**Scuola Internazionale Superiore di Studi Avanzati /
International School for Advanced Studies**

Network functions characterization of random hippocampal neuronal networks using multielectrode array

Thesis submitted for the degree of Doctor Philosophiae

Neurobiology sector

March 2008

Candidate
Frédéric Broccard

Supervisor
Prof. Vincent Torre

Ed. Q1 AREA SCIENCE PARK - S.S.14 Km163,5 - 34012 Basovizza (TS) - ITALY

The external examiner of this thesis was:

Prof. Hugh P.C. Robinson

Department of Physiology, Physiological Laboratory
University of Cambridge, Downing Street, Cambridge CB2 3EG, UK

email: hpcr@cam.ac.uk

. . . ./ à la mémoire de feu Peg

. . . ./ au Dr J. Ubbens

. . . ./ The owls are not what they seem.

Twin Peaks

. . . / We're here to go. That's what we're here for. We're here to go.

William Burroughs, Dead City Radio

Contents

Declaration

The work described in this thesis has been carried out at the International School for Advanced Studies (SISSA/ISAS, Trieste, Italy) between November 2003 and January 2008. All the electrophysiological work on cultured hippocampal networks arises from my own experiments and data analysis with the exception of the work on population coding in which Paolo Bonifazi also performed some preliminary experiments and data analysis. Work on the leech was carried out by Elizabeth Garcia-Perez and Alberto Mazzoni. In the work on stem cells, Jelena Ban carried out all the molecular biological part of the study under the supervision of Elisabetta Ruaro. Data analysis of the computational properties of the stem cells-derived networks was done by Paolo Bonifazi and I. In the work on the plasticity induced by disinhibition, gene microarrays and real-time experiments were done by Silvia Pegoraro and gene microarrays analysis by Daniele Bianchini and Claudio Altafini. TUNEL essay was performed by Daniela Avossa.

List of publications

The results presented in the first two paragraphs of the Results section have been published in the following articles.

Ban J, Bonifazi P, Pinato G, **Broccard FD**, Studer L, Torre V, Ruaro ME (2007) Embryonic derived stem cell-derived neurons form functional networks in vitro. *Stem Cells* 25(3), 738-749.

*Mazzoni A**, *Broccard FD**, *Garcia-Perez E, Bonifazi P, Ruaro ME, Torre V (2007) On the dynamics of spontaneous activity in neuronal networks. *PLoS ONE* **2**(5):e439.
*equally contributed

The third and fourth paragraphs of the Results section correspond to articles in preparation.

Broccard FD, Pegoraro S, Ruaro ME, Pastore G, Avossa D, Bianchini D, Altafini C, Torre V (2008) Sequential events underlying neuronal plasticity induced by a transient exposure to bicuculline. (In preparation).

Broccard FD, Bonifazi P, Ruaro ME, Torre V (2008) Population coding in hippocampal neuronal networks. (In preparation).

Abbreviations

AMPA: α-amino-3-hydroxy-5-methylisoxazole-4-propionic acid

AP: action potential

BIC: bicuculline

EEG: electroencephalography

fMRI: functional magnetic resonance imaging

GABA: γ-aminobutyric acid

GBZ: gabazine

GDPs: giant depolarizing potentials

LFP: local field potential

LTD: long term depression

LTP: long term potentiation

MEA: Multi-electrode array

MEG: magnetoencephalography

NMDA: N-methyl-D-Aspartate

PCS: preferred cortical state

PET: positron emission tomography

PSTH: post-stimulus time histogram

SOC: self-organized criticality

STDP: spike timing dependent plasticity

SPW: sharp population wave

1- ABSTRACT

In nervous systems, behaviors are generated through the activity of ensembles of neurons assembled in networks, where networks become the interface between the cellular and behavioral levels. Uncovering the mechanisms of action of these networks is thus essential in order to fully understand and characterize the nervous systems functions in normal and pathological conditions.

A complete understanding of a given network requires information about its individual component cells, their functional properties, their wiring diagram and their dynamic interactions. Few known networks come close to providing complete information on all these aspects. Moreover, even if complete information were available it would still only provide insights into network functioning. This is because the structural and functional properties of networks are not static but plastic and can vary over time. Reductionist approaches have been successful at identifying and characterizing many components that could contribute to network functions. For example, the contribution of specific individual classes of cells to network functions can be inferred by selectively silencing or activating them by combining genetics and pharmacology (Wulff & Wisden, 2005). However, networks are not the linear sum of its individual parts but instead reflect the spatial and temporal interactions of non-linear properties. Individual cell components influence and are influenced by the network output(s). Thus, a system-level understanding is needed as advocated by cyberneticians (Bertalanffy, 1969) and systems biologists (Kitano, 2002), focusing on the system's interactions and dynamics rather than on the characteristics of the single isolated parts.

The subject of my PhD thesis is to study network functions of neuronal networks composed of dissociated rat hippocampal neurons grown on multielectrode arrays (MEA). On the one hand, *in vitro* cultured neuronal networks with random connections retain universal properties and principles present in artificial and natural neural systems. Indeed, such *in vitro* networks form extensive synaptic connectivity and display complex spontaneous activity and sensitivity to externally applied patterns of activity and are endowed with basic plasticity mechanisms. The organizing principles operating at the level of neuronal populations are intrinsic to neurons and are therefore manifested in *in vitro* cultured networks, thus providing a point of view of neuronal network functions and mechanisms, independent of the network's topology. On the other hand, MEAs offer the

possibility of probing the neuronal activity of a large number of neurons non-invasively and for extensive periods of time, which is a prerequisite to investigate network functions at the population level while keeping in focus the contribution of single neurons.

In this thesis, network functions have been investigated from four different points of view. First, the generation of functional neuronal networks from embryonic mouse stem cells is presented along with a comparison of these networks with those of cultured hippocampal networks. This represents the first demonstration proving that embryonic stem (ES) cells-derived neurons are capable of generating functional neuronal networks. We show that the spontaneous and evoked activities are remarkably similar to those of cultured hippocampal networks. Moreover, ES-derived networks are endowed with basic information properties and are capable of discriminating stimuli of different intensity at a single trial level. Thus, ES-derived neurons provide a novel strategy to design/engineer functional networks with defined computational properties. Second, as recent work showed that spontaneous activity is a hallmark of cultured networks (Maeda et al., 1995; van Pelt et al., 2004), we provide a detailed analysis of its dynamics and compare it with that of intact leech ganglia. We found that the spontaneous activity of these two very different networks share several features, such as the presence of long-range correlations, and that their dynamics can be accounted for the self-organized criticality (SOC) framework (Bak et al., 1988; Jensen, 1998). The SOC theory originates from statistical mechanics and characterizes the system dynamics of interconnected nonlinear threshold units, in which each unit has one or more input/output(s). SOC dynamics has been found in a variety of neuronal preparations with specific functional architecture in vertebrates. Our results provide the first demonstration of SOC in random networks as well as in invertebrate networks, thus generalizing SOC dynamics, and indicating that such dynamics might be a generic property and ubiquitous phenomenon in a large variety of neuronal networks. Third, the time varying aspect of network functions was investigated. In particular, we studied how synaptic plasticity could be induced pharmacologically and the molecular mechanisms allowing its maintenance in cultured hippocampal networks. To this end, we used a top-down approach (recording of the electrical activity with MEA) in combination with a bottom-up one (identification of specific genes by using DNA microarrays) to characterize the time course of the electrical and cellular events up to

24h. Then we investigated how such plasticity affected network functions. In particular, we looked at changes of (i) the spontaneous firing pattern, (ii) the evoked-activity and (iii) the pattern of gene expression. It was found that a transient exposure (30 min.) to inhibitors of $GABA_A$ receptors, such as bicuculline and gabazine, was sufficient to induce network plasticity. On the one hand, inhibitors of $GABA_A$ receptors induced a synchronous bursting pattern of activity that persisted up to 24h following the drug washout. An early component of synchronization was blocked by inhibitors of the MAPK/ERK pathway, whereas a late component was blocked by inhibitors of transcription. Moreover, our results indicate that the regulation of hundreds – rather than tens or thousands – of genes takes place following the drug washout and suggest that a down-regulation of K+ and HCN channels likely underlie the early component of synchronization. On the other hand, the evoked activity was potentiated for several hours following the drug washout, demonstrating the possibility of pharmacologically inducing a form of plasticity in MEAs. This could represent an interesting alternative with regards to the classical electrical protocols for the induction of functional plasticity. Overall, the combination of MEA and DNA microarrays revealed to be a powerful approach to investigate the electrical and molecular events underlying neuronal plasticity in cultured networks. Finally, we investigated the computational abilities of cultured hippocampal networks by comparing several coding schemes and focused on the difference of two forms of population coding: distributed and pooled. By using classification criteria from pattern recognition theory, we found striking similarities with *in vivo* population coding strategies used in the somatosensory cortex of the rat (Petersen et al., 2003) and the monkey (Nicolelis et al., 1998). In order to be able to correctly identify a stimulus' intensity and spatial location, distributed codes proved to be more efficient than the pooling of neuronal responses. Taken together, these results provide the first compelling evidence that simple computational tasks can rely on distributed population coding schemes in random cultured networks, as proposed some years ago (Potter, 2001).

The results reported in the first two paragraphs of the Results section have been published in peer-reviewed journals. The third and fourth paragraphs represent articles in preparation.

2- INTRODUCTION

2.1- MEA technology

Mutli-electrode arrays (MEAs) allow simultaneous recording from, and stimulation of, a large number of neurons for a long period of time, thanks to their non-invasive extracellular electrodes. MEA also referred to as micro-electrode arrays, multi-electrode plates, planar electrode arrays or multi-microelectrode dishes, provide an intermediate level of investigation between patch-clamp studies and animal experimentation. The first recording obtained with MEA was field potentials from cultured chick cardiac myocytes in the early 70s (Thomas et al., 1972). About a decade later an important step was reached when MEAs were developed allowing multi-single-cell recording and electrical stimulation of cultured neuronal networks (Pine, 1980; Gross et al., 1982). Since then, various groups designed and fabricated their own MEA, including hardware and software (Israel et al., 1984; Novaks and Wheeler, 1986; Connolly et al., 1990; Jimbo and Kawana, 1992; Martinoia et al., 1993), and using diverse neuronal cell types (see Stett et al., 2003 for a review of MEA application with other cell types such as cardiac myocytes and retina). Thanks to recent progress in cell culture techniques (Potter & DeMarse, 2001) health and sterility of dissociated cultures can now be maintained for several months, up to a year. Currently, several MEA systems are commercially available. Two companies dominate the market: Multichannel Systems[1] (Reutlingen, Germany) and Panasonic[2] (Tokyo, Japan). Plexon Inc.[3] also offers a MEA system in collaboration with W. Gross (University of N. Texas).

A typical MEA set-up (Fig. 1) consist of a MEA, a multichannel amplifier, a computer for signal processing software and data logging and a life-support system to maintain ideal conditions for the cells. The above mentioned companies provide everything but the life-support part.

[1]http://www.multichannelsystems.com

[2]http://www.panasonic.com/medical_industrial/med-index.html

[3]http://www.plexoninc.com

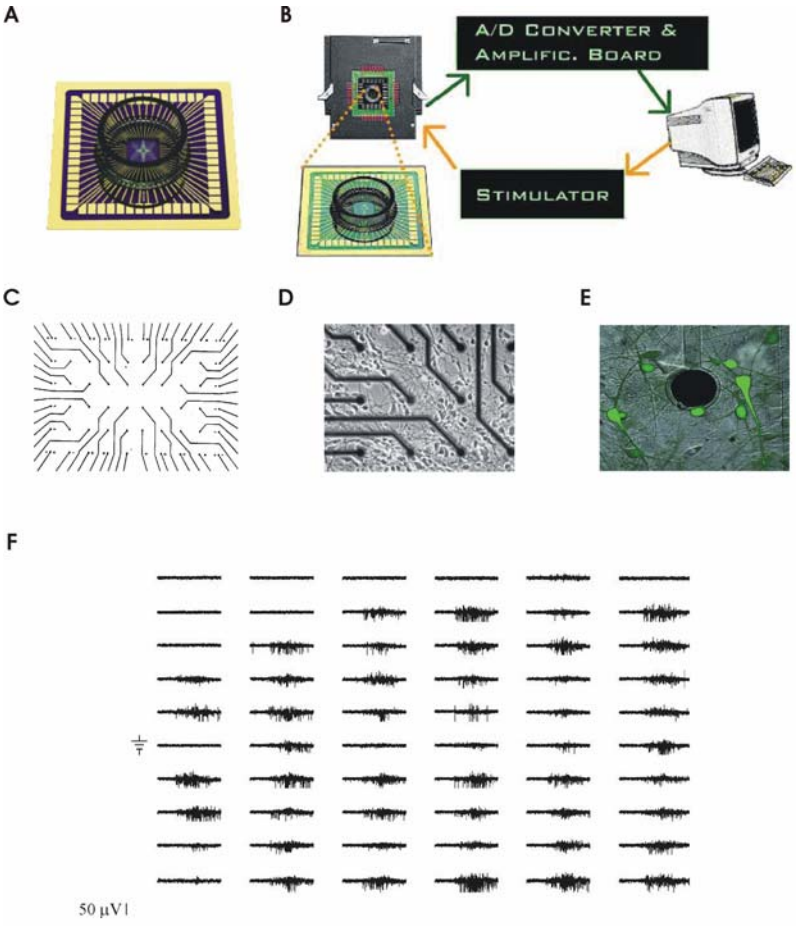

Figure 1 | A. 60 electrodes MEA dish with glass substrate supplied by Multichannelsystems. **B.** Sketch of the MEA set-up. The MEA dish is connected to a 60-channels 10 Hz – 3 kHz bandwidth preamplifier/filter-amplifier which redirects the signals recorded from the neurons towards further electronic processing (i.e. amplification and AD conversion) operated by a board lodged within a high performance PC. Sample data are usually transferred in real time to the hard disk for off-line analysis. Electrodes can also be used for stimulation. In this case, specific patterns of stimulation are designed via software and then loaded into the stimulator. **C.** Layout of the 60 electrodes. Intra-electrodes distance is 500 µm. **D.** Close-up of a dozen of electrodes with neuronal processes. **E.** Close-up of a single electrode with neurons stained with the neuronal marker TUJ-1 (green), recognizing the neuron specific beta III tubulin. The electrode diameter is 30 µm and is made of titanium-nitride. **F.** One second snapshot of the 60 electrodes' activity for a cultured network of rat hippocampal neurons, showing the occurrence of a burst invading almost all the network. Some electrodes are silent probably because of a lack of electrical contact with neurons. One electrode is used as ground.

The substrate of choice for MEAs is glass for its biocompability and transparency property. It allows MEAs to be used in parallel with optical methods (Potter, 2001) making possible to virtually observe, monitor and stimulate every cell in a cultured monolayered network with high temporal (ms) and spatial (μm) resolution. This is currently not achievable in living animals or in other preparations such as brain slices. Generally, the electrodes are made of gold and have a diameter ranging between 10 to 100 μm. They are usually covered with platinum black (porous platinum) or sputtered with iridium oxide or titanium nitride to lower their impedance. Low impedance is needed to detect small extracellular signals (μV range) and to limit the faradaic process that may harm cells when they are stimulated. The number of electrodes ranges from tens to more than a hundred, but progress in computer and data storage technology will certainly allow the creation of MEAs with more electrodes and higher sampling rates. The leads that connect the electrodes to external electronics are made of gold or the transparent conductor indium-tin oxide. A layer of insulating material isolates the MEA' surface and the interconnects from the culture medium and also serves as culture substrate to promote cell adhesion after coating. Biocompatible insulators include (but are not restricted to) SiO_2, SiN_4 and polymers such as polyimide, silicon resin and polyacrylamide. The coating molecules used are generally polyaminoacids, such as polylysine or polyornithine to insure good quality of contact between electrodes and neurons, which is a critical determinant for signal detection. Since more than one neuron can make contact with an electrode, numerous spike sorting algorithms have been developed, allowing the identification of single neurons contribution to the recorded electrode signals.

The rapid development of MEA technology and the widespread use of MEAs arise from several observations. Firstly, as said above, recent technical advances in multi-units recording techniques (including optical ones, such as calcium imaging) now allow researchers to virtually observe, monitor and stimulate every single cell in cultured neuronal networks with high spatiotemporal resolution. The study of network functions in *in vitro* systems offer the possibility to overcome some of the major limitations of their *in vivo* counterparts by allowing to record simultaneously from a large number of cells, non-invasively, and for long periods of time ranging from hours up to months (Potter, 2001;

Potter & DeMarse, 2001). Secondly, similarly to several others *in vitro* preparation, a tight control and manipulation of the neurochemical environment is possible. Thirdly, although the cultured neuronal networks developing *in vitro* lack the functional cytoarchitecture from the brain region – from where the cells are dissociated – and can be considered as random networks, they retain many features and characteristics of real networks (Potter, 2001; Marom & Eytan, 2005). This provides a general view of neuronal networks and cell assemblies, allowing the investigation of universal principles governing network functions and mechanisms. Furthermore, the main electrophysiological, biochemical and pharmacological properties of the individual cells composing cultured neuronal networks are identical to cells *in vivo* (Higgins & Banker, 1998). Fourthly, cultured networks are free to develop and can express their full developmental and adaptation potential whose investigation is limited in slice preparations. Indeed, these latter are cut off from a larger system in which they were intended to function, whereas cultured networks develop from scratch. Finally, on a more functional side, *in vitro* cultured networks form extensive synaptic connectivity and display complex spontaneous activity and sensitivity to externally applied patterns of activity. These features are common to all the nervous systems that learn. Thus, cultured neuronal networks are a useful tool to study synaptic plasticity at the population level while keeping on focus the contribution of single neurons. Furthermore, cultured networks also permit the development of strategies for the future implantation of bionic devices in live animals (Patterson et al., 2004) and represent an ideal platform to study engineered networks in which either the proportion of specific neuronal subtypes (see Ban et al., 2007 for a example) or their properties, or both, are modified.

An alternative solution to the traditional glass substrate is silicon (Pancrazio et al., 1998; Bucher et al., 1999). This is attractive because of years of experience gained by the semi-conductor industry and also thanks to the possibility of interacting electrically excitable cells with field-effect transistors (Vassanelli and Fromherz, 1997). However, this technology is relatively new and the success of its applications is still too sparse to suport firm conclusions.

2.1.1- Biosensors

In vitro cultured neurons have been shown to be very sensitive to neuroactive compounds present in the culture medium (Gross et al., 1992) which modify the pattern of spontaneous activity depending on the cell type (Morefield et al., 2000). Following the pioneer work of Gunter W. Gross and his collaborators, neuronal networks received a lot of attention as biosensors (Gross et al., 1992, 1995, 1997; Morefield et al., 2000) for several analytical properties such as selectivity, sensitivity, stability, robustness, reliability, reproducibility, rapidity and accuracy as well as for their ease of utilization and maintenance. Moreover, the great amount of knowledge accumulated over the past 20 years on the effect of neuroactive compounds (read-out response of the biosensors) facilitated the use of neuronal networks for classification purposes. Indeed, a legion of neuroactive substances have been shown to modify the pattern of spontaneous activity and include (but are not limited to) agonists and antagonists of glutamate, GABA, glycine, dopamine and acetylcholine receptors, as well as several ionic channels (sodium, potassium, calcium) blockers. Furthermore, the rapidity of the response of most of these compounds makes on-line analysis feasible (Selinger et al., 2004) and opens up the possibility of an industrial and/or pharmaceutical use of MEAs as biosensors. Finally, although until now MEAs have only been used to characterize single neuroactive compounds, the possibility of co-culturing networks (Baker et al., 2006) and engineered networks to sense specific biochemical compounds holds great promise to have highly specific and sensitive robust biosensors in the near future.

2.1.2- Stimulating networks

MEAs can also be used to stimulate neuronal networks in diverse locations. Traditionally the electrodes selected for stimulation were unable to simultaneously record electrical activity, but recent technological improvements from Multichannelsystems (Reutlingen, Germany) and several research groups (Jimbo et al., 1999; Wagenaar & Potter, 2004) have overcome this limitation and it is now possible for electrodes to switch from stimulation to recording with a very small delay of a few milliseconds. It has been

shown that a clear electrical response could be elicited over almost the entire network by stimulating one of the extracellular electrodes with a brief and strong voltage pulse (Jimbo et al., 2000). The electrical response of cortical neurons is composed of an early phase of a few tens of milliseconds and a late phase of several hundreds of milliseconds. The early phase is characterized by a precise and reproducible firing timing (small jitter) and by a wave-like spread of the electrical activity over the network. In contrast, the late phase is characterized by clusters of electrical activity with significant spatio-temporal fluctuations. The late phase depends both on cholinergic pathways and NMDA receptors as it is selectively suppressed by application of the cholinergic agonist carbachol (Tateno et al., 2005) or by the NMDA antagonist D(-)-2-amino-5-phosphovaleric acid or an increase of the extracellular Mg^{2+} concentration (Jimbo et al., 2000), respectively. Jimbo and colleagues also investigated the effect of stronger stimulation protocols, using tetanic stimulation, to reveal the distributed changes in the network properties. By serially stimulating all individual electrodes with test stimuli and tetanus, it was found that activity-dependent changes were pathway-specific (Jimbo et al., 1999); the activity between two electrodes was enhanced if their activity was correlated before the application of tetanic stimulation, whereas it was depressed when the correlation fell outside a 40 ms time window. Moreover, although using a more simple protocol in which the tetanus was applied to one or two electrodes only, it has also been shown that the reliability of both the first spike and the interspike interval was modified by tetanic stimulation (Tateno & Jimbo, 1999); either enhancement or reduction of the reliability and reproducibility of the spike train were observed. Compared with the traditional paired-cell technique focusing on two cells considered in isolation though embedded in a network, these two studies represent a significant progress for studying spike timing dependent plasticity (STDP; Markram et al., 1997), because the MEA approach allows to probe changes over the whole network and can reveal the influence of virtually all cells forming the network using spike-sorting algorithms.

Stimulation of cultured rat hippocampal networks grown on MEA with single pulse at low frequency revealed that the timing of the first action potential (AP) was rather precise from trial to trial whereas the timing of later APs was much more variable (Bonifazi et al., 2005). Interestingly, pooling of the neuronal responses reduced response

variability and allowed to reliably distinguish stimuli varying in intensity on a single trial basis. Moreover, the size of the neuronal pool and the time bin necessary to provide reproducible responses were remarkably similar to those previously observed *in vivo* (Nicholelis et al., 1998). Pharmacological dissection of the main excitatory and inhibitory pathways revealed that a reduction of the bursting activity obtained by blocking the NMDA receptors increased the mutual information between the evoked response and the stimuli. Conversely, an increase of the bursting activity by blocking $GABA_A$ receptors decreased it. This is in agreement with previous analysis of the importance of the balance between excitation and inhibition in neuronal networks (Shadlen & Newsome, 1994).

Stimulating cultured networks also revealed that these networks were endowed with the ability of performing some basic forms of learning. The main motivation of using random *in vitro* networks is the assumptions that learning is governed by a set of underlying universal neural principles (Marom & Eytan, 2005) and that the organizing principles operating at the level of neuronal population are intrinsic to neurons and are therefore manifested in *in vitro* cultured networks. This last assumption is justified by the observation that random networks cultured *in vitro* possess two major learning features common to all neural systems; (i) a rich heterogeneous functional connectivity enabling a large repertoire of possible responses to diverse stimuli; and (ii) sensitivity of the functional connectivity to patterns of activity, allowing for selection of responses.

Using a closed-loop set-up in which cortical networks interacted with a computer, Marom and Shahaf (2001) used a rather unusual criterion for learning. MEAs were stimulated through a pair of electrodes and the response of a third probe electrode was monitored. Once a specific response was elicited in the probe electrodes the computer automatically stopped the stimulation, for a period of rest. Then the network was stimulated again. Thus, the stimulation protocol consisted of stimulation periods of different length, interspaced by a period of rest. The probe electrode that responded 50±10 ms after a stimulus with a response-to-stimulus ratio of 1/10 was selected. This means that in average 10 stimuli were necessary to evoke one spike. The criterion for stopping the stimulation was to increase the response-to-stimulus ratio of this probe electrode to 2/10 or greater. After stimulation of pairs of electrode at low frequencies (0.33-1 Hz), it was shown that the response time (i.e. the time for the probe electrode to

fulfill a response-to-stimulus ratio equal or greater than 2/10) decreased with the number of stimulation cycle. In other words, the probe electrode always responded more quickly once the predefined desired response-to-stimulus ratio was fulfilled. The authors concluded that networks *learned* to fulfill the predefined desired criterion. It should be however noted that others failed to repeat this learning protocol (Wagenaar & Potter, 2006). Further work by Marom and colleagues also revealed that networks of cortical neurons were able of selective adaptation (Eytan et al., 2003). Stimulating networks through two different electrodes, one at a frequency of 0.2 Hz and the other at 0.02 Hz, they observed that the response to the rare stimulus (0.02 Hz) was markedly increased whereas the response to the frequent stimulus (0.2 Hz) was attenuated, probably due to short-term depression.

Work in our lab, using *in vitro* random networks of rat hippocampal neurons, demonstrated that these networks could perform some basic image processing operations such as gaussian filtering and pattern recognition (Ruaro et al., 2005). In particular, tetanic stimulation of a given pattern of electrodes (among a total of six) proved to be sufficient to potentiate the response of this particular pattern, indicating that the potentiation of a specific network response was possible, similarly to what is observed in single-cell electrophysiology.

Taken altogether, these results (Marom & Eytan; 2005; Ruaro et al., 2005) indicate that random networks are capable of some form of learning and can be used to investigate their underlying universals. This is both encouraging and a prerequisite for establishing a new generation of analog computing devices, in which the full potential of parallel processing (Rumelhart et al., 1986) will be truly exploitable.

2.2- Spontaneous activity in neuronal networks

Brain functions have been traditionally investigated from an input-output perspective in which a stimulus or task is administered and the resulting changes in neuronal activity and behavior are measured. However, the brain is never at rest and shifting patterns of activity course through it. Spontaneous neuronal activity refers to activity that is not attributable to specific sensory inputs or motor outputs; it represents neuronal activity that is intrinsically generated by the brain. Its most obvious manifestation is during sleep where the main sensory inputs and motor outputs are absent. But neuroimaging studies indicate that even during waking states, brain regions unrelated to a specific task or function are active (Fox & Raichle, 2007). Moreover, most *in vitro* preparations often display spontaneous activity (Maeda et al., 1995; Tscherter et al., 2001; Beggs & Plenz, 2003; van Pelt et al., 2005). Although spontaneous activity seems to be an important feature of neuronal tissues and is well documented, it has not been equally well studied so far and its role remains unclear.

In this section, I will first review the early role of spontaneous neuronal activity and its importance for the formation and maturation of developing networks and circuits. A primitive form of network-driven activity will be discussed and although this spontaneous activity differs from the one encountered in mature networks, it nevertheless shares some similar aspects, such as circuit homeostatic plasticity to maintain the proper level of network activity. Then, I will review the contribution of spontaneous neuronal activity to neuronal computation and information processing in mature networks, a view that challenges the long-held assumption according to which background synaptic activity simply represents noise.

2.2.1- Patterns of spontaneous activity and development of neural circuits

Research over the last 20 years has clearly established that electrical activity is essential for the development of neuronal circuits in many part of the brain (Zhang & Poo, 2001). Experience-dependent activity is only one facet of a more general principle

for neuronal activity in transforming young and immature circuit into mature and functional networks subserving adult brain function. Indeed, a hallmark of developing neuronal circuit is the presence of internally generated primitive patterns of spontaneous activity that transform circuits into mature ones (Katz & Shatz, 1996; O'Donovan, 1999; Ben-Ari, 2001). This spontaneous activity can already be detected in utero in several species, arguing for a critical role of spontaneous activity in circuits' formation before the onset of sensory experience. For example, in the visual system of nonhuman primates, ocular dominance columns are fully formed by birth (Horton & Hocking, 1996) indicating that the initial formation of the stripes is independent from visual experience. Hamburger (1976) who studied chick embryos, identified two general features characterizing the spontaneous activity found in all parts of the developing nervous system examined so far: i) the activity is restricted to a limited period of time during development and ii) it is organized into bursts of activity separated by periods of quiescence.

Typically, one distinguishes the activity generated before and after the formation of chemical synaptic networks. Before the formation of synaptic contacts, activity produced in the early mammalian cortex (Yuste et al., 1992) and in the retina (Feller et al., 1996) depends on calcium transients that are synchronized in groups of cells coupled by gap junctions. In cells of the amphibian neural tube, this calcium-dependent activity can take the form of calcium spikes or waves (Spitzer, 1994; Gu & Spitzer, 1997). Calcium spikes rise rapidly and decay over several minutes and appear to be important for transmitter and ion channel expression. In contrast, calcium waves rise and decay slowly and appear to be associated with neurite extension at growth cone. Potential sources for these calcium transients are Ca^{2+} influx via membrane depolarization through NMDA receptors and voltage-gated Ca^{2+} channels or Ca^{2+} release from internal store.

Before the establishment of the first synaptic contacts, the prevailing view concerning the early formation of neuronal circuit was that it was mainly directed by molecular interactions. Pathfinding of growing axons was thought to be independent from electrical activity and to only require molecular guidance signals provided by the surrounding developing tissues; a process known as chemotaxis (Kandel et al., 2000). However, electrical activity in growing axons can trigger secretion of neurotrophins and

neurotransmitters from growth cones; neurotransmitters, such as glutamate and GABA for example, can act as trophic factors and subserve an identical role as neurotrophins (Mattson, 1988; Lauder, 1993). Moreover, in cultured *Xenopus* spinal neurons, brief trains of action potentials could convert the response of the growth cone towards repulsive cues into attraction (Ming et al., 1999) and in hippocampal cultures, growth cone motility is dynamically regulated by transient bursts of spontaneous activity (Ibarretxe et al., 2007). Thus, electrical activity can directly influence axonal growth. In some preparations, a more clear role for activity in axon pathfinding has been reported as for growing thalamic axons to reach their appropriate targets (Catalano & Shatz, 1998) or for axons of cortical pyramidal cells to form layer-specific intracortical connections (Dantzker & Callaway, 1998). Further evidence in favor of a role of spontaneous electrical activity for axon pathfinding was provided by Hanson and Landmesser (2004, 2006). They showed that, in chick spinal cord, lowering the frequency of rhythmic activity using the $GABA_A$ antagonist picrotoxin resulted in dorsoventral pathfinding errors (Hanson and Landmesser, 2004). In contrast, doubling the frequency of the rhythmic activity by blocking the glycine transporter GlyT1 with sarcosine, perturbed the anteroposterior pathfinding process (Hanson and Landmesser, 2006). On the other hand, in other preparations like the mouse olfactory system, projection of olfactory sensory neurons to specific glomeruli in the olfactory bulb was largely unaffected in odorant-evoked neuronal activity deficient mice (Lin et al., 2000), although others reported minor alterations in path findings (Zheng et al., 2000). Thus, although a large body of evidence identifies a role of patterned neural activity in early axon guidance, it remains an open issue why the guidance behavior of axons in some preparations is insensitive to such patterns of activity. It seems however clear that there is a reciprocal influence between the development of neuronal connectivity on the one hand, and the intrinsic spontaneous network electrical activity on the other hand (Corner, 1994).

Recurrent patterns of spontaneous activity are also observed after synaptogenesis in a large variety of systems from different species. By using direct recording of electrical activity and/or optical method such as fluorescence Ca^{2+} imaging, they have been studied most extensively in the hippocampus (Ben-Ari et al., 1989; Leinekugel, 2003), spinal cord (O'Donovan, 1989), retina and lateral geniculate nucleus (Galli & Maffei, 1988;

Katz & Schatz, 1996) and have also been observed in the neocortex (Garaschuk et al., 2000) and cultured cortical neurons (Maeda et al., 1995; van Pelt et al., 2005), in the auditory system (Lippe, 1994) and in the trigeminal nucleus (Ho & Waite, 1999). In many of these structures, these network-driven patterns of spontaneous activity provide most of the activity required for the maturation and refinement of the synapses and the establishment of functional circuits. Current evidence suggests that these patterns involve spontaneous bursts of activity correlated both in space and time (O'Donovan, 1999; Feller, 1999; Ben-Ari, 2001). In general, these spontaneous synchronous bursts last for tens to hundreds of milliseconds, are separated by intervals of several seconds to a few minutes, and involve the correlated firing of large population of neurons.

In the next paragraphs, I will review patterns of spontaneous activity on the hippocampus, retina and spinal cords as they share striking features.

In vivo recording in the CA1 region of the hippocampus of freely moving rat pups (P4-P6) with bundles of 8 extracellular electrodes revealed multi-unit bursts which recurred at 0.1-0.3 Hz (Leinekugel et al., 2002). This profile of neuronal activity was similar to the spontaneous sharp population waves bursts (SPW) observed in adult rat during immobility or slow-wave sleep (Fig. 2A) and is similar to the giant depolarizing potentials (GDPs) described *in vitro* in brain slices (Ben-Ari et al., 1989; for a review, see Ben-Ari, 2001).

As GDPs (Fig. 2B) bear striking similarities with their *in vivo* counterparts, SPWs, a certain number of observations accumulated over the last 20 years are likely to be relevant to the *in vivo* situation.

GDPs appear in the last days of the embryonic life and last until around the end of the second postnatal week (Fig. 2C). GDPs constitute the first pattern of synchronized activity and in fact, other adult oscillatory hippocampal patterns, including theta activity (5-10 Hz) and faster ripple oscillations (150-200 Hz), emerge at later developmental stages (Leblanc & Bland, 1979). GDPs (Ben-Ari, 2001) and other patterns of spontaneous population discharges in the retina (Feller et al., 1997; Wong, 1999) and in the spinal cord (O'Donovan, 1999) are slow-propagating waves of activity with a periodicity of the order of minutes (Feller, 1999). In the hippocampus, GDPs originate mainly in the CA3 region and propagate to the CA1 region and the fascia dentata

(Leinekugel et al., 1998; Menendez de la Prida et al., 1998). Its mechanisms of generation will be explored further in this work as they are well-characterized and share several common principles with the population discharges observed in the spinal cord and in the retina.

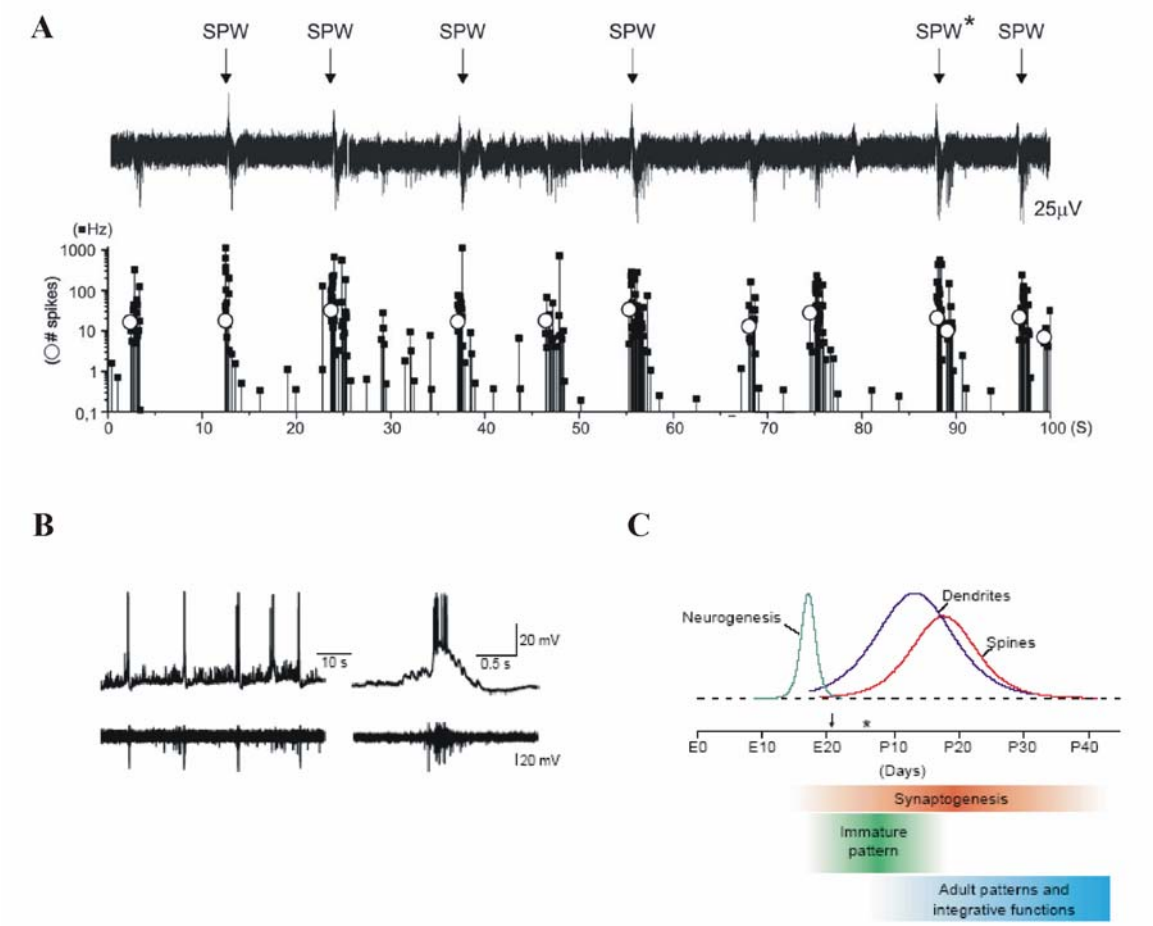

Figure 2 | Spontaneous activity in the developing hippocampus. **A.** Multi-unit activity recorded extracellularly in the CA1 pyramidal layer of a freely moving rat (P4-6). **B.** Pattern of synchronous activity in the neonatal rat hippocampus known as giant depolarizing potential (GDP). Simultaneous intracellular recording of CA3 pyramidal cell (i) and extracellular field of CA3 pyramidal layer in hippocampal slice (P6). **C.** Time course of the principal events occurring in the developing rat hippocampus. Neurogenesis occurs in major part before birth (at E21, indicated by arrow). Synaptic connections begin to form around birth and continue to form during two postnatal weeks. During this time, most of the synchronized activity is provided by GDPs. Panel A is modified from Leinekugel, 2003. Panel B and C are reproduced from Ben-Ari, 2001.

Retinal waves are robust phenomena that have been observed in several species, including rat, mouse, chick, cat, rabbit and turtle. They are generated by ganglion cells (Galli & Maffei, 1988) and sweep across a restricted portion of the retina. Calcium imaging studies revealed that amacrine cells are also required (Wong et al., 1995). At the developmental stage where retinal waves are observed, the major synaptic connections are between amacrine and retinal ganglion cells. The amacrine cells are connected to each other and project to ganglion cells. Several pieces of evidence point out the critical role of cholinergic (Feller et al., 1997; Penn et al., 1998) and GABAergic (Fisher et al., 1998) transmission for the generation of retinal waves. Although the majority of amacrine cells are GABAergic, a significant fraction, called the starburst amacrine cells, are cholinergic. Cholinergic synaptic inputs depolarize ganglion cells during the waves and cholinergic antagonists block retinal waves (Penn et al., 1998). Similarly, $GABA_A$ antagonists can reduce the frequency of the wave and even block them (Fisher et al., 1998). Interestingly, the mechanisms of retinal wave generation change with age. In chick (>P18) and ferrets (>E11), retinal waves are insensitive to cholinergic antagonists and instead are blocked by glutamate antagonists (Wong, 1999). Thus, in several species, a variety of synaptic mechanisms at different developmental stages can lead to the generation of similar propagating waves of activity in the retina.

As stated above, spontaneous activity in the spinal cord is similar to the one encountered in the retina and hippocampus in several aspects. Early spinal cord activity consists of periodic bursts, synchronized across several segments (O'Donovan, 1989). This rhythmic activity is driven by excitatory neurotransmitters and there is a switch from acetylcholine at an early stage (E5; Milner & Landmesser, 1999) to glutamate at a later stage (E10; Chub & O'Donovan, 1998) as observed in the retina (Wong, 1999). Moreover, in the hippocampus, retina and spinal cord, these patterns of rhythmic spontaneous activity are all network-driven, independent of pacemaker or oscillatory neurons. In all these different networks, the most important property necessary to generate spontaneous activity is hyperexcitability (Feller, 1999; O'Donovan, 1999). This may result from functional recurrent connectivity, with probable excess innervation which is later pruned, and from the depolarizing nature of all the major neurotransmitters in early development. Indeed, apart from acetylcholine and glutamate, which are

excitatory and have a depolarizing effect like in the retina and spinal cord, neurotransmitters usually considered as inhibitory in adult brains, such as glycine and GABA, are also excitatory in immature neurons (Ben-Ari et al., 1989, 1997; Ben-Ari, 2002). The depolarizing action of GABA was suggested in the pioneer study demonstrating the existence of GDPs in hippocampal slices (Ben-Ari et al., 1989) and is a milestone for developing networks, because it has been then confirmed in every species and structures studied (Ben-Ari, 2002; for an exhaustive review, see Ben-Ari et al., 2007). The excitatory action of GABA is mediated by $GABA_A$ receptors and is critical for GDPs generation. However, recent studies indicate that GABA can exert dual – both excitatory and inhibitory – actions during development. This is due to the reversal potential of GABA (E_{GABA}). In immature neurons $E_{GABA} \approx -35mV$, due to the high intracellular chloride ions (Ben-Ari et al., 1989). On the one hand, $GABA_A$ currents depolarize the immature neurons and this could activate voltage-gated Ca^{2+} channels and potentiate the activity of NMDA by releasing the Mg^{2+} block (Leinekugel et al., 1997). On the other hand, the reverse potential of the glutamate receptor-mediated currents (near 0 mV) is more positive than E_{GABA}. Therefore, during co-activation of $GABA_A$ and glutamate receptors (like during GDPs, see below), $GABA_A$ receptor-mediated conductance shunts the glutamate receptor-mediated currents, preventing excitotoxicity and epileptiform activity (Wells et al., 2000). Thus, the action of GABA in the immature neurons depend on complex interactions between GABA and glutamate conductances (ratio of the GABA:NMDA:AMPA receptor-activated conductances, timing of activation) as well as on the value of E_{GABA}.

While GABAergic transmission via $GABA_A$ receptors is critical for GDPs, there is also a substantial contribution of glutamatergic transmission via NMDA and, to a less extent, via AMPA receptors (Khazipov et al., 1997; Bolea et al., 1999). This is because at early developmental stages, AMPA synaptic transmission is relatively quiescent. Thus, in neonatal neurons, the depolarization needed to remove the Mg^{2+} block of NMDA receptors is provided by the $GABA_A$ receptors activation. Augmentation of intracellular Ca^{2+}, revealed by simultaneous electrophysiological recordings and Ca^{2+} imaging, has also been observed during GDPs (Leinekugel et al., 1997). The main source of Ca^{2+} is via voltage-dependent Ca^{2+} channels, depolarized by the excitatory action of $GABA_A$

receptors. However, augmentation of intracellular Ca^{2+} has also been observed when activation of voltage-dependent Ca^{2+} channels was prevented (Leinekugel et al., 1997), suggesting that NMDA receptors provide another important source of Ca^{2+}. Altogether, these observations led to the hypothesis that during GDPs the neuronal excitation results from a synergy between $GABA_A$ and NMDA receptors activation (Khazipov et al., 1997; Leinekugel, 2003). Another important factor to consider is the sequential maturation of the GABAergic and glutamatergic synaptic transmission (Tyzio et al., 1999; Ben-Ari, 2002) that can explain the relative contribution of these two neurotransmitters in GDPs generation and reconcile some previous conflicting observations.

Thus, it seems clear that the generation of early spontaneous patterns of activity in the hippocampus, spinal cord and retina is due to purely excitatory synapses. In contrast, the mechanism dictating the rhythmicity and termination of these spontaneous patterns of activity is less clear and likely involve a depression of the network excitability. However, the way this "network depression" is obtained has not yet reached a general consensus and probably involves different mechanisms in different preparations. In rat hippocampal slices, it has been shown that $GABA_B$ antagonist lengthened GDPs (McLean et al., 1996), probably via a blockade of $GABA_B$ receptors that are functional earlier than postsynaptic receptors (Gaiarsa et al., 1995). However, it is currently unknown if a similar effect is present in the spinal cord and the retina. Other possible sources of network depression could be depletion of the readily releasable pool of transmitters, which has been shown in adult hippocampal slices (Staley et al., 1998), and/or inactivation of voltage-gated currents (Franklin et al., 1992).

The similarities between all these network-driven patterns of rhythmic spontaneous activity, led Ben-Ari (2001) to propose that these patterns of activity share the following common properties:

i) they are the first pattern of spontaneous activity in immature circuits and are restricted during a limited developmental period of time;

ii) they are globally similar and are characterized by slowly propagating recurrent waves of activity;

iii) they propagate both within structures and between connected structures that will form a functional network/circuit;

iv) they coincide with the depolarizing action of GABA and glycine;

v) the mechanism of generation switches during development;

vi) they are associated with intracellular Ca^{2+} oscillations;

On a functional level, rhythmic pattern of spontaneous activity provide hebbian conditions for the modulation and rewiring connectivity of synaptic connections. Hebb's postulate (Hebb, 1949) – coincident pre- and postsynaptic firing leads to synapse strengthening – has been further extended by assuming that noncoincident pre- and postsynaptic firing leads to synapse weakening (Stent, 1973). Moreover, the rearrangement of connectivity is similar to LTP and LTD, which are the classical models of activity-dependent synaptic plasticity. LTP and LTD of GABAergic synapses have been observed in the newborn rat hippocampus and were shown to involve both NMDA-dependent and independent pathways (Durand et al., 1996; McLean et al., 1996b). In the *Xenopus* developing visual system, LTP/LTD could be triggered by artificial or natural stimuli (Zhang et al., 1998; 2000), but the possibility that rhythmic pattern of spontaneous activity could trigger LTP/LTD has not been addressed. Thus, although immature tissues show an ability to express both LTP and LTD, it is not clear whether such plastic modifications are triggered by a rhythmic pattern of spontaneous activity at an earlier stage of development.

Besides modifying synaptic connections, rhythmic patterns of spontaneous activity can change intrinsic excitability of neurons as well as patterns of gene expression and protein synthesis. An important factor involved in these processes, and in some form of LTP/LTD, is calcium, which indeed increases transiently in developing neurons (see point vi) above and discussion on calcium spikes and waves, p. 14). Another effect of the electrical activity is the generation of electric fields that may induce electroosmotic or electrophoretic migration of cellular components in the membrane or cytoplasm (Zhang & Poo, 2001). These migrations create gradients in the distribution of cellular components that facilitate specific molecular interactions and localizations at pre- and post-synaptic sites that can serve for activity-dependent synaptic modifications. Rhythmic patterns of spontaneous activity could contribute to this phenomenon but to which extent, it is currently unknown.

MEAs have been largely used to study synchronized patterns of bursting activity in developing networks *in vitro* (Maeda et al., 1995, 1998; van Pelt et al., 2004, 2005), as they allow the simultaneous recording of a large number of neurons over long periods of time. Moreover, unlike brain slices, immature random *in vitro* networks are free to develop in response to experimental manipulations, thus providing a system of choice for the investigation of structural and functional network development. Patterns of bursting activity have been mainly studied in cortical neurons and have been followed from few days to several weeks after plating (Maeda et al., 1995; van Pelt et al., 2004). Spontaneous activity usually appears at the end of the first week after plating and synchronized bursts emerge during the second week (van Pelt et al., 2004). A recent observation suggests that the cell density can influence the emergence of spontaneous bursting patterns (Arnold et al., 2005). Synchronized bursts, also called network bursts, occur spontaneously and are network-driven, initiated and governed by spatial and temporal summation of synaptic events in the culture and not by pacemaker cells (Maeda et al., 1995), as observed in the hippocampus, retina and spinal cord (see above). Furthermore, their source varies randomly with each burst (Maeda et al., 1995), excluding any deterministic phenomenon for their generation. Although these synchronized bursts are always present during a culture's life time, they change systematically in shape as a function of age *in vitro*, with the more drastic changes, in terms of number of spikes and recruited sites, taking place during the first four weeks *in vitro* (van Pelt et al., 2004). From then on, the bursts are relatively stable and similar. Likewise, the burst frequency and propagation velocity also change with age and markedly increase as networks grow (Maeda et al., 1995). As networks mature they establish more synaptic contact that will influence bursts features. Remarkably the time point of maximal synapse number appears to coincide with the time in which network bursts reach their longest durations (van Pelt et al., 2005).

Further studies on the modification of synchronized activity in response to electrical stimulation using MEAs (Maeda et al., 1998; van Pelt et al., 2005) have begun to address issues on the reciprocity between electrical activity and network development (Corner, 1994). A single stimulation session of a single electrode for an hour (van Pelt et al., 2005) was able to modify the network burst properties of 11 days old cultures to the

ones of a 3 weeks old culture, whereas such changes occur spontaneously in about 20 days. Although preliminary, this result suggests that modifying or altering the electrical properties of developing networks can cause drastic changes of the connectivity. This is supported by another study showing that a potentiation of activity could be reached by applying repeatedly strong inducing stimuli to a set of electrode. The potentiation of activity represented an increased probability of generating bursts by a test stimulus, an increased frequency and number of spikes of spontaneous network bursts along with an increased speed of burst propagation (Maeda et al., 1998). These changes lasted more than 20 minutes, indicating that changes occurred at the cellular level.

These *in vitro* studies and others (Ming et al., 1999; Hanson and Landmesser 2004, 2006; Catalano & Shatz, 1998; Dantzker & Callaway, 1998; Ibarretxe et al., 2007) clearly show that modification of the pattern of electrical activity influences network connectivity. However, these studies only investigated the effects of chronic stimulations, or perturbations, and it remains to see what could be the influence of more prolonged modifications of the electrical activity on network development.

2.2.2- Self-organized criticality and neuronal networks

Neuronal networks exhibit distinct modes of correlated population activity, including waves, oscillations and synchrony (for review, see Singer & Gray, 1995; Engel et al., 2001; Ermentrout & Kleinfeld, 2001). These patterns of activity have been experimentally identified *in vivo* and are also present in cortical networks *in vitro* (Plenz & Kitai, 1996; Kamioka et al., 1996; Nakagami et al., 1996). Recently, neural network models (Chen et al., 1995; Herz & Hopfield, 1995; Eurich et al., 1999, 2002; Lin & Chen, 2005) suggested a new mode of spontaneous activity called self-organized criticality (SOC).

SOC originates from statistical mechanics (Bak et al., 1988; Jensen, 1998) and characterizes the dynamics of systems of interconnected nonlinear threshold units, in which each unit has one or more input/outputs. In these systems, the redistribution of the

activity of one unit to others initiates a cascade that can propagate through the entire system. Over time, these systems evolve into a critical state characterized by event sizes with no characteristic time scale (scale free). This critical state is usually a stable attractor of the system dynamics. Numerous systems display SOC and include the sandpile model (Bak et al., 1988), the forest fire model (Malamud et al., 1998), neural networks models (Chen et al., 1995; Herz & Hopfield, 1995; Eurich et al., 1999, 2002; Lin & Chen, 2005) and solar wind (Freeman et al., 2000) to name only a few. The self-organizing term means that such state is reached without any tuning of a specific parameter. SOC systems display the following features:

i) they are far from equilibrium
ii) there is a separation of time scales (the external driving force is very slow compared to the rate of the cascades)
iii) the activity has a 1/f power spectrum at low frequencies
iv) activation in the system spread as cascades (also called avalanches) having size and duration distribution described by power laws with characteristic exponents (-3/2 for size and -2 for duration)

In neural systems, the basic process of neuronal integration and redistribution is similar to that seen in many other SOC systems. Herz and Hopfield (1995) first noticed the similarities between earthquake dynamics and neural model dynamics. Thus, neuronal activity could be considered as a kind of neuronal avalanche in which the activity propagates as individual neurons trigger action potential firing in subsequent neurons. Recent experimental findings give support to this hypothesis. In agreement with the scale free property cited above, SOC has been described at several levels of investigation from MEG and EEG time series in the developing and adult human brain (Linkenkaer-Hansen et al., 2001; Freeman, 2004; Tatcher et al., 2008) to LFP in acute slices and organotypic cultures of rat cortex using multielectrode arrays (Beggs & Plenz, 2003). Two of these studies deserve a particular attention.

The first one is the study by Linkenkaer-Hansen and colleagues (2001) because SOC was concluded solely on the basis of the 1/f behavior of the power spectrum. Firstly,

1/f noise is ubiquitous in physics and all the systems displaying it do not necessarily follow SOC. Secondly, a recent paper by Bedard et al. (2006) indicates that special attention has to be paid in interpreting 1/f noise as the authors show that the 1/f power spectrum of the EEG in the cat is due to the frequency-dependent filter of the brain tissue. Thus, although 1/f power spectrum at low frequencies is indicative of the presence of correlations at long timescales (of the order of seconds), its presence is a necessary but not sufficient condition for the existence of SOC and further analysis is needed to undoubtedly claim SOC in these EEG time series.

The second study is a work by Beggs and Plenz (2003). They recorded spontaneous activity in organotypic cultures and acute slices of rat somatosensory cortex using 60-channels multielectrode arrays. The events of interest were LFP and neuronal avalanches were defined according the following way: i) LFP of interest crossing a given threshold were defined as events; ii) the recording time was binned for bin width varying from 1 to 16 ms and the number of events in each bin was counted; iii) bins in which at least one event occurred were called "active" and the ones were no events occurred were called "silent"; iv) neuronal avalanche was defined as a strip of consecutive active bins preceded and ended by a silent bin. Then the duration of an avalanche was defined as the number of bins composing it and its size as the total number of electrodes involved. Avalanche size and duration followed power laws over one to two orders of magnitude with a slope varying in function of the chosen bin width. When the bin width was chosen in order to correspond to the average interval between two events, the slope of the avalanche size and duration distribution was respectively –3/2 and –2, exactly as predicted by SOC. They also considered different subsets of electrodes to show that the avalanche distributions exhibited scale invariance. Moreover, they also computed the branching parameter σ, i.e. the ratio of descendent electrodes to ancestor electrodes for two consecutive time bins at the beginning of an avalanche. This corresponds to the expected number of active electrodes that will be active in the next time step (corresponding to the bin width in this case) after that a single or more electrodes initiated an avalanche. The value of σ was close to 1, meaning that activity in one electrode would lead to activity in one other electrode in average. Finally, numerical simulations of avalanche dynamics in a feedforward network demonstrated that

information transmission was optimal for a value of $\sigma = 1$. These findings suggest that the dynamics underlying spontaneous activity in organotypic cultures and acute slices of rat cortex can be described by SOC and that information transmission is optimized at the critical state (see also Beggs, 2008). Moreover, avalanches of LFP can occur in spatio-temporal patterns that repeat more often than expected by chance and have been proposed to play a role in information storage (Beggs & Plenz, 2004). In addition, according to critical branching process (Zapperi et al., 1995), networks are in a critical state at the edge of stability for $\sigma = 1$ (Fig. 3, top). For a value of $\sigma < 1$, networks are in a subcritical state and activity will quickly die out, unable to sustain any input pattern. In contrast, networks with a value of $\sigma > 1$ are in a supercritical state in which an increasing number of electrodes would be activated at each step, eventually leading to an unstable runaway activation or saturation of the network. Recent numerical simulations suggest that the critical state optimizes the dynamic range (Fig. 3) by being simultaneously extremely sensitive to small perturbations and able to detect large inputs without saturation (Chialvo, 2006; Kinouchi & Copelli, 2006).

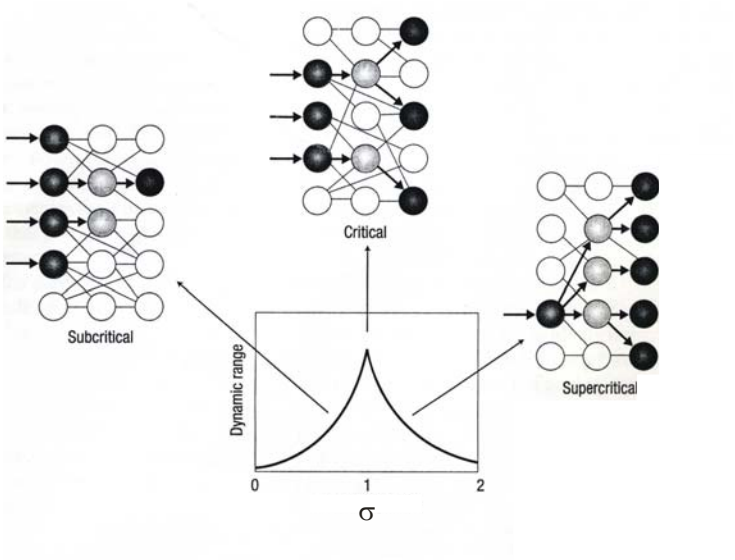

Figure 3 | Critical branching process optimizes the dynamic range. Networks with branching parameter σ close to one maintain on average the input activity (black followed by gray and black) thus optimizing the dynamic range. In the subcritical state (left), networks are unable to sustain any input pattern, whereas in the supercritical state (right) networks will saturate. (Modified from Chialvo, 2006).

2.2.3- Spontaneous activity and neuronal computation

In absence of sensory stimuli the brain is never at rest and neurons are continuously active. This ongoing activity requires energy to be sustained. It is estimated that 60 to 80% of the energy budget of the brain supports neuronal signaling, i.e. communication among neurons and their supporting cells (Raichle & Mintun, 2006). However, in humans, task-related increases in neuronal metabolism are usually very small (<5%) when compared with the large resting energy consumption, as revealed by functional neuroimaging (Raichle & Mintun, 2006), such as positron emission tomography (PET) and functional magnetic resonance (fMRI) that measure changes in brain circulation and metabolism (energy consumption). Thus, from a metabolic point of view, this means that the intrinsic spontaneous activity may be far more important that the evoked activity in term of overall brain function (Raichle & Mintun, 2006). So far, much of the knowledge about brain function comes from the study of the evoked activity and random spontaneous activity was traditionally considered to be noise (Shadlen & Newsome, 1998), but it could be that we studied only a minor component of total brain activity. Hopefully, recent computational and experimental studies at different levels of investigation have begun to unravel the functional role of spontaneous activity in neuronal systems.

A plethora of recent studies indicate that spontaneous activity has in fact a highly coherent spatiotemporal structure and should not be considered anymore as random noise (Arieli et al., 1995, 1996; Kenet et al., 2003; Fiser et al., 2004). As a consequence, in the brain, and more generally in any neuronal system exhibiting spontaneous ongoing activity, incoming (sensory) inputs will interact, likely nonlinearly, with this ongoing activity and the output(s), or response(s), will depend upon internal network dynamics (Tsodyks et al., 1999; Destexhe & Contreras, 2006). Using simultaneous real-time optical imaging and single-unit recordings in *in vivo* anesthetized cats, Tsodyks and colleagues (1999) showed that the spontaneous and evoked firing of single neurons was tightly linked to the network states in which they are embedded. Individual neurons tended to fire maximally when the network was active. A more common example illustrating the relation between neuronal responsiveness and spontaneous activity is the comparison of

waking and sleep states. The spontaneous activity recorded in the electroencephalogram (EEG) from cortex and thalamus is highly different during waking and sleep. During sleep and anesthesia, EEG is dominated by high-amplitude waves with high spatiotemporal coherence, whereas in contrast, during waking state, coherence is low and EEG contains mainly low-amplitude waves (Steriade et al., 1993). By looking at the drastic changes taking place during the transition between waking and sleep states and during various anesthetized states, it has been clearly established that reduced neuronal responsiveness and selectivity, in diverse modalities, was directly associated with the high-amplitude activity in the EEG (Morrow & Casey, 1992; Steriade, 2000; Edeline et al., 2001; Murakami et al., 2005). To better understand why and how neuronal responsiveness is reduced during sleep and anesthetized states, we need to look at the changes of the cellular properties occurring during these states.

During sleep or anesthesia, the spike threshold increases in cortical and thalamic cells because these cells progressively hyperpolarize (Steriade et al., 1993b), thus reducing intrinsic excitability. Moreover, hyperpolarization of the membrane potential activates intrinsic currents underlying burst firing, particularly in thalamic cells (Janhsen & Llinas, 1984). This burst firing impedes thalamic cells to normally function as sensory relay. Cortical and thalamic cells are further hyperpolarized by synchronized inhibitory inputs that generate large membrane shunting. This results in a highly reduced responsiveness and large increase in response variability that renders networks less reliable. In contrast, during waking state, the membrane potential is more depolarized (Steriade et al., 2001) and close to the spike threshold, allowing neurons to respond more reliably and with less variability. As the response of any individual neuron is determined by the influence of thousands of synaptic inputs, a fine balance of excitation and inhibition (Haider et al., 2006) is fundamental to keep the membrane potential of neurons into a depolarized state – also known as UP states – thus increasing the reliability and decreasing the variability of responses as it happens during waking. On the contrary, when this balance is disrupted like during sleep, neurons respond with greater variability and less reliability. Thus, the dynamical states of a network profoundly affect the way individual neurons will respond to stimuli. Haider and colleagues (2007) took advantage of the anesthesia induced by ketamine-xylazine to investigate this issue *in vivo* in the cat.

The interest of this approach is that under ketamine-xylazine anesthesia, cortical neurons oscillate at low frequency (<1 Hz) between two states: they are either quiescent (DOWN states) or show active periods of depolarization and firing (UP states). UP states display a pattern of activity mimicking the waking state i.e. they are characterized by low amplitude and high frequencies EEG. Combined intra- and extracellular recordings in the cat primary visual cortex under ketamine-xylazine anesthesia revealed that the visual responsiveness of cortical neurons was enhanced during periods of spontaneous depolarizations. Neurons fired more spikes in response to flashed bright and dark bars and a multiplicative gain of the contrast response function was observed during the UP states (Haider et al., 2007). In other studies of the cat visual cortex, and without considering the stimuli contrast by using high-contrast drifting grids, larger evoked responses correlated with spontaneous depolarizations and increased network activity (Arieli et al., 1996; Azouz & Gray, 1999). These studies indicate that networks' spontaneous depolarizations enhance neuronal responsiveness. Moreover, this effect seems independent of the modality investigated as it also has been found in the sensorimotor cortex. Indeed, cortical responses to electrical stimulation of both peripheral nerve (Rosanova & Timofeev, 2005) and prethalamic pathways (Timofeev et al., 1996) are facilitated during UP states in ketamine-xylazine-anesthetized cats.

So far only the facilitating effects of increased network activity have been described. But the opposite holds as well. Decreased background activity leads to decreased responsiveness. The generalization of the principle that the level of network activity influences the way individual neurons respond to stimuli/inputs has been shown in an elegant experiment using the dynamic clamp technique (Fellous et al., 2003). A computer model of *in vivo* synaptic background activity was used to inject conductance in an *in vitro* rat neuron from the layer 5 of the prefrontal cortex. This allowed to assess individually the effects of inhibition and excitation and showed that the level of background synaptic activity dynamically modulated the input/output properties of individual neocortical neurons, thus clearly identifying the differential contribution of inhibitory and excitatory conductances (Fellous et al., 2003). More specifically, the mean inhibitory and excitatory synaptic input level set the "working point" of the neuron by shifting the firing rate-current curve rightward or leftward respectively. The dynamic

clamp technique has also been widely used by Destexhe and his collaborators in conjunction with computational models and they showed that the integrative properties of neocortical neurons are strongly affected by the level of background activity (for a review see Destexhe et al., 2003). The impact of background activity can be summarized as follow: the presence of stochastic background activity (i) enhances the cortical neurons' responsiveness (Fellous et al., 2003) and allows detectable responses to be evoked by weak inputs (Rudolph & Destexhe, 2003b), (ii) allows dendritic action potentials to propagate up to the soma and consequently reduce the location dependency of synaptic inputs (Destexhe & Paré, 1999; Rudolph & Destexhe, 2003), and (iii) increases the temporal resolution of synaptic inputs due to a marked reduction of the membrane time constant, allowing neurons to respond reliably to higher frequencies (Rudolph & Destexhe, 2003b). Finally, in a model of the suprasylvian cortex, constrained by *in vivo* intracellular data obtained in the in ketamine-xylazine-anesthetized cats, Destexhe & Paré (1999) stressed that a large number of synaptic events were required to evoke spiking reliably. This condition is likely to occur *in vivo* during UP states in which large populations of neurons are depolarized (Haider et al., 2007).

Another striking example of the role of intrinsic ongoing activity in influencing neuronal responsiveness is the effect of attention. Increase in background activity and responsiveness has been observed in primate visual areas during selective attention (Luck et al., 1997; Willliford & Maunsell, 2006) and this can be explained by a concomitant increase in synaptic bombardment of neurons in this area (Murphy & Miller, 2003). Although the mechanisms underlying attentional shifts are still unknown, this is a clear indication that increased network activity enhances neuronal responsiveness.

More importantly, the spontaneous background activity also affects networks' plastic properties. A series of experiments in different preparations in the cat showed that the probability to induce plasticity and the ability to induce potentiation or depression was strongly dependent on the level of the background neuronal activity (Crochet et al. 2006). The level of plastic changes was first determined in cats under barbiturate anesthesia by stimulating cortical neurons located in layers II to VI (with a majority in layers II/III) in the suprasylvian association areas 5 and 7. The conditioning stimulus consisted of 30 rhythmic pulse-trains (five stimuli) of different frequencies (10, 40 and

100 Hz) applied every 2s through two to three bipolar electrodes. This protocol triggered changes in almost all neurons (77%). Both potentiation and depression were observed but depression was more prevalent than potentiation. Then the level of background activity was either increased by inducing the anesthesia with ketamine-xylazine or a mixture of barbiturate and ketamine-xylazine, or decreased by using small isolated cortical stabs. Comparison of the EEG and intracellular recordings in these three conditions revealed that under ketamine-xylazine anesthesia (high level of neuronal activity) the probability of inducing plasticity was the lowest but potentiation was more easily induced than depression. Conversely, in isolated cortical stabs (low level of neuronal activity), the probability of inducing plasticity was the highest but the probability of inducing potentiation was the lowest. Thus, the level of spontaneous activity strongly affects both the probability to induce plasticity and its sign (potentiation or depression). On the one hand, the higher is the spontaneous neuronal activity, the fewer are the synapses affected by additional activation; on the other hand, the lower is the neuronal activity, the more sensitive the synapses are to activation. These results are a nice demonstration of the concept of metaplasticity (Abraham and Bear, 1996) – the plasticity of synaptic plasticity – which states that the activity of a synapse modifies the threshold for induction of plasticity; so changing the level of background activity should affect the expression of plasticity, which is exactly what Crochet and his colleagues observed (Crochet et al., 2006).

Taking together, these studies clearly indicate that neuronal processing is significantly modulated by ongoing network spontaneous activity, and that this spontaneous activity is a direct reflection of the intrinsic dynamical state of the network. In this context it can be said that spontaneous activity provides the context under which the network operates by determining which cells are responsive and just how responsive they are.

Interestingly, *in vivo* studies in the visual cortex noted that, in addition of being dynamically modulated by the network state, the response of cortical neurons was not a direct reflection of the input. Tsodyks and collaborators (1999) focused on the relation between the activity of single neurons and the dynamics of the network in which they are embedded by carrying out simultaneous single-unit and optical recordings in the cat

striate cortex after presentation of drifting grids. The striate cortex was chosen because a majority of neurons are specifically tuned for orientation direction from which tuning curve can be easily determined in this region. Furthermore, the functional architecture and intracortical wiring are well known. After having determined the population state for which the neuron firing was maximal – called the preferred cortical state (PCS) – the similarity (correlation coefficient) between the underlying functional architecture and the PCS was estimated and indicated that nearly the same population state occurred during both spontaneous and evoked activity. Similarly, correlations in the spontaneous neuronal firing are only slightly modified by visual stimulation (Fiser et al., 2004). These authors concluded that during evoked activity, the presentation of a stimulus pushed the network into the neuron's PCS, which represents the stimulus. This suggests that rather than directly encoding the structure of the input signal, sensory inputs modulate the intrinsic circuit dynamical behavior. Other studies in the visual cortex support this conclusion (Arieli et al., 1996; Fiser et al., 2004). This is very important as, in the framework of modulation of inputs by ongoing spontaneous activity discussed above, it represents the other side of the same coin. Therefore, in the visual cortex, there is a reciprocal influence between spontaneous patterns of ongoing background activity and sensory inputs; spatiotemporal patterns of network activity influence information processing, and vice versa, sensory inputs modify ongoing network activity. However, if this holds on other sensory modalities is currently unknown. Interestingly, it has been shown that the level of spontaneous ongoing activity modulated the trial-to-trial variability of evoked responses in the rat auditory cortex (Kisley & Gerstein, 1999). In this study, the level of spontaneous ongoing activity was modified using different depths of anesthesia induced by ketamine/xylazine. It was found that the trial-to-trial variability was the lowest under light anesthesia in which the firing pattern of spontaneous activity was mainly tonic. Conversely, the trial-to-trial variability was the highest under medium anesthesia which was characterized by a clear rhythmic bursting pattern.

Thus, the pattern of ongoing spontaneous activity can modulate sensory inputs in various ways and this should be kept in mind when analyzing evoked responses. Traditionally, the approach of dealing with trial-to-trial variability consists in averaging over many trials. However, such an approach requires the assumption of linear

superposition between random background activity and a highly stereotyped, repeatable evoked response. Although this can be true for some preparations (Arieli et al., 1996; Azouz & Gray, 1999), there could be apparent violations of this assumption in some case, especially when the spatiotemporal patterns of background activity exhibits a high coherence (Arieli et al., 1995; Kisley & Gerstein, 1999; Tsodyks et al., 1999; Kenet et al., 2003; Fiser et al., 2004).

In the first part of my thesis, due to the importance of ongoing spontaneous activity and bursting patterns in neuronal networks, I investigated spontaneous activity dynamics in cultured hippocampal networks and compared it with that of intact leech ganglia (see Results, section 3.2). Currently, spontaneous activity dynamics has been investigated in several systems but a general framework is still lacking. As SOC has been described in several vertebrate preparations with functional architecture, we tested if SOC could also describe the spontaneous activity of cultured hippocampal networks with random connectivity and invertebrate networks (leech ganglia). Moreover, since spontaneous activity influences drastically the computational properties of neuronal networks, characterizing its dynamics could provide valuable insights on the information processing abilities of neuronal networks.

So far, the role of synchronous bursting (and the underlying hyperexcitability) has been mainly studied in developing networks. In order to shed light on their influence on mature networks, I focused on the relationship between hyperexcitability and synchronous bursting pattern in the second part of my thesis. To this end, networks were disinhibited pharmacologically by a transient exposure to antagonists of $GABA_A$ receptors. This led to the appearance of a synchronous bursting pattern of activity that persisted for hours following the drug washout, indicating that plastic changes occurred in the networks during the drug application (see Results, section 3.3). This protocol allowed us to investigate both spontaneous and evoked activity network plasticity at the molecular and electrical level. In particular, we characterized in great details the plastic changes for several hours (up to 24h) at the electrical level using MEA and at the molecular level using DNA microarrays (in collaboration with Silvia Pegoraro). Indeed, previous works combining MEA and DNA microarrays focused mainly on the patterns of

gene expression without much emphasis on the functional characterization of the concomitant electrical changes (Valor et al., 2006; Xiang et al., 2007).

2.3- Neural Coding schemes

The nervous system is a communication machine and deals with information that is conveyed to the brain and processed within it primarily in the form of action potentials (APs). Neural coding refers to the representation and transformation of information in the nervous system. The study of neural coding involves measuring and characterizing how stimulus attributes are represented by APs or train of APs and how such stimulus attributes change over time. Formally, two opposite but complementary approaches are used to study the link between stimulus and response. Neural encoding refers to the map from stimulus to response, whereas neural decoding refers to the reverse map, from response to stimulus (Dayan & Abbott, 2001).

What do we know about coding in the nervous system? Although the kinds of coding used in real neural systems is still the topic of an intense debate, it is now clear that the nervous system does not employ one code, or a small number, or an infinity of different codes, but many (Bear et al., 1996; Rieke et al., 1997; Dayan & Abbott, 2001). Relevant neural codes or representation of information by neuronal activities may depend on the circuits or on the situations. This is further complicated as other carriers than APs, such as local field potential or subthreshold membrane fluctuations may be functional.

There is an ongoing vigorous debate about the nature of the neural code between the partisans for a rate code (Shadlen & Newsome, 1994; Buracas et al., 1998) and those for a timing code (Softky, 1995; Rieke et al., 1997). Despite this controversial issue (Rieke et al., 1997; Dayan & Abbott, 2001) and the nature of the carrier, most of neuroscientists agree that coding schemes depends on the situation and on the system under investigation.

Functionally, the approach to investigate neural coding can be summarized as follows: consider a sensory modality, for example audition. First, the different relevant properties of the stimulus (sounds) have to be distinguished (frequency, intensity, phase

relationship) along with their temporal aspects – such as those that give rise to rhythm and melody in the case of audition. Then, each of the stimulus properties has to be investigated the way it is represented at various levels: at the receptors, at the efferent fibers (auditory fibers), at various relay nuclei, and so on, as far centrally as these representations – or responses to a given stimulus – can be followed. Once the responses are recorded, neural encoding and decoding approaches can be used to investigate the relationship between the applied stimulus and the recorded response(s). Although the functional approach is an indispensable part of the biological significance of neural coding, it generally requires detailed knowledge about neural processing of information, and some of it may not be, or poorly, known at present. Another difficulty is that in some cases, the different relevant properties of the physiological stimuli may not be known at all and have to be discovered experimentally before any inference could be made. This is especially true in the case of animals using senses other than those used by humans like for example electroception in some fish species, echolocation in bats, magnetoception in birds, or pressure detection in fish and some aquatic amphibians.

Another, heuristic, approach to investigate neural coding is to set out and deal with the properties or aspects of each code in a formal manner.

In the following sections I will first describe rate and temporal coding in single neurons and population of neurons. I will then briefly review other possible coding schemes used by the nervous systems.

2.3.1- Rate coding

The rate code is a code in which information is represented by the firing rates. It is also sometimes named frequency coding. It was first described more than 80 years ago by Adrian and Zotterman (1926). By hanging different weights from a muscle, they showed that the number of spikes recorded from sensory nerves innervating the muscle increased as the weight increased. The rate, or frequency, of the APs thus indicated the intensity of the stimulus. That is to say, the number of spikes in a fixed time window following the onset of the stimulus represents the intensity of the stimulus, which is the

main idea of rate coding. Thus, in a rate code the information about a stimulus resides in the mean firing rate of a spike train taken over a relatively long time window (several tens of ms). From this point of view, the observed variability is considered to be noise (Shadlen & Newsome, 1994) and reliable estimates are generally obtained by averaging neural responses over several trials and over substantial time windows. As much of the information is carried by the mean firing rate, the precise timing of individual APs does not matter. When it does, the code is called temporal.

So defined, a wide variety of problems arise if one wants to adopt a rate code as being a general feature of neural systems. First, while carrying out tasks in the natural world, animals must quickly extract information about single stimuli. Moreover, some signals change very rapidly which is incompatible with integration over an extended period of time. Second, in auditory neurons, the same firing rate can be observed both for sounds with high amplitude that are not at the preferred frequency of a neuron and sounds with low amplitude at the neuron's preferred frequency. This ambiguity can be resolved by a timing code but not by a rate code (Bialek and Rieke, 1992). Third, there is experimental evidence that different input spike trains, with the same mean firing rate, but different temporal structures produce significantly different outputs from the same cell (Segundo et al., 1963). Fourth, the information transmission drops in redundant synaptic connections when a rate code is considered (Zador, 1998). However, such connections are commonly observed in neural systems, contradicting the ubiquity of rate codes. Finally, rate codes cannot support the information transmission rates observed in real neurons (Rieke et al., 1997), whereas timing code can (MacKay & Culloch, 1952).

Although these limitations of rate coding suggest that temporal coding is a more plausible candidate code, we have to bear in mind that : (i) nervous systems are unlikely to use a single coding scheme (as discussed above); and (ii) some of these limitations can be circumvented when considering populations of neurons rather than single isolated neurons. Thus, although rate coding is certainly not a ubiquitous phenomenon in nervous systems, population rate coding has nevertheless been observed in several neural systems and can account for a wide variety of computationally demanding tasks.

Population codes are robust and offer several computational advantages such as mechanisms for noise removal, short-term memory and the instantiation of complex

nonlinear functions (Pouget et al., 2000; Sanger, 2003). Two types of strategy can be distinguished based on the tuning curves properties of the individual neurons. On the one hand, the *local strategy* appears when a large number of highly specific neurons, narrowly-tuned, respond optimally to a very narrow range of stimuli. This strategy provides a convenient ease of decoding and one needs only to know which neuron is active to identify which stimulus is present. In the visual system for example, the representation of visual space among sensory receptors is a clear example of a local code where individual receptors respond to stimulation of small patches of the retinal surface. This local representation, or topographic map, is maintained throughout the visual system in such a way that neighboring cortical neurons respond to neighboring regions of visual space (Bear et al., 1996). Similar topographic maps are also seen in the somatotopic projections from the skin surface to the somatosensory cortex and in the cochleotopic projections from the inner ear to the auditory cortex (Bear et al., 1996).

In the *distributed strategy*, on the other hand, the tuning curves are broadly-tuned and the responses of individual neurons are not specific to a particular stimulus. Rather, the information is represented by the collective response of many neurons. Distributed representations generally require fewer neurons than local representations and are more robust to degradation of individual neurons. An example of this type of strategy in the visual system is the representation of color information by photoreceptors in the retina (DeValois & DeValois, 1993). Cones respond to a wide range of wavelengths and only three channels of information are sufficient to encode a large range of different colors (Bear et al., 1996). In the motor cortex, Georgopoulos and colleagues showed in a seminal paper that the precise direction of arm movement in the rhesus monkey could be predicted by the firing activity of population of broadly-tuned neurons (Georgopoulos et al., 1986). Other examples of distributed representations can be found in the olfactory and chemosensory systems, where information is carried by patterns of activation across a limited set of receptor types. In general, it seems that distributed representations are used by the cortex wherever the number of receptors or effector channels is limited.

A central tenet of parallel distributed processing theory (Rumelhart et al., 1986) is that neural information is spread across populations of neurons, and that each neuron contributes to the processing of many informational factors. Recent development of

multi-unit recording techniques has permitted to directly address this and other related issues *in vivo* (Nicolelis et al., 1997, 1998; Chapin & Nicolelis, 1999; Panzeri et al., 2001; Petersen et al., 2001). An *in vitro* approach, using MEAs, has also been proposed (Potter, 2001), yet very few studies have been carried out in this direction. Although *in vitro* cultured networks lack any functional cytoarchitectural organization, some basic questions regarding information processing by population of neurons can nevertheless be addressed. Furthermore, the *in vitro* approach allows a tight control of the pharmacological environment difficultly achievable *in vivo*. Previous work in our lab (Bonifazi et al., 2005; discussed in more detail in section 2.1.2), using rat hippocampal neurons grown on MEAs, demonstrated that studying population coding with MEAs is feasible and actually represented the first proof of concept of the *in vitro* approach proposed by Potter (2001).

2.3.2- Temporal coding

Temporal codes are based on the timing of APs and try to account for short-term stimuli producing a very small number of APs, unlike rate codes. To estimate firing rates, a given neuron must fire at least two APs. Considering for example a maximum firing rate of 100 Hz, then a stimulus smaller than 10 ms would likely trigger a single AP, rendering the estimation of the mean firing rate impossible. Actually many biologically significant sound variations (speech, bat echolocation, frog calls) can occur as fast as 5-20 ms and a neuron firing at 100 Hz will generate one or two spikes. Indeed, several empirical reports in a variety of systems support the hypothesis that small numbers of spikes are relevant and important for information processing. Neurons in many brain regions of different species have time to fire at most one AP, so even the ensemble firing rate in such a short period might be similar for many stimuli, thus providing a weak discrimination power.

Recordings from the bat auditory system revealed that an average of just one spike was produced by cells in response to pairs of ultrasonic pulses simulating the bat's own sonar call and a returning echo (Dear et al., 1993). No more than three spikes were

produced in primary visual cells during texture discrimination tasks in monkey (Knierem & van Essen, 1992) and cats (Reid et al., 1991). Moreover, it seems likely that the importance of a small number of spikes is not restricted to the early stages of neural signal processing. For example, in the rat hippocampus, which receives input only from higher sensory cortices, the so-called place cells fire at peak rates of ~30 spikes/s (Wilson & McNaughton, 1993). Assuming that the rat's accuracy of its own position is on the centimeter order and since a rat moves at speeds of ~20 cm/s, hippocampal signaling about position must therefore be based on 1 or 2 spikes per cell, of the same order as in the sensory cortex.

Conceptually, the hypothesis that small numbers of spikes are relevant for information processing has received a lot of attention at the behavioral level. The short response latency of neurons in human and primate visual system imposes strong constraints on visual processing. Complex stimuli such as faces, food, familiar 3D objects and even complex scenes that have never been seen before can be successfully categorized on the basis of only 100-150 ms in humans (Antal et al., 2000) and monkeys (Thorpe & Imbert, 1989; Fabre-Thorpe et al., 1998). While visual processing is fast, processing in other sensory pathways can be even faster in many cases. In the bat auditory cortex briefly discussed above, neurons can respond as fast as 8 ms after stimulus onset (Jen et al., 1989), which, given the number of subcortical processing stages, imposes that neurons have only a couple of milliseconds to respond at each stage. There are also major constraints in invertebrate sensory systems (Carr, 1993). Taken altogether these various lines of experimental evidence strongly argue in favor of the generality of the processing speed constraint in sensory pathways. It stands that the speed of sensory processing is so fast in some systems that few if any of the neurons at each level of the processing hierarchy will have enough time to emit more than one spike before those in the next layer have to respond (Thorpe et al., 2001).

At the population level, the encoding of information by the relative timing or latency of the first spike was named Rank Order Coding (Thorpe et al., 2001) or recruitment order (Richmond & Wiener, 2004). Modeling studies of visual processing revealed that such a population temporal code could resolve the processing speed constraint (Delorme & Thorpe, 2001; Thorpe et al., 2001). This coding scheme (Fig. 4A)

is very efficient, fast and ideally suited for certain types of rapid processing tasks as well as robust and easy to implement in biological hardware. Moreover, information theoretic analysis of spike-patterns of the auditory cortex, during a sound localization task, revealed that for many neurons the latency of the first spike transmitted more information about the stimulus location than did spike count (Furukawa & Middlebrooks, 2002). Similar results have been observed in the rat somatosensory cortex in which temporal precision of firing in an ensemble of neurons, of the millisecond order, was shown to encode a larger amount of information than the mean firing rate (Panzeri et al., 2001; Petersen et al., 2001). Interestingly, the first evoked spike could carry more than 80% of the total spike train information.

Recently, the first experimental evidence of Rank Order Coding was demonstrated in the human somatosensory cortex (Johansson & Birznieks, 2004). Recordings were carried out from peripheral somatosensory nerve fibers with tungsten needle electrodes while different forces were applied on various locations of the fingertips by a flat or two small spherically curved objects of different diameter. It was shown that the relative timing of the first-spike carried reliable information about direction of fingertip force and object shape and that the recruitment order was able to discriminate among four directions of fingertip forces and the three different shapes used. Furthermore, the information was available faster than the fastest rate codes and quick enough to account for the behavioral reactions occurring during natural objects manipulation. It remains to be seen how generally applicable recruitment order is as an ensemble code and if it can be generalized to other modalities.

Another line of evidence in favor of temporal coding, underlying the importance of the precise timing of APs, is the discovery of spike timing dependent plasticity (STDP). In this form of plasticity, the functional changes in neurons and at synapses are sensitive to the relative timing of APs of the pre- and post-synaptic neurons. Using dual patch-clamp, it has been shown that the strength of a synapse was increased if the pre-synaptic neuron fired 10 ms before the post-synaptic one (Markram et al., 1997). In contrast, when the order of activation was reversed so that the post-synaptic neuron fired before the pre-synaptic one, the strength of the synapse decreased. STDP implies that a time-window of a few tens of milliseconds is important for synaptic plasticity and that the

polarity of the plastic changes depends on the relative timing between the pre- and post-synaptic neurons. Revisiting the Hebbian rule of plasticity according which, synapses increase their efficacy if they cause a persistent activation of their post-synaptic target, it can be said that synapses increase their efficacy if the pre-synaptic neuron is activated *shortly before* the post-synaptic neuron is activated.

Finally, synchrony and rhythmic or oscillatory activity are other examples of temporal coding (Gray et al., 1989; DeCharms & Merzenich, 1996; Ritz & Sejnowski, 1997) in which temporal relationships among neurons matters. Cortical networks are known to exhibits a wide range of oscillations (Buzsáki & Draguhn, 2004) that are thought to subserve diverse processes, such as facilitation of synaptic plasticity and attention (Salinas & Sejnowski, 2001; Buzsáki & Draguhn, 2004). Furthermore, there are numerous cases in which cortical neurons have been shown to convey information by their relative timing when information is absent from the firing rate (Gray et al., 1989; DeCharms & Merzenich, 1996). For example, it has been shown, in the monkey auditory cortex, that temporally coordinated APs can systematically signal sensory object features, even in the absence of changes in firing rate (DeCharms & Merzenich, 1996). Synchrony has also been found in the frontal and motor cortex (Murthy & Fetz, 1992; Prut et al., 1998). Such synchrony of spike timing has been proposed as a possible coding scheme involved in 'binding' together individual firing-rate feature representations into a unified object percept – the so-called binding problem (Roskies, 1999). The binding problem has been thoroughly studied in the visual cortex (Singer & Gray, 1995). In the awake monkey for example, presenting one or two objects in the receptive fields of two visual neurons evoked nearly the same firing rate (Kreiter & Singer, 1996). However, in this case, synchrony between pairs of neurons reflected whether one or two stimuli were shown, even when both firing rates did not vary across conditions (Kreiter & Singer, 1996). Neurons in the visual cortex can thus act as coincidence detectors able to detect synchronous firing.

Whereas synchronization is thought to play important computational roles in forming dynamic neuronal assemblies, a recent study in the weakly electric fish suggests that the opposite phenomenon, desynchronization, is just as important (Benda et al., 2006). According to the authors, transient desynchronization can be used by a neural

system as a code for a short but important signal. They concluded that both synchronization and desynchronization, as well as *changes* between synchrony or asynchrony or vice versa might be relevant signals for neural information processing.

To summarize, temporal coding can take several forms and temporal relationships among neurons can carry information that would be missed if only rate coding is considered.

Beyond the distinction between rate and temporal codes in a given neural system, the identification of a specific code can sometimes be ambiguous and the possibility of using different encoding strategies to represent the same information also exists. Indeed, in a very interesting paper, Nicolelis and colleagues provided evidence that the location of tactile stimuli could be represented by different encoding strategies by broadly-tuned population of neurons in diverse brain area of the adult owl monkey (Nicolelis et al., 1998). By using multielectrode recordings, they showed that small neural ensembles (formed by 30 to 40 neurons) used a distributed strategy to encode simultaneously the same information in different brain areas of the somatosensory cortex (area 3b, 2 and SII). Furthermore, the brain areas 3b and 2 encoded tactile location information based on the mean firing rate, whereas a code based on the temporal patterns of ensemble firing was used in area SII.

Fundamentally, both rate codes and temporal codes are time dependent codes and the temporal character of the neural code might be determined by the behavior of the firing rate (Dayan & Abbott, 2001). If the time-dependent firing rate varies slowly with time, the code is typically called a rate code whereas it can be called a temporal code when the time-dependent firing rate varies rapidly and spike time precision is important to extract most of the information. Figure 4B provides an example of different firing rate behaviors for a neuron of a visual area (MT) recorded over multiple trials. The activity in the top panel would typically represent rate coding, and the activity in the bottom panel would reflect temporal coding. Although the criterion to distinguish changes of firing rates as slow or rapid is far from being obvious in certain situations (middle panel of Fig. 4B), in some other clear-cut ones, the dynamic evolution of the firing rate can still provide valuable information about the kind of code being used. Thus the distinction

between rate and temporal codes is rather subtle and care has to be taken before drawing any strong conclusion about the identification of a specific code in a given situation.

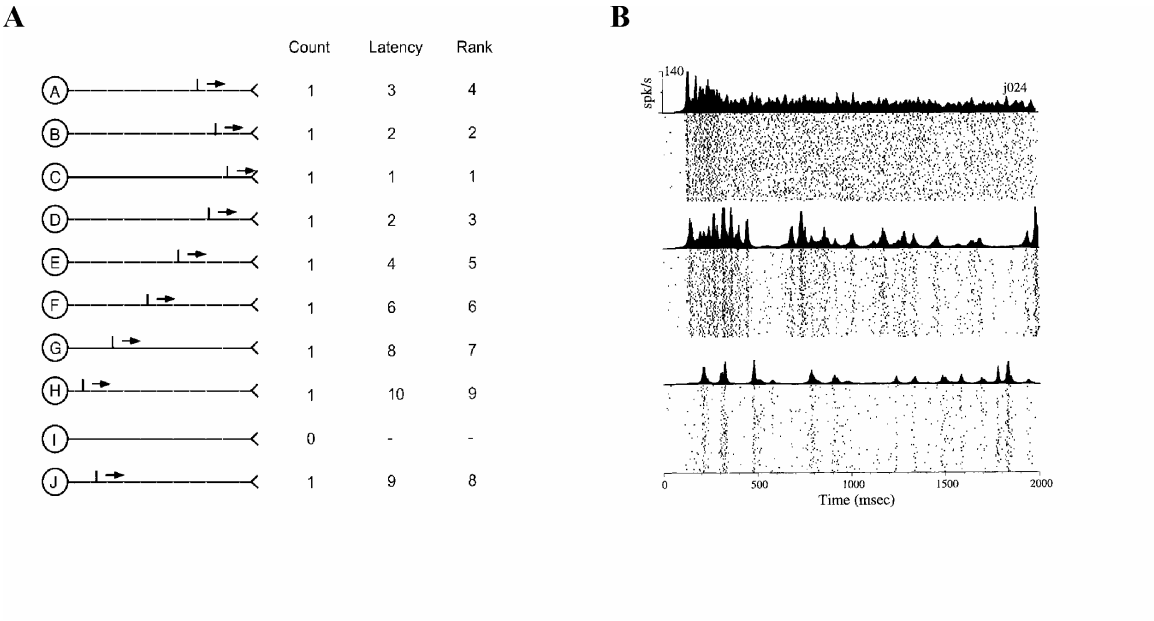

Figure 4 | **A.** Comparison of three coding schemes operating in short time windows. Spikes are generated by the 10 neurons A-J at different times. By using a count code, to count the number of neuron that have spiked during a particular time, corresponding to a population rate code, only 10+1 states are available. In a binary code (not shown), there would be 2^{10} possible states. In a latency code, with millisecond precision, there are 10^{10} possible states. Finally, with a rank order code (recruitment order), there are 10! possible states. **B.** Time-dependent firing rates of a single neuron for different stimuli. In the rasters every dot represents a spike and every line a single trial of a MT neuron. The stimulus consisted of moving random-dots. The three different firing rates are for the same neuron but for different stimulus coherence (decreasing from top to bottom). (Panel A reproduced from Thorpe et al., 2001 and panel B adapted from Bair & Koch, 1996.)

2.3.3- Other coding schemes

Beyond the controversial debate between rate and temporal codes, other biologically plausible coding schemes have recently received considerable attention. Due to space limitation I will here only review two other coding schemes that that can be potentially used in many nervous systems.

Based on the switching between tonic and burst firing of thalamic neurons (Llinas & Jahnsen, 1982), the possibility that burst firing plays an important role in sensory processing was postulated almost 25 years ago (Crick, 1984). However, only recently the first *in vivo* experimental evidence has begun to emerge (reviewed in Krahe & Gabbiani, 2004). Bursts could filter noise and improve the signal-to-noise ratio of neuronal responses as it has been found in the cat and monkey visual cortex (Cattaneo et al., 1981; Livingstone et al., 1996). In the weakly electric fish, pyramidal cells reliably indicate the time course of amplitude modulation of electric fields and the performance of detecting such amplitude modulation was greater when bursts rather than isolated spikes were considered (Metzner et al., 1998). Feature extraction by bursts also seems to be performed in high vocal centre of the zebrafinch songbird (Lewicki & Konishi, 1995). When sequences of the bird's own song were played back to a bird, neurons selective to its own song generated bursts, whereas they did not when permutations of the sequences were played back. Some details are still unknown, such as the exact biophysical mechanisms for burst generation in a specific context, and, above all, if bursts convey information as unitary events or whether the fine temporal structure matters. However, the possibility that bursts have a distinct function in sensory information transmission remains and further theoretical and experimental work is needed to shed light on this plausible coding scheme.

Another kind of coding scheme is the possibility that dual or multiple codes carrying different modes of information are embedded in one neural system (Masuda & Aihara, 2007). A simple example would be the combination of a rate code and a temporal code in a spike train. In this case the precise timing of individual spikes could carry additional information that would be missed if only a rate code was considered and *vice-*

versa. Although experimental evidence is relatively scarce, this possibility of dual coding seems to be employed at least in the retina. Recordings from rabbit and salamander retina suggest that information on object identity is encoded by the spike counts, whereas information on time is encoded in spike timing (Berry et al., 1997). Another theoretical possibility of dual coding would be the coding of significant information by the interspike interval that would be missed if only individual spikes were considered independently from each other. In this case, one would speak about a correlation code. But the simultaneous use of multiples codes is not the only possible way of dual coding. The results of Nicolelis and colleagues (1998) described previously on the use of rate and temporal codes in the owl monkey somatosensory cortex suggest that using multiple codes in different locations in a neural system (segmentation of the neural resource space according to Masuda & Aihara nomenclature) might be another mode of dual coding.

Although proposed some years ago, the possibility of using distributed coding scheme in cultured networks (Potter, 2001) has received little attention in the MEA community. In the third part of my thesis, motivated by previous work in our lab demonstrating the feasibility of using MEAs to study population coding (Bonifazi et al., 2005), I investigated basic computational properties of neuronal networks. Because of the large variety of possible coding schemes reviewed above and of the *in vivo* studies suggesting that different coding schemes could be used by the same neuronal network (Nicolelis et al., 1998), I tested the relevance of diverse decoding schemes to discriminate patterns varying both in their location and intensity (see Results, section 3.4). A comparison of the efficiency of two population codes, namely distributed and pooling, and the influence of the neuronal population size and the critical time window adapted for analysis is also presented. Finally, we compared our results obtained *in vitro* with those recently obtained *in vivo* (Nicolelis et al., 1997, 1998; Chapin & Nicolelis, 1999; Panzeri et al., 2001; Petersen et al., 2001).

3 - RESULTS

- 3.1 -

Embryonic derived stem cell-derived neurons form functional networks in vitro

Ban J, Bonifazi P, Pinato G, **Broccard FD**, Studer L, Torre V, Ruaro ME

Stem Cells **25**(3), 738-749 (2007)

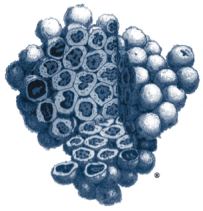

STEM CELLS®

Embryonic Stem Cell-Derived Neurons Form Functional Networks In Vitro

Jelena Ban, Paolo Bonifazi, Giulietta Pinato, Frederic D. Broccard, Lorenz Studer, Vincent Torre and Maria Elisabetta Ruaro

Stem Cells 2007;25;738-749; originally published online Nov 16, 2006;
DOI: 10.1634/stemcells.2006-0246

STEM CELLS®, an international peer-reviewed journal, covers all aspects of stem cell research: embryonic stem cells; tissue-specific stem cells; cancer stem cells; the stem cell niche; stem cell genetics and genomics; translational and clinical research; technology development.

STEM CELLS® is a monthly publication, it has been published continuously since 1983. The Journal is owned, published, and trademarked by AlphaMed Press, 318 Blackwell Street, Suite 260, Durham, North Carolina, 27701. Print ISSN: 1066-5099. Online ISSN: 1549-4918.

AlphaMed Press

STEM CELLS®

EMBRYONIC STEM CELLS

Embryonic Stem Cell-Derived Neurons Form Functional Networks In Vitro

JELENA BAN,[a] PAOLO BONIFAZI,[a] GIULIETTA PINATO,[a] FREDERIC D. BROCCARD,[a] LORENZ STUDER,[b] VINCENT TORRE,[a] MARIA ELISABETTA RUARO[a]

[a]International School for Advanced Studies-via Beirut 2-4, Trieste, Italy; [b]Laboratory of Stem Cell and Tumor Biology, Division of Neurosurgery and Developmental Biology Program, Memorial Sloan-Kettering Cancer Center, New York, New York, USA

Key Words. ES cells • In vitro differentiation • Neuronal network • Hippocampus

ABSTRACT

Embryonic stem (ES) cells provide a flexible and unlimited source for a variety of neuronal types. Because mature neurons establish neuronal networks very easily, we tested whether ES-derived neurons are capable of generating functional networks and whether these networks, generated in vitro, are capable of processing information. Single-cell electrophysiology with pharmacological antagonists demonstrated the presence of both excitatory and inhibitory synaptic connections. Extracellular recording with planar multielectrode arrays showed that spontaneous bursts of electrical activity are present in ES-derived networks with properties remarkably similar to those of hippocampal neurons. When stimulated with extracellular electrodes, ES-derived neurons fired action potentials, and the evoked electrical activity spread throughout the culture. A statistical analysis indicated that ES-derived networks discriminated between stimuli of different intensity at a single trial level, a key feature for an efficient information processing. Thus, ES-derived neurons provide a novel in vitro strategy to create functional networks with defined computational properties. STEM CELLS *2007;25:738–749*

INTRODUCTION

Systems neuroscience aims at understanding how neuronal networks operate in a concerted way and, in particular, how information is processed [1–8]. A fundamental prerequisite to investigate how neuronal networks process information is to monitor simultaneously the electrical activity of a large population of neurons in the networks. In the last decade, the application of new electrophysiological and optical techniques in vivo [9–11] allowed better characterization of the functional properties of neuronal networks, giving the possibility of studying neural coding mechanisms, and distributed representations in different parts of the brain. In this way, it was shown how information can be encoded in the firing rate of an ensemble of neurons or in the synchrony of firing [6, 12], in the relative timing of action potentials (APs) [4, 13, 14], or in the latency of first evoked APs [8, 15]. However, due to the variability of the experimental conditions and the intrinsic complexity of the investigated system, it is very difficult to obtain a detailed analysis in vivo. Many of these problems are bypassed by studying neuronal networks in in vitro cultures, where experimental conditions and properties can be controlled in a more reliable way. Moreover, the chronic monitoring and stimulation of in vitro preparations for long-term periods provides a unique way to investigate developmental and plasticity mechanisms in a variety of systems [16–19].

When neurons are isolated and plated on an appropriate substrate, they readily grow, forming axodendritic arborization extending up to some millimeters and covered by a large number of functional synapses [16, 20, 21]. Distribution and cell types present in cultures are similar to those found in vivo [22–24], and, although they have lost the original connectivity of the intact tissue, they represent a good system to study how neuronal networks operate as a whole under controlled conditions. Multielectrode arrays (MEAs) represent a unique tool to investigate network dynamics, allowing the recording of the electrical activity of neuronal networks in both space and time [25], and have been used widely to characterize the spontaneous and the evoked activity of neuronal networks [1, 16, 19, 21, 26–33].

The use of ES cells allows the generation of an unlimited number of different cell types, including neurons [34–41]. Several protocols have been developed to derive neurons from ES cells in vitro [36, 38, 42], and some differentiation procedures allow the selective derivation of specific neuron types [38, 43–46]. Electrophysiological data from ES-derived neurons with different protocols validate their functional differentiation [34, 38, 41, 47–51], as well as the formation of synapse between ES-derived neurons [52] or between an ES-derived neuron and a mature neuron in organotypic slices [53] or in vivo [38, 54, 55]. ES cells provide a source of specialized cells for regenerative medicine [56–60], and it has been shown that ES cells or ES-derived neuronal precursors can incorporate into the nervous system and differentiate into neurons and glia [55, 61–64]. However, little is known of the capability of ES-derived neurons to form functional networks and their properties. Because the main function of neurons is communication, we decided to test the ability of ES-derived neurons to form functional networks and, in particular, to process information reliably.

Correspondence: Maria Elisabetta Ruaro, International School for Advanced Studies, via Beirut 2-4, 34014 Trieste, Italy. Telephone: +39 040 3756510; Fax +39 040 3756502; e-mail eruaro@sissa.it Received April 21, 2006; accepted for publication November 9, 2006; first published online in STEM CELLS *EXPRESS* November 16, 2006. 1066-5099/2007/$30.00/0 doi: 10.1634/stemcells.2006-0246

In the present work, by combining intracellular recordings and extracellular recordings obtained with MEAs, we have analyzed how and to what extent ES cells form functional networks in vitro, and compared the properties of these networks with those of dissociated hippocampal neuronal networks [1]. ES-derived networks exhibited spontaneous activity, similar to that observed in primary networks in vitro [16, 19, 31, 65]. When stimulated with extracellular electrodes, ES-derived neurons fired action potentials, and the evoked electrical activity spread throughout the culture. A statistical analysis of the pattern of firing indicates that ES-derived networks have properties similar to those of primary adult neurons and can process information in a reproducible way in different trials; therefore, ES-derived networks behave as reliable computing elements.

MATERIALS AND METHODS

Neuronal Culture Preparation

Hippocampal neurons from Wistar rats (P0-P2) were prepared as previously described [33]. Cells were plated on polyornithine/matrigel precoated MEA [33] at a concentration of 8×10^5 cells/cm^2 and maintained in minimal essential medium with Earle's salts (Invitrogen Corp., Carlsbad, CA, http://www.invitrogen.com) supplemented with 5% fetal calf serum, 0.5% D-glucose, 14 mM Hepes, 0.1 mg/ml apo-transferrin, 30 μg/ml insulin, 0.1 μg/ml D-biotin, 1 mM vitamin B_{12}, and 2 μg/ml gentamycin. After 48 hours, 5 μM cytosine-β-D-arabinofuranoside (Ara-C) was added to the culture medium to block glial cell proliferation. Half of the medium was changed twice a week. Neuronal cultures were kept in an incubator, providing a controlled level of CO_2 (5%), temperature (37°C), and moisture (95%). In all experiments, hippocampal cells were used after 3 weeks in culture.

ES-Derived Neuron Differentiation

ES cells were induced to differentiate into neurons using the protocol for GABAergic neurons described in Barberi et al. [43], only slightly modified. Undifferentiated BF1/lacZ ES cells were plated on mitomycin-treated MS5 cells as single-cell suspension at a density of 250 cells/cm^2 in Knockout Serum Replacement (KSR) medium and cultured for 6 days. The ES-derived epithelia structures were then mechanically separated from MS5 cells monolayer, by flushing Hanks' balanced salt solution through the pipette tip near the colony. The detached ES cells colonies were resuspended with KSR medium and plated on polyornithine-fibronectin-coated dishes. After 2–3 hours, the medium was changed with N2 medium containing basic fibroblast growth factor (bFGF) 10 ng/ml and 1 μg/ml fibronectin (amplification medium), and cells were induced to proliferate in presence of bFGF for 4 days. During the last 2 days, 200 ng/ml Sonic Hedgehog (SHH) and 100 ng/ml fibroblast growth factor (FGF)8 were added as patterning factors. Cells were then trypsinized and plated on polyornithine-laminin-coated MEA plates or glass coverslips in N2 medium containing 10 ng/ml brain-derived neurotrophic factor, 10 ng/ml NT4, and 1 μg/ml laminin (differentiation medium). Half of the differentiation medium was then changed twice a week. The postmitotic neurons were maintained in culture up to 10 weeks. All recombinant proteins were from R&D Systems (Minneapolis, http://www.rndsystems.com/).

Immunocytochemistry

Cells were fixed in 4% paraformaldehyde containing 0.15% picric acid (in phosphate-buffered saline [PBS]), saturated with 0.1 M glycine, permeabilized with 0.1% Triton X-100, saturated with 0.5% bovine serum albumin (BSA) in PBS and then incubated for 1 hour with primary antibodies. The primary antibodies were (a) rabbit polyclonal antibodies: against GABA, serotonin, CaMKII (all from Sigma Chemicals, St. Louis, http://www.sigmaaldrich.com/), and tyrosine hydroxylase (TH; Pel Freeze, Rogers, AR, http://www.pelfreez-bio.com/); (b) mouse monoclonal antibodies: TUJ1 (Covance, Berkeley, CA, http://www.crpinc.com), GFAP (Sigma Chemicals), nestin (Chemicon, Temecula, CA, http://www.chemicon.com/); and (c) guinea pig polyclonal antibody against V-GLUT2 (Chemicon).

The secondary antimouse fluorescein isothiocyanate (FITC) and anti-rabbit-tetramethylrhodamine isothiocyanate (TRITC) antibodies were from Sigma (Sigma Chemicals), goat anti-mouse immunoglobulin (Ig) G_1-FITC and IgG_{2a}-TRITC were from Southern Biotech (Birmingham, AL, http://www.southernbiotech.com/), anti-guinea pig-488 Alexa (Molecular Probes). Total nuclei were stained with 2 μg/ml in PBS Hoechst 33342 (Sigma Chemicals).

Electrophysiological Recordings

Dissociated hippocampal and ES-derived neuronal cultures were transferred in a recording chamber, perfused in Ringer's solution (145 mM NaCl, 3 mM KCl, 1.5 mM $CaCl_2$, 1 mM $MgCl_2$, 5 mM glucose, 10 mM Hepes; adjusted to pH 7.3 with NaOH) and visualized with an upright microscope (Olympus) with differential interference contrast optics. Patch-clamp recordings were performed with an Axoclamp 2-B amplifier (Axon Instruments/Molecular Devices Corp., Union City, CA, http://www.moleculardevices.com). Experiments were performed at room temperature (20°C–22°C). Electrodes were pulled (Narishige, Tokyo, http://www.narishige.co.jp/main.htm) and filled with an intracellular solution containing 120 mM potassium-gluconate, 10 mM sodium-gluconate, 10 mM Hepes, 10 mM sodium-phosphocreatine, 4 mM MgATP, 4 mM NaCl, 2 mM Na_2ATP and 0.3 mM Na_3GTP (adjusted to pH 7.3 with KOH); in these conditions, the electrode resistance was 15–20 MΩ. To enhance the driving force for chloride currents, some experiment were performed in symmetrical chloride conditions by substituting potassium-gluconate with KCl in the pipette solution; in these conditions, the resistance of the electrodes was 5–10 MΩ. The data were digitized at 20 kHz (Digidata 1200, Axon Instruments) and analyzed using pClamp9 software (Axon Instruments). Values of membrane potentials were corrected for the effects of liquid junction potential during seal formation.

Pharmacological identification of postsynaptic responses was performed by application of the following synaptic blockers: 30 μM D-AP5, 20 μM 6-cyano-7-nitroquinoxaline-2,3-dione (CNQX); 10 μM SR-95531 (gabazine). All reagents were purchased from Tocris (Bristol, United Kingdom, http://www.tocris.com/).

MEA Electrical Recordings and Electrode Stimulation

ES-derived neurons cultured on MEAs, were kept in an incubator with a controlled level of CO_2 (5%), temperature (37°C), and moisture (95%). Before electrical recordings, dishes were sealed with a cap distributed by MultiChannel Systems (Reutlingen, Germany, http://www.multichannelsystems.com/) to reduce gas exchange and eliminate evaporation and contamination and transferred from the culture incubator to a different incubator with controlled CO_2 (5%), and temperature (37°C) where the electrical recording system was placed. Before starting the recordings, the neuronal culture was allowed to settle for approximately 30 minutes. After termination of the experiment, usually after 2–3 hours, the medium was changed, and the dish was moved back to the incubator.

MultiChannel Systems commercially supplied the multielectrode array system used for electrophysiology. MEA dishes had 10×6 TiN electrodes with an interelectrode spacing of 500 μm, and each metal electrode had a diameter of 30 μm. The MEA is connected to a 60-channel, 10–3-kHz bandwidth preamplifier/filter-amplifier (MEA 1,060 AMP), which redirects the signals toward a further electronic processing (i.e., amplification and analog to digital [AD] conversion), operated by a high-performance computer. Signal acquisitions are managed under software control, and each channel was sampled at a frequency of 20 kHz. One electrode was used as ground. Sample data were transferred in real time to the hard disk for off-line analysis. Each metal electrode could be either used for recording or for stimulation. The voltage stimulation used consisted of bipolar pulses lasting 100 μs at each polarity, of amplitude varying from 200 to 900 mV, injected through a single channel of the STG1004 Stimulus Generator [66]. The voltage pulse generated by the STG1004 was applied in parallel with the set of electrodes

manually selected for stimulation (simultaneous multisite stimulation). An artifact lasting 5–20 ms, caused by the electrical stimulation, was induced on the recording electrodes but was removed from the electrical recordings during data analysis [33, 67]. For each stimulus, the culture was stimulated for 100 trials every 4 seconds.

Data Analysis

Acquired data were analyzed using MATLAB (The Mathworks, Inc., Natick, MA, http://www.mathworks.com/). For each individual electrode, we computed the SD (σ) of the noise, which ranged from 3 to 6 μV, and only signals crossing the threshold of -5σ were counted as APs and used for data analysis. AP sorting was obtained by using principal component analysis and open source toolboxes for the analysis of multielectrode data [68] with MATLAB. To quantify the amount of small amplitude spikes, a fixed threshold of -50 μV was used, and the number of APs recorded was then compared with that obtained with a threshold of -5σ. The firing rate (FR(t)) of Figure 3B and the probability distribution of the number of spikes per bin of Figure 4A and 4B were computed by counting the number of spikes recorded by the whole MEA in time bins of 250 ms. To compute the average firing rate (AFR) of the neurons, peristimulus time histograms (PSTHs) were calculated for the sorted neurons (Fig. 6A, 6C) using a 10-ms time bin, where time 0 ms corresponds to the delivery of the stimulation. Similarly, when APs recorded by the whole array of electrodes were pooled, the array PSTHs (APSTHs) were calculated (Fig. 6B, 6D). The coefficient of variation (CV) of any variable analyzed is the SD over the mean of the variable. To test the difference of firing between the spontaneous activity and the activity after the extracellular stimulation, we considered the number of APs, respectively, in the 50 ms preceding and in the 50 ms after the stimulus. To test the significant difference in the variation between the two quantities, we used one-way analysis of variance.

Calculation of the Mutual Information

With the aim of decoding the stimulus intensity, we considered the array response (AR_t). We used information theory [69] and, in particular, mutual information to estimate the amount of information that can be decoded in different time bins (i.e., varying t) and for different extents of pooling (i.e., different numbers of electrodes). In particular, the mutual information was calculated as follows:

$$I_t \equiv I_t(R, S) = \sum_{s \in S} p(s) \sum_{r \in R} p_t\,(r|s) \cdot \log_2 \left(p_t(r|s)/p_t(r)\right)$$

where

$$p_t(r) = \sum_{s \in S} p(s) \cdot p_t(r|s)$$

I_t quantifies in bits the amount of information that a single response, r, (i.e., AR_t,) provides about the intensity of the stimulus, s. $p_t(r)$ is the total probability of observing the response r considering the time bin 0 to t ms after the stimulus, averaged over all stimuli. In our case, all stimuli occurred with equal probability, $p(s)$. In order to minimize the effects of finite sample size on our estimates of information, the real response r has been binned into different intervals, following the methods of Panzeri and Treves [70].

Calculation of Correlation

The degree of correlation of firing in the network was measured comparing the multiunit recordings of pairs of electrodes. The spontaneous activity was recorded for approximately 30 minutes and, to convert it into a time series ($SA_1, \ldots, SA_n$), it was binned into firing rate with a bin width Δt. For each pair of electrodes (i, j), the cross-correlation $\rho_{i,j}$ between the time series ($SA_{i1}, \ldots, SA_{in}$; $SA_{j1}, \ldots, SA_{jn}$) was calculated according to the equation:

$$\rho_{i,j} = \frac{\sum_{n=1}^{N} (SA_{in} - <SA_i>)(SA_{jn} - <SA_j>)}{\sqrt{\left(\sum_{n=1}^{N} (SA_{in} - <SA_i>)^2\right)\left(\sum_{n=1}^{N} (SA_{jn} - <SA_j>)^2\right)}}$$

and the average cross correlation $<\rho>$ over all the possible pairs of electrodes was calculated. The cross-correlation analysis for the spontaneous activity shown in Figure 4 was obtained varying the size of the bin width Δt.

RESULTS

Differentiation of ES Cells

Neuronal differentiation was induced by coculturing ES cells on MS5 murine bone marrow-derived stromal cells as described in Barberi et al. [43]. ES cells seeded at low density on this feeder layer and exposed to serum replacement medium formed small epithelial structures, so that after 6 days many cells in the structure were positive for nestin, a marker for precursors (Fig. 1A; Barberi et al. [43]). For further propagation and selection, these structures were detached from the MS5 feeders, transferred, disaggregated, plated on polyornithine-fibronectin coated dishes, and propagated in the presence of bFGF. After a few days, almost all of the cells were positive for nestin (Fig. 1A, right panel).

Removal of bFGF and addition of specific neurotrophins allowed differentiation to occur. Figure 1B compares the expression of different markers in ES-derived neurons at 3 weeks of differentiation, with dissociated hippocampal cells cultivated for 3 weeks. ES-derived neurons expressed the postmitotic neuronal marker β-tubulin III starting from 3 days after differentiation induction, and this marker was present throughout the observation period (TUJ1-positive). Of these postmitotic neurons, approximately 30% were GABAergic (positive to GABA), less than 5% were dopaminergic (positive for tyrosine hydroxylase) and very few (less than 1%) serotonergic (positive for 5-HT). The remaining neurons were glutamatergic (positive CaMKII or vesicular glutamate transporter 2 [VGLUT2]). Very few astrocytes (cells positive for GFAP) were observed during the first week, whereas their percentage progressively increased, reaching approximately 50% of the population at 4 weeks of differentiation. An increase in glial cells reflected the prolonged period of in vitro differentiation required for network formation. Increased numbers of GFAP+ cells over time is in agreement with in vivo developmental progression and with neural stem cell differentiation studies in vitro [69, 70]. In the hippocampal culture, the fraction of glial cells was approximately 20% during the observation period. Approximately 10% of the neurons were GABAergic, and approximately 90% were glutamatergic (positive to VGLUT2); no serotonin or dopaminergic neurons were detected. (Fig. 1 and [1]).

To confirm that differentiation of ES cells produced functional neurons, intracellular recordings with patch pipettes were performed at 7, 14, 21, and 28 days after differentiation induction (41 cells). The resting membrane potential was -43 ± 4 mV after 1 week ($n = 8$), and increased to -68 ± 7.8 mV after 3 weeks ($n = 13$). In the control hippocampal cells, the resting membrane potential was -63 ± 5.9 ($n = 18$). The input resistance was 2 ± 1.3 GΩ during the first week, and decreased subsequently to 1.4 ± 0.6 GΩ in the ES-derived neurons. In the control hippocampal cells, the input resistance was 0.4 ± 0.1 GΩ. After 1 week, a depolarizing current pulse evoked, at most, one AP with mean amplitude of 12.9 ± 5 mV SD ($n = 8$). After 2 weeks of differentiation, ES-derived neurons produced APs with amplitude of about 50 mV, but a tonic discharge of APs

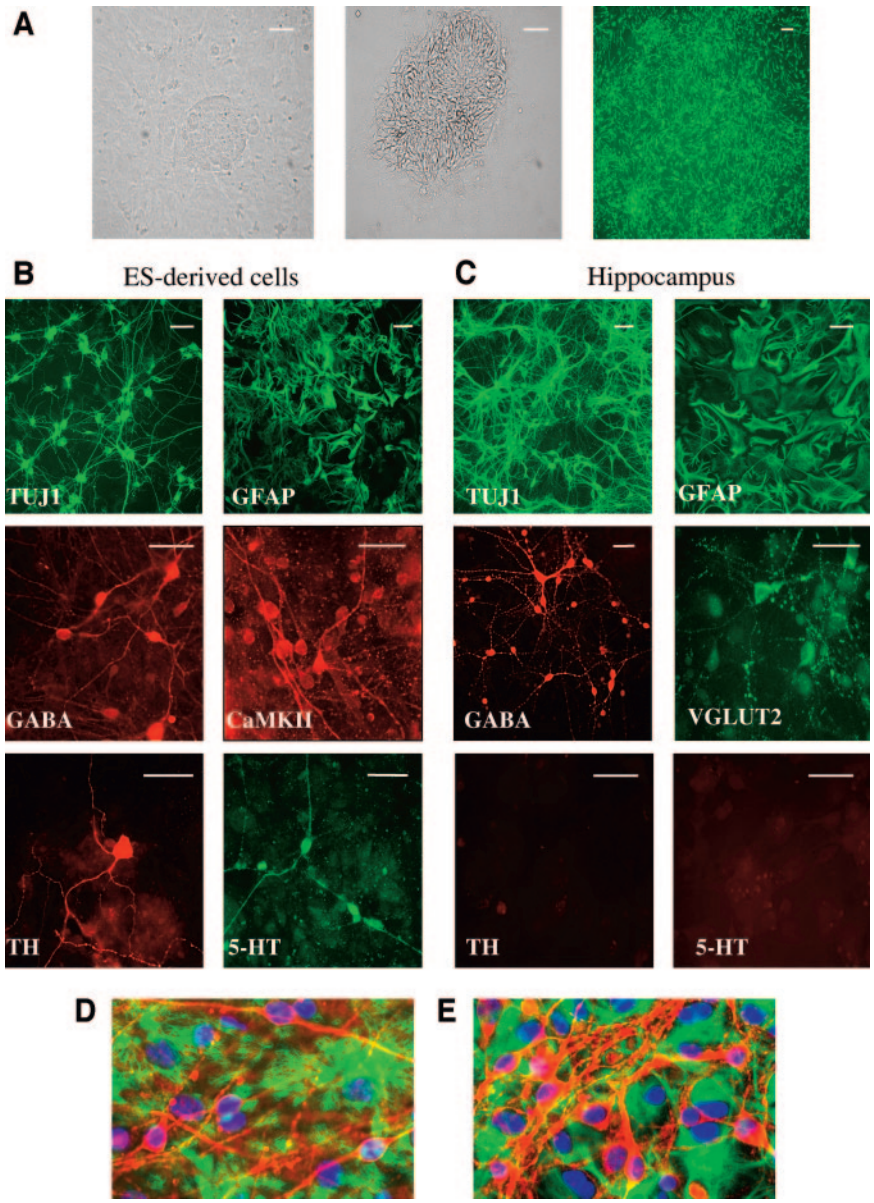

Figure 1. Cellular composition of ES-derived and hippocampal cultures. **(A):** Embryonic stem (ES) cells grown on MS5 cells feeder in KSR medium at day 4 (left) and day 6 (middle); nestin-positive neural precursors (right). **(B):** ES-derived neurons at 3 weeks of differentiation stained with anti-β-tubulin III (TUJ1), glial cells (GFAP positive), GABAergic neurons (GABA positive), glutamatergic neurons (CaMKII positive), dopaminergic neurons (TH positive), and serotonergic neurons (5-HT positive). **(C):** Immunofluorescence analysis as in **B** for the hippocampal neurons kept 3 weeks in culture. Glutamatergic neurons are marked with anti-VGLUT2 antibody. **(D, E):** Double staining of neurons (TUJ1) and glia (GFAP) with total nuclei marked by Hoechst 33342 in ES-derived neurons and hippocampal neurons respectively. Scale bar = 50 μm. Abbreviations: ES, embryonic stem; GFAP, glial fibrillary acidic protein; 5-HT, 5-hydroxytryptophan; TH, tyrosine hydroxylase.

was evoked only in one of eight cells analyzed. After 3 weeks, 4 of 12 cells fired trains of APs, and after 4 weeks, 9 of 13 cells discharged APs in a sustained way, but neurons with a transient firing were still observed.

Examples of current-clamp recordings of ES-derived neurons at 7, 14, 21, and 28 days of differentiation are shown in supplemental Figure 1. After 4 weeks of differentiation, in some cells, a depolarizing current pulse did not evoke APs, and voltage clamp recordings from these cells indicated the presence of voltage gated K^+ currents but not of Na^+ current (not shown). As the percentage of glial cells in the culture increased with time, these recordings were presumably obtained from glial cells.

The basis of network connectivity is the formation of functional synapses among different components. Therefore, we analyzed pharmacologically the different transmitters contribution to spontaneous postsynaptic events.

Starting from 14 days of differentiation, in most cultures, intracellular recordings showed both excitatory and inhibitory spontaneous synaptic activity (Fig. 2). The identification of inhibitory synaptic contributions was performed by current-clamp whole-cell patch-clamp recordings. To enhance the contribution of chloride currents, some experiments were performed in symmetrical chloride conditions, where chloride mediated synaptic events result as depolarizing potentials. Addition of glutamate receptor blockers D-AP5 (30 μM) and CNQX (20 μM) allowed isolating inhibitory contributions. At resting potential, the cells showed strong spontaneous depolarizing events that could trigger action potential initiation (Fig. 2A, left trace).

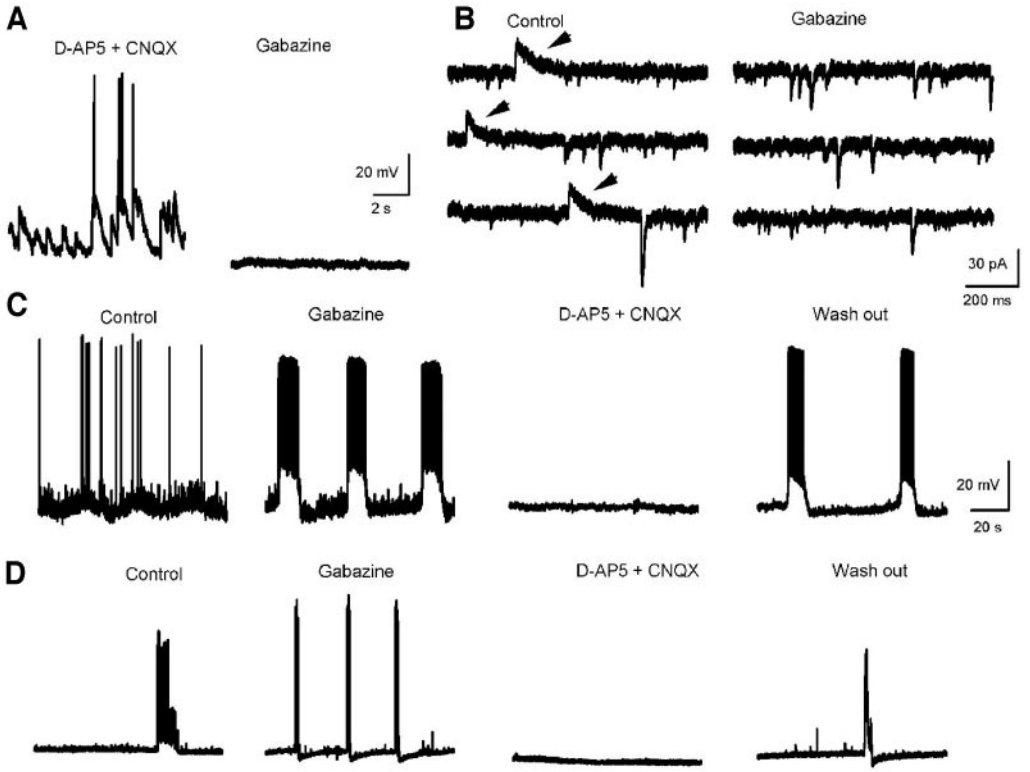

Figure 2. Electrophysiological and pharmacological identification of spontaneous synaptic inputs. **(A):** Whole-cell current-clamp patch-clamp recording at 0 bias current of an embryonic stem cell (ES)-derived neuron in presence of D-AP5 (30 μM) and CNQX (20 μM). The recording was performed in symmetrical chloride conditions in order to enhance the contribution of chloride currents (first trace). Addition of gabazine (10 μM) abolished the spontaneous activity, with a hyperpolarizing effect on the membrane potential (second trace). **(B):** Spontaneous outward (arrows) and inward currents were observed in voltage clamp recordings at −50 mV with potassium-gluconate-based pipette solution. Traces in left column are representative of control conditions, showing both outward and inward currents. Addition of gabazine completely prevented outward currents, but did not influence inward currents occurrence (representative traces in right column). **(C):** Spontaneous activity of ES-derived neuron recorded in current clamp at 0 bias with potassium-gluconate-based pipette solution (first trace). Application of gabazine synchronized excitatory synaptic inputs with consequent onset of bursts of action potentials (second trace). Further application of D-AP5 and CNQX completely abolished the occurrence of bursts (third trace). After wash out, bursting activity regenerated (last trace). **(D):** Hippocampal neuron spontaneous activity recorded in current clamp at 0 bias with potassium-gluconate-based pipette solution (first trace); effect of gabazine (second trace); effect of further addition of D-AP5 and CNQX (third) trace; and wash out (last trace). Traces scale as in C.

Further addition of the GABA-A antagonist SR-95531 (gabazine, 10 μM) completely canceled this spontaneous activity (Fig. 2A, right trace; $n = 3$). These results demonstrate the contribution of GABAergic transmission in the spontaneous activity of ES-derived neurons. The averaged membrane potential before application of gabazine (Fig. 2A, left trace) calculated in a time window without occurrence of APs was -56 ± 5.4 mV, whereas after the application of gabazine, the averaged value in a time window of the same duration was -70 ± 1.1 mV. The decrease in the SD reflected the block of chloride-mediated depolarization after gabazine treatment.

Further evidence for inhibitory contributions in the spontaneous synaptic activity could be found by recording the cells in voltage clamp conditions with potassium-gluconate based intracellular pipette solution (see Materials and Methods; Fig. 2B). By clamping the cell at −50 mV, spontaneous occurring outward currents were recorded at a frequency of approximately 1 Hz (Fig. 2B, arrows). Subsequent application of gabazine completely prevented the occurrence of such events.

Excitatory synaptic input was also present in the spontaneous activity (Fig. 2C, control). Application of gabazine in potassium-gluconate-based intracellular pipette solution to block inhibition both isolated excitatory contributions in whole-cell patch-clamp recordings and increased the synaptic coupling among the neurons participating to the network. This resulted in synchronous excitatory synaptic inputs in the recorded cells, often triggering bursts of APs (Fig. 2C, gabazine). In these conditions addition of glutamate receptor blockers D-AP5 and CNQX completely abolished the occurrence of such events (Fig. 2C, AP5; CNQX) that reappeared after wash out (Fig. 2C, wash out; $n = 3$).

The same experiment was also performed in hippocampal cells, and data are shown in Figure 2D ($n = 3$). These results show the presence of inhibitory and excitatory synaptic contributions for both ES-derived and hippocampal neurons. However, difference in the firing pattern between the two networks was observed. In particular, the duration of the burst in the ES-derived neurons was significantly longer (13.4 ± 5.2 seconds) than the hippocampal bursts (3.5 ± 1.3; Student's t-test $p < .0005$).

Spontaneous Activity of Maturing ES-Derived Neurons

Spontaneous activity is a common characteristic of developing neuronal networks both in vivo and in vitro, which is believed to play an important role in network development [16, 19, 73–76]. To evaluate the distribution and propagation of the spontaneous activity in ES-derived neuronal culture, neuronal precursors were plated and induced to differentiate directly on the MEA. In parallel, hippocampal networks grown on MEA

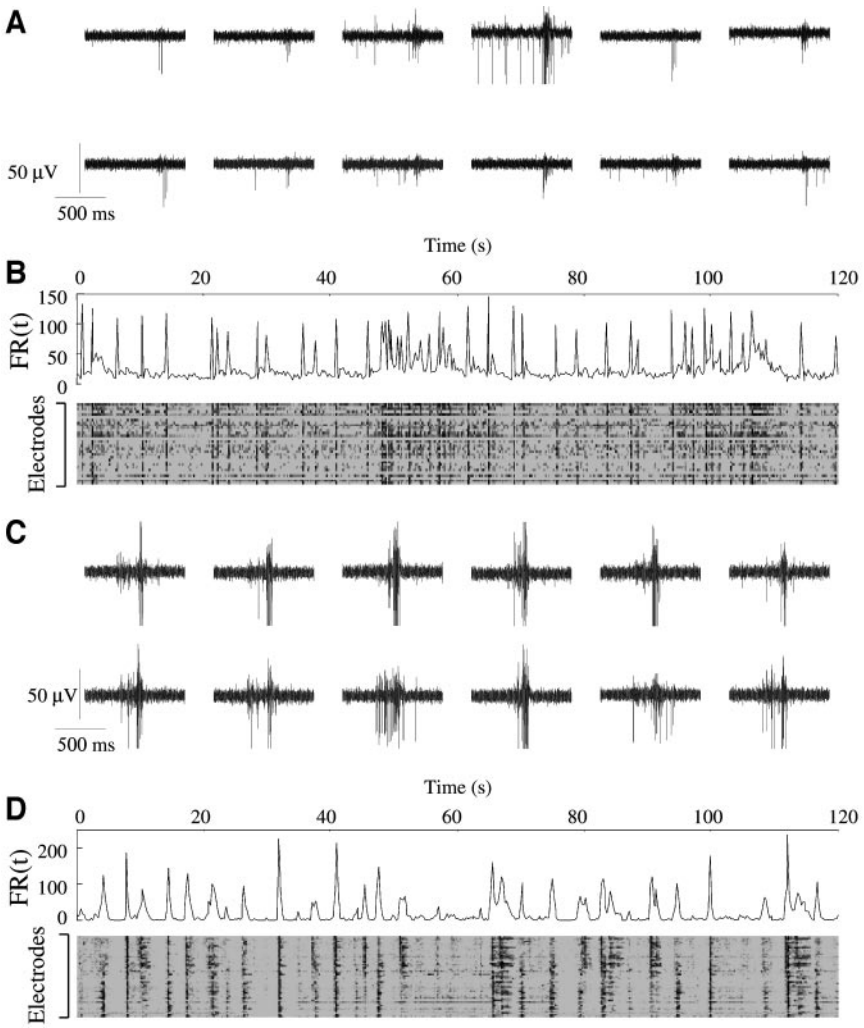

Figure 3. Multielectrode recording of spontaneous activity of an embryonic stem cell (ES)-derived network at 25 days of differentiation. **(A):** Snapshot of 1 second of spontaneous activity at selected electrodes of the multielectrode array (MEA) during a burst. **(B):** Temporal analysis of 2 minutes of spontaneous activity. Upper panel: 2 minutes of global activity of the network; firing rate (number of action potentials [APs] in a bin width of 250 ms) recorded by all electrodes of the MEA. Lower panel: spontaneous activity recorded by each single electrode in time bins of 250 ms; the intensity of the activity at the electrode in a particular time bin is represented in grayscale (see Materials and Methods). **(C)** and **(D)** represent the same analyses as in **(A)** and **(B)** for a hippocampal network after 3 weeks in culture.

were analyzed for comparison. After 1 week of differentiation of ES-derived neurons on the MEA, it was possible to record the extracellular voltage signals with a shape very similar to those observed in cultures obtained from neonatal hippocampal rat neurons (supplemental Fig. 2). Extracellularly recorded APs varied in a number of active sites and amplitude of spikes in different cultures because it depends on the quality of the contact of the cells with the electrodes. Figure 3 illustrates the spontaneous activity of ES-derived networks (3A and 3B) and of hippocampal networks (3C and 3D). Simultaneous extracellular recordings are shown in Figure 3A and 3C for ES-derived and hippocampal networks, respectively. The spike trains of ES-derived neurons contained a greater proportion of small spike amplitudes than present in hippocampal ones (Fig. 3A, 3B). In fact, less than 5% (4.22% $\pm$ 0.57%) had amplitude higher than 50 μV (see Materials and Methods) although amplitude as large as 100 μV could be observed. In the hippocampus, the percentage of spikes with amplitude higher that 50 μV was more than double (10.14% $\pm$ 2.22%) and spikes could reach 200 μV.

APs were detected on different electrodes, and bursts of APs recorded simultaneously from several electrodes invading the entire network were often observed. The global electrical activity of the network was described by computing the firing rate of the entire network FR(t) (see Materials and Methods) counting the total number of recorded APs in a given bin width. As shown in the upper panels of Figure 3B and 3D, the FR(t) of both ES-derived and hippocampal networks had large peaks corresponding to the simultaneous firing of several neurons, separated by periods where only occasional APs were observed. The global electrical activity of the network can also be visualized by considering raster plots, where a dot represents the occurrence of an AP, of several electrodes. Raster plots from ES-derived and hippocampal networks are shown on the bottom panel of Figure 3B and 3D, respectively. In raster plots, a vertical black line indicates that APs were recorded simultaneously from all, or most, extracellular electrodes of the MEA.

A comparison between the FR(t) and raster plots from ES-derived and hippocampal networks shows that, in both net-

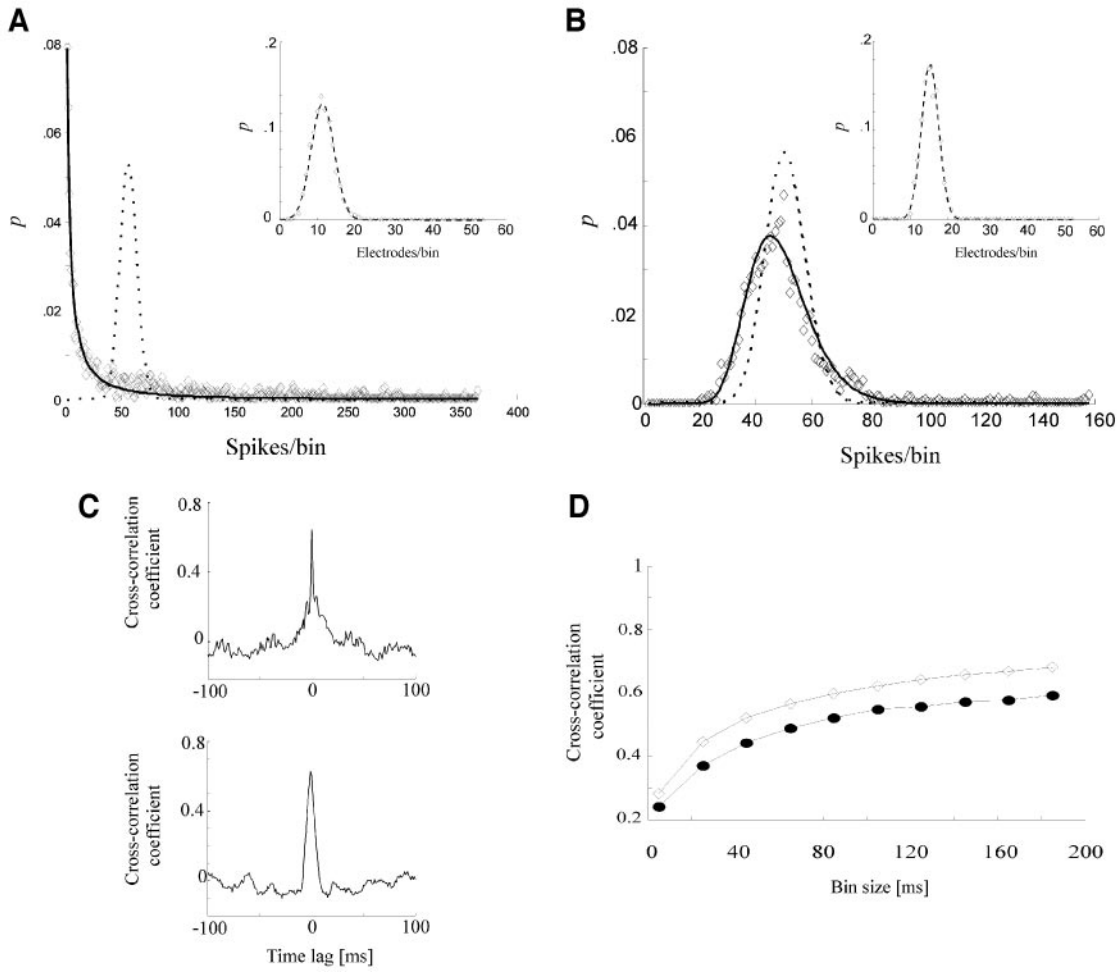

Figure 4. Correlated firing. **(A, B):** Probability distribution of the number of spikes per bin (250 ms) in the hippocampal- and embryonic stem cell (ES)-derived networks, respectively. Both networks are fitted by a lognormal distribution (solid line) and not by a Poissonian distribution (dashed line), as expected in the case of random firing among neurons. The skewed lognormal distribution and its long right tail account for the presence of few large bursts, containing several hundreds of spikes, and occurring in both networks. Insets: probability distribution of the number of active electrodes per bin. The dashed line represents a Poissonian fit, indicating that the pattern of active electrodes in each time bin occurs at random. **(C):** Examples of cross correlation between couple of electrodes 1 mm apart, in the hippocampal- (top panel) and ES-derived networks (bottom panel). **(D):** Dependency of the network cross correlation on the bin size used for both ES-derived networks (filled circle) and hippocampal networks (open diamond).

works, large bursts of simultaneous activity were observed. The size of these bursts was random and did not have any regular structure. These bursts did not have any obvious periodicity, and their occurrence could not be predicted. We observed spontaneous activity in these cultures ($n = 5$) for more than 2 months and, in one case, up to 3 months. Although the firing pattern of both types of networks was quite similar, the spontaneous activity baseline was slightly higher in ES-derived networks than in hippocampal networks (compare upper panels of Fig. 3B and 3D). This was likely due to the presence of a tonic firing of small amplitude, resulting in rare periods of quiescent activity (compare bottom panels of Fig. 3B and 3D). This tonic firing of small amplitudes spikes (Fig. 3A) was reminiscent of that of immature hippocampal networks (data not shown).

To further investigate the firing pattern of both networks, the firing rate was binned and the probability distribution of the number of spikes and active electrodes present in each bin was computed (see Materials and Methods). Both networks had a probability distribution of the number of spikes per bin fitted by lognormal distributions (Fig. 4A and 4B), indicating the presence of multiplicative effects [77] among the firing pattern of individual electrodes, broadening the range over which large numbers of spikes per bin can be observed.

The lognormal fit, characterized by a long right tail, also excluded a random firing pattern typically described by Poissonian distributions [78]. Moreover, the presence of tonic firing in ES-derived networks was further revealed by the presence of a peak in the lognormal distribution, centered on the number of active electrodes. This means that at least one spike was present in each bin most of the time, in contrast to hippocampal networks, where small numbers of spikes fired in each time bin have the highest probability.

Although the network firing pattern was not random and was dependent of multiplicative interactions among neurons, the number of active electrode in each bin followed a Poissonian distribution (Fig. 4A and 4B, insets), suggesting that the pattern of active electrode in during each time bin occurred at random. In both network types, cooperative effects between neurons recorded at distant electrodes were also indicated by their high cross-correlation coefficient (Fig. 4C).

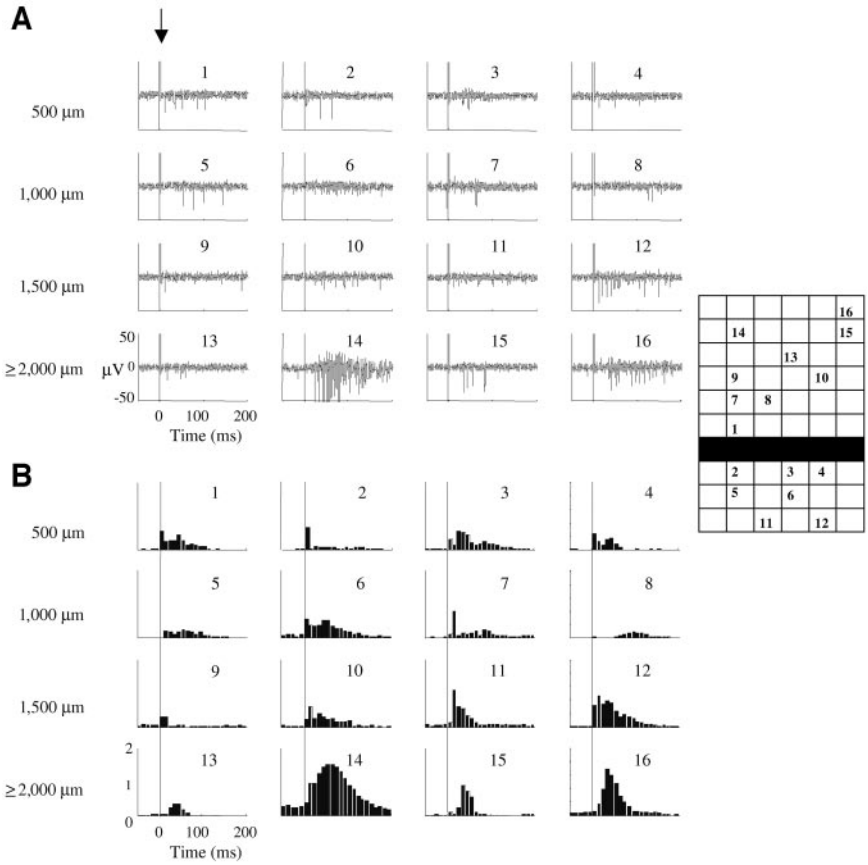

Figure 5. Evoked electrical activity in embryonic stem cell (ES)-derived networks. **(A):** Examples of extracellular voltage recordings after the stimulation of a bar of electrodes (black line in the scheme on the right) with a bipolar voltage pulse of 900 mV. **(B):** Peristimulus time histogram (PSTH) of the evoked activity from 16 electrodes of the multielectrode array (MEA). The thin vertical line indicates the stimulation artifact. Data averaged over 100 repetitions of the same stimulation.

The degree of connectivity within the network was quantified by computing the network correlation, defined as the average cross-correlation $<\rho>$ among electrical recordings from active electrodes (i.e., exhibiting evident APs; see Materials and Methods). As shown in Figure 4D, $<\rho>$ increased with the size of the bin width (i.e., the size of the time window over which correlations were considered). For small values of the bin width (i.e., less than 20 ms), the value of $<\rho>$ was lower than 0.1, indicating that spontaneously occurring APs were almost completely uncorrelated on a short time scale. At larger bin width (around 200 ms), as there is an increasing number of observations per bin, there is an increasing probability of observing correlations, and the value of $<\rho>$ increased to approximately 0.5 in both networks. This observation indicates a larger correlation of spontaneously occurring APs on a longer time scale. The dependence of $<\rho>$ on the used bin width is a consequence of the biophysical mechanisms underlying synaptic transmission and the generation of APs [1]: synaptic release and AP initiation in different neurons is statistically independent at the ms level, but becomes correlated in the presence of a common input lasting some hundreds of milliseconds.

Spread of the Evoked Electrical Activity in the Network

The propagation of electrical excitation in a network is a proof of the presence of chemical and electrical synaptic pathways and of functional network formation as has been previously shown in different studies on hippocampal [33] and cortical networks [20, 79, 80].

Therefore, the spread of the evoked activity was studied in ES-derived network cells cultured on MEA. Electrical activity was evoked by delivering brief voltage pulses to the extracellular electrodes of the MEA (see Materials and Methods) These voltage pulses induced a transient depolarization of neurons in good electrical contact with the stimulating electrode, possibly triggering the initiation of an AP. When a bar of electrodes was stimulated (black squares in the grid of Fig. 5), APs were evoked in neurons on nearby electrodes with a latency of some milliseconds. These evoked APs propagated over almost the entire network, with a progressively longer delay (Fig. 5A). The latency of the first evoked AP at electrodes near the stimulating bar, as the one indicated by the number 1 was less than 10 ms. Clear burst of evoked APs at electrodes more than 3 mm from the stimulating electrodes, as electrodes 14, 15, and 16 were observed. The latency of the first evoked APs at these more distant electrodes was around 40 ms. The results shown here are very similar to those previously described for hippocampal cultures [1, 33] and for cortical cultures [17, 21, 81].

The variability of the evoked electrical response was characterized by computing the peristimulus time histograms, obtained by averaging evoked response over 100 repetitions of the same stimulus (Fig. 5B). The peak of the PSTH of the activity recorded on more distant electrodes occurred at progressively longer times: at a distance of approximately 2,000 μm from the stimulating electrodes, the peak amplitude of the PSTH occurred with a delay of approximately 40 ms from the stimulus. The evoked response was usually composed of a first reproducible

AP, occurring with a similar timing in every trial, followed by less reproducible APs (Fig. 5B), as previously described for cortical networks [81]. The standard deviation of the latency of the first evoked AP, usually referred to as its "jitter," was used to measure the reproducibility of the evoked AP. A significant correlation between jitter and latency of the first evoked AP was observed in ES-derived networks ($\rho = .63$, $n = 4$; supplemental Fig. 3A) similarly to what observed in hippocampal networks ($\rho = .8$, $n = 5$; supplemental Fig. 3B and Bonifazi et al. [1]). The average latency increased with the physical distance between the recording electrode and the stimulating electrodes in both ES-derived and in hippocampal networks. The maximal speed of AP propagation was approximately 400 mm/s in both ES-derived and in hippocampal networks (supplemental Fig. 3C, 3D; Bonifazi et al. [1]).

The results shown in Figure 5 and in supplemental Figure 3 indicate that the evoked electrical activity in ES-derived networks spread with properties that are very similar to those observed in hippocampal networks.

Reproducibility of the Response and Information Processing

Neurons under certain network conditions fire APs in a poorly reproducible way, and, in particular, neurons receiving the same stimulation in different trials fire a variable number of APs or the same number of APs but with a different timing [1, 82, 83]. In most trials, the first evoked AP occurred with approximately the same latency, and it is considered reliable [1, 81]. Variability is characterized by repeatedly applying the same stimulation and analyzing the evoked average firing rate and the corresponding coefficient of variation ($CV = \sigma_{AFR}/AFR$) defined as the ratio between the standard deviation of the AFR (σ_{AFR}) and the AFR itself. As shown in Figure 6A, for selected individual ES-derived neurons, the CV (black dots) of the AFR (white bars) was rarely lower than 0.5, indicating that the evoked electrical activity was not reproducible.

The variability of the evoked electrical activity can be significantly reduced when several neurons are considered, and evoked APs are averaged or pooled together [1, 15, 82, 84]. When APs recorded from all the active electrodes (i.e., therefore from an ensemble of more than 30 ES-derived neurons) were pooled, the CV of the evoked activity was lower than 0.5 for 60 ms (Fig. 6B). A similar behavior was observed when the firing of individual hippocampal neurons was analyzed (Fig. 6C) and when their evoked electrical activity was pooled together, as shown in Figure 6D.

Functional neuronal networks can process information by encoding important features of the stimulus, such as its intensity [1]. Therefore, coding of stimulus intensity in ES-derived networks was investigated at the level of a single neuron or when APs from a population of cells were pooled. The same analysis was carried out in hippocampal networks (Fig. 7). Because pooling APs in ES-derived neurons exhibited a reproducible response ($CV < 0.5$), we investigated whether ES-derived networks distinguish the stimulus intensity, as observed in hippocampal networks [1]. Voltage pulses of different intensities were applied to the same row of electrodes. Raster plots of the evoked electrical activity from four distinct electrodes are shown in the four columns of Figure 7A. Similar data obtained from hippocampal networks are shown for comparison in Figure 7D. In both networks, by increasing the intensity of the voltage pulse from 300–600 to 900 mV, the number of APs recorded on each electrode increased, and the evoked APs became more frequent and more reliable. When the evoked electrical activity among several dozens of ES-derived neurons was pooled, it was possible to reliably distinguish the three stimulus intensities. As shown in Figure 7B, the histograms of the evoked electrical activity from about three dozen of neurons for the three voltage stimuli were well separated. Therefore, ES-derived networks were able to distinguish the stimulus intensity as hippocampal networks do (Fig. 7E). To quantify the ability of ES-derived networks to process information, we computed the mutual information IM, calculating the amount of information that could be decoded. As shown in Figure 7C, IM depended on the considered bin width and the size of neuronal pooling. With a bin width of 35 ms, and by pooling the electrical activity from 20 electrodes, approximately 1.3 bits of information were extracted from a theoretical maximum of 1.52 bits.

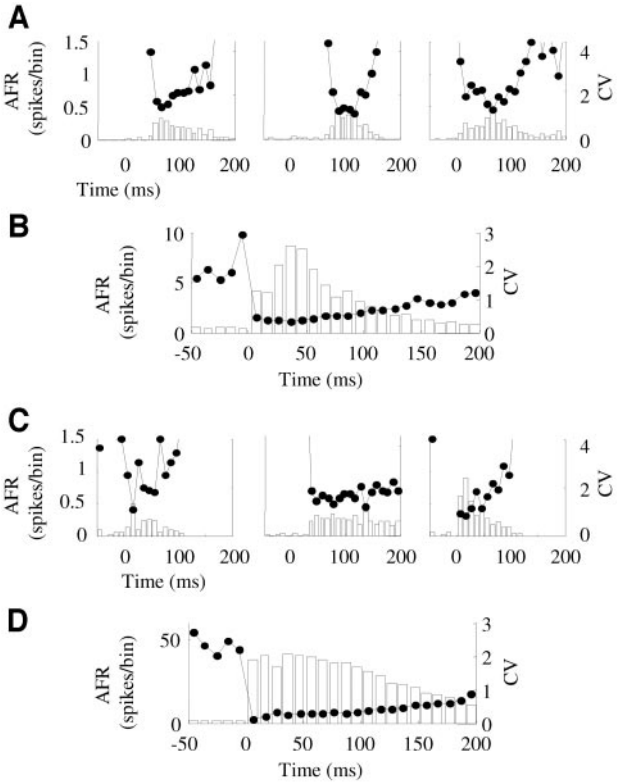

Figure 6. Reproducibility and coding. Average firing rate (AFR; open bars) and coefficient of variation (CV; black dots) of the firing from three selected embryonic stem cell (ES)-derived neurons **(A)** and from the entire network **(B)**. **(C)** and **(D)** as in **(A)** and **(B)**, but for neurons from hippocampal culture.

Similar results were obtained in hippocampal networks, where a maximum of 1.4 bits could be extracted by using a bin width of 25 ms and pooling the activity over 20 electrodes. These results show that ES-derived networks possess some basic computational properties, as we previously demonstrated for hippocampal networks [1].

DISCUSSION

In the present article, we provide the first investigation to our knowledge of the parallel processing of ES-derived networks. The study of neuronal networks in vitro is conceivable because it has been shown that functional characteristics of ex vivo neuronal networks are similar to those observed in vivo in terms

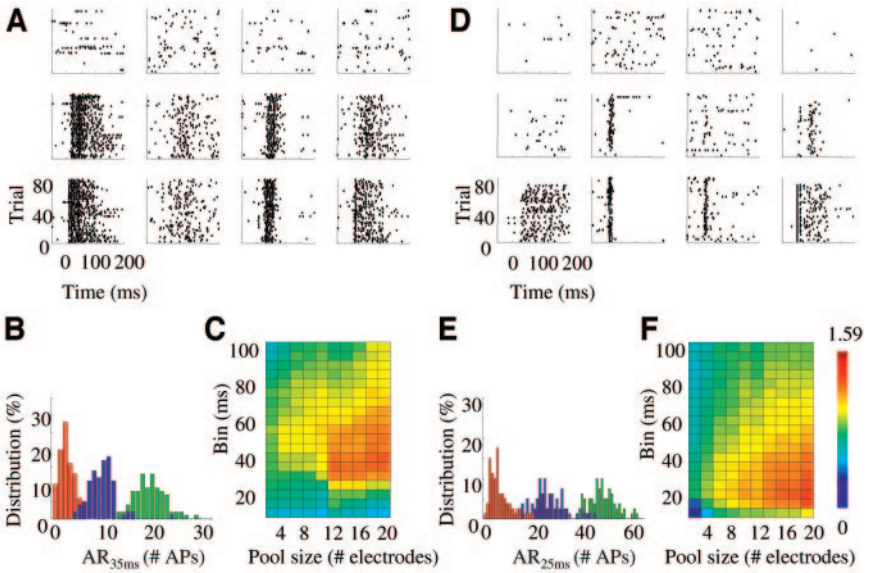

Figure 7. Information processing in embryonic stem cell (ES)-derived and hippocampal networks. **(A):** Raster plots of evoked action potentials (APs) recorded from four different electrodes (each column) by voltage pulses of 300, 600, and 900 mV (each row). **(B):** frequency histograms of all APs recorded in a time window from 0 to 51 ms from the stimulus evoked by the three different voltage stimulations. **(C):** Dependence of the mutual information on bin width and number of pooled electrodes. **(D, E, F):** As in **(A)**, **(B)**, and **(C)**, but from hippocampal cultures. In **(B)** and **(E)**, red corresponds to 300 mV, blue to 600 mV, and green to 900 mV.

of connectivity, inhibition/excitation ratio, electrophysiological and electrical stimuli (for a review, see Van Pelt et al. [19]). Moreover, in vitro networks possess information-processing ability with basic computational properties similar to those found in in vivo networks [35]. Recent work in our laboratory using dissociated hippocampal networks has also shown that different decoding strategies can be used to extract relevant features [1], giving the appropriate parameters to investigate ES-derived networks. By culturing ES-derived neurons over an MEA, we show that these networks are functional and exert some computational properties similar to those of hippocampal networks in culture.

When an extracellular voltage pulse was applied to the MEA electrodes, electrical activity was evoked and propagated for several millimeters in the culture with a velocity of approxiamtely 400 mm/second, similar to that observed in hippocampal cultures. The firing pattern of neurons in response to the stimulus was mainly composed by a first, reliable AP followed by less reliable APs, again comparable to hippocampal [1] and cortical [81, 85] neuronal networks in vitro. The variability of firing in ES-derived neurons was reduced when the APs were pooled over a population of neurons, and the high reproducibility of the pooled response allowed distinguishing, at the level of a single trial, stimuli varying in intensity. The ability of ES-derived neurons to process information was illustrated by measuring the mutual information between the evoked response and the stimulus intensity. This analysis indicates that a population of ES-derived neurons can reliably discriminate three stimulus intensities (corresponding to 1.52 bits of information) as observed in naturally matured neurons [1] and that ES-derived neurons can process information as mature neurons do.

Despite the striking similarity observed in the evoked activity, we observed some differences in the spontaneous activity. Although bursts of synchronous firing were present in both networks, interburst activity was more prominent in the ES-derived networks (Fig. 3), reminiscent of immature hippocampal networks (data not shown). This could reflect a difference in the ongoing maturational process characterized by different numbers of gap junctions, differential voltage-gated channel and ligand receptor expression and/or composition, difference in the rectifying function of the chloride ions [86–91], or percentage of glia in the cultures. One or more of these factors could also explain the difference in the duration of firing observed in the patch-clamp experiments between the two networks (Fig. 2C, 2D).

Our data also demonstrate that purely ES-derived neurons undergo functional maturation at a rate comparable to that observed after coculturing ES cells on top of hippocampal slice [53]. The appearance of neuronal postmitotic markers occurred much earlier than did the electrophysiological maturation of neurons. Moreover, the composition of the culture changed in terms of presence of glial cells during the observation period, indicating that a prolonged follow-up of the culture for therapeutic purposes is required.

The finding that ES-derived neurons form functional networks in vitro opens up a variety of new perspectives for future applications. ES cells are a potent source for the generation of various neuronal cell types, and by changing the composition of the culture, it is possible to promote the differentiation in specific neuronal types [38, 43–46]. Therefore, in the near future, it will be feasible to engineer neuronal networks with different neuronal types and to investigate the properties of the resulting networks. Similarly, because ES cells are amenable to genetic modification [92, 93], it will be possible to obtain neuronal types with modified properties in which selected ion channels or synaptic receptors are over- or underexpressed. This technology will allow the construction of neuronal networks with entirely new computational properties. The same technology can provide valid models of neuronal networks linked to a variety of neurodegenerative diseases and can verify the action of new ES-derived neurons on these model networks, providing a new perspective for therapeutic recovery.

The availability of unlimited number of ES-derived neurons paired with an intrinsic ability of these cells to form neuronal networks suggests the potential of this system to establishing large-scale, self-assembling networks. Such complex networks could provide a first key step towards ES cell-based neurocomputing [1, 33].

ACKNOWLEDGMENTS

This work was supported by the EU Grant 12788 NEURO, and by a FIRB grant from the Italian Ministers. We thank Manuela Schipizza Lough for carefully reading the manuscript. P.B. is currently affiliated with the University of Cambridge, Department of Physiology, Cambridge, U.K.

DISCLOSURES

The authors indicate no potential conflicts of interest.

REFERENCES

1 Bonifazi P, Ruaro ME, Torre V. Statistical properties of information processing in neuronal networks. Eur J Neurosci 2005;22:2953–2964.
2 Hopfield JJ. Neural networks and physical systems with emergent collective computational ability. Proc Nat Acad Sci U S A 1982;79:2554–2558.
3 Rumelhart DE, McClelland JL. Explorations in Parallel Distributed Processing. Cambridge, MA: MIT Press, 1998.
4 DeCharms RC, Merzenich MM. Primary cortical representation of sounds by the coordination of action-potential timing. Nature 1996;381:610–613.
5 Georgopoulos AP, Schwartz AB, Kettner RE. Neuronal population coding of movement direction. Science 1986;233:1416–1419.
6 Gray CM, Konig P, Engel AK et al. Oscillatory responses in cat visual cortex exhibit inter-columnar synchronization which reflects global stimulus properties. Nature 1989;338:334–337.
7 Nicolelis MA, Ghazanfar AA, Stambaugh CR et al. Simultaneous encoding of tactile information by three primate cortical areas. Nat Neurosci 1998;1:621–630.
8 Thorpe S, Delorme A, Van Rullen R. Spike-based strategies for rapid processing. Neural Network 2001;14:715–725.
9 Nicolelis MA, Ghazanfar AA, Faggin BM et al. Reconstructing the engram: Simultaneous, multisite, many single neuron recordings. Neuron 1997;18:529–537.
10 Kerr JND, Greenberg D, Helmchen F. Imaging input and output of neocortical networks in vivo. Proc Natl Acad Sci U S A 2005;102:14063–14068.
11 C Stosiek, O Garaschuk, K Holthoff et al. In vivo two-photon calcium imaging of neuronal networks. Proc Natl Acad Sci U S A. 2003;100:7319–7324.
12 Singer W, Gray CM. Visual feature integration and the temporal correlation hypothesis. Ann Rev Neurosci 1995;18:555–586.
13 O'Keefe J, Recce MLP. hase relationship between hippocampal place units and the EEG theta rhythm. Hippocampus 1993;3:317–330.
14 Hopfield JJ. Pattern recognition computation using action potential timing for stimulus representation. Nature 1995;376:33–36.
15 Johansson RS, Birznieks I. First spikes in ensembles of human tactile afferents code complex spatial fingertip events. Nat Neurosci 2004;7:170–177.
16 Van Pelt J, Vajda I, Wolters PS et al. Dynamics and plasticity in developing neuronal networks in vitro. Prog Brain Res 2005;147:173–188.
17 Jimbo Y, Tateno T, Robinson H Simultaneous induction of pathway-specific potentiation and depression in networks of cortical neurons. Biophys J 1999;76:670–678.
18 Welsh DK, Logothetis DE, Meister M, et al. Individual neurons dissociated from rat suprachiasmatic nucleus express independently phased circadian firing rhythm. Neuron 1995;14:697–706.
19 Van Pelt J, Wolters PS, Corner MA et al. Long-term characterization of firing dynamics of spontaneous burst in cultured neural networks. IEEE Trans Biomed Eng 2004;51:2051–2062.
20 Marom S, Shahaf G. Development, learning and memory in large random networks of cortical neurons: Lessons beyond anatomy. Q Rev Biophys 2002;35:63–87.
21 Potter SM. Distributed processing in cultured neuronal networks. Prog Brain Res 2000;130:49–62.
22 Neale EA, Oertel WH, Bowers LM et al. Glutamate decarboxylase immunoreactivity and gamma-[3H] aminobutyric acid accumulation within the same neurons in dissociated cell cultures of cerebral cortex. J Neurosci 1983;3:376–382.
23 Huettner JE, Baughman RW. Primary culture of identified neurons from the visual cortex of postnatal rats. J Neurosci 1986;6:3044–3060.
24 Nakanishi K, Kukita F. Intracellular [Cl(-)] modulates synchronous electrical activity in rat neocortical neurons in culture by way of GABAergic inputs. Brain Res 2000;863:192–204.
25 Morin FO, Takamura Y, Tamiya E. Investigating neuronal activity with planar microelectrode arrays: Achievements and new perspectives. J Biosci Bioeng 2005;100:131–143.
26 Jimbo Y, Kawana A. Electrical stimulation and recording from cultured neurons using a planar microelectrode array. Bioelectrochem Bioenerg 1992;29:193–204.
27 Robinson HP, Kawahara M, Jimbo Y et al. Periodic synchronized bursting and intracellular calcium transients elicited by low magnesium in cultured cortical neurons. J Neurophysiol 1993;70:1606–1616.
28 Robinson HP, Torimitsu K, Jimbo Y et al. Periodic bursting of cultured cortical neurons in low magnesium—cellular and network mechanisms. Jpn J Physiol 1993;(Suppl 43):l25–130.
29 Maeda E, Robinson HP, Kawana A. The mechanisms of generation and propagation of synchronized bursting in developing networks of cortical neurons. J Neurosci 1995;15:6834–6845.
30 Maeda E, Kuroda Y, Robinson HP et al. Modification of parallel activity elicited by propagating bursts in developing networks of rat cortical neurones. Eur J Neurosci 1998;10:488–496.
31 Kamioka H, Maeda E, Jimbo Y et al. Spontaneous periodic synchronized bursting during formation of mature patterns of connections in cortical cultures. Neurosci Lett 1996;206:109–112.
32 Shahaf G, Marom S. Learning in networks of cortical neurons. J Neurosci 2001;21:8782–8788.
33 Ruaro ME, Bonifazi P, Torre V. Toward the neurocomputer image processing and learning with a neuronal culture. IEEE Trans Biomed Eng 2005;52:371–383.
34 Bain G, Kitchens D, Yao M et al. Embryonic stem cells express neuronal properties in vitro. Dev Biol 1995;168:342–357.
35 Fraichard A, Chassande O, Bilbaut G et al. In vitro differentiation of embryonic stem cells into glial cells and functional neurons. J Cell Sci 1995;108(Pt 10):3181–3188.
36 Kawasaki H, Mizuseki K, Nishikawa S et al. Induction of midbrain dopaminergic neurons from ES cells by stromal cell-derived inducing activity. Neuron 2000;28:31–40.
37 Keller GM. In vitro differentiation of embryonic stem cells. Curr Opin Cell Biol 1995;7:862–869.
38 Lee SH, Lumelsky N, Studer L et al. Efficient generation of midbrain and hindbrain neurons from mouse embryonic stem cells. Nat Biotechnol 2000;18:675–679.
39 Li M, Pevny L, Lovell-Badge R, et al. Generation of purified neural precursors from embryonic stem cells by lineage selection. Curr Biol 1998;8:971–974.
40 Ying QL, Stavridis M, Griffiths D et al. Conversion of embryonic stem cells into neuroectodermal precursors in adherent monoculture. Nat Biotechnol 2003;21:183–186.
41 Nakayama T, Momoki-Soga T, Yamaguchi K et al. Efficient production of neural stem cells and neurons from embryonic stem cells. Neuroreport 2004;15:487–491.
42 Okabe S, Forsberg-Nilsson K, Spiro AC et al. Development of neuronal precursor cells and functional postmitotic neurons from embryonic stem cells in vitro. Mech Dev 1996;59:89–102.
43 Barberi T, Klivenyi P, Calingasan NY et al. Neural subtype specification of fertilization and nuclear transfer embryonic stem cells and application in Parkinsonian mice. Nat Biotechnol 2003;21:1200–1207.
44 Morizane A, Takahashi J, Takagim Y. Optimal conditions for in vivo induction of dopaminergic neurons from embryonic stem cells through stromal cell-derived inducing activity. J Neurosci Res 2002;69:934–993.
45 Westmoreland JJ, Hancock CR, Condie BG. Neuronal development of embryonic stem cells: A model of GABAergic neuron differentiation. Biochem Biophys Res Commun 2001;284:674–680.
46 Park C-H, Minn Y-K, Lee J-Y et al. In vitro and in vivo analyses of human embryonic stem cell-derived dopamine neurons. J Neurochem 2005;92:1265–1276.
47 Bibel M, Richter J, Schrenk K et al. Differentiation of mouse embryonic stem cells into a defined neuronal lineage. Nat Neurosci 2004;7:1003–1009.
48 Finley MF, Kulkarni N, Huettner JE. Synapse formation and establishment of neuronal polarity by P19 embryonic carcinoma cells and embryonic stem cells. J Neurosci 1996;16:1056–1065.
49 Hancock CR, Wetherington JP, Lambert NA et al. Neuronal differentiation of cryopreserved neural progenitor cells derived from mouse embryonic stem cells. Biochem Biophys Res Commun 2000;271:418–421.
50 Jüngling K, Nägler K, Pfrieger FW et al. Purification of embryonic stem cell-derived neurons by immunoisolation. FASEB J 2003;7:2100–2102.

51 Strübing C, Ahnert-Hilger G, Shan J et al. Differentiation of pluripotent embryonic stem cells into neuronal lineage in vitro gives rise to mature inhibitory and excitatory neurons. Mech Dev 1995;53:275–287.
52 Miles GB, Yohn DC, Wichterle H et al. Functional properties of motoneurons derived from mouse embryonic stem cells. J Neurosci 2004; 24:7848–7858.
53 Benninger F, Beck H, Wernig M et al. Functional integration of embryonic stem cell-derived neurons in hippocampal slice cultures. J Neurosci Neurosci 2003;23:7075–7083.
54 Ruschenschmidt C, Koch PG, Brustle O et al. Functional properties of ES cell-derived neurons engrafted into the hippocampus of adult normal and chronically epileptic rats. Epilepsia 2005;46(suppl 5):174–178.
55 Wernig M, Benninger F, Schmandt T et al. Functional integration of embryonic stem cell-derived neurons in vivo. J Neurosci 2004;24: 5258–5268.
56 Baizabal JM, Furlan-Magaril M, Santa-Olalla J et al. Neural stem cells in development and regenerative medicine. Arch Med Res 2003;34: 572–588.
57 Kim J-H, Auerbach JM, Rodriguez-Gomez JA et al. Dopamine neurons derived from embryonic stem cells function in an animal model of Parkinson's disease. Nature 2002;418:50–56.
58 Perrier AL, Studer L. Making and repairing the mammalian brain—in vitro production of dopaminergic neurons. Semin Cell Dev Biol 2003; 14:181–189.
59 Sánchez-Pernaute R, Studer L, Bankiewicz KS et al. In vitro generation and transplantation of precursor-derived human dopamine neurons. J Neurosci Res. 2001;65.
60 Tabar V, Panagiotakos G, Greenberg ED et al. Migration and differentiation of neural precursors derived from human embryonic stem cells in the rat brain Nat Biotechnol 2005;23:601–606.
61 Brüstle O, Spiro AC, Karram K et al. In vitro-generated neural precursors participate in mammalian brain development. Proc Natl Acad Sci U S A 1997;94:14809–14814.
62 Brüstle O, Jones KN, Learish RD et al. Embryonic stem cell-derived glial precursors: A source of myelinating transplants. Science 1999;285: 754–756.
63 Hara A, Niwa M, Kunisada T et al. Embryonic stem cells are capable of generating a neuronal network in the adult mouse retina. Brain Res 2004;999:216–221.
64 McDonald JW, Liu XZ, Qu Y et al. Transplanted embryonic stem cells survive, differentiate and promote recovery in injured rat spinal cord. Nat Med 1999;5:1410–1412.
65 Tateno T, Kawana A, Jimbo Y. Analytical characterization of spontaneous firing in networks of developing rat cultured cortical neurons. Phys Rev E Stat Nonlin Soft Matter Phys Phys 2002;65 (5 Pt 1):051924.
66 Wagenaar DA, Pine J, Potter SM. Effective parameters for stimulation of dissociated cultures using multi-electrode arrays. J Neurosci Methods 2004;138:27–37.
67 Wagenaar DA, Potter SM. Real-time multi-channel stimulus artifact suppression by local curve fitting. J Neurosci Methods 2002;120: 113–120.
68 Egert U, Knott T, Schwarz C et al. MEA-Tools: An open source toolbox for the analysis of multi-electrode data with MATLAB. J Neurosci Meth 2002;17:33–42.
69 Shannon CE, Weaver W. The Mathematical Theory of Communication. Urbana, IL: University of Illinois Press, 1949.
70 Panzeri S, Treves A. Analytical estimates of limited sampling biases in different information measures. Network 1996;7:87–107.
71 Sauvageot CM, Stiles CD. Molecular mechanisms controlling cortical gliogenesis. Curr Opin Neurobiol 2004;12:244–249.
72 Sun YE, Martinowich K, Ge W. Making and repairing the mammalian brain-signaling toward neurogenesis and gliogenesis. Sem Cell Dev Biol 2003;14:161–168.
73 Lestienne R. Spike timing, synchronization and information processing on the sensory side of the central nervous system. Prog Neurobiol 2001;65:545–591.
74 Lahtinen H, Palva JM, Sumanen S et al. Postnatal development of rat hippocampal gamma rhythm in vivo. J Neurophysiol 2002;88: 1469–1474.
75 Leinekugel X, Khazipov R, Cannon R et al. Correlated bursts of activity in the neonatal hippocampus in vivo. Science 2002;296:2049–2052.
76 Demas J, Eglen SJ, Wong RO. Developmental loss of synchronous spontaneous activity in the mouse retina is independent of visual experience J Neurosci 2003;23:2851–2860.
77 Limpert E, Stahel WA, Abbot M. Log-normal distributions across the sciences: Keys and clues. Bioscience 2001;51:341–352.
78 Dayan P, Abbott LF. Theoretical Neuroscience. Computational and Mathematical Modeling of Neural Systems. Cambridge, MA: MIT Press, 2001.
79 Corner MA. Reproducibility of structure-function relations in developing neuronal networks- the odyssey of self-organizing brain through research fads, fallacies and prospects. Prog Brain Res 1994;102:3–31.
80 Canepari M, Bove M, Maeda E et al. Experimental analysis of neuronal dynamics in cultured cortical networks and transition between different patterns of activity. Biol Cybern 1997;77:153–162.
81 Jimbo Y, Kawana A, Parodi P et al. The dynamics of a neuronal culture of dissociated cortical neurons of neonatal rats. Biol Cybern 2000;83: 1–20.
82 Zoccolan D, Pinato G, Torre V. Highly variable spike trains underlie reproducible sensorimotor responses in the medicinal leech. J Neurosci 2002;22:10790–10800.
83 Arisi I, Zoccolan D, Torre V. Distributed motor pattern underlying whole-body shortening in the medicinal leech. J Neurophysiol 2001;86: 2475–2488.
84 Pinato G, Battiston S, Torre V. Statistical independence and neural computation in the leech ganglion. Biol Cybern 2000;83:119–130.
85 Tateno T, Jimbo Y, Robinson HP. Spatio-temporal cholinergic modulation in cultured networks of rat cortical neurons: Spontaneous activity. Neuroscience 2005;134:425–437.
86 Antonucci DE, Lim ST, Vassanelli S et al. Dynamic localization and clustering of dendritic Kv2.1 voltage-dependent potassium channels in developing hippocampal neurons. Neuroscience 2001;108:69–81.
87 Connors BW, Bernardo LS, Prince DA. Coupling between neurons of the developing neocortex. J Neurosci 1983;3:773–782.
88 Clayton GH, Staley KJ, Wilcox CL et al. Developmental expression of C1C-2 in the rat nervous system. Brain Res Dev Brain Res 1998;108: 307–318.
89 Smith RL, Clayton GH, Wilcox CL et al. Differential expression of an inwardly rectifying chloride conductance in rat brain neurons: A potential mechanism for cell-specific modulation of postsynaptic inhibition. J Neurosci 1995;15:4057–4067.
90 Ben-Ari Y. Excitatory actions of GABA during development: The nature of the nurture. Nat Rev Neurosci 2002;3:728–739.
91 Cherubini E, Gaiarsa JL, Ben-Ari Y. GABA: An excitatory transmitter in early postnatal life.Trends Neurosci. 1991;14:515–519.
92 Friedrich G, Soriano P. Promoter traps in embryonic stem cells: A genetic screen to identify and mutate developmental genes in mice. Genes & Dev 1991;5:1513–1523.
93 Thomas KR, Capecchi MR. Site-directed mutagenesis by gene targeting in mouse embryo-derived stem cells. Cell 1987;51:503–512.

See www.StemCells.com for supplemental material available online.

- 3.2 -

On the dynamics of the spontaneous activity in neuronal networks

Mazzoni A, **Broccard FD**, Garcia-Perez E, Bonifazi P, Ruaro ME, Torre V

PLoS ONE **2**(5):e439 (2007)

OPEN ACCESS Freely available online

PLoS one

On the Dynamics of the Spontaneous Activity in Neuronal Networks

Alberto Mazzoni[9], Frédéric D. Broccard[9], Elizabeth Garcia-Perez[9¤a], Paolo Bonifazi[¤b], Maria Elisabetta Ruaro, Vincent Torre*

International School for Advanced Studies, Trieste, Italy

Most neuronal networks, even in the absence of external stimuli, produce spontaneous bursts of spikes separated by periods of reduced activity. The origin and functional role of these neuronal events are still unclear. The present work shows that the spontaneous activity of two very different networks, intact leech ganglia and dissociated cultures of rat hippocampal neurons, share several features. Indeed, in both networks: i) the inter-spike intervals distribution of the spontaneous firing of single neurons is either regular or periodic or bursting, with the fraction of bursting neurons depending on the network activity; ii) bursts of spontaneous spikes have the same broad distributions of size and duration; iii) the degree of correlated activity increases with the bin width, and the power spectrum of the network firing rate has a 1/f behavior at low frequencies, indicating the existence of long-range temporal correlations; iv) the activity of excitatory synaptic pathways mediated by NMDA receptors is necessary for the onset of the long-range correlations and for the presence of large bursts; v) blockage of inhibitory synaptic pathways mediated by $GABA_A$ receptors causes instead an increase in the correlation among neurons and leads to a burst distribution composed only of very small and very large bursts. These results suggest that the spontaneous electrical activity in neuronal networks with different architectures and functions can have very similar properties and common dynamics.

Citation: Mazzoni A, Broccard FD, Garcia-Perez E, Bonifazi P, Ruaro ME, et al (2007) On the Dynamics of the Spontaneous Activity in Neuronal Networks. PLoS ONE 2(5): e439. doi:10.1371/journal.pone.0000439

INTRODUCTION

The spontaneous firing of spikes accounts for almost 80% of the metabolic energy consumed by the brain [1] and therefore this spontaneous electrical activity is expected to have a major neurobiological function. In vertebrate and invertebrate species, spontaneous activity in the nervous system has been studied primarily in rhythm-generating networks called central pattern generators (CPG) [2]. Some patterns of periodic spontaneous activity, like those underlying heartbeat [3] and respiration [4] are active throughout life, even if their frequency can be modulated. Other CPGs, like those responsible for locomotion [5], are triggered by signals coming from the environment, and are then able to sustain a periodic activity without further inputs [6]. Periodic spontaneous bursts of spikes can convey information about sensory stimuli [7] and are important also during development [8], since they contribute to determine the structure of neuronal networks [9,10].

Neuronal networks, however, often display irregular spontaneous activity characterized by intermittent bursts separated by periods of reduced activity. From the point of view of information processing, arrhythmic spontaneous bursts represent the noise of the system under investigation [11] and it is important to determine their statistical properties. *In vivo* studies have revealed that evoked activity in stimuli driven experiments is always superimposed on this ongoing background activity, which contributes to the trial-to-trial variability [12,13]. Most importantly, the spontaneous background activity displays spatial and temporal correlation [14,15]. Long-range correlations of the irregular spontaneous activity have been studied in *in vitro* neuronal networks [16].

In order to identify general dynamical properties of the arrhythmic spontaneous firing, we analyzed and compared the spontaneous electrical activity of two very different networks: intact leech ganglia and dissociated cultures from hippocampal rat neurons. In the present manuscript we show that despite their differences in origin and function, the spontaneous activity of both networks has similar statistical properties. The firing of neurons exhibits a strong correlation for bin widths of hundreds of milliseconds, corresponding to low frequency correlations. Burst size and duration follow power law distributions with the same slope in both preparations.

As the dynamics of the spontaneous activity is shaped by the balance between excitation and inhibition [17] and its alteration underlies a transition between diverse bursting regimes [18,19], we have modified this balance by means of pharmacological manipulations.

When excitatory synaptic pathways mediated by NMDA receptors are blocked, both neuronal networks are driven into a regime where large bursts are absent. In contrast, blockage of inhibitory synaptic pathways mediated by $GABA_A$ receptors drives both networks into a regime characterized by large and highly synchronous bursts.

These results show that the spontaneous electrical activity of intact leech ganglia and hippocampal cultures share several properties and respond to pharmacological manipulations with very similar dynamical changes. These results also provide the

Academic Editor: Olaf Sporns, Indiana University, United States of America

Received March 15, 2007; **Accepted** April 17, 2007; **Published** May 9, 2007

Funding: This work was supported by the EU grant NEURO, by a FIRB grant from the Italian Government and by the GRAND grant from CIPE/FVG.

Competing Interests: The authors have declared that no competing interests exist.

* **To whom correspondence should be addressed.** E-mail: torre@sissa.it

9 These authors contributed equally to this work.

¤a **Current address:** Departamento de Neurociencias, Centro de Investigación Médica Aplicada (CIMA), Pamplona, Spain
¤b **Current address:** Institut de Neurobiologie de la Méditerranée (INMED), Parc Scientifique de Luminy, Marseille, France

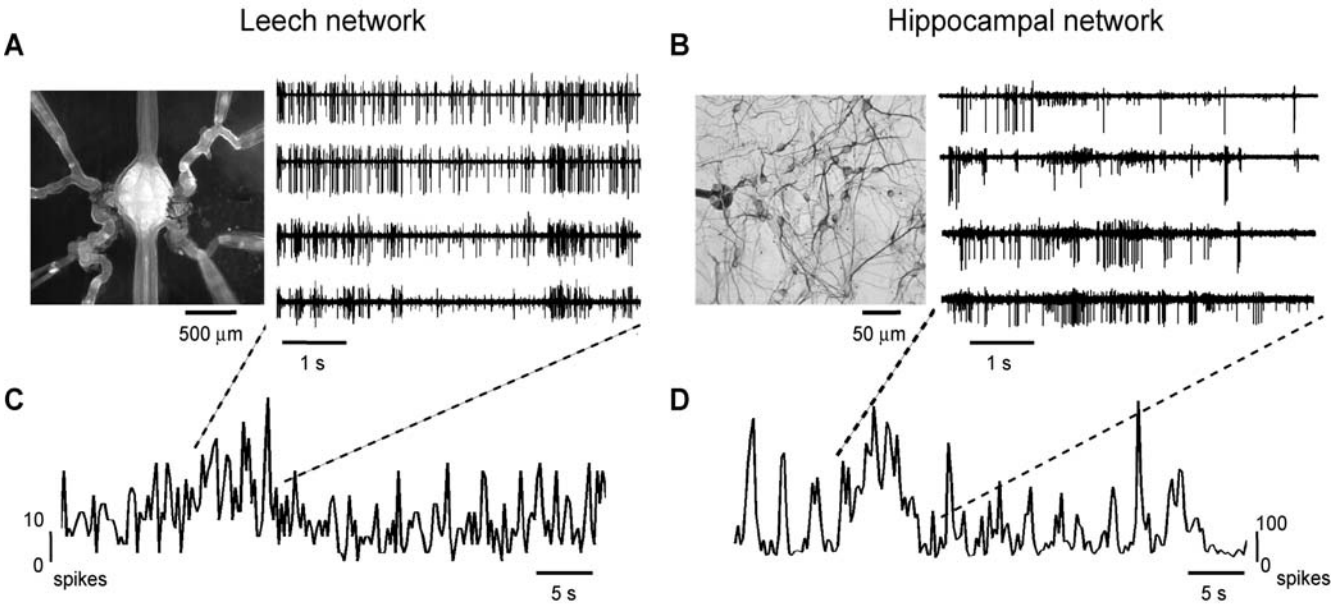

Figure 1. Spontaneous bursting activity in the leech and hippocampal networks. (A) Left: isolated leech ganglion with eight suction pipettes recording from different roots. Right: Extracellular recordings showing the spontaneous electrical activity monitored from four different roots. (B) Left: close-up of dissociated hippocampal neurons grown on MEA. The black dot corresponds to an individual electrode. Right: spontaneous activity recorded from four extracellular electrodes (out of 60). (C–D) Network firing rate binned at 500 ms for a representative leech network (C) and a representative hippocampal network (D). Note the presence of large peaks corresponding to concerted bursts of electrical activity and the difference between the two spike scales.
doi:10.1371/journal.pone.0000439.g001

background for understanding the origin and functional role of spontaneous bursting.

RESULTS

We investigated the spontaneous firing of spikes in the leech nervous system and in dissociated cultures of rat hippocampal neurons. Leech ganglia were isolated and 6 to 8 emerging roots were dissected and inserted into suction pipettes, from which extracellular voltage recordings were obtained (Figure 1A, left, see Methods). Dissociated neuronal cultures from neonatal hippocampal neurons were grown [20] on 60-channel multielectrode arrays (MEA) (Figure 1B, left, see Methods) with 50 to 55 active sites. We will hereafter refer to leech ganglia and hippocampal neuronal cultures as leech and hippocampal networks, respectively. In both preparations spontaneous activity was recorded for periods that ranged from 30 minutes to 2 hours. The firing pattern in both networks was characterized by intermittent bursts of activity with a broad variety of sizes separated by episodes of low firing activity (Figure 1A and 1B, right).

The network firing rate (see Methods) fluctuated significantly, showing large peaks corresponding to bursts of concerted electrical activity (Figure 1C and 1D). Synchronous firing was observed also in electrical recordings obtained from spatially distant extracellular electrodes of the MEA and from suction electrodes on roots emerging from opposite sides of leech ganglia.

Network correlation at short and long time scales

In both networks, the shape of the spike per bin distribution of the network firing rate depended on the bin width. When the activity was binned in time windows of 20 ms, the spike per bin distribution was fitted by a Poisson function in all the leech networks ($n = 15$, χ^2 test, $p > 0.05$, Figure 2A), and in most

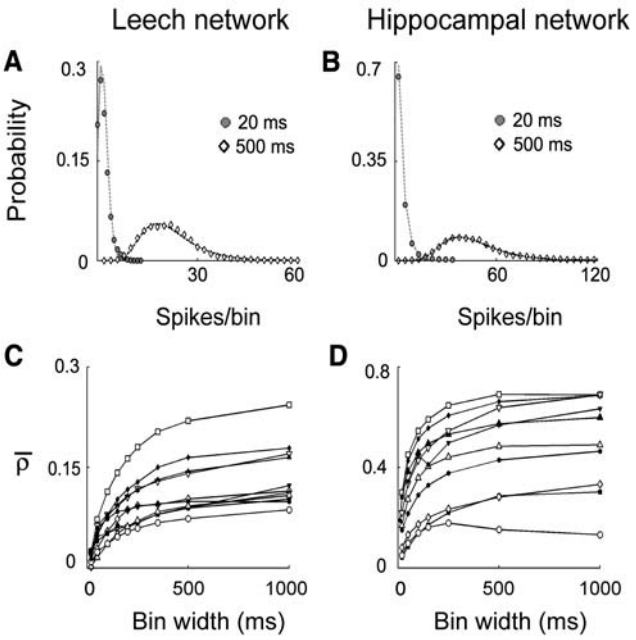

Figure 2. Network firing correlation. (A–B) Spikes per bin distribution of the network firing rate binned at 20 ms (filled symbols) and 500 ms (open symbols), in leech (A) and hippocampal networks (B). Data binned at 20 ms are fitted by a Poisson distribution. Data binned at 500 ms are fitted by a lognormal distribution. (C–D) Network correlation coefficient $\bar{\rho}$ as a function of the bin width for 10 leech (C) and 10 hippocampal networks (D) showing a bin width-dependent growth. Each symbol corresponds to a different preparation.
doi:10.1371/journal.pone.0000439.g002

hippocampal networks (7/10, χ^2 test, $p>0.05$, Figure 2B). In a Poisson process, leading to a Poisson distribution, the occurrence probability of a spike does not depend on the occurrence of other spikes. These results are consistent with an independent firing among neurons [21]. In contrast, when the activity was binned in time windows of 500 ms, the spike per bin distribution was fitted by a lognormal function for both networks (Figure 2A and 2B, leech, $n=15$, hippocampal network, $n=10$; χ^2 test $p>0.05$), suggesting that the networks activity is - at this time scale - regulated by interactions leading to a correlated firing [22,23].

As different functions fitted the spike per bin distribution when different bin widths were used, the degree of correlation observed in the network could depend on the time scale in which spikes were counted. We measured the degree of correlation present in the entire network by averaging the cross-correlation at lag 0 over all pairs of neurons, thus obtaining the network correlation coefficient $\bar{\rho}$ (see Methods). As shown in Figure 2C and 2D, $\bar{\rho}$ grew with the bin width for most leech (14/15, $r>0.5$) and hippocampal networks (9/10, $r>0.5$). At a bin width of 20 ms, for leech networks, $\bar{\rho}$ was less than 0.05 and increased by 3 ± 1 times at a bin width of 500 ms, reaching a mean value of 0.14 ± 0.04 ($n=15$). In hippocampal networks, $\bar{\rho}$ was 0.21 ± 0.1 at a bin width of 20 ms, and similarly to leech networks, it increased by 2.5 ± 1 times at a bin width of 500 ms reaching a mean value of 0.49 ± 0.15 ($n=10$). These results indicate that interactions leading to episodes of intense network activity take place on a timescale of hundreds of milliseconds.

The spontaneous activity of single neurons

We have studied the spontaneous activity of single neurons in both networks. From the extracellular recordings it was possible to sort spikes fired by the same single neuron (see Methods). The extracellular recordings shown in Figure 3A and 3E were obtained from the left posterior posterior root emerging from the 12th ganglion of the leech, and from a single MEA electrode, respectively. The spike sorting procedure identified in both recordings two distinct action potential shapes, one with a large and the other with an intermediate amplitude, generated by different neurons. As evident by visual inspection, in both traces one neuron fired in a regular fashion, whereas the other fired in a more irregular way, with occasional bursts of spikes.

The inter-spike intervals (ISI) of the spontaneous firing of the neurons of both networks have three stereotyped distributions: i - exponentially distributed (Figure 3B and 3F); ii - bi-exponentially distributed (Figure 3C and 3G) where the ISI probability is given by the sum of two exponential functions; iii - with a pronounced peak at a time T superimposed on either an exponential or a bi-exponential distribution (Figure 3D and 3H). The first distribution corresponds to a Poissonian firing [21], the second to a bursting neuron characterized by intervals of high frequency firing, and the last one to a neuron displaying episodes of almost periodic firing, with an average period between successive spikes equal to T. Characteristic times of each dynamics and fraction of neurons belonging to it for the two preparations are summarized in Table 1.

Since the activity of the neurons was correlated (see Figure 2), the high firing frequency corresponding to small ISI occurred in different neurons in a quasi-synchronous way: bi-exponential neurons were bursting at similar times (see Figure 4A and 4B). Indeed, raster plots (bottom of panels 4A and 4B) clearly showed that bursts in different neurons occurred simultaneously.

It was possible to reliably identify specific leech motoneurons (motoneuron 3 and motoneuron 107, see Methods) and to analyze the variability of their spontaneous firing in different leeches. This analysis showed that leech motoneurons have a characteristic pattern of spontaneous firing, i.e. their ISI was either exponentially distributed or it had a pronounced peak indicating an almost periodic firing. However, these motoneurons could vary their behavior from a regular to a bursting firing. We then measured the percentage of neurons spontaneously firing with a bi-exponential ISI distribution across different experiments; this percentage was positively correlated to the network correlation coefficient in both leech ($n=15$, $r=0.76$, Figure 4C) and hippocampal network ($n=10$, $r=0.85$, Figure 4D), indicating that bursts were associated to an increase in correlation.

Neuronal correlations

The three kinds of neuronal activity were associated to different autocorrelation and power spectral density functions (PSD, see Methods): i - Poisson firing neurons had an autocorrelation with a peak at zero lag, and an almost flat power spectrum (lowest traces of Figure 5A and 5B); ii - bi-exponential neurons displayed an exponential decay of the autocorrelation function with time constants ranging from 2 to 10 seconds, and an higher power associated to low frequencies, indicating that long-range temporal correlations were present during bursting activity (intermediate and highest traces of Figure 5A and 5B); iii - periodic neurons had peaks in the autocorrelation function and a single peak in the PSD, not always evident since they were superimposed on one of the two previous behaviors (data not shown).

We then analyzed the correlations of pairs of neurons in both networks (see Methods). At short time scales every neuron was correlated with only a small fraction of the network (Pearson test for independence, $p>0.05$). For both networks at a bin width of 20 ms every neuron was correlated with less than 10% of the network ($4.6\pm1.5\%$ for the leech, $n=15$; $8\pm4\%$ for hippocampal network, $n=10$). At this time scale every neuron of the leech network was then correlated only to 1 or no other neuron, and hippocampal network neurons were correlated only to the neighboring and sometimes to a few not-neighboring neurons. The number of correlated neurons grew with the bin width, and at a time scale of 500 ms every neuron was instead correlated to approximately 60% of the neurons in both cases ($57\pm6\%$ for the leech, $n=15$; $64\pm6\%$ for hippocampal network, $n=10$), indicating the presence of a coherent activity in the network. In both cases these values were not significantly different from the values obtained with a bin width of 1000 ms ($60\pm5\%$ for the leech, $n=15$, t-test $p=0.4$; $64\pm7\%$ for hippocampal network, $n=10$, t-test $p=0.9$). Even if the extent of the spatial correlation was similar in the two networks, the synchronization was more precise among hippocampal neurons (data not shown), so the resulting network correlation coefficient was higher (Figure 2). A change in dynamics for time scales between 1 and 2 Hz was also evident as shown in the frequency analysis.

The power spectrum of the network firing rate of both networks was flat for frequencies above 2 Hz and decreased as $f^{-\text{slope}}$, with a slope close to 1, (leech, $n=15$, mean slope $=0.97\pm0.3$; hippocampal, $n=10$, mean slope $=1.15\pm0.2$), for frequencies ranging from 0.1 to 1 Hz (Figure 5C and 5D). This indicated long-range temporal correlations in the network activity, as a result of the structure of the activity of the single neurons and of their correlation. These results show that in both cases neurons are neither independently firing nor precisely synchronized during spontaneous activity, but that they are correlated through processes acting on the hundreds of milliseconds time scale. A bin width of 500 ms was used thereafter, since it was large enough to capture the cooperative behavior in both networks.

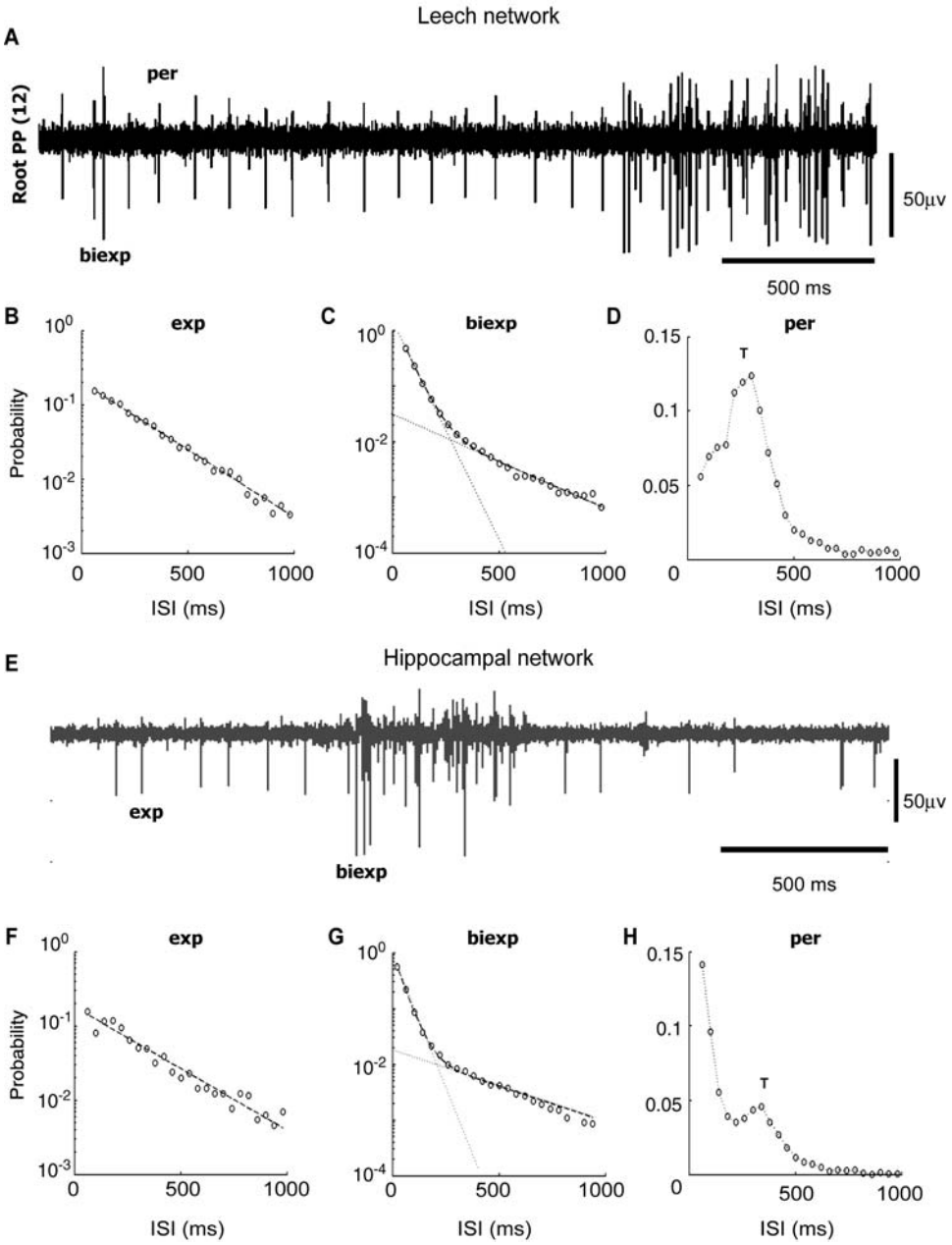

Figure 3. Single neurons dynamics. (A and E) Extracellular recording from a single electrode in the leech (A) and in the hippocampal network (E) showing the activity of neurons with periodic (A), Poissonian (E) and bursting (A and E) firing. (B and F) ISI distribution of identified neurons with exponential dynamics for leech (B) and hippocampal (F) network. Black dashed lines indicate exponential fit. (C and G) ISI distribution of identified neurons with bi-exponential dynamics for leech (C) and hippocampal (G) network. Black dashed lines indicate bi-exponential fit. (D and H) ISI distribution of identified neurons with periodic dynamics for leech (D) and hippocampal (G) network. Label T indicates the position of the peak, corresponding to the period of the firing.
doi:10.1371/journal.pone.0000439.g003

Blockage of excitatory and inhibitory synaptic pathways

To assess more accurately the role of neurons' interactions in the spontaneous activity in both networks, we investigated the action of antagonists of excitatory and inhibitory transmission. The blockage of the excitatory transmission mediated by NMDA receptors with APV (see Methods) decreased the bursting activity (Figure 6A and 6B, blue trace) in both networks, whereas the blockage of the inhibitory pathways mediated by $GABA_A$ receptors with bicuculline or PTX (see Methods) increased the bursting activity (Figure 6A and 6B, red trace), in agreement with previous results [24,25].

It was also possible to monitor the activity of identified neurons before and after the application of receptor blockers in both preparations (see Methods) and to see that the modulation of the interactions among neurons affected the dynamics of single neurons.

In both networks the presence of APV led to an increase of the fraction of neurons displaying an exponential ISI distribution, i.e. Poissonian firing (leech: from 37% to 56% n = 6; hippocampal:

Table 1. Single neurons dynamics.

Inter spike intervals distribution	Leech network (n = 15)		Hipp. network (n = 10)	
	char. time	% neurons	char. time	% neurons
Exponential	175±76 ms	37% (27%–56%)	290±90 ms	19% (9%–26%)
Bi-exponential	42±24 ms	35% (18%–54%)	47±19 ms	70% (53%–88%)
	331±117 ms		378±194 ms	
Periodic	167±91 ms	27% (18%–33%)	280±74 ms	11% (0%–25%)

In the left rows for both networks characteristic times of different single neuron dynamics, i.e. time constants of exponential distributions and peak position of periodic distributions. In the right rows fraction of neurons displaying different dynamics (numbers in brackets indicate the range of the values across different experiments).
doi:10.1371/journal.pone.0000439.t001

from 19% to 28% n = 5). ISI distributions of neurons of both preparations switching from bursting to regular firing in presence of APV are displayed in Figure 7A and 7B. In both networks the blockage of $GABA_A$ receptors had an opposite effect decreasing the fraction of neurons displaying an exponential ISI distribution (leech: from 37% to 14% n = 6; hippocampal culture: from 19% to 8% n = 5). ISI distributions of neurons switching from regular firing to bursting in both preparations are displayed in Figure 7C and 7D.

The cooperative behavior observed in both networks was investigated by studying the action of antagonists of excitatory and inhibitory transmission on the degree of correlation. We analyzed their effect on the spike per bin distribution, the power spectrum of the firing rate and the network correlation coefficient.

The blockage of the excitatory transmission mediated by NMDA receptors with APV (see Methods) diminished considerably the degree of correlated firing (leech: n = 6, $\bar{\rho} = 0.05 \pm 0.01$,

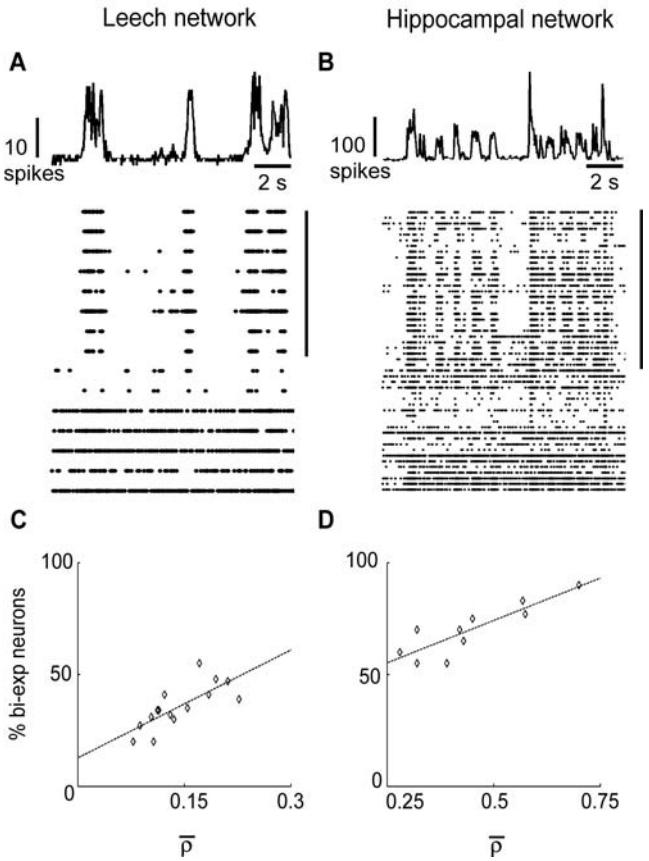

Figure 4. Single neurons dynamics and network bursts. (A–B) Network firing rate (upper panel) and raster plot (lower panel) for leech (A) and hippocampal (B) network. Each line of the raster plot represents the activity of a single neuron. Bi-exponential neurons have been clustered and are indicated by the black vertical bar. (C–D) Fraction of neurons displaying bi-exponential ISI distribution as a function of the network correlation coefficient for leech (C) and hippocampal networks (D). Each point represents a different experiment. Black dashed lines indicate linear regression.
doi:10.1371/journal.pone.0000439.g004

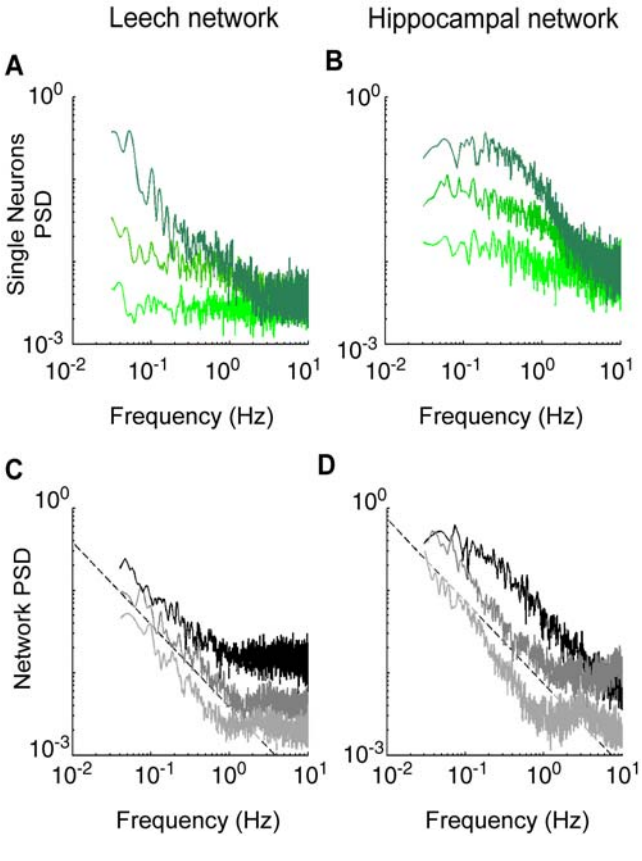

Figure 5. Single neurons and network frequency analysis. (A–B) Power spectral density (PSD) of representative neurons in different green shades from leech (A) and hippocampal networks (B). The PSD of the firing of a single neuron ranges from an almost flat behavior to very high power associated to low frequencies. (C–D) PSD of the network firing rate for representative experiments from leech (C) and hippocampal networks (D). Black dashed lines correspond to 1/f slope, describing the PSD for frequencies smaller than 1 Hz. In both panels, higher and lower traces are vertically shifted for clarity, by factors 1.2 and 0.8 respectively.
doi:10.1371/journal.pone.0000439.g005

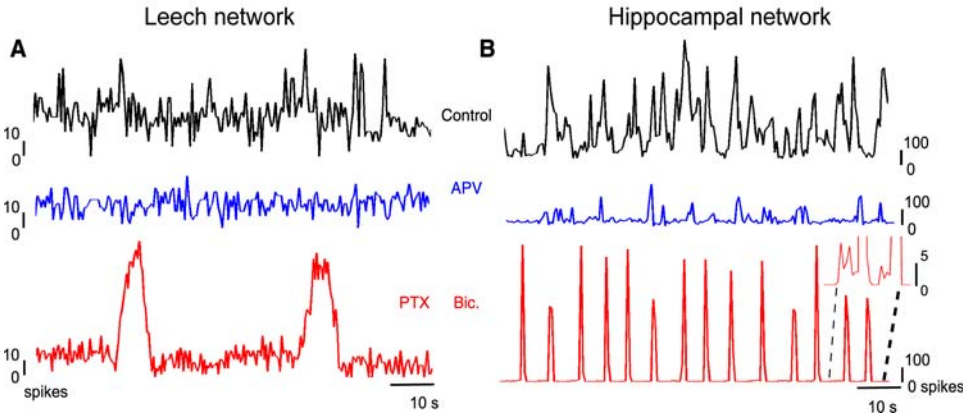

Figure 6. Effects of synaptic blockers on the network activity. (A–B) Changes in the network firing rates binned at 500 ms for leech (A) and hippocampal (B) networks, in control (black trace), in the presence of 20 μM APV (blue trace) and 10 μM PTX (red trace, panel A) or bicuculline (red trace, panel B). Note the residual spiking activity between periods of synchronous activity in the hippocampal network (inset, right red trace; large peaks have been truncated for clarity).
doi:10.1371/journal.pone.0000439.g006

hippocampal: $n=5$, $\bar{\rho}=0.14\pm0.03$; Figure 8A and 8B). In both networks the two values were significantly smaller than in control conditions (t test, leech: $p<0.05$, hippocampal: $p<0.05$). In leech networks, the spike per bin distribution, which was fitted by a lognormal distribution in normal conditions (Figure 8C, black trace), became either a Poisson distribution (Figure 8C, blue trace; 3/6, χ^2 test, $p>0.05$) or a lognormal distribution (3/6, χ^2 test, $p>0.05$) with a reduced skewness (between 40% and 60% of the control values, see Methods) as expected from a more uniform activity with less bursts. Similarly, in hippocampal networks, the skewness of the lognormal function decreased significantly (between 5% and 20% of the control values; black and blue trace in Figure 8D).

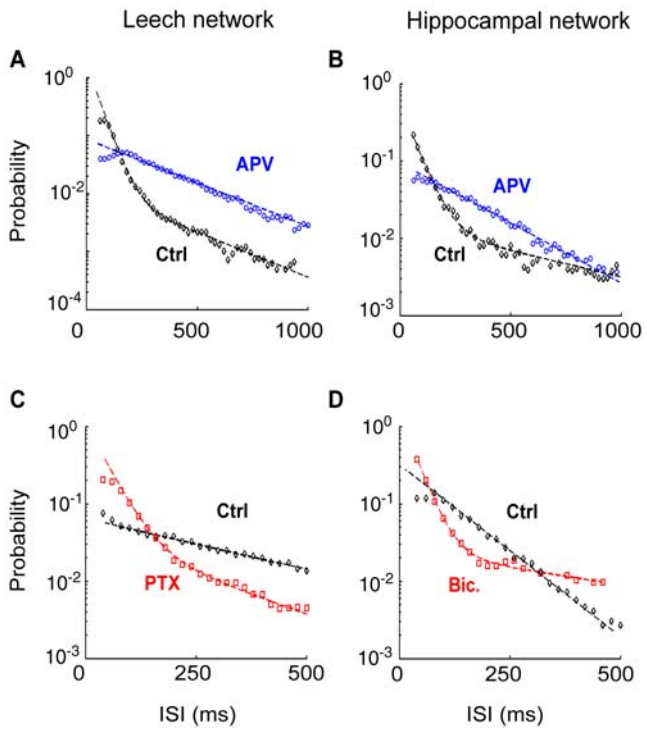

Figure 7. Effects of synaptic blockers on single neurons dynamics. (A–B) Neurons from leech (A) and hippocampal (B) networks, having a bi-exponential ISI distribution in control (black trace), and an exponential ISI distribution in the presence of 20 μM APV (blue trace). (C–D) Neurons from leech (C) and hippocampal (D) networks, having an exponential ISI distribution in control (black trace), and a bi-exponential ISI distribution in the presence of 10 μM PTX (red trace, panel C) or bicuculline (red trace, panel D).
doi:10.1371/journal.pone.0000439.g007

In normal conditions, the firing rate power spectrum decreased as 1/f (Figure 8E and 8F, black traces) for frequencies between 0.1 and 1 Hz as shown above. In the presence of APV, the power spectrum was almost flat (Figure 8E and 8F, blue traces) at all analyzed frequencies (leech: $n=6$, slope between 0 and -0.2; hippocampal: $n=5$, slope between 0 and -0.4), as expected in the absence of correlation [26]. In contrast, when inhibitory pathways mediated by $GABA_A$ receptors were blocked (see Methods), we observed an increase of correlation (leech: $n=5$, $\bar{\rho}=0.22\pm0.05$, hippocampal: $n=5$, $\bar{\rho}=0.7\pm0.1$ see Figure 8A and 8B). This increase of correlation was significant in both networks (t test, leech: $p<0.05$, hippocampal: $p<0.05$) and also modified the shape of the power spectrum, leading to a broad peak at low frequencies (Figure 8E and 8F, red trace; leech, $n=5$; hipp, $n=5$). In the presence of bicuculline the firing rate power spectrum of hippocampal networks exhibited a pronounced peak at frequencies between 0.2 and 0.6 Hz, while PTX in leech networks increased the power associated to frequencies between 0.1 and 0.3 Hz.

These results show that excitatory synaptic pathways mediated by NMDA receptors increase firing correlation of both networks, and that inhibitory synaptic pathways mediated by $GABA_A$ receptors have an opposite effect.

Spontaneous bursting activity

Power law dynamics and long-range interactions have been found in *in vitro* cortical cultures [16], and in the propagation of spontaneous local field potentials in organotypic and acute cortical slices [27,28]. We investigated whether the burst size and the burst duration distributions in leech and hippocampal networks also followed a power law distribution. Since there is no standard way to define a burst, we have used three different definitions (1, 2 and 3, see Methods). The definitions are based on the analysis of the ISI and on the network average firing rate. In Definition 1, the network ISI distribution is fitted with a bi-exponential function, leading to two characteristic time scales: the short time scale corresponding to the activity during the bursts, and the long time

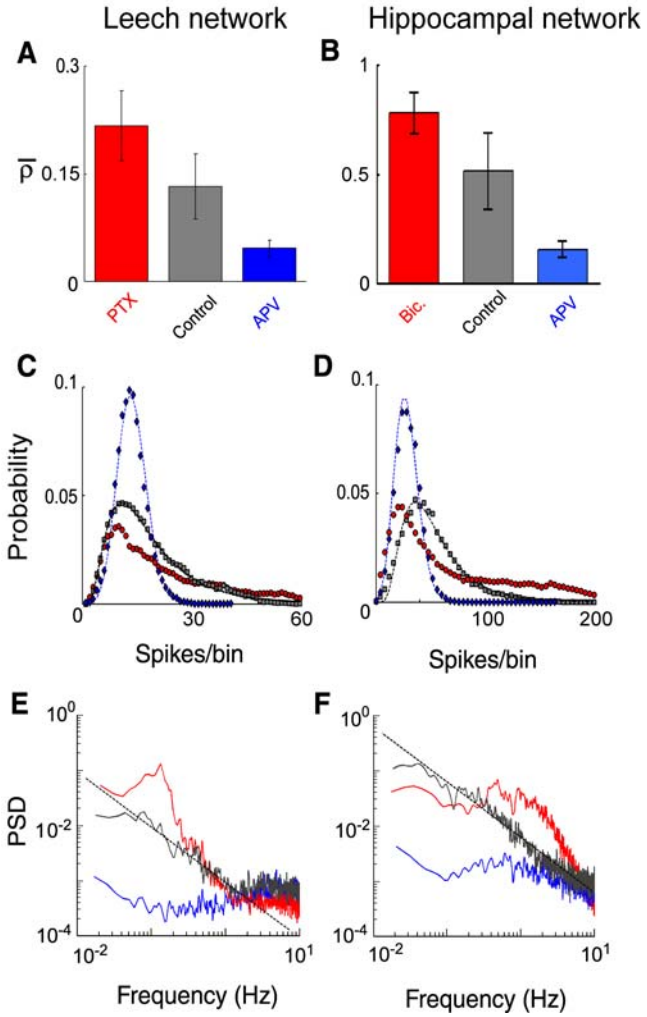

Figure 8. Effects of synaptic blockers on network correlation. (A–B) Network correlation coefficient rate in leech (A) and hippocampal (B) networks in the different pharmacological conditions considered. (C–D) Spikes per bin distribution of the network firing rate in leech (C) and hippocampal (D) networks. Data were fitted by a lognormal function in normal conditions (grey symbols). In the presence of 20 μM APV (blue symbols) data were fitted by a Poisson distribution for the leech network and by a lognormal distribution for the hippocampal network. Note the reduction of skewness in the presence of APV in both preparations (see text). Red symbols correspond to spike per bin distribution in the presence of 10 μM PTX (C) and bicuculline (D). (E–F) PSD of the network firing rate in control (black trace), in the presence of APV (blue trace), PTX (E, red trace) or bicuculline (F, red trace). Black dashed lines have 1/f slope.
doi:10.1371/journal.pone.0000439.g008

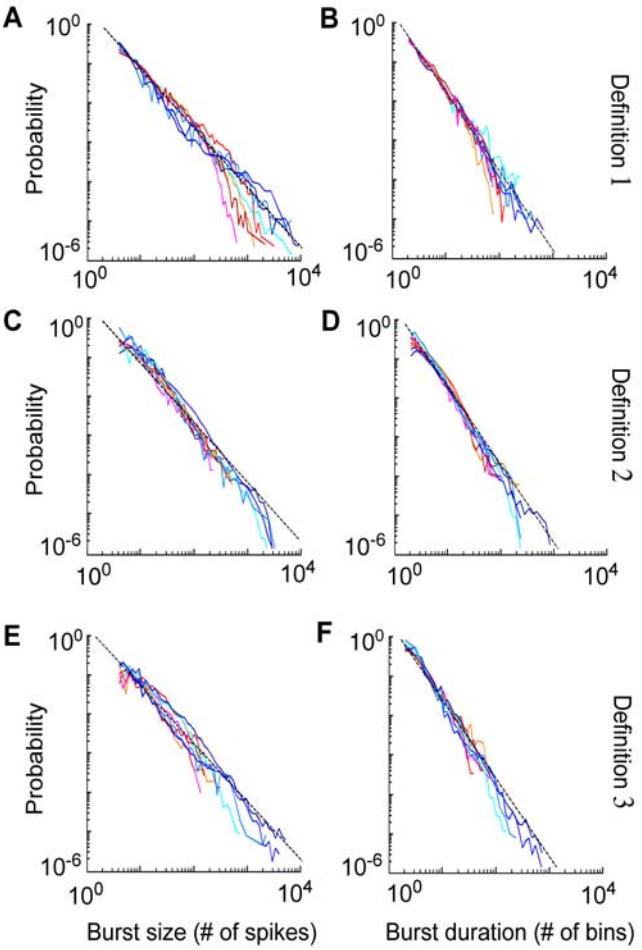

Figure 9. Burst statistics. Probability distributions of burst size and duration computed according to 3 different burst definitions. Data from representative experiments obtained in leech (reddish lines) and hippocampal networks (bluish lines). Bursts size (on the left) and duration (on the right) distributions are calculated according to definition 1 (A, B), definition 2 (C, D), and definition 3 (E, F). Black dashed lines are power laws with a slope of −1.5 in the left column and −2 in the right column. Note the power law behavior of bursts size distribution of hippocampal networks for 3 log units.
doi:10.1371/journal.pone.0000439.g009

scale to the inter-burst activity. Bursts are then identified by strips of bins where the network firing rate is two times higher than the inter-burst average firing rate. Definition 2 identified bursts as collections of spikes separated by an interval smaller than the average ISI. Definition 3 identified bursts by strips of bins where the network firing rate is above its average, similarly to the procedure used in [27,28]. Results were largely independent of the definition adopted.

For leech networks and for the three burst definitions, the distributions of the bursts size and bursts duration (see shades of red in Figure 9) followed a power law over two log units. In hippocampal networks (see shades of blue in Fig. 9), where we recorded the activity of a number of neurons approximately 10 times higher than in leech networks (see Methods), we could verify power law behavior over an extended range. As shown by the blue shaded lines, the distribution of bursts size and bursts duration had a power law distribution over three log units. The average slope of the bursts size distribution (Figure 9A, 9C and 9E) was -1.6 ± 0.2 (Def. 1), -1.55 ± 0.2 (Def. 2), and -1.6 ± 0.2 (Def. 3) for leech networks ($n=15$) and -1.55 ± 0.2 (Def. 1), -1.65 ± 0.2 (Def. 2), and -1.6 ± 0.2 (Def. 3) for hippocampal networks ($n=10$). We also verified that the duration distribution of the bursts followed a power law distribution (Figure 9B, 9D and 9F) and we found an average slope of -2.1 ± 0.2 (Def. 1), -2.2 ± 0.2 (Def. 2), -2.1 ± 0.2 (Def. 3) for leech networks ($n=15$) and -2.1 ± 0.1 (Def. 1), -2.15 ± 0.2 ((Def. 2), -2.1 ± 0.2 (Def. 3) for hippocampal networks ($n=10$). The statistics of bursts obtained with the three definitions was not significantly different (ANOVA, $p>0.05$ for both leech and hippocampal networks). However, definition 1 was able to characterize bursts over a more extended range and it was therefore used for later analysis.

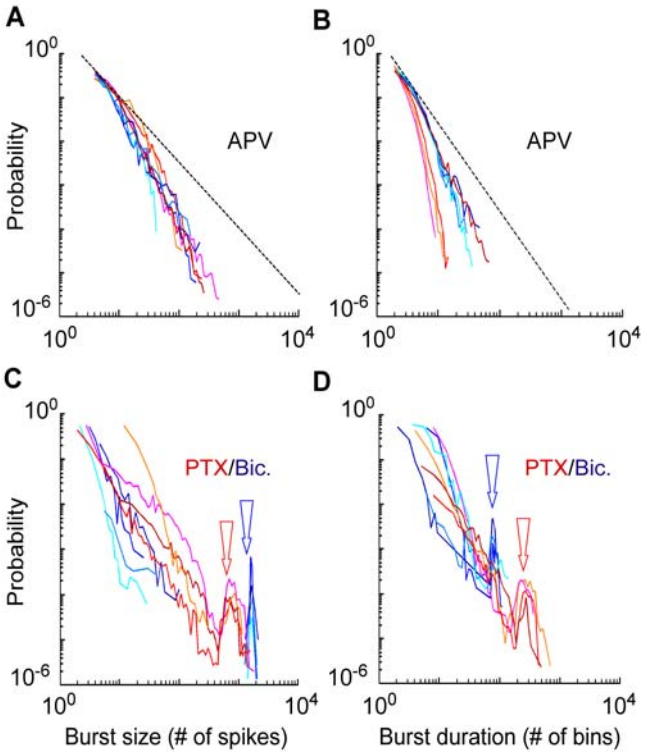

Figure 10. Bursts statistics in the presence of synaptic blockers. Bursts size and duration distributions for leech (reddish lines) and hippocampal (bluish lines) networks obtained using burst definition 1. (A–B) In the presence of APV, the number of large bursts decreased. The black dashed line has a slope of −1.5 in (A) and of −2 in (B), as in the right and left column of Figure 9, respectively. (C–D) In the presence of $GABA_A$ receptor blockers (PTX/bicuculline), peaks corresponding to large bursts appeared (indicated by the arrows). Traces were shifted to superimpose peaks of each preparation. In hippocampal networks, intermediate size bursts are absent as shown by the discontinuity of the distributions.
doi:10.1371/journal.pone.0000439.g010

As changing the balance of excitation and inhibition significantly affected the degree of correlated firing among neurons, we analyzed how pharmacological modulations of excitation and inhibition modified the distribution of bursts size and duration.

In the presence of APV, distributions of bursts size and duration (Figure 10A and 10B) of leech (shades of red) and hippocampal (shades of blue) networks were concave and did not follow a power law. In contrast, in the presence of PTX or bicuculline, very large bursts became more frequent, as indicated by the presence of a peak in the burst size and duration distributions (arrows in Figure 10C and 10D). In these conditions the probability of finding bursts of intermediate size was close to zero.

These results show that when synaptic pathways mediated by NMDA receptors are blocked, and the excitatory interaction among neurons is reduced, both networks enter a regime where large bursts are absent. In contrast, blockage of inhibitory $GABA_A$ synaptic pathways drives the networks towards a regime showing large and highly synchronous bursts.

DISCUSSION

The present study provides a detailed analysis of the spontaneous activity in two very different neuronal networks: intact leech ganglia and dissociated cultures of rat hippocampal neurons. Bursts of spontaneous spikes were observed in both neuronal networks. Despite their different origin and connectivity, several properties of spontaneous firing were present in both neuronal networks, indicating that these properties could be general features of the spontaneous activity dynamics.

Statistical properties of the spontaneous activity

The spontaneous activity of leech and hippocampal networks, analyzed in the present manuscript, was primarily composed of irregular and arrhythmic bursts of spikes (Figure 1). These spontaneous spikes were poorly correlated when they were counted on small bin widths of tens of milliseconds. However, in both networks, the degree of correlation increased when larger bin widths of some hundreds of milliseconds were considered (Figure 2). This observation indicated the existence of temporal correlation on long time scales in both networks. Indeed the power spectrum of the network firing rate had significant components below 1 Hz, displaying a 1/f behavior in this range (Figure 5). These results are in agreement with previous analysis of cultured cortical networks [16] describing long-lasting correlation of the spontaneous activity.

The ISI distribution of the spontaneous firing of single neurons (Figure 3) was either exponential or bi-exponential or with a pronounced peak comprised between 100 and 400 ms (see Table 1). An exponentially distributed ISI was consistent with a Poisson process controlling spontaneous firing [21], whereas an ISI distribution with a pronounced peak indicated the presence of episodes of almost periodic firing. When the overall activity of the network increased, most neurons showed a bursting dynamics in which intervals of intense firing were alternated with less active periods (Figure 4 and 7). This bursting dynamics was characterized by an ISI with a bi-exponential distribution. Shifts between periodic or Poissonian firing and bursting activity produced by synaptic inputs are well known [29], and have been extensively studied in leech heartbeat interneurons [30].

The power spectra of single neuron firing could have different shapes (Figure 5A and 5B) consistent with the different ISI distributions. However, when the overall firing of the network was considered (Figure 5C and 5D) in both networks - and in all preparations - the same 1/f behavior was observed. Taken together, these observations showed that global properties of neuronal networks average specific properties of individual neurons.

The probability distributions of size and duration of bursts in both networks (see Figure 9) had a power law behavior with slopes close to −3/2 and −2 respectively.

A similar network activity dynamics is described by the Self-Organized Criticality (SOC) paradigm [31–33]. SOC models display long-range correlations like those of Figs 2 and 5 and when the interaction strength in SOC networks is increased or decreased, their activity distributions are very similar to the bursts distributions displayed in Figure 10. Neuronal activity was described in the SOC framework in human electroencephalogram [34,35] (but see also [36]) and in local field potentials from cultured and acute cortical rat slices [27], but this is the first time to our knowledge that similar phenomena are found: i - at the spike level, ii - in a random neuronal network and iii - in a invertebrate network. The SOC paradigm is an interesting descriptive model for spontaneous bursts, but does not offer insights into their biological origin and into their functional role.

Origin of the spontaneous activity

Blockage of excitatory and inhibitory synaptic pathways produced very similar effects in both networks providing some hints of the synaptic origin of the observed bursts.

Since the spontaneous bursting activity was determined by network interactions, altering the balance between excitation and inhibition caused a transition towards diverse bursting regimes. In both networks, blockage of excitatory postsynaptic potentials (EPSPs) mediated by NMDA receptors with APV reduced the degree of correlation of the spontaneous activity (Figure 8) and the occurrence of large bursts (Figure 10). Not only were networks' bursts suppressed, but also single neuron's bursts (Figure 7), supporting the finding that the single neuron behavior depends on the global correlation (Figure 4). The prominent effect of APV was unexpected in leech networks, as most of the known glutamate receptors in the leech are non-NMDA [37,38]. However, when we applied the selective antagonist APV (see Methods) we always obtained a clear reduction of the bursting activity (Figure 6A, blue trace), suggesting that NMDA receptors are present in the leech ganglion [39]. These experimental observations indicate that excitatory synaptic pathways mediated by NMDA receptors are necessary for the correlated activity and for the presence of bursts in both networks; indeed EPSP mediated by NMDA receptors have a slow decay kinetics with a time constant of some hundreds of milliseconds [40,41], providing the biophysical mechanism for sustained and correlated firing on longer time scales [42] (see Figure 2).

On the other hand, when inhibitory $GABA_A$ synaptic pathways were blocked, a highly bursting regime appeared, with a bi-stable dynamics alternating large bursts with silent periods (Figure 6 and 10), single neurons started to burst (Figure 7) and the correlation of their activity increased (Figure 8). The spontaneous bursts became larger as excitation spread in the network more easily. In this regime, bursts duration was expected to be determined by intrinsic properties of excitatory synapses such as synaptic depletion [43,44] and inactivation of voltage-gated currents [45]. As a consequence, the duration of the bursts became more stable (see peaks in Figure 10C and 10D).

In normal conditions, long lasting EPSP were balanced by inhibitory synaptic inputs and bursts were then likely to be terminated by inhibitory inputs that cause a propagation failure of the activity [46]: burst duration depended on the excitation/inhibition interplay in the whole network and could have a broad range of values (Figure 9). In the presence of APV, inhibition was predominant thus reducing the burst duration. Inactivation of voltage-gated currents [45] could as well influence the burst duration and time course in these two regimes.

Based on these results we propose a common mechanism for the spontaneous bursting activity of both networks: i - neurons fire spontaneously according to a Poisson process; ii - the spontaneous firing of these neurons activates long lasting EPSP, mediated by NMDA receptors, initiating a burst; iii - these bursts spread in the networks and are terminated, by the combination of several mechanisms, as discussed above. A mathematical model of these mechanisms and a comparison with experimental data is in preparation and will be presented elsewhere.

In this work we analyzed an intact and functional invertebrate network, and a dissociated mammalian neuronal network. A leech ganglion contains approximately 400 neuronal somata, as well as axonal projections from other ganglia, whereas between 10 and 100 thousand neurons form the investigated hippocampal cultures. More importantly, the leech ganglion is a hierarchical neuronal network and the hippocampal culture is a random neuronal network. In dissociated cultures, the original cytoarchitectural organization is lost during the dissociation and neurons re-wire with random connections. In contrast, leech ganglia retain a specific internal structure suitable for specific behaviors, structured for instance in mechanosensory neurons, interneurons and motoneurons. Our results showed that most features of the spontaneous activity were nonetheless shared between the two networks. This suggests that some synaptic interactions among neurons are sufficient to determine a global behavior, poorly dependent on the specific wiring of the network itself. In this view, the wiring of leech networks becomes evident when specific behaviors, such as swimming [47,48], or crawling [49,50] are initiated by sensory stimuli and/or command neurons [5].

The spontaneous activity in leech and hippocampal networks was not entirely similar and some features distinguished the functional leech network. The degree of correlated activity in leech networks was significantly lower than that observed in hippocampal networks (Figure 2). The dynamics of single neurons were also very different: the fraction of single neurons with a bi-exponential ISI distribution was approximately 70% in hippocampal networks and only 35% in leech networks, while the periodic neurons were 11% and 27%, respectively. Despite these differences, the similarity in the statistical properties of the spontaneous bursting activity between leech and hippocampal networks was remarkable.

Functional role of the spontaneous activity

Spontaneous bursts play a fundamental role during neuronal development [8]. In this early phase, chloride mediated neurotransmission is excitatory [51], so the spontaneous activity is intense and in the form of long-lasting bursts alternated by periods of quiescent activity, due to the hyper excitable nature of the networks. Intense spontaneous activity is essential for the development of the functional architecture of neuronal networks [52–54] and for the incorporation of newly born neurons in the adult nervous system [55]. Spontaneous bursts of electrical activity of developing neurons are not only important for the refinement of neuronal projections but are also necessary for finding the correct pathways [56]. The developmental mechanisms are sensitive to activity in the time scale of several hundreds of milliseconds, and the unit of information at this stage could consequently be the burst rather than the single spike [57].

Large bursts are associated with an unblockage of NMDA receptors [58], causing a large influx of Ca^{2+} ions inside the cytoplasm [59]. This Ca^{2+} influx initiates a variety of intracellular signalling pathways, possibly also involving changes of gene expression [60,61]. In this view, bursts of spikes have the major function of triggering fundamental biological process.

The spontaneous activity during development is also able to modulate both excitatory and inhibitory synaptic efficacy [10], thus setting the balance between inhibition and excitation present in adult neuronal networks [62]. Therefore, the interplay between growth and efficacy of neuronal connections and spontaneous activity seems to determine general features of the spontaneous activity of neuronal networks with different architectures, like those described in this work.

Global dynamical properties of the spontaneous activity of different networks can be very similar, but their neurobiological functions are expected to be different. The presence of large bursts and strong correlation impairs information processing, and indeed in dissociated hippocampal networks, a reduced spontaneous activity and a lower degree of correlation decrease response variability to the same stimulation and increase correlation between stimulus and response [63]. In intact animals large spontaneous bursts could instead have an important role acting as internal triggers in the initiation of movements, also in the absence of external stimulation [64,65]. In fact, large bursts of spontaneous activity are statistically related to the initiation of motion in resting leeches (Garcia-Perez et al., in preparation).

As different dynamical regimes seem more suitable for different functions, it is very useful to drive a neuronal network from one regime to another. These transitions can be achieved by modifying the balance between excitation and inhibition by means of neuromodulators [66] and can also occur during development, when $GABA_A$ mediated synaptic potential reverse polarity and pass from excitatory to inhibitory [67]. The spontaneous activity pattern strongly influences neuronal networks' information processing [68], and thus modulation of neuronal networks' spontaneous activity is likely to be a basic feature of neural computation [69], essential for tuning the function of neuronal networks.

MATERIALS AND METHODS

Physiology

Leech preparations Adult leeches *Hirudo medicinalis* were obtained from Ricarimpex and kept at 5°C in tap water dechlorinated by aeration for 24 hours. Leech ganglia were isolated as previously described [70] and the roots emerging from the exposed ganglion were cleaned for suction pipette recordings [71]. In each experiment we recorded from 6–8 roots the activity of 15 to 25 motoneurons. All preparations were kept in a Sylgard-coated dish at room temperature (20–24°C) and bathed in Ringer solution (in mM: 115 NaCl, 1.8 $CaCl_2$, 4 KCl, 12 glucose, 10 Tris maleate buffered to pH 7.4) [70].

Hippocampal cultures Hippocampal neurons were obtained from Wistar rats (P0–P2) and plated on 60-channel multielectrode array (MEA, MultiChannelSystems) enabling extracellular recordings as previously described [20,63]. As it was possible to sort spikes from 1 to 5 neurons for an individual electrode, we were able to record the activity of a maximum of 300 neurons. The age of the cultures varied from 22 to 35 days *in vitro*. Extracellular recordings were digitized at 10 or 25 kHz, and recorded with MCRack (MultiChannelSystems, Reutlingen, Germany).

Pharmacological manipulations To reduce the excitation in the two neuronal networks, we bath-applied the non-competitive NMDA receptor antagonist 2-amino-5-phosphonopentanoic acid (APV) (final concentration, 20 μM; TOCRIS). To reduce inhibition, we bath-applied the ionotropic $GABA_A$ receptors antagonists picrotoxin (PTX, final concentration, 10 μM; Sigma) and bicuculline (final concentration, 10 μM; Sigma) to leech ganglia and to hippocampal dissociated cultures, respectively.

Data Analysis

Acquired data were analyzed using MATLAB (The Mathworks,Inc.).

Spike sorting Spike sorting was carried out using principal component analysis and a custom software [71] for leech networks and open source MATLAB toolboxes for the analysis of multielectrode data [72] for hippocampal networks.

In some experiments it was necessary to identify neurons to find changes in their dynamics due to pharmacological manipulation. We identified the neurons assuming that the relative action potential amplitude was not affected by these modulations. In both preparations, for each electrode, the behavior of the neurons producing the two or three largest action potentials was analyzed in control conditions and in the presence of drugs.

The position of most motoneurons in the leech ganglion is known [70]. Thus it was possible to simultaneously record intracellularly from specific motoneurons and extracellularly from the roots. Motoneurons 3 and 107 reliably produced the largest action potentials in the dorsal posterior and anterior anterior roots, respectively. Thanks to this, we could compare the activity of these identified neurons in different preparations.

Network firing rate The duration of the recording was divided into bins of constant width. Different widths were used to compare properties at different time scales. For each single neuron the number of spikes occurring in each bin was counted and the resulting discrete time series represented the *neuron firing rate*. The *network firing rate* was defined as the sum of all neuron firing rates (i.e. the number of all spikes recorded in the network from each bin).

In both preparations more than one electrode can record the activity of the same neuron. In the leech, some motoneurons project their axons in more than one root. To avoid double recording, spikes separated by less than 2 ms, occurring in different roots of the same side, were counted as a single spike in the network firing rate. MEA can record the activity of a single neuron in several sites, but we estimate that this has a low probability to occurr, as the spatial density of the electrodes is low (inter-electrode distance = 500 μm).

Spike per bin distribution The probability distribution *P(S)* of the number of spikes S per bin of the network firing rate was fitted either by a Poisson or by a lognormal function:

$$P(S) = \frac{1}{S\sqrt{2\pi}\sigma}\exp\left[-\frac{(\ln S-\mu)^2}{2\sigma^2}\right]$$

where μ and σ are the mean and the variance of the distribution of the logarithm of *S*.

Skewness The skewness of a distribution, a measure of the degree of asymmetry, is defined as:

$$\gamma_1 = \frac{\bar{\mu}_3}{\bar{\mu}_2^{3/2}}$$

where $\bar{\mu}_i$ is the i-*th* central moment of the distribution [26].

Firing rate power spectrum The power spectral density of the network firing rate obtained with a bin width of 10 ms was computed by using Welch's averaged modified periodogram method (*pwelch* function in Matlab) after a low pass filtering with a cut-off frequency of 25 Hz to prevent aliasing.

Network correlation coefficient For each pair (i,j) of neurons the correlation coefficient [26] $\rho_{i,j}$

$$\rho_{ij} = \frac{\sum_n (FR_i(n) - <FR_i>)(FR_j(n) - <FR_j>)}{\sqrt{<(FR_i(n) - <FR_i>)^2> \cdot <(FR_j(n) - <FR_j>)^2>}}$$

of the neuron firing rates *FR(n)* was computed in a bin width varying from 20 to 1000 ms. $\rho_{i,j}$ was then averaged over all pairs to obtain the *network correlation coefficient* $\bar{\rho}$.

Burst definitions As there is no standard definition of *burst*, we considered three alternative definitions.

Definition 1 : The distribution of inter-spike intervals (ISI) between successive spikes in the network was computed and fitted by a bi-exponential function:

$$P(ISI = t) = C_1 e^{-t/\tau_{long}} + C_2 e^{-t/\tau_{short}}$$

where C_1 and C_2 are two constants and τ_{short} and τ_{long} are a fast and a slow time constant, respectively. The network firing rate with a bin width equal to τ_{long} was calculated and strips of adjacent bins, each counting more than two spikes, were considered as bursts.

Definition 2: a burst was identified as an ensemble of consecutive spikes separated by a time interval smaller than the average inter-spike interval (ISI). ISI varied from 2 to 20 ms for hippocampal networks and from 10 to 50 ms for leech networks.

Definition 3: the network firing rate with a bin width equal to ISI was calculated, as well as its average value. A burst was identified in the network firing rate as a strip of adjacent bins in which each bin has a number of spikes higher than the average firing rate (see [27,28]).

For the three burst definitions, only bursts containing more than three spikes were considered. The *burst size* is the total number of spikes within the burst, and its *duration* is the time interval between the first and the last spike of the burst.

ACKNOWLEDGMENTS

We thank G. Bianconi for her comments, G. Pastore for preparing some of the hippocampal cultures and M. Lough for carefully reading the manuscript.

Author Contributions

Conceived and designed the experiments: AM VT FB MR EG PB. Performed the experiments: AM FB MR EG PB. Analyzed the data: AM VT FB EG PB. Wrote the paper: AM VT FB MR EG PB.

REFERENCES

1. Raichle M (2006) The brain dark energy. Science 314: 1249–1250.
2. Marder E, Calabrese RL (1996) Principles of rhythmic motor pattern generation. Physiol Rev 76: 687–717.
3. Calabrese RL, Nadim F, Olsen OH (1995) Heartbeat control in the medicinal leech: a model system for understanding the origin, coordination and modulation of rhythmic motor patterns. J Neurobiol 27: 390–402.
4. Bianchi AL, Denavit Saubie M, Champagnat J (1995) Central control of breathing in mammals: neuronal circuitry, membrane properties, and neurotransmitters. J Am Phys Soc 75: 1–4.
5. Kristan WB Jr, Calabrese RI, Friesen WO (2005) Neuronal control of leech behavior. Prog Neurobiol 76: 279–327.
6. Grillner S (2003) The motor infrastructure: from ion channels to neuronal networks. Nat Rev Neurosci 4: 573–586.
7. Krahe R, Gabbiani F (2004) Burst firing in sensory systems. Nat Rev Neurosci 5: 13–23.
8. O'Donovan MJ (1999) The origin of spontaneous activity in developing networks of the vertebrate nervous system. Curr Opin Neurobiol 9: 94–104.
9. Leinekugel X, Khazipov R, Cannon R, Hirase H, Ben-Ari Y, Buszaki G (2002) Correlated bursts of activity in the neonatal hippocampus *in vivo*. Science 296: 2049–2053.
10. Gonzales-Islas C, Wenner P (2006) Spontaneous network activity in the embryonic spinal cord regulates AMPAergic and GABAergic synaptic strength. Neuron 29: 563–575.
11. Zohary E, Shadlen MN, Newsome WT (1994) Correlated neuronal discharge rate and its implications for psychophysical performance. Nature 370: 140–143.
12. Arieli A, Sterkin A, Grinvald A, Aertsen A (1996) Dynamics of ongoing activity: explanation of the large variability in evoked cortical responses. Science 273: 1868–1871.
13. Azouz R, Gray CM (1999) Cellular mechanism contributing to response variability of cortical neurons *in vivo*. J Neurosci 19: 2209–2223.
14. Chiu C, Weliki M (2001) Spontaneous activity in developing ferret visual cortex *in vivo*. J Neurosci 21: 8906–8914.
15. Fiser J, Chiu C, Weliky M (2004) Small modulation of ongoing cortical dynamics by sensory input during natural vision. Nature 431: 573–578.
16. Segev R, Benveniste M, Hulata E, Cohen N, Palevski A, et al. (2002) Long term behavior of litographically prepared in vitro neuronal networks. Phys Rev Lett 88: 118102 1–4.
17. Shadlen MN, Newsome WT (1994) Noise, neural codes and cortical organization. Curr Opin Neurobiol 4: 569–579.
18. Canepari M, Bove M, Maeda E, Cappello M, Kawana A (1997) Experimental analysis of neuronal dynamics in cultured cortical networks and transitions between different patterns of activity. Biol Cybern 77: 153–162.
19. Kudela P, Franaszczuzuk PJ, Bergey GK (2003) Changing excitation and inhibition in simulated neural networks: effects on induced bursting behavior. Biol Cybern 88: 276–285.
20. Ruaro ME, Bonifazi P, Torre V (2005) Toward the neurocomputer: image processing and pattern recognition with neuronal cultures. IEEE Trans Biomed Eng 52: 371–383.
21. Rieke F, Warland D, de Ruyter van Steveninck R, Bialek W (1997) Spikes. Exploring the Neural Code. Cambridge (MA): MIT Press.
22. Crow EL, Shimitzu K (1987) Lognormal Distributions. New York: Marcel Dekker.
23. Limpert EL, Stahel WA, Abbt M (2001) Log-normal distributions across the sciences: keys and clues. BioSci 51: 341–351.
24. Cline HT (1986) Evidence for GABA as a neurotransmitter in the leech. J Neurosci 6: 2848–2856.
25. Traub RD, Jefferys JG (1994) Are there unifying principles underlying the generation of epileptic afterdischarges in vitro? Prog Brain Res 102: 383–94.
26. Papoulis A (1984) Probability, Random Variables, and Stochastic Processes 2nd ed. New York: McGraw-Hill.
27. Beggs JM, Plenz D (2003) Neuronal avalanches in neocortical circuits. J Neurosci 23: 11167–11177.
28. Beggs JM, Plenz D (2004) Neuronal avalanches are diverse and precise activity patterns that are stable for many hours in cortical slice cultures. J Neurosci 24: 5216–5229.
29. Turrigiano G, Abbott LF, Marder E (1994) Activity-dependent changes in the intrinsic properties of cultured neurons. Science 264: 974–977.
30. Cymbaluk GS, Gaudry Q, Masino MA, Calabrese RL (2002) Bursting in leech heart interneurons: cell-autonomous and network-based mechanisms. J Neurosci 22: 10580–10592.
31. Bak P, Tang C, Wiesenfeld K (1988) Self-organized criticality. Physical Review A: Atomic, Molecular, and Optical Physics 38: 364–374.
32. Jensen HJ (1998) Self-Organized Criticality – Emergent Complex Behavior in Physical and Biological Systems. Cambridge: Cambridge University Press.
33. Vespignani A, Zapperi Z (1998) How self organized criticality works: a unified mean field picture. Physical Review E: Statistical, Nonlinear, and Soft Matter Physics 57: 6345–6363.
34. Linkenkaer-Hansen K, Nikouline VV, Palva JM, Ilmoniemi RJ (2001) Long range temporal correlations and scaling behavior in human brain oscillations. J Neurosci 21: 1370–1377.
35. Freeman WJ (2004) Origin, structure, and role of background EEG activity. Part 2. Analytic phase. Clin Neurophysiol 115: 2089–2107.
36. Bedard C, Kroger H, Destexhe A (2006) Does the 1/f frequency scaling of brain signals reflect self-organized critical states? Phys Rev Lett 97: 118102 1–4.
37. Thorogood MS, Brodfuehrer PD (1995) The role of glutamate in swim initiation in the medicinal leech. Invert Neurosci 1: 223–233.
38. Wu E (2002) Evidence against the presence of NMDA receptors at a central glutamatergic synapses in leeches. Invert Neurosci 4: 157–164.
39. Burrell BD, Sahley CL (2004) Multiple forms of Long-Term Potentiation and Long-Term-Depression converge on a single interneuron in the leech CNS. J Neurosci 24: 4011–4019.
40. Hestrin S, Nicoll RA, Perkel DJ, Sah P (1990) Analysis of excitatory synaptic action in pyramidal cells using whole-cell recording from rat hippocampal slices. J Physiol (Lon) 422: 203–225.
41. Koch C (1999) Biophysical computation. Oxford: Oxford University Press.
42. Wang XJ (1999) Synaptic basis of cortical persistent activity: the importance of NMDA receptors to working memory. J Neurosci 19: 9587–9603.
43. Stevens CF, Tusjimoto T (1995) Estimates for the pool size of releaseble quanta at a single central synapse and for the time required to refill the pool. Proc Natl Acad Sci USA 92: 846–849.
44. Staley KJ, Longacher M, Bains JS, Yee A (1998) Presynaptic modulation of CA3 network activity. Nat Neurosci 1: 201–209.
45. Franklin JL, Fickbohm DJ, Willard AL (1992) Long-term regulation of neuronal calcium currents by prolonged changes of membrane potential. J Neurosci 12: 1726–1735.
46. Maeda E, Robinson HP, Kawana A (1995) The mechanisms of generation and propagation of synchronized bursting in developing networks of cortical neurons. J Neurosci 15: 6834–6845.
47. Brodfuehrer PD, Friesen WO (1986) Control of leech swimming activity by the cephalic ganglia. J Neurobiol 17: 697–705.
48. Brodfuehrer PD, Thorogood MSE (2001) Identified neurons and leech swimming behavior. Prog Neurobiol 63: 371–381.
49. Cacciatore TW, Rozenshteyn R, Kristan WB (2000) Kinematics and modelling of leech crawling: evidence for an oscillatory behavior produced by propagating waves of excitation. J Neurosci 20: 1643–1655.
50. Eisenhart FJ, Cacciatore TW, Kristan WB (2000) A central pattern generator underlies crawling in the medicinal leech. J Comp Physiol A 186: 631–643.
51. Ben Ari Y, Cherubini E, Corradetti R, Gaiarsa JL (1989) Giant synaptic potentials in immature rat CA3 hippocampal neurones. J Physiol 416: 303–325.
52. Jones TA, Jones SA (2000) Spontaneous activity in the statoacoustic ganglion of the chicken embryo. J Neurophysiol 83: 1452–1468.
53. Baker RE, Corner MA, van Pelt J (2006) Spontaneous neuronal discharge patterns in developing organotypic mega-co-cultures of neonatal rat cerebral cortex. Brain Res 1101: 29–35.

54. Huberman DA, Speer MC, Chapman B (2006) Spontaneous Retinal Activity Mediates Development of Ocular Dominance Columns and Binocular Receptive Fields in V1. Neuron 52: 247–254.
55. Spitzer NC (2006) Electrical activity in early neuronal development. Nature 444: 107–172.
56. Hanson MG, Landmesser LT (2006) Increasing the frequency of spontaneous rhythmic activity disrupts pool-specific axon fasciculation and pathfinding of embryonic spinal motoneurons. J Neurosci 49: 12769–12780.
57. Butts DA, Rokhsar DS (2001) The information content of spontaneous retinal waves. J Neurosci 27: 961–973.
58. Bliss TVP, Collingridge GL (1993) A synaptic model of memory: long-term potentiation in the hippocampus. Nature 361: 31–39.
59. Van Pelt J, Wolters PS, Corner MA, Rutten WLC (2004) Long-term characterization of firing dynamics of spontaneous bursts in cultured neural networks. IEEE Trans Biom Eng 11: 2051–2062.
60. Arnold FJ, Hofmann F, Bengston CP, Wittmann M, Vanhoutte P, Bading H (2005) Microelectrode array recordings of cultured hippocampal networks reveal a simple model for transcription and protein synthesis-dependent plasticity. J Physiol 564: 3–19.
61. West AE, Chen WG, Dalva MB, Dolmetsch RE, Kornhauser JM, et al. (2001) Calcium regulation of neuronal gene expression. Proc Natl Acad Sci USA 98: 11024–11031.
62. Haider B, Duque A, Hasenstaub AR, McCormick DA (2006) Neocortical activity *in vivo* is generated trough a dynamic balance of excitation and inhibition. J Neurosci 26: 4535–4545.
63. Bonifazi P, Ruaro ME, Torre V (2005) Statistical properties of information processing in neuronal networks. Eur J Neurosci 22: 2953–2964.
64. Lee IH, Assad JA (2003) Putaminal activity for simple reactions or self-timed movements. J Neurophysiol 89: 2528–2537.
65. Maimon G, Assad JA (2006) Parietal area 5 and the initiation of self time-movements versus simple reactions. J Neurosci 26: 2487–2498.
66. Tateno T, Jimbo Y, Robinson HP (2005) Spatio-temporal cholinergic modulation in cultured networks of rat cortical neurons: spontaneous activity. Neuroscience 134: 425–437.
67. Cherubini E, Gaiarsa JL, Ben-Ari Y (1991) GABA: an excitatory transmitter in early postnatal life. Trends Neurosci 14: 515–519.
68. Destexhe A, Contreras D (2006) Neuronal computation with stochastic network states. Science 314: 85–90.
69. Marder E, Thirumalai V (2002) Cellular, synaptic and network effects of neuromodulation. Neural Netw 15: 479–493.
70. Muller KJ, Nicholls JG, Stent GS (1981) Neurobiology of the Leech. New York: Cold Spring Harbor Laboratory.
71. Arisi I, Zoccolan D, Torre V (2001) Distributed motor pattern underlying whole-body shortening in the medicinal leech. J Neurophysiol 86: 2475–2488.
72. Egert U, Knott TH, Schwarz C, Nawrot M, Brandt A, Rotter S, Diesmann, M (2002) MEA-Tools: an open source toolbox for the analysis of multi-electrode data with MATLAB. J Neurosci Meth 17: 33–42.

- 3.3 -

Sequential events underlying neuronal plasticity induced by a transient exposure to gabazine

Broccard FD, Pegoraro S, Ruaro ME, Pastore G, Avossa D, Bianchini D, Altafini C, Torre V

Submitted to the Journal of Physiology

Sequential events underlying neuronal plasticity induced by a transient exposure to gabazine

Running title: Neuronal plasticity and gene regulation

Frédéric D. Broccard[1], *Silvia Pegoraro*[1], *Maria Elisabetta Ruaro*[1], *Daniele Bianchini*[1], *Daniela Avossa*[1], *Giada Pastore*[1], *Claudio Altafini*[1] *and Vincent Torre*[1,2]

[1] International School for Advanced Studies- Area Science Park SS 14 Km 163.5 Edificio Q1 34012- Basovizza, Trieste (Italy), [2] Italian Institute of Technology (IIT)

Corresponding author:
Vincent Torre
Scuola Superiore di Studi Avanzati (SISSA)
Area Science Park, SS 14 Km 163.5, Edificio Q1
34012 Basovizza (TS), Italy
Phone: +39 040 3756513
Fax: +39 040 3756502
E-mail: torre@sissa.it

Number of figures and tables: 10
Supplementary material: Supplementary table 1
Number of pages: 45
Number of words: 6343
Keywords: network, plasticity, multielectrode array, gene expression, DNA microarray, electrical activity

Abstract

Periods of intense electrical activity can initiate neuronal plasticity leading to long lasting changes of network properties. By combining multielectrode extracellular recordings with DNA microarrays, we have investigated in rat hippocampal cultures the time course of neuronal plasticity triggered by a transient exposure to gabazine. The spontaneous electrical activity remained synchronized up to 24 h after gabazine washout and the evoked electrical activity was potentiated for several hours. An early component of synchronization (E-Sync) was blocked by PD98059 and UO126, inhibitors of the MAPK/ERK pathway, and a late component (L-Sync) was blocked by inhibitors of transcription. Potentiation of the evoked response was reduced but not abolished by PD98059. Gabazine exposure initiated significant changes of gene expression: several transcription factors were maximally up-regulated within 90 minutes, and more than 200 genes - many of which known to be involved in LTP - were up-regulated in the following 1-2 h. A down-regulation of some genes coding for K^+ and HCN channels was observed 24 h after treatment, possibly underlying L-Sync.

Introduction

When the electrical activity of neuronal networks is elevated, even transiently, several properties of synapses and neurons are modified. These changes provide the basis for long term memory (Goelet et al., 1986; Malenka and Nicoll 1999), which can be initiated by electrical stimulation with intracellular and/or extracellular electrodes (Bliss and Lomo, 1973). Bursts of electrical activity can also be induced by pharmacological manipulations, such as elevation of extracellular K^+ (Jensen and Yaari, 1997) or addition of drugs such as bicuculline (Arnold et al., 2005) and kainic acid (Westbrook and Lothman, 1983) or by elevation of the intracellular concentration of second messengers such as cAMP, using forskolin (Otmakhov et al., 2004). These phenomena, usually referred to as neuronal plasticity, are mediated by several signalling pathways leading to the modulation of synaptic strength, density of ionic channels and shape of neurons (Carlisle and Kennedy, 2006). On a time scale of a few minutes, neuronal plasticity is mediated by local protein trafficking, leading to the insertion or removal of proteins into and from the membrane (Lau and Zukin, 2007; Groc and Choquet, 2007). In order to sustain modifications beyond 2-3 h, changes of gene expression are required (Martin et al., 2000; Rao et al., 2006) occurring at different time scales: the mRNA of immediate early genes (c-fos, jun,….), increases within 15 minutes following glutamate application (Bading et al., 1993; Zhang et al., 2007) but other genes are up- or down-regulated at later times. Following intense electrical activity, transcription factors of the " Early Growth Response (EGR) " family such as the EGR1 mRNA and protein increase within 1-2 h, but changes of EGR3 are seen only after 2-4 h (O'Donovan et al., 1999). In order to unravel these complex events it is necessary to relate modifications of network electrical properties to concomitant protein and gene turnover and to understand the fine orchestration between local protein trafficking and timing of gene expression changes (Martin and Zukin, 2006; Tzingounis and Nicoll, 2006).

The present work aims to analyze the time course of neuronal plasticity and the concomitant changes of gene expression in cultures of hippocampal neurons from neonatal rats following a 30 minutes gabazine or bicuculline treatment. As bicuculline is known to block also SK K^+ channels (Khawaled et al., 1999), experimental results obtained primarily following gabazine treatment (GabT) are described. We used multi-electrode-

arrays (MEAs) on which the neuronal culture were grown (Arnold et al., 2005; Ruaro et al., 2005; Mazzoni et al., 2007). MEAs represent a non-invasive technique based on extracellular electrodes allowing electrical recordings lasting for several hours or even days. Changes of gene expression were followed with DNAchips and with real-time PCR analysis harvesting the mRNA at different times after GabT from networks in which the electrical activity was recorded.

Methods

Neuronal culture preparation.

Hippocampal neurons dissociated from Wistar rats (P0-P2) were plated on polyorhitine/matrigel pre-coated MEA at a concentration of 8 x 10^5 cells/cm^2 and maintained in a neuron medium as previously described (Ruaro et al., 2005). After 48 h, 5 μM cytosine-β-D-arabinofuranoside (Ara-C) was added to the culture medium in order to block glial cell proliferation. Neuronal cultures were kept in an incubator providing a controlled level of CO_2 (5%), temperature (37°C) and moisture (95%).

Electrical recordings and electrode stimulation.

Multi electrode array (MEA) recordings were carried out with a MEA60 system (Multi Channel Systems, Reutlingen, Germany). Stimulations and recordings were carried out after 21-35 days *in vitro*. Synchronous network bursting was induced by 30 min. treatment with $GABA_A$ receptor antagonists, such as bicuculline methiodide (50 μM) or gabazine (20 μM). $GABA_A$ antagonists were washed out by changing the medium three times. In some experiments, PD98059 (50 μM), U0126 (20 μM) or Actinomycin D (8 μM) were pre-incubated before application of a $GABA_A$ antagonist (see Results). In other experiments, K^+ channel blockers such as 4-aminopyridine (4-AP, 100μM), tetra-etylammonium chloride (TEA, 10mM), apamin (100nM), Heteropodatoxin 2 (HpTx2, 10μM) or arachidonic acid (AA, 40μM) or the inhibitor of HCN ZD7288 (100μM) were added to the cultures. AA was dissolved in Tocrisolve® and cultures were first treated with Tocrisolve® as negative control. Bicuculline methiodide, TEA and HpTx2 were obtained from Sigma-Aldrich (St. Louis, MO, USA); gabazine, PD98059, U0126, Actinomycin D, 4-AP and arachidonic acid were obtained from Tocris Cookson Ltd (Bristol, UK). The amplitude of the bipolar voltage pulse (200 μs) required to evoke an electrical response varied between 200 and 450 mV. Cultures were stimulated with a train of 40 bipolar pulses separated by an inter-pulse interval of 4s. The pattern of stimulation consisted of a bar of six neighbouring electrodes.

Data analysis.

Acquired data were analyzed using MATLAB (The Mathworks, Inc.) as previously described (Wagenaar and Potter, 2002; Ruaro et al., 2005). The *network firing rate (NFR)* is defined as the sum of all electrodes firing rates (i.e. the number of all spikes recorded in the network in each bin). The average network correlation, ρ, was computed by averaging the cross-correlation of individual pairs over all the possible pairs of electrodes as previously described (Mazzoni et al., 2007). The total number of spikes as a function of the distance d was fitted by the exponential function $Ae^{-d/\lambda}$ from which λ was obtained (inset Fig.3*G*).

RNA extraction.

The total RNA was extracted using TRIzol reagent (Sigma) according to the manufacturer's instructions followed by a DNase I (Invitrogen, Carlsbad, CA, USA) treatment to remove any genomic DNA contamination. The total RNA was further purified using RNeasy Mini Kit Column (Qiagen, Milan, Italy) and subsequently quantified by ND-1000 Nanodrop spectrophotometer (Agilent Technologies, Milan, Italy).

DNAchips analysis.

Neuronal cultures grown on MEA were treated for 30 minutes with 50 μM gabazine. Gabazine was removed and RNAs were extracted from cultures 1.5, 3, 6 and 24 h from start of GabT or from untreated cultures. Ten minutes of electrical recording was collected at each time point before harvesting RNAs. At each time point at least 3 biological replicates were collected and Standard Affymetrix protocols were applied for amplification and hybridization. Gene profiling was carried out with the Affymetrix RAT230_2 platform containing 31099 probes, corresponding to 14181 probes with a gene symbol. Low level analysis was performed using an RMA (Robust Multi-array Average) algorithm (Irizarry et al., 2003) directly on the scanned images. Because of high dimensionality, we removed

probe sets labeled as ambiguous and those without any gene symbol. The variance σ^2 of mean value of expression changes (in $\log_2$ units) relative to untreated controls was computed considering collectively samples collected at 1.5,3, 6 and 24 h after GabT. Genes with a variance σ^2 lower than 0.6 were filtered out. The profiles of the three Clusters evident in Fig.4*B* were fitted by the curve:

$$x_i = F(t, \theta) = A + \theta_1 t^{\theta_2} \cdot e^{-\theta_3 t} - \theta_4 t$$

where x_i is the log ratio treatment/control of the i-th gene, t is time in hour and A and Θ are appropriate parameters which were obtained using a nonlinear curve-fitting procedure. Each cluster was then enriched by considering genes with a time course highly correlated to one of the three profiles.

Quantitative RT-PCR.

RNA (250ng) was reverse transcribed using SuperScript II reverse transcriptase and random hexamer (Invitrogen, Milan, Italy). Real-time PCR was performed using iQ SYBR Green supermix (Biorad, Milan, Italy) and the iQ5 LightCycler. Gene specific primers were designed using Beacon Designer (Premier Biosoft, Palo Alto, CA, USA). The thermal cycling conditions comprised 3 min at 95°C, and 40 cycles of 10 seconds for denaturation at 95°C and 45 sec for annealing and extension at 58°C. The expression level of the target mRNA was normalized to the relative ratio of the expression of *Gapdh* mRNA. The forward primer for *Gapdh* was 5'-CAAGTTCAACGGCACAGTCAAGG-3', reverse primer was 5'-ACATACTCAGCACCAGCATCACC-3'. Fold changes calculations were made between treated and untreated samples at each time point using the $2^{-\Delta\Delta CT}$ method. The forward primer for *Egr1* was 5'-AAGGGGAGCCGAGCGAAC-3', reverse primer was 5'-GAAGAGGTTGGAGGGTTGGTC-3'; forward primer for *Egr2* was 5'-CTGCCTGACAGCCTCTACCC-3', reverse primer was 5'-ATGCCATCTCCAGCCACTCC-3'; forward primer for *Egr3* was 5'-ACTCGGTAGCCCATTACACTCAG-3', reverse primer was 5'-GTAGGTCACGGTCTTGTTGCC-3'; forward primer for *Nr4a1* was 5'-GGTAGTGTGCGAGAAGGATTGC-3', reverse primer was 5'-GGCTGGTTGCTGGTGTTCC-3'; forward primer for *Arc* was 5'-

AGACTTCGGCTCCATGACTCAG-3', reverse primer was 5'-GGGACGGTGCTGGTGCTG-3'; forward primer for *Homer1a* was 5'-GTGTCCACAGAAGCCAGAGAGGG-3', reverse primer was 5'-CTTGTAGAGGACCCAGCTTCAGT-3'; forward primer for *Bdnf* was 5'-CGATTAGGTGGCTTCATAGGAGAC-3', reverse primer was 5'-GAAACAGAACGAACAGAAACAGAGG-3'.

Terminal deoxynucleotidyl transferase (TdT)-mediated fluorescein-dUTP nick-end labeling (TUNEL) analysis and immunofluorescence.

Hippocampal cultures were fixed with 4% paraformaldehyde in PBS 24 or 48 h after gabazine treatment. TUNEL histochemistry (Roche, Germany) was performed according to manufacturer's instructions. Cultures were then labelled with anti-β tubulin III (TUJ1, Covance, Denver, PA, USA, 1:500) followed by Alexa 594 goat anti-mouse (Invitrogen, Milan, Italy) and nuclei stained with DAPI (Sigma, Saint Louis, MO, USA) for 10 min, coverslipped with Vectashield mounting medium (Vector, Burlingame, CA, USA).

Results

Cultures of dissociated neonatal rat hippocampal neurons grown over MEAs form functional networks of interacting neurons (Ruaro et al., 2005). We increased synaptic efficacy by exposing hippocampal cultures for 30 min to the $GABA_A$ receptor antagonist gabazine (gabazine treatment, GabT). After GabT, gabazine was washed out and the time course of electrical activity and gene expression was followed. Ten minutes of spontaneous activity was recorded at each time point before harvesting RNAs (see Methods). In another series of experiments, we characterized changes of the evoked activity induced by GabT.

Gabazine treatment induces an early (E-Sync) and a late synchronization (L-Sync)

Spikes were clearly detected from voltage recordings obtained from MEA extracellular electrodes and their frequency was monitored during development of neuronal plasticity (first three rows of Fig.1*A*-*C*). In control conditions, neuronal firing was usually incoherent, but occasional synchronous bursts were observed (see raster plot in Fig.1*B*). The global electrical activity was analyzed by computing the network firing rate (NFR_{250ms}), i.e. the total number of spikes recorded from all MEA electrodes in a 250 ms bin width (Fig.1*C*, see Methods).

(Fig.1 near here)

During GabT the electrical activity became highly synchronous, and the NFR exhibited large peaks separated by silent periods (compare raster plots in Fig.1*B*). Five minutes after GabT (third column of Fig.1*A*-*C*) the spontaneous activity was more synchronous than in control conditions and very few spikes among burst were detected. These changes were observed for several hours after drug removal (fourth and fifth column of Fig.1*A*-*C*), as previously reported (Arnold et al., 2005). Changes of the spontaneous activity were quantified by computing three quantities: (i) the NFR averaged over 10 minutes (NFR_{10min}); (ii) the average network cross-correlation ρ (see Methods) and (iii) the occurrence of silent electrical periods determined as the fraction of 100 ms

periods with less than a total of 10 spikes. NFR_{10min} more than doubled during GabT and after its termination remained higher reaching a maximum value at 3-6 h and then slowly returning to control values (Fig.1*D*, n=6). During GabT, ρ more than 50% (59.5 ± 13.4 % of control value; Fig.1*E*). When gabazine was removed, ρ slightly decreased and was still 28 ± 24 % higher than what originally observed 3 h after GabT. At later times, however, ρ increased again and 24 h after GabT it was 51 ± 45 % higher. During GabT, the occurrence of silent periods drastically increased to 244 ± 63 % and remained higher than control value at all time following GabT, being still 65 ± 36 % larger than control values 24 h after GabT (Fig.1*F*, n=6).

These results indicate that the NFR and ρ had a different time course: NFR reached a maximum value at about 6 h, but ρ showed a biphasic behavior with a minimum value at 6 h. This biphasic behavior is consistent with the existence of two components: one component acting at early times (E-Sync) and a later component clearly visible from 6 to 24 h after GabT (L-Synch). This is reminiscent to what is observed for LTP, where an early component (E-LTP) independent of transcription, precedes a later component (L-LTP) associated to new transcription and translation (Lynch 2004; Malenka and Bear 2004; Raymond and Redman 2006; Raymond 2007).

E-Sync and L-Sync depend on different signalling pathways

Treatment with bicuculline within 2 minutes activates ERK in post-synaptic dendrites, which then translocates to the nucleus within 15-30 minutes (Wiegert et al., 2007). E-LTP and L-LTP are selectively blocked by PD98059 (Sweatt, 2001) or U0126 (Favata et al., 1998) and Actinomycin D (Raymond and Redman 2006) respectively. PD98059 and UO126 are known to be blockers of the MAPK/ERK pathway (Thomas and Huganir, 2004) and Actinomycin D is a general blocker of DNA transcription. We then investigated the effects of these drugs on NFR, ρ and the occurrence of silent periods. PD98059 and UO126 were pre-incubated for 45 minutes before GabT and were washed out together with gabazine.

Treatment with PD98059 (50 μM) or U0126 (20 μM) did not interfere with gabazine-induced synchronization but completely blocked the GabT-induced

synchronization: NFR_{10min} did not change and remained similar or lower to what observed in untreated cultures (red trace in Fig.2*A*, left panel) and ρ remained lower than the control value (Fig.2*B*, left panel). Similarly, the occurrence of silent periods decreased under control value (Fig.2*C*, left panel): silent periods dropped to 26 ± 19 % 1 h after GabT before returning to the control value after 24 h (Fig.2*C*, left panel). On the other hand, when neuronal cultures (n=3) were treated with 8 μM Actinomycin D, NFR_{10min} remained under the control value at all times after GabT (Fig.2*A*, right panel). In contrast, ρ more than doubled during GabT (223 ± 32%) and remained relatively high up to 3 h after GabT (20 ± 9 % larger than the control value), subsequently returning to the control value (Fig.2*B*, right panel). During GabT and in the presence of Actinomycin D, the occurrence of silent periods increased by 237 ± 55 % and 1 and 3 h after GabT it was 79 ± 28 % and 46 ± 32 % larger than in control value, respectively (Fig.2*C*, right panel).

(Fig.2 near here)

These results show that in the presence of blockers of the MAPK/ERK pathway, changes of NFR_{10min}, ρ and the occurrence of silent periods induced by GabT were abolished. In contrast, when Actinomycin D was added, GabT still evoked a significant increase of ρ and of silent periods lasting for 1-3 h. However, changes of NFR_{10min}, ρ and of silent periods observed 24 h after GabT were abolished. Therefore, E-Sync seems to be mediated by the activity of the MAPK/ERK complex, possibly through the phosphorylation of some target proteins (Wiegert et al., 2007; Sweatt, 2001; Schrader et al., 2006), while L-Sync appears to be mediated by changes of gene expression, as it is eliminated by drugs blocking the transcription.

The evoked response is maximally potentiated 3 hours after GabT

MEA's extracellular electrodes can be used for recording and stimulation. In another series of experiments, we quantified changes of the evoked activity. Brief (200 μs) bipolar pulses were applied to a row of electrodes (black bar in the grid of Fig.3*A*) and the propagation of evoked spikes throughout the network was recorded. In order to avoid saturation, the lowest voltage pulse evoking some spikes was used, before, during and after

GabT (Fig.3). After GabT, the number of evoked spikes increased in almost all trials (Fig.3*B*) and at all time points (Fig.3*C*).

(Fig.3 near here)

Changes of the evoked response were quantified by computing the total number of evoked spikes in a time window of 100 ms from the stimulus onset (NRF_{100ms}). NRF_{100ms} significantly increased between 1 and 6 h after GabT (Fig.3*D*): the evoked response was maximally potentiated 3 h after GabT and started to decline after 6 h, returning almost to control level 24 h after GabT. Neuronal plasticity induced by GabT caused evoked spikes to travel through the network in a faster and more reliable way. In some experiments, we could identify a spike produced by the same neuron, and we measured how its latency and jitter changed during neuronal plasticity (Fig.3*E,F*). The latency in control conditions from the stimulus was between 6 and 9 ms and was reduced by 2-3 ms after GabT. The standard deviation of the latency (jitter) similarly decreased (blue and red symbols in Fig. 3*F*). A clear reduction of latency and jitter of evoked spikes were observed in at least 31 identified single neurons (n=5 cultures). We also analyzed how spikes propagated in the network by measuring the space constant λ of the evoked activity (see Methods and inset of Fig.3*G*). Collected data from 4 cultures showed that λ increased by about 25 % within 1 h after GabT and remained larger than the control values up to 24 h (Fig.3*G*). These results show that GabT – also in the absence of a concomitant strong or tetanic electrical stimulation – potentiated the electrical response propagating in the culture, inducing in this way a form of LTP.

Changes of gene expression

In order to understand the molecular changes underlying the modification of the electrical activity induced by GabT, we investigated changes of gene expression with DNA microarrays and real-time PCR. Gene expression was analysed 1.5, 3, 6 and 24 h

after the onset of GabT and the variance of changes relative to the control observed at all these times was computed (see Methods). After GabT, the mean value of expression changes (in $\log_2$ units) relative to untreated controls did not change for the great majority of genes (see Fig.4*A*).

(Fig.4 near here)

As the standard deviation σ of changes of housekeeping genes was about 0.25, we filtered out genes with a variance σ^2 lower than 0.6, obtaining 132 genes significantly modulated (Fig.4*B*). Visual inspection of expression changes of these genes (Fig.4*B*) indicated three distinct temporal profiles: genes maximally up-regulated 1.5, 3 and 24 h after GabT were grouped in Cluster 1, 2 and 3, respectively. The precise time course of these three profiles was identified (black traces in Fig.4*B-E*; see Methods) and the population of the three Clusters was enriched by reanalyzing the data with a lower variance (see Methods) looking for genes whose changes were highly correlated with one of the three profiles. By using this procedure, 25, 318 and 93 genes were present in Clusters 1, 2 and 3, respectively (see Fig.4*C-E*). The complete list of identified genes can be found in Supplementary Table 1. Changes of gene expression occurring 1.5 and 3 h after GabT were checked by real-time PCR for some selected genes, namely *Egr1, Egr2, Egr3*, *Nr4a1*, *Bdnf*, *Homer1a* and *Arc* (Fig.4*F*). Genes in Cluster 1 (see Table 1) had a 2-fold up-regulation 1 h after GabT, returning to the control level or slightly below 6 h after drug removal (Fig.4*C*). Gene Ontology (GO) analysis indicated that 44% (11/25) of these genes were regulators of transcription, such as members of the Egr (Hughes and Dragunow, 1995) and Nr4a families (Giguere, 1999). The identification of genes in Cluster 1 as transcription factors was statistically more significant compared to a similar identification for the other clusters (p value<0.01 Fisher's exact test; see Methods). Five of these transcription factors (*Egr1-3*, *Nr4a1* and *Junb*) have been shown to play a major role also in LTP. Cluster 1 contained additional genes such as *Arc, Homer1, Ptgs2* and *Dusp5* known to be effector genes in LTP (see Table 2 and references therein).

Several genes in Cluster 2 were maximally up-regulated 3 h after gabazine removal (Fig.4*D*) i.e. at the same time of maximal potentiation of the evoked response (Fig.3*D*).

GO analysis indicated that 28 % of these genes are involved in neuronal electrical transmission and could be grouped in three classes: genes involved in "ion transport" (such as *Kcnd2*, *Cacna2d3*, and *Gria1*), in "signal transduction" (such as *Cck* and *Homer1*), and in "transmission of nerve impulse" (such as *Rab3a Snsap25*, *Syn1* and 2. Of the 435 genes identified, 361 are annotated. To better investigate the functionalities of these genes, we performed an extensive PubMed search to extract functional information for all these genes. 43 genes belonging to Cluster 1 and 2 are known to be involved in LTP (see Table 2) strongly suggesting that the up-regulation of genes in Cluster 2 mediated the electrophysiological changes described in Figure 3. The list of LTP genes in Table 2 contains many transcription factors and genes encoding for ion channels. Besides these, most of the remaining genes could be categorized as *structural*, *pre-* and *post-synaptic* based on their biological function. We therefore decided to classify all the other 318 genes in these three groups based on the PubMed search. The results of this search are listed in Table 3. 39 genes have been classified as *structural genes* for their structural role in cellular function and their up-regulation could underlie structural and morphological changes associated to LTP. Analogously the 26 *pre-synaptic* and the 24 *post-synaptic* genes found in our screening and listed in Table 3 could mediate changes of synaptic properties occurring during LTP.

Several genes in Cluster 3 were down-regulated by GabT 3 h after drug removal (like *Abcb1a, Ccnd1, Il1rl1, Tcf19*), and conversely, they were up-regulated at later times (Fig.4*E*). 11% of the genes belonging to this cluster were put in the "apoptosis" category by GO and included both pro-apoptotic (such as *Casp4* and *Unc5c*) and pro-survival (such as *Tgfb3* and *Gadd45a*) genes. *Structural genes* were also found in Cluster 3 suggesting their possible involvement in the reinforcement and consolidation of LTP.

The effect of ERK inhibitors on the potentiation of the evoked response

As PD98059 and U0126 blocked changes of the spontaneous activity induced by GabT (Fig.2), we investigated their effect on the potentiation of the evoked response (Fig.3). Application of these inhibitors to neuronal cultures decreased the recorded spontaneous activity measured at all extracellular electrode (Fig.5*A*). The NFR_{250ms}, used

to describe the global spontaneous activity (see Fig.2) was almost halved (Fig.5*B*) in all tested cultures (n=4), but periods of larger electrical activity could be still observed. In these cultures, inhibitors of the MAPK/ERK were incubated for 20 minutes before GabT and changes of the evoked response were analyzed. In the presence of these inhibitors, GabT still potentiated the evoked response, although in a lesser extent (red trace in Fig.5*C*), with a time course similar to that observed in the absence of these inhibitors (black trace in Fig.5*C*). 3 h after GabT, the number of evoked spikes reached 198 ± 41 % in normal conditions, but increased only by 39 ± 15 % in the presence of PD98059 and U0126. Therefore, inhibition of the MAPK/ERK pathway reduced but not abolished the potentiation of the evoked response caused by GabT.

(Fig.5 near here)

In order to understand the nature of potentiation of the evoked response observed in the presence of inhibitors of the MAPK/ERK pathway, we analyzed with real-time PCR some selected genes up-regulated by GabT (Fig.4). As shown in Figure 5*D*, the up-regulation induced by GabT of genes of the EGR family, *Nr4a1* and *Arc* was significantly reduced and almost blocked by inhibitors of the MAPK/ERK pathway, but not the up-regulation of *Bdnf* and *Homer1a*.

Several genes coding for K^+ channels are down-regulated 24 hours after GabT

The NFR of both the spontaneous (Fig.1*D*) and evoked activity (Fig.3*D*) returned almost to the control level 24 h after GabT, but not the network cross-correlation ρ (Fig.1*E*) and the occurrence of silent periods (Fig.1*F*) observed during the spontaneous activity. L-LTP is mediated by multiple changes occurring in the pre- and post-synaptic machinery (Lisman, 2003) but also involves changes in the density and/or properties of ionic channels present in the dendritic arborization and axon of neurons forming the network (Frick et al., 2004). These changes could affect the degree of synchronization of the spontaneous activity. To test this possibility, we investigated in detail changes of genes encoding for subunits and/or ancillary regulatory subunits of Na^+, K^+, Ca^{2+}, HCN ionic

channels, as well as GABA and glutamate receptors. The majority of these genes were not affected by GabT (Fig.6*A-F*), but some of them were significantly down-regulated 24 h after GabT (red crosses). Down-regulated genes related to K^+ channels (Fig.6*B*) were *Kcnc1, Kcnj6, Kcna4, Kcnn2, Kcnc2, Kcnip3, Ki55.1, Kcnab1, Kcnd2* and *Kcnip4*. Also some genes coding for subunits of Ca^{2+} (*Cacng2, Cacng3, Cacnb4* and *Cacna2d3*; Fig.6*C*), Na^+ channels (S*cn1a* and *Scn2a1*; Fig.6*A*) and for glutamate (*Gria1* and *Gria2*; Fig.6*D*) and GABA (*Gabrb1, Gabra5, Gabra1, Gabbr2* and *Gabrg2*; Fig.6*E*) receptors were down-regulated. The gene coding for HCN1 channels was significantly down-regulated, but not those coding for HCN2-4 channels, in agreement with the larger expression of HCN1 channels in rat hippocampus (Richichi et al., 2008). As the degree of correlated activity of neuronal networks can also depend on the amount of electrical coupling among neurons, we looked for possible changes of genes expressing connexins, i.e. the ionic channels mediating electrical coupling. No significant changes of genes coding for connexins were found.

(Fig.6 near here)

None of the Ca^{2+} and Na^+ channels or GABA receptors genes found here has been reported to be involved in neuronal plasticity. K^+ channels encoded by the *Kcna4 Kcnn2 Kcnab1* and *Kcnd2* genes (see references in Table 2) are known to be involved in neuronal plasticity and HCN1 down-regulation has been observed following seizure like events (Shah, 2004; Richichi et al., 2008). These observations suggest that a down-regulation of HCN1 and K^+ channels could underlie or contribute to L-Sync. In order to test this possibility, we pharmacologically blocked HCN1 and K^+ channels. We first analyzed the effect of unspecific K^+ channels blockers, such as 4-aminopyridine (4-AP) and TEA. In the presence of 100 μM 4-AP, synchronous bursts appeared (Fig.6*G*) and ρ increased by 304 ± 156 % (Fig.6*J*, *t*-test, $p<0.05$, n=4). In the presence of 10 mM TEA, the network firing became more synchronous (Fig.6*H*) and ρ almost doubled (Fig.6*J*; 195 ± 67 % of the control value, n=3). Synchronization induced by TEA treatment was transient and in fact, after 10 minutes or so, the value of ρ substantially decreased (data not shown). We also tested the effect of arachidonic acid, a known blocker of the A-current (Villarroel,

1993) and in the presence of 40 μM of this drug the spontaneous firing was slightly more synchronous (data not shown). Addition of 100 μM of ZD7288, a known blocker of HCN channels, also induced a large and clear synchronization of the electrical spontaneous activity (Fig.6*I,J*; 202 ± 59 % of the control value, n=3). Taken together, these data indicate that a down-regulation of genes coding for HCN and K^+ channels could contribute to L-Sync.

Integrity of neuronal cultures after gabazine exposure

The presence of genes linked to apoptosis in Cluster 3, raises the possibility of permanent damage induced in the neuronal culture by GabT. Indeed, bursts of electrical activity caused by GabT are expected to release large amounts of glutamate in synapses, possibly causing spillover reaching extra-synaptic NMDA receptors, known to trigger neuronal death (Hardingham et al., 2002). Thus, we checked the integrity of neuronal cultures in several ways. Tunel assays (Fig.7*A,B*) did not show a significant increase in apoptotic nuclei after GabT. In fact we counted 9.2 ± 3.3 % of apoptotic nuclei (positive for tunel: green nuclei in left panel of Fig.7*A*) in control conditions, 9.5 ± 5.0 % and 6.7 ± 2.3 % 24 and 48 h after GabT (Fig.7*B*), respectively.

(Fig.7 near here)

GABA in the mature hippocampus hyperpolarizes neurons, but can have a depolarizing effect in the immature hippocampus (Ben-Ari et al., 1989) or following insults such as trauma, ischemia or seizures (Galanopoulou, 2007). As GabT caused electrical bursts reminiscent of epileptic seizures, we verified that GabT did not modify the hyperpolarizing effect of the activation of GABA receptors. Addition of 30 μM GABA before GabT blocked almost completely the spontaneous activity by silencing the great majority of the MEA's electrodes and switching to a tonic mode of firing (Fig.7*C*), consistently with the activation of inhibitory synaptic pathways. When the same amount of GABA was added 24 h following GabT, the spontaneous activity was similarly blocked (Fig.7*D*). We also verified that subsequent GabT 24 or 48 h after the first GabT had the

same effect (Fig.7*E*): the network cross-correlation ρ more than doubled for the three consecutive GabTs. These results show that a transient exposure to blockers of inhibitory GABAergic synaptic pathways initiate neuronal plasticity without causing significant damage to neuronal cultures and changes of the hyperpolarizing effect of GABA.

Discussion

The present work identifies several sequential steps underlying neuronal plasticity induced by a transient gabazine treatment. Immediately after termination of GabT, the spontaneous electrical activity becomes more synchronous (E-Sync) than in control conditions. Following GabT, ERK proteins are phosphorylated and activated within less than 5 minutes (Wiegert et al., 2007). E-Sync is blocked by inhibitors of the MAPK/ERK pathway but is not affected by inhibitors of gene transcription (Fig.2), suggesting that local protein trafficking underlies it. Late synchronization however is blocked by both inhibitors demonstrating a major role of MAPK/ERK signalling pathway in neuronal plasticity and showing the requirement of new gene transcription for synchronicity consolidation. Some tens of genes (Cluster 1), primarily composed by transcription factors such as members of the *Egr*, *Dusp* and *Nr4a* families, are maximally up-regulated 1.5 h after GabT. Another cluster of genes (Cluster 2), is maximally up-regulated about 3 h after GabT and many of these genes are known to be involved in LTP. At the same time or slightly later the evoked and spontaneous electrical activity are strongly potentiated (Figure 1 and 3). From 6 to 24 h after GabT, the spontaneous electrical activity becomes progressively more synchronous (L-Sync) concomitantly to a late down-regulation of genes coding for several K^+ channels and the HCN1 channel. A third group of genes (Cluster 3) involved in cellular homeostasis is up-regulated 24 h after GabT. From these results it is possible to relate specific events occurring during neuronal plasticity to changes of expression of specific gene clusters.

Comparison with previous investigations

Several previous investigations have identified hundreds of genes up-regulated by an intense electrical activity in mouse hippocampus (Zhang et al., 2007), in rat hippocampus and cerebral cortex (Altar et al., 2004) and in mouse dentate gyrus (Park et al., 2006). Zhang et al. (2007) evoked electrical activity either by stimulating synaptic NMDA

receptors by using bicuculline or extra-synaptic NMDA receptors by adding glutamate to the medium (Zhang et al., 2007). Altar et al. (2004) induced electroconvulsive seizures while Park et al. (2006) used direct electrical stimulations of the hippocampus. The present investigation used GabT to elevate the global electrical firing. In all these investigations an elevated global firing initiates the transcription of several genes associated to metabolic and structural components and synaptic functions.

A parallel analysis of genes up-regulated in these experiments shows a significant number of commonly regulated genes. 13 (out of 25) genes in Cluster1 and also some genes in Cluster 2 (like *Pnoc*, *Rgs2* and *Ntrk2*) of the present investigation are also up-regulated in mouse hippocampal cultures following a permanent stimulation of synaptic NMDA receptors with bicuculline (Zhang et al., 2007). Similarly, 16 genes (*Bdnf, Ptgs2, Homer1,Tac2, Egr1,2,4, Arc, Nrp1, TrkB, Vegf, Vgf, JunB, Nr4a3, cFos,* and *Syn2*) regulated by increasing the electrical activity with electroconvulsive seizures *in vivo* were also up-regulated in our system. Moreover, 5 LTP genes (*Egr2, Fos, Homer1, Nrgn,* and *Rab3a*) found in our investigation and listed in Table 2 were also up-regulated by a tetanic stimulation of the perforant path, a well known protocol for LTP induction in the hippocampus (Park et al., 2006). Therefore, despite experimental differences, these investigations identify several genes commonly up-regulated in many forms of LTP.

E-Sync of spontaneous activity

As shown in Fig.2, E-Sync is not blocked by Actinomycin D but by inhibitors of the MAPK/ERK pathways. Therefore E-Sync is very likely to be dependent on local protein trafficking controlled by the MAPK/ERK pathway. In this regard, E-Sync is very similar to a component of LTP, referred as Early LTP, which is not blocked by inhibitors of gene expression (Sweatt 2001; Raymond and Redman 2006; Raymond 2007). Local protein synthesis and regulation of ionic channels, such as phosphorylation of the Kv4.2 channel by ERK (Schrader et al., 2006) PKA or CaMKII are likely mechanisms.

Potentiation of evoked activity

Potentiation of the spontaneous and evoked electrical activity (Fig.1 and 3) and up-regulation of genes in Cluster 2 have a very similar time course suggesting of a causal relationship between gene activation and electrical potentiation. Potentiation of the evoked activity was reduced, but not eliminated by inhibitors of the MAPK/ ERK pathway (Fig.5). Therefore potentiation of the evoked response is mediated by several pathways likely to be working in unison. Many genes belonging to Cluster 1 and 2 are well known players in LTP (see Table 2) such as *Bdnf* and its receptor TrkB (Barco et al., 2005) (referred to as *Ntrk2* in Table 2), *Arc* (Messaoudi et al., 2007), *Egr1* (Davis et al., 2003) and *Homer1* (Hernandez et al., 2005). We hypothesize that the large majority of genes of Clusters 1 and 2 underlie induction of LTP and that their activation orchestrates neuronal plasticity. The latter most likely depends on the activation of hundreds - rather than tens or thousands - of genes, in agreement with our findings. In fact, of the 361 annotated genes in our clusters from the PubMed search, we found that one third is, or could be, involved in changes of synaptic strength related to LTP. 43 genes have already been implicated in LTP (Table2), 39 genes have been classified as *Structural genes* for their structural role in cellular function and their up-regulation could underlie structural and morphological changes associated to LTP. Analogously the 26 *Pre-synaptic* and the 24 *Post-synaptic* genes found in our screening and listed in Table 3 could mediate changes of synaptic properties occurring during LTP.

Structural genes

Among structural genes in Cluster 1 and 2 there are elements that control properties of the cytoskeleton and the dynamics of microtubules and neurofilaments like *Arc, Homer1, Mapt, or Stmn3* or the formation of new dendritic arborisation like *Dscam or Nxph1*. Many genes of the cadherin family (*Cdh10, Cdh11*,….), controlling cell to cell

adhesion are also member of these category. The gene *Dscam* (Down Syndrome Cell Adhesion Molecule) plays a major role in axon guiding and development of neuronal circuits (Yamagata et al, 2008; Fuerts et al, 2008) and is well known to be involved in neuronal plasticity. *Nrxn3* (Neurexin) in conjunction with neuroligin is thought to play a major role in the formation of new synapses and in particular in adhesion complex (Fabrichny, 2007) and therefore besides being structural they can be also classified as pre-post synaptic. *Structural Genes* were also found in Cluster 3 and they could be involved in the reinforcement and consolidation of LTP.

Pre- and post -synaptic genes

Several pre-synaptic genes such as synapsin I e II (James et al., 2004), syntaxin1A Yamakawa et al., 2007), *Snap25* (Bailey and Lahiri, 2006) code for proteins involved in vesicle release from pre-synaptic terminals, and their up-regulation could be associated to an increase of vesicle release during synaptic transmission.

Among the post-synaptic genes there are elements associated to Post Synaptic Density complex like *Cnksr2 and Opcml*: to the regulation and local trafficking of post-synaptic glutamate ionic channels like *Nsf or Ptpn5* and to the regulation of post-synaptic spines like *Slc12a5* and therefore could be involved in the reinforcement of the synaptic strength.

As shown in Fig.6, many genes coding for ionic channels and their accessory proteins belong to Cluster 2. Their up-regulation closely follows the time course of potentiation of the evoked response, suggesting that they also could participate to the regulation and orchestration of LTP.

For these reasons, we propose that genes found in this screening could represent a template – to be verified - for genes involved in neuronal plasticity in several other preparations.

L-Synch of spontaneous activity

L-Sync could be mediated by a down-regulation of K^+ and HCN channels and in fact, blockers of K^+ channels with a wide spectrum of action, such as TEA and 4-AP, increase the degree of synchronization of the spontaneous activity (Fig.6). Blockage of HCN1 channels by changing dendritic excitability modulates LTP (Narayanan and Johnston, 2007) and contributes to neuronal plasticity by prolonging the entry of Ca^{2+} in distal dendrites (Tsay et al., 2007). Synchronous bursts induced by blockage of K^+ channels are more frequent and less regular and therefore the down-regulation of K^+ channels can be one of the several mechanisms underlying neuronal plasticity. In addition, network synchronization was not observed or was rather small when specific K^+ channels blockers (Apamin for *Kcnn2*, Heteropodatoxin 2 and arachidonic acid for *Kcnd2*) were used (data not shown), indicating that a fine tuning and a precise regulation of several ionic channels (Fig.6) underlie L-Sync.

Genes of Cluster 3

Genes belonging to Cluster 3 are up-regulated 24 h after GabT and some of them (5/93) are also up-regulated in mouse hippocampal cultures 2-4 h after addition of glutamate or bicuculline (Zhang et al., 2007). Several genes from Cluster 3 are associated to apoptosis, with pro-apoptotic (such as *Casp4* and *Unc5c*) and pro-survival (such as *Tgfb3* and *Gadd45a*) genes. The homeostatic mechanisms present in neuronal cultures – both in the cytoplasm and at the network level – minimize the number of apoptotic neurons (Fig.7) and provide a way to safely return to control conditions 24 h after GabT.

Figure Legends

Figure 1. Synchronization of the spontaneous electrical activity induced by GabT. The spontaneous electrical activity of hippocampal cultures grown on MEAs for three weeks was recorded for 10 min before the addition (control) and during treatment with gabazine (50 μM for 30min, GabT). ***A,*** Representative traces from three individual extracellular electrodes showing the presence of synchronized bursts of electrical activity during GabT and at different time points following gabazine washout. ***B***, Raster plots of the activity of all 60 MEA electrodes. Each horizontal line represents the activity of a single electrode. Synchronous bursts are represented by black vertical lines. Spikes between synchronous bursts are drastically reduced during GabT and after the drug washout. ***C***, Network firing rate (NFR) expressed as the total number of spikes recorded from all the MEA electrodes in bins of 250 ms. The scale bar on the left is similar for all conditions except during GabT. Data from a single experiment shown in ***A-C***. ***D***, Time course of the average NFR. ***E***, Time course of the average network synchronicity. The degree of network synchronization was estimated by averaging the network cross-correlation ρ over all electrode pairs (see Methods). ***F***, Time course of the fraction of silent periods, defined as the fraction of frames containing ten or less spikes, showing the reduction of the number of individual spikes during and after GabT. Bin size was 250 ms. n = 5 cultures for ***D***, ***E*** and ***F***. Values were normalized relative to control values. Error bars are mean ± s.e.m.

Figure 2. Effects of MAPK inhibitors and Actinomycin D on early and late gabazine-induced synchronization ***A***, Left, Average NFR time course in the presence of the MAPK

cascade inhibitors PD98059 and U0126 (red trace). Data for PD98059 (50 μM; n = 3) and U0126 (20 μM; n = 3) were pooled together as they affected similarly network properties. The NFR fluctuates around the baseline after GabT and is not potentiated unlike in control conditions (black trace). U0126 and PD98059 were preincubated 20 and 45 minutes before GabT, respectively, and washed out with gabazine. Right, Actinomycin D decreases slightly the NFR. ***B***, E-Sync and L-Sync depend on different signaling pathways. Left, network synchronicity is abolished in the presence of PD98059 or U0126. Right, in the presence of Actinomycin D, L-Sync but not E-sync is blocked, indicating that L-Sync depends on gene transcription. ***C***, Time course of the fraction of silent periods containing ten or less spikes. Left, blockers of the MAPK pathway reduces the fraction of silent periods following GabT, i.e. the number of individual spikes increase in the network. Right, in presence of Actinomycin D, the fraction of silent periods is smaller than control value after tens of hours. Bin size was 250ms. Values were normalized relative to control values.

Figure 3. Potentiation of the evoked response induced by GabT. ***A***, Examples of the evoked activity's time course for a single trial for three representative electrodes located at 0.5, 1 and 2 mm distance (see *inset*) from the stimulating electrode respectively (black bar in *inset*). The number of evoked spikes increases following the GabT. Hippocampal cultures were stimulated with the lowest intensity (200-450 mV) evoking a response. 40 pulses (trials) with an inter-pulse interval 4s were used. Inset, graphical representation of the MEA grid. Each square represents an electrode. Distance between electrodes is 500 μm. Black bar corresponds to the stimulated electrodes and grey numbered squares to the

electrodes whose activity is shown in ***A***. ***B***, Raster plots of the spikes evoked in one electrode at each time point analyzed. Each horizontal line represents the response to one trial recorded up to 250 ms after the stimulus onset. ***C***, Time course of the NFR. The total number of evoked spikes was counted in 10 ms bins, following electrical stimulation. The increase of evoked spike is especially pronounced in the first 100 ms following stimulation. Data from a single experiment shown in ***A-C***. ***D***, Average time course of the NFR (n=5 cultures). The NFR was normalized relative to control values. Bin size was 250 ms. ***E***, Ten overlapping spike traces in control conditions (black traces) and 3h after gabazine washout (red traces) of an individual electrode showing the decrease of the latency of the first evoked spike. Artifacts have been truncated for clarity. ***F***, Time course of the latency (blue traces) and jitter (red traces) of the first spike for three neurons showing that the latency and jitter decrease after GabT. Each symbol corresponds to a different neuron. ***G***, Time course of the activity propagation constant (λ, see Methods) showing the increase of the activity spread following GabT. Inset, the number of spikes in a 100 ms time window was counted and averaged, for electrodes located at 0.5, 1 and 2 mm from the stimulated bar of electrodes, and fitted with an exponential function $Ae^{-d/\lambda}$ (grey line). Colours as in ***E***.

Figure 4. Gene expression profile revealed by DNA microarrays. ***A***, Time course of all the probe sets unequivocally hybridized. ***B***, Time course the 132 probe sets in **A** whose variance is bigger than 0.6 over the entire time course. ***C-E***, Time course of three gene clusters identified in ***B***. The clusters were identified using the K-means method between the specific time profiles (blue traces in ***B***) and the entire probe set shown in ***A***. ***F***,

Changes of gene expression occurring 1.5 h and 3 h after GabT measured by Real-Time PCR for Egr1, Nr4a1, Arc, Homer1a and Bdnf. See also Table 1 for a list of genes up-regulated 1.5h after gabazine washout in cluster 1 and Table 2 for a list of genes known to be involved in neuronal plasticity and belonging to Cluster 1 and 2.

Figure 5. Effect of inhibitors of the MAPK pathway. ***A***, Representative traces from two individual extracellular electrodes in control conditions (left) and in presence of 50 μM PD98059 (right). ***B***, Corresponding network firing rate computed with a bin width of 25 ms, in normal conditions (left) and in presence of 50 μM PD98059 (right) showing a depression of the spontaneous electrical activity by PD98059. Dotted line indicates zero spike. ***C***, The evoked activity is still potentiated when the MAPK pathway was blocked before GabT (see Results). Dashed line corresponds to potentiation of the evoked activity without blocking the MAPK pathway before GabT. Data for PD98059 (50 μM; n = 3) and U0126 (20 μM; n = 3) were pooled together as they affected similarly network properties. ***D***, Changes of gene expression occurring 1.5 h after GabT measured by Real-Time PCR for Egr1, Egr2, Egr3, Nr4a1, Bdnf, Homer1a and Arc in presence of gabazine and PD98059 (gray bars) relative to normalized expression in presence of gabazine alone (black bar).

Figure 6. Ionic channels expression and K^+ channel blockers induced-synchronization. ***A-F***, Time course of the ionic channels and receptors channels expression induced by GabT. Red bars correspond to the mean. Horizontal blue bars correspond to the first and third quartile. Red crosses represent deviation from the mean. ***G-I***, Effects of K^+ channels

blockers on the network synchronization. Three representative electrodes showing the synchronous bursting induced by 100 μM 4-aminopyridine (4-AP**,** ***G***), 10 mM tetra-etylammonium (TEA**,** ***H***) and 100 μM ZD7288 (***I***), respectively. Bottom panels show the average network firing rate computed with a bin width of 100ms. Dashed lines correspond to zero spike. Note the absence of individual spikes in the intra-burst intervals in ***H***. ***J***, Summary of the effect of diverse K^+ and HCN channel blockers on the average network correlation coefficient ρ (see Methods).

Figure 7. Gabazine treatment does not interfere with the cell culture integrity. ***A***, Staining of hippocampal cells in control conditions with different markers. Nuclei positive to TUNEL assay (green, left panel). Neurons expressing type III tubulin recognized by TUJ1 antibody (red, middle panel); total nuclei stained with DAPI (blue, right panel). Scale bar 20 μm. ***B***, Merge pictures of the three markers shown in ***A*** in control conditions (left), 24 h (middle) and 48 h (right) after gabazine treatment demonstrating the absence of apoptosis by this treatment. Scale bar as in ***A***. ***C***, Modification of the network activity by GABA. Top panels, The NFR and bursting activity in control conditions (left) are drastically reduced in the presence of 30 μM GABA (right). Bottom panels, raster plots. ***D***, Similar to ***C*** but 24h after gabazine washout. The same reduction of bursting activity by GABA is observed for cultures treated with gabazine. ***E***, Time course of the network synchronicity following repeated GabT. GBZ 1, 2 and 3 correspond to the first, second and third GabT, respectively.

Table 1: List of genes present in Cluster 1, i.e. maximally up-regulated at 1.5h after gabazine wash-out.

Table 2: List of genes present in Cluster 1 and 2 known to be involved in LTP.

Table 3: List of genes involved in structural, pre- and post-synaptic processes.

References

Altar CA, Laeng P. Jurata LW, Brockman JA, Lemire A, Bullard J, Bukhman YV, Young TA, Charles V & Palfreyman MG (2004) Electroconvulsive seizures regulate gene expression of distinct neurotrophic signaling pathways. *J Neurosci* **24**, 2667-2677.

Arnold FJ, Hofman F, Bengston CP, Wittmann M, Vanhoutte P & Bading H (2005) Microelectrode array recordings of cultured hippocampal networks reveal a simple model for transcription and protein synthesis-dependent plasticity. *J Physiol* **564**, 3-19.

Bading H, Gintly DD & Greenberg ME (1993) Regulation of gene expression in hippocampal neurons by distinct calcium signaling pathways. *Science* **260**, 181-186.

Bailey JA & Lahiri DK (2006) Neuronal differentiation is accompanied by increased levels of SNAP-25 protein in fetal rat primary cortical neurons: implications in neuronal plasticity and Alzheimer's disease. *Ann NY Acad Sci* **1086**, 54-65.

Barco A, Patterson S, Alarcon JM, Gromova P, Mata-Roig M, Morozov A & Kandel ER (2005) Gene expression profiling of facilitated L-LTP in VP16-CREB mice reveals that BDNF is critical for the maintenance of LTP and its synaptic capture. *Neuron* **48**, 123-137.

Ben-Ari Y, Cherubini E, Corradetti R & Gaiarsa JL (1989) Giant synaptic potentials in immature rat CA3 hippocampal neurones. *J Physiol* **416**, 303-325.

Benjamini Y & Yekutieli D (2001) The control of the false discovery rate in multiple testing under dependency. *Ann Stat* **29**, 1165-1188.

Bliss TV & Lomo T (1973) Long-lasting potentiation of synaptic transmission in the dentate area of the anaesthetized rabbit following stimulation of the perforant path. *J Physiol* **232**, 331-356.

Carlisle HJ & Kennedy MB (2005) Spine architecture and synaptic plasticity. *Trends Neurosci* **28**, 182-187.

Davis S, Bozon B & Laroche S (2003) How necessary is the activation of the immediate early gene zif268 in synaptic plasticity and learning? *Behav Brain Res* **142**, 17-30.

Fabrichny IP, Leone P, Sulzenbacher G, Comoletti D, Miller MT, Taylor P, Bourne Y & Marchot P (2007) Structural analysis of the synaptic protein neuroligin and its beta-neurexin complex: determinants for folding and cell adhesion. *Neuron* **56**, 979-91.

Favata MF, Horiuchi KY, Manos EJ, Daulerio AJ, Stradley DA, Feeser WS, Van Dyk DE, Pitts WJ, Earl RA, Hobbs F, Copeland RA, Magolda RL, Scherle PA & Trzaskos JM (1998) Identification of a novel inhibitor of mitogen-activated protein kinase kinase. *J Biol Chem* **273**, 18623-18632.

Fuerts PG, Koizumi A, Masland RH & Burgess RW (2008) Neurite arborisation and mosaic spacing in the mouse retina requires DSCAM. *Nature* **451**, 470-474.

Frick A, Magee J & Johnston D (2004) LTP is accompanied by an enhanced local excitability of pyramidal neuron dendrites. *Nat Neurosci* **7**, 126-135.

Galanopoulou AS (2007) Developmental patterns in the regulation of chloride homeostasis and GABA(A) receptor signaling by seizures. *Epilepsia* **48**, 14-18.

Gao FB (2007) Molecular and cellular mechanisms of dendritic morphogenesis. *Curr Opin Neurobiol* **17**, 525-32.

Goelet P, Castellucci VF, Schacher S & Kandel ER (1986) The long and the short of long-term memory--a molecular framework. *Nature* **322**, 419-422.

Groc L & Choquet D (2007) AMPA and NMDA glutamate receptors trafficking: multiple roads for reaching and leaving the synapse. *Cell Tissue Res* **326**, 423-438.

Giguere V (1999) Orphan nuclear receptors: from gene to function. *Endocr Rev* **20**, 689–725.

Hardingham GE, Fukunaga Y & Bading H (2002) Extrasynaptic NMDARs oppose synaptic NMDARs by triggering CREB shut-off and cell death pathways. *Nat Neurosci* **5**, 405-414.

Hernandez PJ, Schlitz CA & Kelley AE (2005) Dynamic shifts in corticostriatal expression patterns of the immediate early genes Homer 1a and Zif268 during early and late phases of instrumental training. *Learn Mem* **13**, 599-608.

Hughes P & Dragunow M (1995) Induction of immediate-early genes and the control of neurotransmitter-regulated gene expression within the nervous system. *Pharmacol Rev* **47**, 133-178.

Irizarry RA, Bolstad BM, Collin F, Cope LM, Hobbs B & Speed TP (2003) Summaries of Affymetrix GeneChip probe level data. *Nucleic Acids Res* **31**, e15.

James AB, Conway AM, Thiel G & Morris BJ (2004) Egr-1 modulation of synapsin I expression: permissive effect of forskolin via cAMP. *Cell Signal* **16**, 1355-62.

Jensen MS & Yaari Y (1997) Role of intrinsic burst firing, potassium accumulation, and electrical coupling in the elevated potassium model of hippocampal epilepsy. *J Neurophysiol* **77**, 1224-1233.

Khawaled R, Bruening-Wright A, Adelman JP & Maylie J (1999) Bicuculline block of small-conductance calcium-activated potassium channels. *Eur J Physiol* **438**, 314-321.

Lau CG & Zukin RS (2007) NMDA receptor trafficking in synaptic plasticity and neuropsychiatric disorders. *Nat Rev Neurosci* **8**, 413-426.

Lisman J (2003) Long-term potentiation: outstanding questions and attempted synthesis. *Phil Trans R Soc Lond B* **358**, 829-842.

Lynch MA (2004) Long-term potentiation and memory. *Physiol Rev* **84**, 87-136.

Malenka RC & Nicoll RA (1999) Long-term potentiation – A decade of Progress ? *Science* **285**, 1871-1876.

Malenka RC & Bear MF (2004) LTP and LTD: an embarrassment of riches. *Neuron* **44**, 5-21.

Martin SJ, Grimwood PD & Morris RG (2000) Synaptic plasticity and memory: an evaluation of the hypothesis. *Annu Rev Neurosci* **23**, 649-711.

Martin KC & Zukin RS (2006) RNA trafficking and local protein synthesis: an overview. *J Neurosci* **26**, 7131-7134.

Mazzoni A, Broccard FD, Garcia-Perez E, Bonifazi P, Ruaro ME & Torre V (2007) On the dynamics of spontaneous activity in neuronal networks. *PLoS ONE* **2**(5), e439.

Mead AN & Stephens DN (2003a) Involvement of AMPA receptor GluR2 subunits in stimulus-reward learning: evidence from glutamate receptor gria2 knock-out mice. *J Neurosci* **23**, 9500-9507.

Mead AN & Stephens DN (2003b) Selective disruption of stimulus-reward learning in glutamate receptor gria1 knock-out mice. *J Neurosci* **23**, 1041-1048.

Messaoudi E, Kanhema T, Soulé J, Tiron A, Dagyte G, da Silva B & Bramham CR (2007) Sustained Arc/Arg3.1 synthesis controls long-term potentiation consolidation through regulation of local actin polymerization in the dentate gyrus in vivo. *J Neurosci* **27**, 10445-10455.

Narayanan R & Johnston D (2007) Long-term potentiation in rat hippocampal neurons is accomplished by spatially widespread changes in intrinsic oscillatory dynamics and excitability. *Neuron* **56**, 1061-1075.

O'Donovan KJ, Tourtellotte WG, Millbrandt J & Baraban JM (1999) The EGR family of transcription-regulatory factors: progress at the interface of molecular and systems neuroscience. *Trends Neurosci* **22**, 167-173.

Otmakhov N, Khibnik L, Otmakhova N, Carpenter S, Riahi S, Asrican B & Lisman J (2004) Forskolin-induced LTP in the CA1 region of the hippocampus is NMDA receptor dependent. *J Neurophysiol* **91**, 1955-1962.

Park CS, Gong R, Stuart J & Tang SJ (2006) Molecular network and chromosomal clustering of genes involved in synaptic plasticity in the hippocampus. *J Biol Chem* **281**, 30195-30211.

Rao VR, Pintchovski SA, Chin J, Peebles CL, Mitra S & Finkbeiner S (2006) AMPA receptors regulate transcription of the plasticity-related immediate-early gene Arc. *Nat Neurosci* **9**, 887-895.

Raymond CR & Redman SJ (2006) Spatial segregation of neuronal calcium signals encodes different forms of LTP in rat hippocampus. *J Physiol* **570**, 97-111.

Raymond CR (2007) LTP forms 1, 2 and 3: different mechanisms for the "long" in long-term potentiation. *Trends Neurosci* **30**, 167-175.

Richichi C, Brewster AL, Bender RA, Simeone TA, Zha Q, Yin HZ, Weiss JH & Baram TZ (2008) Mechanisms of seizure-induced 'transcriptional channelopathy' of hyperpolarization-activated cyclic nucleotide gated (HCN) channels. *Neurobiol Dis* **29**, 297-305.

Ruaro ME, Bonifazi P & Torre V (2005) Towards the neurocomputer: image processing and pattern recognition with neuronal cultures. *IEEE Trans Biomed Eng* **52**, 371-383.

Shah MM, Anderson AE, Leung V, Lin X & Johnston D (2004) Seizure-induced plasticity of h channels in entorhinal cortical layer III pyramidal neurons. *Neuron* **44**, 495-508.

Schrader LA, Birnbaum SG, Nadin BM, Ren Y, Bui D, Anderson AE & Sweatt JD (2006) MAPK regulates the Kv4.2 potassium channel by direct phosphorylation of the pore-forming subunit. *Am J Physiol Cell Physiol* **290**, C852-861.

Sweatt JD (2001) The neuronal MAP kinase cascade: a biochemical signal integration system subserving synaptic plasticity and memory. *J Neurochem* **76**, 1-10.

Thomas GM & Huganir RL (2004) MAPK cascade signalling and synaptic plasticity. *Nat Rev Neurosci* **5**, 173-183.

Tsay D, Dudman JT & Siegelbaum SA (2007) HCN1 channels constrain synaptically evoked Ca^{2+} spikes in distal dendrites of CA1 pyramidal neurons. *Neuron* **56**, 1076-1089.

Tzingounis AV & Nicoll RA (2006) Arc/Arg3.1 : linking gene expression to synaptic plasticity and memory. *Neuron* **52**, 403-407.

Villarroel A (1993) Suppression of neuronal potassium A-current by arachidonic acid. *FEBS Lett* **335**, 184-188.

Wagenaar DA & Potter SM (2002) Real-time multi-channel stimulus artifact suppression by local curve fitting. *J Neurosci Meth* **120**, 113-120.

Westbrook GL & Lothman EW (1983) Cellular and synaptic basis of kainic acid-induced hippocampal epileptiform activity. *Brain Res* **273**, 97-109.

Wiegert JS, Bengston CP & Bading H (2007) Diffusion and not active transport underlies and limits ERK1/2 synapse-to-nucleus signaling in hippocampal neurons. *J Biol Chem* **282**, 29621-29633.

Yamagata M & Sanes JR (2008) Dscam and Sidekick proteins direct lamina-specific synaptic connections in vertebrate retina. *Nature* **451**, 465-469.

Yamakawa T, Saith S**,** Li Y**,** Gao X**,** Gaisano HY & Tsushima RG (2007) Interaction of syntaxin 1A with the N-terminus of Kv4.2 modulates channel surface expression and gating. *Biochemistry* **46**, 10942-10949.

Zhang SJ, Steijaert MN, Lau D, Schütz G, Delucinge-Vivier C, Descombes P & Bading H (2007) Decoding NMDA receptor signaling: identification of genomic programs specifying neuronal survival and death. *Neuron* **53**, 549-562.

Aknowledgements

Thanks to M. Lough for critically reading the manuscript, Prof. E. Cherubini for helpful comments on a previous version of this manuscript and to H. Bading for useful discussion. This work was supported by the grant from CIPE (GRAND FVG), by the FP6 grant NEURO (12788) from the European Community and by the FIRB grant RBLA03AF28 007 from the Italian Ministry of Research (MIUR).

TABLE 1 Genes belonging to Cluster 1 and up-regulated at 90 minutes after gabazine wash-out

Gene Symbol	Gene Name	TF*	LTP	Reference
Arc	Activity regulated cytoskeletal-associated protein		+	Rodriguez JJ et al. (2005) Eur. J. Neurosci. 21:2384
Arf4l_pred.	ADP-ribosylation factor-like 4D			
Dusp5	Dual specificity phosphatase 5		+	Hevroni D et al. (1998) J. Mol. Neurosci.10:75
Egr1	Early growth response 1	+	+	M. W. Jones et al.(2001) Nat. Neurosci. 4: 289
Egr2	Early growth response 2	+	+	Williams J et al. (1995) Mol. Brain Res. 28: 87
Egr3	Early growth response 3	+	+	Li L et al. (2007) Mol. Cell. Neurosci. 35:76
Egr4	Early growth response 4	+		
Gem_pred.	GTP binding protein (expressed in skeletal muscle)			
Homer1	Homer homolog 1 (Drosophila)		+	Kato A et al. (2003) Mol. Brain Res. 118: 33
Jmjd3_pred.	Jumonji domain containing 3			
Junb	Jun-B oncogene	+	+	Abraham WC et al. (1991) Mol Neurobiol. 5:297
Klf2_predicted	Kruppel-like factor 2	+		
Klf7_predicted	Kruppel-like factor 7	+		
LOC684871				
LOC686523				
Mmp12	Matrix metallopeptidase 12			
Nfil3	Nuclear factor, interleukin 3 regulated	+		
Nr4a1	Nuclear receptor subfamily 4, group A, member1	+	+	Dragunow M. et al. (1996) Mol. Brain Res.36:349
Nr4a2	Nuclear receptor subfamily 4, group A, member2	+		
Nr4a3	Nuclear receptor subfamily 4, group A, membe 3	+		
Ptgs2	Prostaglandin-endoperoxide synthase 2		+	Slanina KA et al. (2005) Neuropharmacol. 49:660
RGD1306880_pred.				
Rgs4	Regulator of G-protein signaling 4			
Serpinb2	Serpin peptidase inhibitor, clade B member2			
Tfpi2	Tissue factor pathway inhibitor 2			

* TF Transcription factor

TABLE 2 Genes involved in LTP in cluster 1 and 2

*	Gene Symbol	Gene Name	Cluster 1	Cluster 2	Reference
S	Arc	Activity regulated cytoskeletal-associated protein	+		Rodriguez JJ et al. 2005 Eur. J. Neurosci. 21:2384
p	Bdnf	Brain derived neurotrophic factor		+	Ying S-W et al. (2002) J. Neurosci. 22:1532
P	Camk2a	Calcium/calmodulin-dependent protein kinase II, □		+	Wang H et al. (2004) Nat. Neurosci. 7:635
-	Cck	Cholecystokinin		+	Balschun D et al (1994) Neuropeptides 26:421
p	Cplx2	Complexin 2		+	Gibson HE (2005) Eur J Neurosci.22:1701
-	Dusp5	Dual specificity phosphatase 5	+		Hevroni D et al. (1998) J. Mol. Neurosci.10:75
T	Egr1	Early growth response 1	+		M. W. Jones et al.(2001) Nat. Neurosci. 4: 289
T	Egr2	Early growth response 2	+		Williams J et al. (1995) Mol. Brain Res. 28: 87
T	Egr3	Early growth response 3	+		Li L et al (2007) Mol. Cell. Neurosci. 35:76
T	Fos	FBJ murine osteosarcoma viral oncogene homolog		+	Dragunow M et al. (1989) Neurosci Lett. 101:274
C	Gria1	Glutamate receptor, ionotropic, AMPA1 (alpha 1)		+	Mead AN et al (2003a) J. Neurosci. 23:1041
C	Gria2	Glutamate receptor, ionotropic, AMPA1 (alpha 2)		+	Mead & Stephens (2003b) J Neurosci. 23:9500
-	Grp	Gastrin releasing peptide		+	Shumyatsky GP et al. (2002) Cell 111: 905
S	Homer1	Homer homolog 1 (Drosophila)	+	+	Kato A et al. (2003) Mol. Brain Res. 118: 33
T	Junb	Jun-B oncogene	+		Abraham WC et al (1991) Mol Neurobiol. 5:297
C	Kcna4	Potassium voltage-gated channel, shaker-related, 4		+	Meiri N et al (1998)Proc Natl Acad Sci U S A. 95:15037
C	Kcnab1	Potassium voltage-gated channel shaker-related, □ 1		+	Murphy GG et al (2004) Curr Biol 14:1907
C	Kcnd2	Potassium voltage-gated channel, Shal-related, 2		+	Chen X et al (2006) J Neurosci 26:12143
C	Kcnn2	Potassium calcium-activated channel subfamily N, 2		+	Kramar EA et al. (2004) J. Neurosci. 24:5151
p	L1cam	L1 cell adhesion molecule		+	Itoh K et al(2005) Mol CellNeurosci. 29:245
p	Nptx1	Neuronal pentraxin 1		+	Ring et al. (2006) J. Neurobiol. 66:361
T	Nr4a1	Nuclear receptor subfamily 4, group A, member 1	+		Dragunow M. et al. (1996) Mol. Brain Res.36:349
P	Nrgn	Neurogranin		+	Kuo-Ping Huang et al. (2004) J. Neurosci. 24:10660
-	Nsg1	Neuron specific gene family member 1		+	Ernfors et al.(2003)TRENDS in Neuroscience 26: 171
P	Ntrk2	Neurotrophic tyrosine kinase, receptor, type 2 (TrkB)		+	Gooney M. et al (2001) J. Neurochem. 77: 1198
P	Ntrk3	Neurotrophic tyrosine kinase, receptor, type 3 (TrkC)		+	Bramham CR (1996) J. Comp. Neurol. 368:371
-	Pnoc	Prepronociceptin		+	Ring et al. (2006) J. Neurobiol. 66:361
-	Prkar1b	Proteinkinase,cAMPdependent regulatory, type1, beta		+	Hensch TK et al (1998) J.Neurosci. 18:2108
-	Prkcc	Protein kinase C, gamma		+	Gärtner A (2006) J. Neurosci. 26:3496
P	Ptgs2	Prostaglandin-endoperoxide synthase 2 (Cox2)	+		Slanina KA et al., (2005) Neuropharmacol. 49:660
p	Rab3a	RAB3A, member RAS oncogene family		+	Castillo PE et al. (1997) Nature 388: 590
-	Reln	Reelin		+	Weeber et al. (2002) J.Biol. Chem. 277:39944
p	Rgs2	Regulator of G-protein signaling 2		+	Ingi T et al (1998) J. Neurosci. 19:7179
-	Rnf39	Ring finger protein 39		+	Matsuo R et al. (2001) BBRC 288: 479
-	Ryr2	Ryanodine receptor 2		+	Welsby P. et al. (2006) Eur. J. Neurosci. 24: 3109
P	Shank1	SH3 and multiple ankyrin repeat domain 1			Hung AY et al (2008) J.Neurosci. 28:1697
p	Snap25	Synaptosomal-associated protein 25		+	Roberts LA et al (1998) Neuroreport 9:33
p	Stx1a	Syntaxin 1A (brain)		+	Fujiwara et al. (2006) J. Neurosci. 26:5767
p	Stx1b2	Syntaxin 1B2		+	Helme-Guizon et al. (1998) Eur. J. Neurosci. 10:2231
p	Syn1	Synapsin I		+	Sato K et al. 2000 Brain Res. 872:219
p	Syn2	Synapsin II		+	Spillane et al. (1995) Neuropharmacol 34:1573
p	Syp	Synaptophysin		+	Janz R. et al.(1999) Neuron 24: 687
-	Vsnl1	Visinin-like 1		+	Brackmann M.et al. (2004) BBRC 322: 1073

* S= Structural p=presynaptic P=postsynaptic T= transcription factor C= channel

TABLE 3 List of genes involved in structural, pre- and post-synaptic processes

Gene Name	Gene Symbol	Cluster
Presynaptic		
ATPase, Ca++ transporting, plasma membrane 2	Atp2b2	2
ATPase, H+ transporting, V1 subunit G isoform 2	Atp6v1g2	2
Complexin 1	Cplx1	2
Dynamin 1	Dnm1	2
EF hand calcium binding protein 2	Efcbp2 o NECAB2	2
Kinesin family member 1A	Kif1a	2
Protein kinase C and casein kinase substrate in neurons 1	Pacsin1 o syndapin I	2
Protein tyrosine phosphatase, receptor type, f polypeptide, interacting protein (liprin), α3	Ppfia3	2
Regulator of G-protein signaling 4	Rgs4	2
Regulator of G-protein signaling 7	Rgs7	2
Solute carrier family 17 (Na-dependent inorganic phosphate cotransporter), member 6	Slc17a6	2
Solute carrier family 17 (Na-dependent inorganic phosphate cotransporter), member 7	Slc17a7	2
Solute carrier family 32 (GABA vesicular transporter), member 1	Slc32a1	2
Solute carrier family 6 (neurotransmitter transporter, GABA), member 1	Slc6a1 o GAT1	2
Somatostatin	Sst	2
Spectrin beta 3	Spnb3	2
Synaptic vesicle glycoprotein 2a	Sv2a	2
Synaptogyrin 3 (predicted)	Syngr3_predicted	2
Synaptoporin	Synpr	2
Synaptotagmin I	Syt1	2
Synaptotagmin XIII	Syt13	2
Synaptotagmin-like 2 (predicted)	Sytl2_predicted	3
Synuclein, alpha	Snca	2
Synuclein, beta	Sncb	2
Vesicle-associated membrane protein 1	Vamp1	2
Vesicular membrane protein p24 (predicted)	Vmp_predicted	2
Postsynaptic		
Calcium binding protein 1	Cabp1	2
Calcium/calmodulin-dependent protein kinase II, alpha	Camk2a	2
Connector enhancer of kinase suppressor of Ras 2	Cnksr2	2
Dendrin	Ddn	2
Dipeptidylpeptidase 10	Dpp10	2
Discs, large homolog 2 (Drosophila)	Dlgh2	2
Dopamine receptor D1 interacting protein	Drd1ip	2
G protein-coupled receptor 85	Gpr85	2
Glycine receptor, alpha 2 subunit	Glra2	2
Guanine nucleotide binding protein, gamma 2	Gng2	2
Inositol 1,4,5-trisphosphate 3-kinase A	Itpka	2
Junctophilin 3 (predicted)	Jph3_predicted	2
Kinesin family member C2	KIFC2	2
Leucine rich repeat and fibronectin type III domain containing 5 (predicted)	Lrfn5_predicted	2
Lin-7 homolog b (C. elegans)	Lin7b o MALS	2
N-ethylmaleimide sensitive fusion protein	Nsf	2
Opioid binding protein/cell adhesion molecule-like	Opcml o OBCAM	2
Protein kinase C, epsilon	Prkce	2
Protein tyrosine phosphatase, non-receptor type 5	Ptpn5 o STEP	2

Protein tyrosine phosphatase, receptor type, R	Ptprr	2
Rap guanine nucleotide exchange factor (GEF) 4	Rapgef4	2
Solute carrier family 12, (potassium-chloride transporter) member 5	Slc12a5 o KCC2	2
Somatostatin receptor 1	Sstr1	2
Somatostatin receptor 2	Sstr2	2
Structural		
Cadherin 10	Cdh10	2
Cadherin 11	Cdh11	2
Calcium/calmodulin-dependent protein kinase II, beta	Camk2b	2
Doublecortin	Dcx	2
Down syndrome cell adhesion molecule	Dscam	2
Fibulin 2	Fbln2	3
Integrin alpha 1	Itga1	3
Lysyl oxidase	Lox	3
Microtubule-associated protein tau	Mapt	2
Neurexin 3	Nrxn3	2
Neurexophilin 1	Nxph1	2
Neurofilament, heavy polypeptide	Nefh	2
Neurofilament, light polypeptide	Nefl	2
Neurotrimin	Hnt	2
Nexilin	Nexn	3
Nidogen 2	Nid2	3
Plakophilin 2	Pkp2	3
Plasticity related gene 1	Prg1	2
Pregnancy upregulated non-ubiquitously expressed CaM kinase	Pnck	2
Procollagen, type I, alpha 2	Col1a2	3
Procollagen, type IV, alpha 1	Col4a1	3
Procollagen, type V, alpha 2	Col5a2	3
Procollagen, type XI, alpha 1	Col11a1	3
Protocadherin 17 (predicted)	Pcdh17_predicted	2
Protocadherin 20 (predicted)	Pcdh20_predicted	2
Protocadherin 8	Pcdh8	2
Rho guanine nucleotide exchange factor 7	Arhgef7	2
Seizure related 6 homolog (mouse)	Sez6	2
SLIT and NTRK-like family, member 1 (predicted)	Slitrk1_predicted	2
Stathmin-like 3	Stmn3 o SCLIP	2
Stathmin-like 4	Stmn4 o RB3	2
T-cell lymphoma invasion and metastasis 1	Tiam1	2
Thrombospondin 1	Thbs1	3
Tissue inhibitor of metalloproteinase 3	Timp3	3
Transgelin	Tagln	3
Tubulin, beta 3	Tubb3	2
Tubulin, beta 4	Tubb4	2
Unc-5 homolog C (C. elegans)	Unc5c	3
Vasoactive intestinal polypeptide	Vip	2

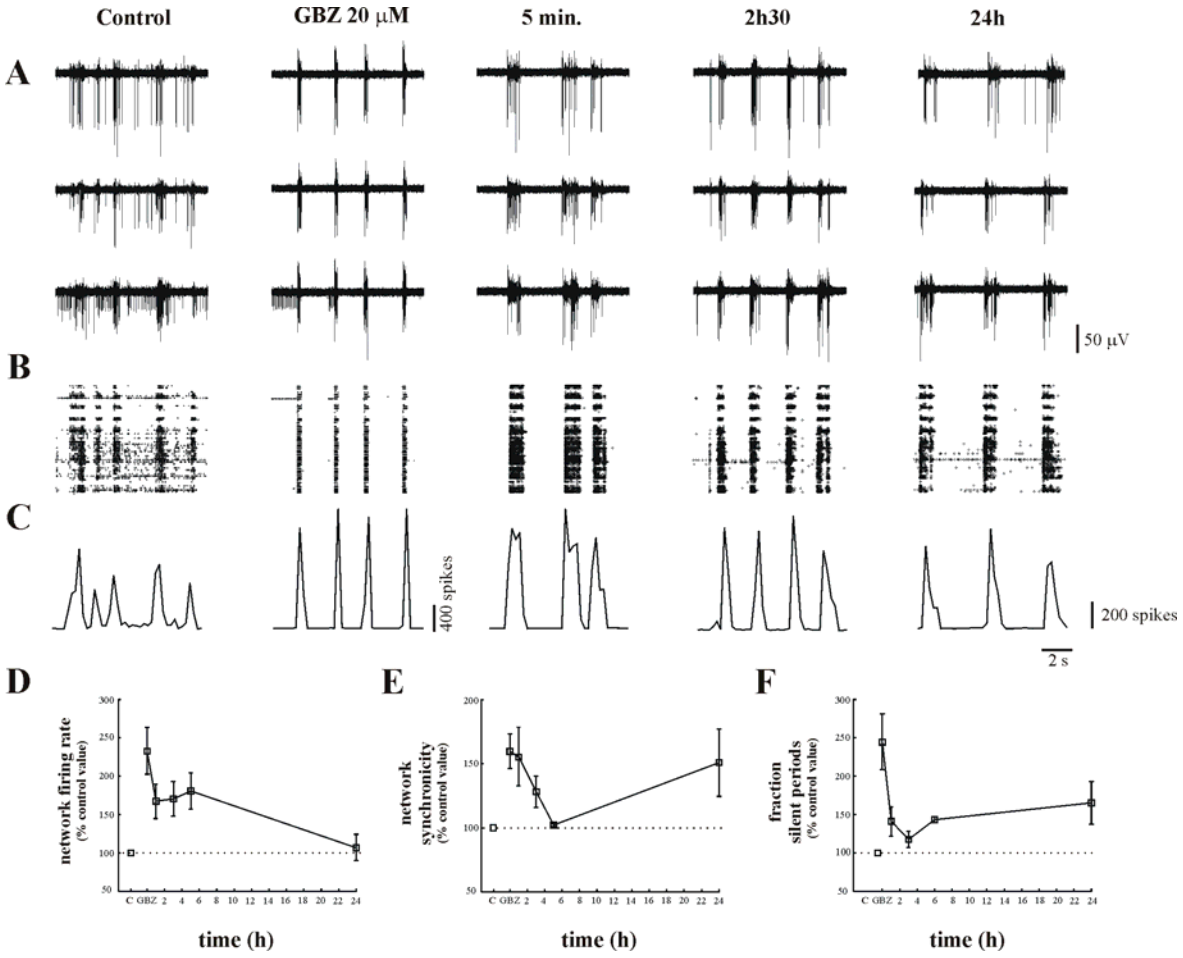
Control
GBZ 20 μM
5 min.
2h30
24h
A
50 μV
B
C
400 spikes
200 spikes
2 s
D
E
F
network firing rate
(% control value)
network
synchronicity
(% control value)
fraction
silent periods
(% control value)
time (h)
time (h)
time (h)

Fig. 1

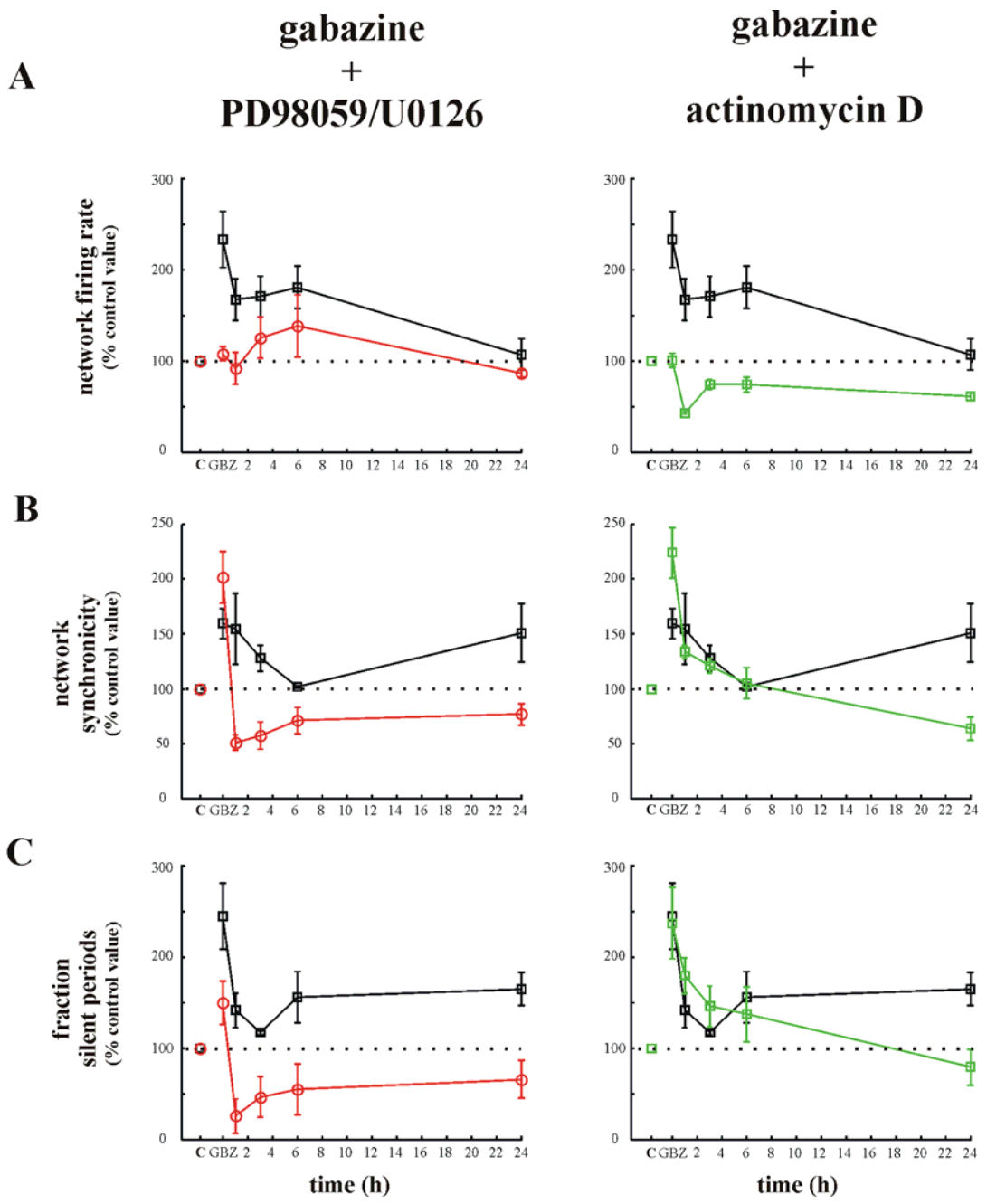
A
gabazine
+
PD98059/U0126
gabazine
+
actinomycin D
network firing rate
(% control value)
B
network
synchronicity
(% control value)
C
fraction
silent periods
(% control value)
C GBZ 2 4 6 8 10 12 14 16 18 20 22 24
time (h)

Fig. 2

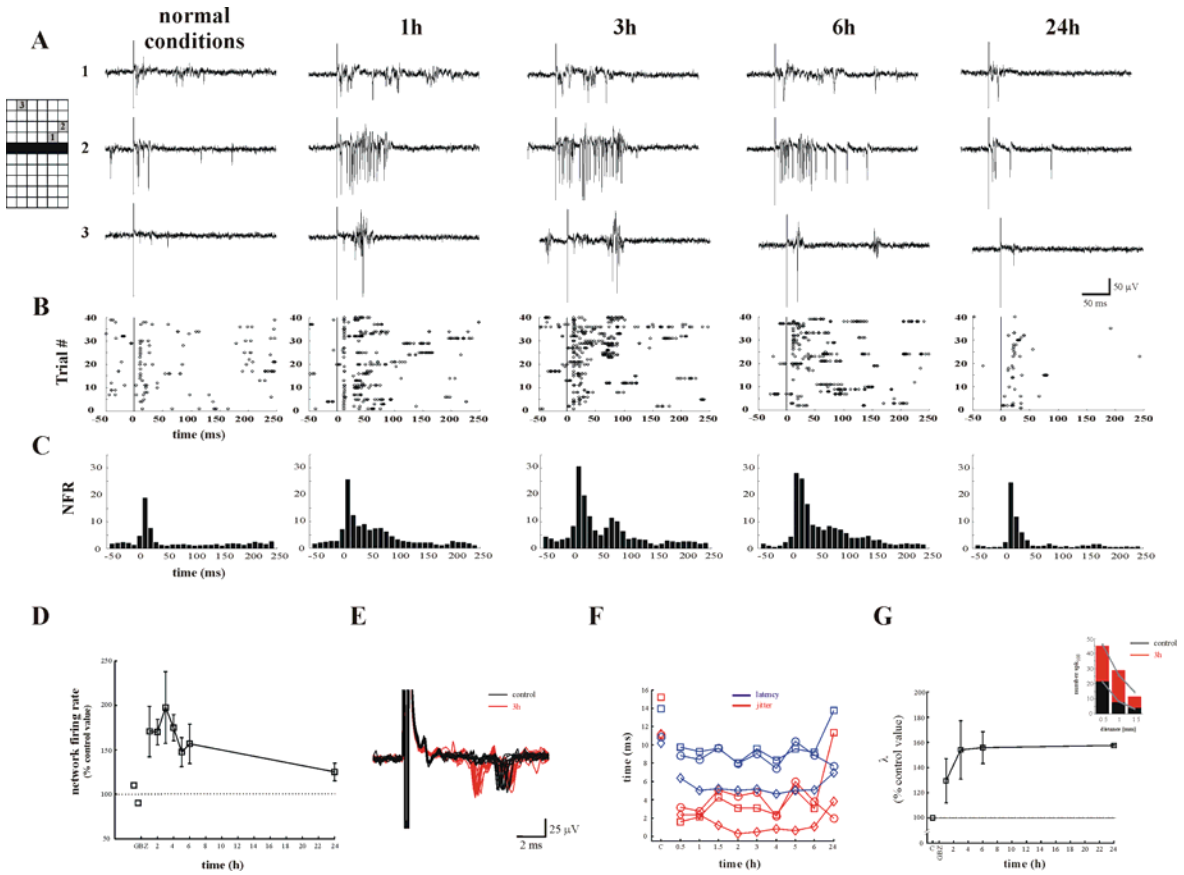
A
normal conditions
1h
3h
6h
24h
1
2
3
50 µV
50 ms
B
Trial #
time (ms)
C
NFR
time (ms)
D
network firing rate (% control value)
time (h)
E
control
3h
25 µV
2 ms
F
latency
jitter
time (ms)
time (h)
G
control
3h
λ (% control value)
time (h)

Fig. 3

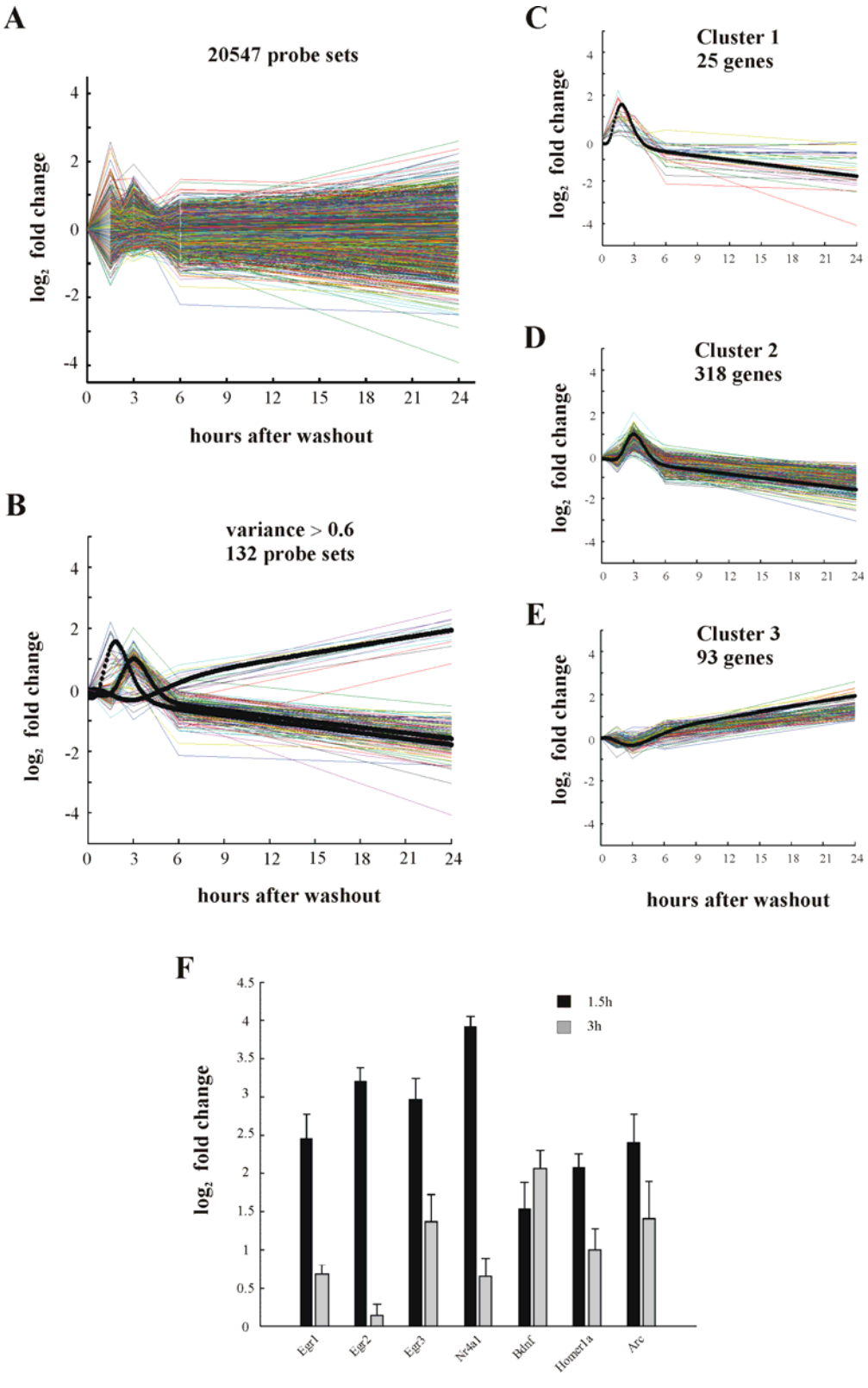
A
20547 probe sets
log2 fold change
hours after washout
B
variance > 0.6
132 probe sets
log2 fold change
hours after washout
C
Cluster 1
25 genes
log2 fold change
D
Cluster 2
318 genes
log2 fold change
E
Cluster 3
93 genes
log2 fold change
hours after washout
F
log2 fold change
1.5h
3h
Egr1
Egr2
Egr3
Nr4a1
Bdnf
Homer1a
Arc

Fig. 4

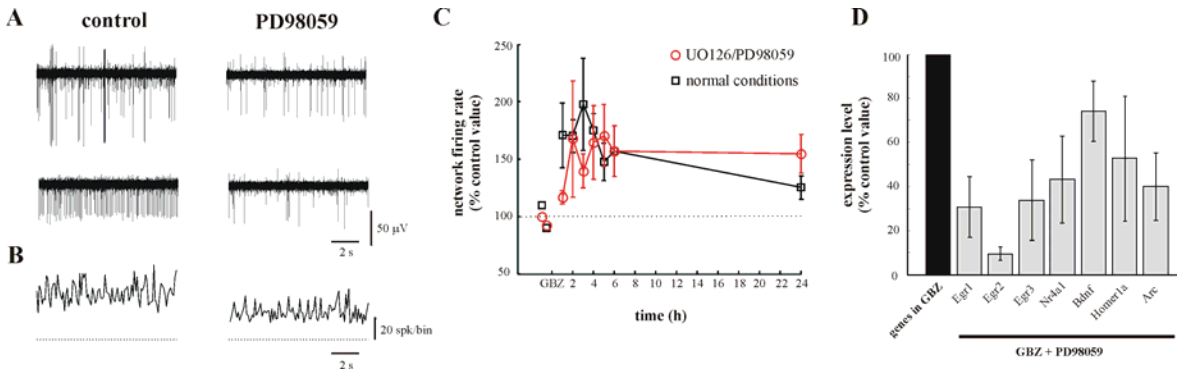
A
control
PD98059
50 µV
2 s
B
20 spk/bin
2 s
C
UO126/PD98059
normal conditions
network firing rate
(% control value)
GBZ
time (h)
D
expression level
(% control value)
genes in GBZ
Egr1
Egr2
Egr3
Nr4a1
Bdnf
Homer1a
Arc
GBZ + PD98059

Fig. 5

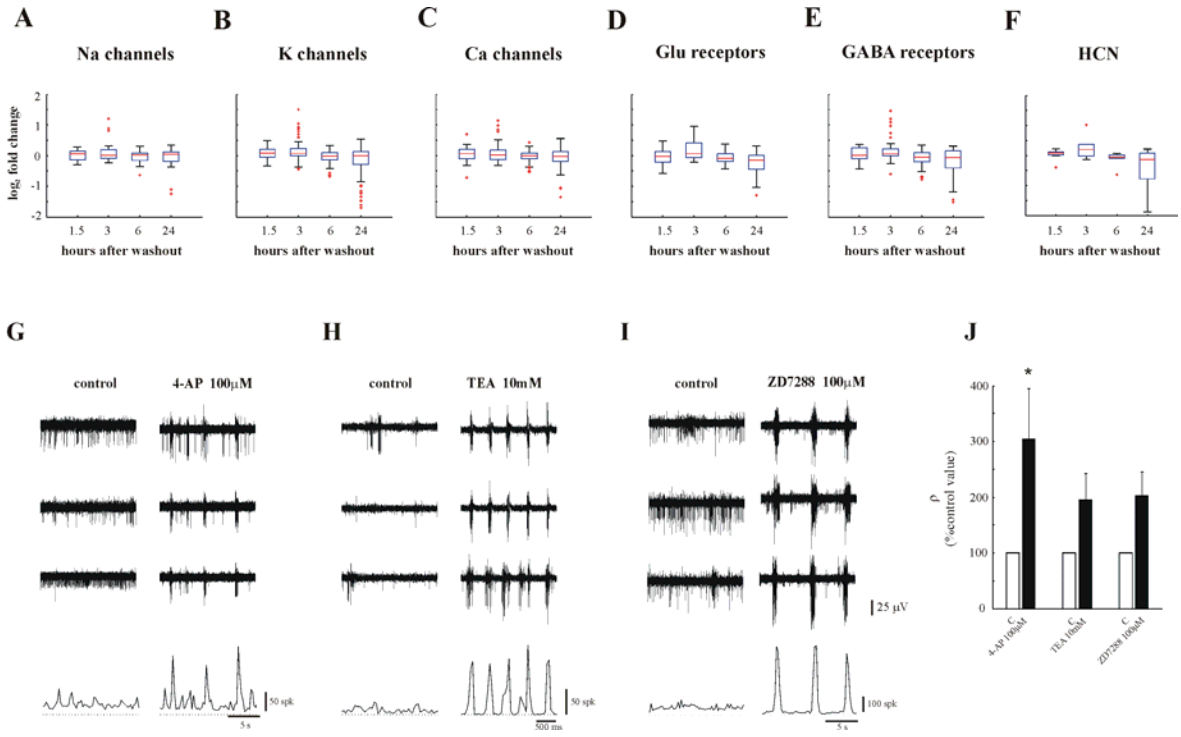
A
Na channels
B
K channels
C
Ca channels
D
Glu receptors
E
GABA receptors
F
HCN
log2 fold change
hours after washout
G
control
4-AP 100µM
H
control
TEA 10mM
I
control
ZD7288 100µM
25 µV
50 spk
100 spk
J
ρ
(*control value)
4-AP 100µM
TEA 10mM
ZD7288 100µM

Fig. 6

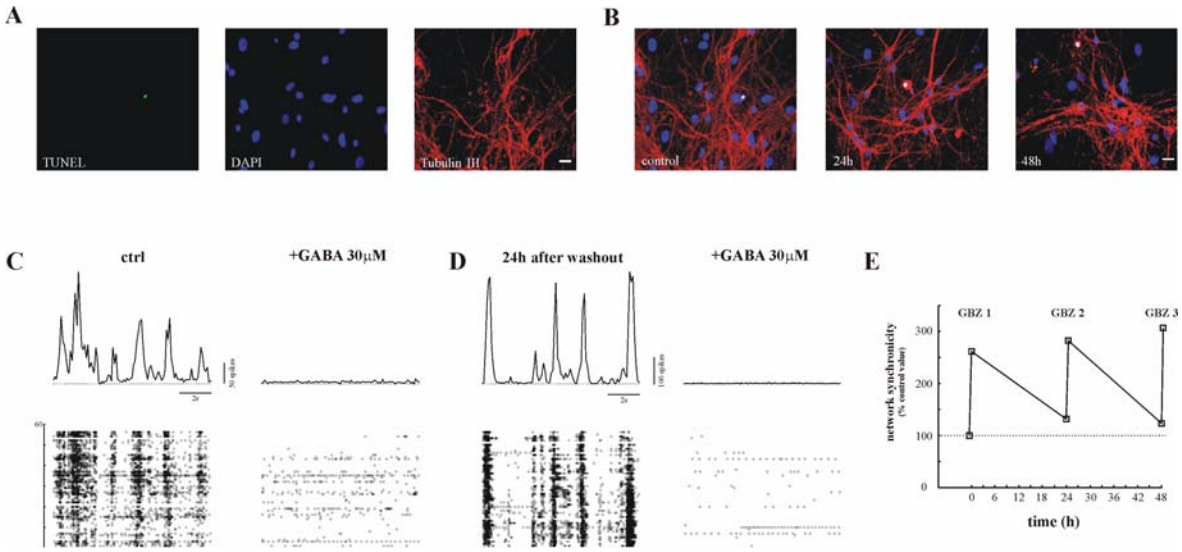
A
TUNEL
DAPI
Tubulin III
B
control
24h
48h
C
ctrl
+GABA 30μM
D
24h after washout
+GABA 30μM
E
GBZ 1
GBZ 2
GBZ 3
network synchronicity
(% control value)
300
200
100
0
0 6 12 18 24 30 36 42 48
time (h)

Fig. 7

Supplementary Table S1

List of all genes present in clusters 1, 2 and 3

CLUSTER 1			
Affymetrix ID	**GenBank ID**	**Gene Name**	**Gene Symbol**
1387068_at	NM_019361	activity regulated cytoskeletal-associated protein	Arc
1380383_at	AI030650	ADP-ribosylation factor 4-like (predicted)	Arf4l_predicted
1368124_at	NM_133578	dual specificity phosphatase 5	Dusp5
1368321_at	NM_012551	early growth response 1	Egr1
1387306_a_at	NM_053633	early growth response 2	Egr2
1392791_at	AA964492	Early growth response 3	Egr3
1387442_at	NM_019137	early growth response 4	Egr4
1382351_at	AI069972	GTP binding protein (gene overexpressed in skeletal muscle) (predicted)	Gem_predicted
1370997_at	AF030088	homer homolog 1 (Drosophila)	Homer1
1390000_at	BE118720	jumonji domain containing 3 (predicted)	Jmjd3_predicted
1387788_at	NM_021836	Jun-B oncogene	Junb
1376569_at	BM385790	Kruppel-like factor 2 (lung) (predicted)	Klf2_predicted
1380363_at	BF420490	Kruppel-like factor 7 (ubiquitous) (predicted)	Klf7_predicted
1373403_at	AI230625	similar to Protein C8orf4 (Thyroid cancer protein 1) (TC-1)	LOC684871
1397460_at	BE119491	Similar to G protein-coupled receptor 158 isoform a	LOC686523
1368530_at	NM_053963	matrix metallopeptidase 12	Mmp12
1368488_at	NM_053727	nuclear factor, interleukin 3 regulated	Nfil3
1386935_at	NM_024388	nuclear receptor subfamily 4, group A, member 1	Nr4a1
1369007_at	L08595	nuclear receptor subfamily 4, group A, member 2	Nr4a2
1369067_at	NM_031628	nuclear receptor subfamily 4, group A, member 3	Nr4a3
1368527_at	U03389	prostaglandin-endoperoxide synthase 2	Ptgs2
1397241_at	BE101570	similar to hypothetical protein MGC47816 (predicted)	RGD1306880_predicted
1368506_at	U27767	regulator of G-protein signaling 4	Rgs4
1368487_at	NM_021696	serine (or cysteine) proteinase inhibitor, clade B, member 2	Serpinb2
1377340_at	AI179507	tissue factor pathway inhibitor 2	Tfpi2

CLUSTER 2			
Affymetrix ID	**GenBank ID**	**Gene Name**	**Gene Symbol**
1384869_at	AW531594	abhydrolase domain containing 7 (predicted)	Abhd7_predicted
1370206_at	BM386997	amiloride-sensitive cation channel 4, pituitary	Accn4
1382608_at	BI281712	actin-like 6B (predicted)	Actl6b_predicted
1370638_at	AF069525	ankyrin 3, epithelial	Ank3
1385910_at	AW533307	Rho guanine nucleotide exchange factor 7	Arhgef7
1376198_at	BI303342	adipocyte-specific adhesion molecule	Asam
1393141_at	BF285419	Aspartate-beta-hydroxylase (predicted)	Asph_predicted
1383340_at	BG671011	ataxia, cerebellar, Cayman type (caytaxin) (predicted)	Atcay_predicted
1368701_at	NM_012506	ATPase, Na+/K+ transporting, alpha 3 polypeptide	Atp1a3
1368698_at	J03754	ATPase, Ca++ transporting, plasma membrane 2	Atp2b2
1388037_at	J05087	ATPase, Ca++ transporting, plasma membrane 3	Atp2b3
1377722_at	BE100072	ATPase, H+ transporting, V1 subunit G isoform 2	Atp6v1g2
1369755_at	AF106624	beta-1,3-glucuronyltransferase 2 (glucuronosyltransferase S)	B3gat2
1383010_at	AW531880	B-cell CLL/lymphoma 11A (zinc finger protein)	Bcl11a
1391948_at	BM390227	B-cell leukemia/lymphoma 11B (predicted)	Bcl11b_predicted
1368677_at	NM_012513	brain derived neurotrophic factor	Bdnf

1388802_at	AI579422	brain expressed X-linked 1	Bex1
1381995_at	AW530502	bruno-like 4, RNA binding protein (Drosophila) (predicted)	Brunol4_predicted
1376707_at	AW918311	C1q and tumor necrosis factor related protein 4 (predicted)	C1qtnf4_predicted
1386922_at	AI408948	carbonic anhydrase 2	Ca2
1369886_a_at	AJ315761	calcium binding protein 1	Cabp1
1390358_at	BF405996	calcium channel, voltage-dependent, alpha 2/delta 3 subunit	Cacna2d3
1382898_at	BG376849	calcium channel, voltage-dependent, beta 4 subunit	Cacnb4
1368759_at	NM_053351	calcium channel, voltage-dependent, gamma subunit 2	Cacng2
1370757_at	AF361340	calcium channel, voltage-dependent, gamma subunit 3	Cacng3
1387133_at	NM_053988	calbindin 2	Calb2
1391229_at	BG381458	calcium/calmodulin-dependent protein kinase I gamma	Camk1g
1388187_at	BM384558	calcium/calmodulin-dependent protein kinase II, alpha	Camk2a
1398251_a_at	NM_021739	calcium/calmodulin-dependent protein kinase II, beta	Camk2b
1368845_at	NM_024000	CaM kinase-like vesicle-associated	Camkv
1370438_at	AF037071	C-terminal PDZ domain ligand of neuronal nitric oxide synthase	Capon
1385519_at	BE105678	CBFA2T1 identified gene homolog (human) (predicted)	Cbfa2t1_predicted
1387032_at	NM_012829	cholecystokinin	Cck
1369670_at	NM_031518	Cd200 antigen	Cd200
1391127_at	BF400818	Cell division cycle 42 homolog (S. cerevisiae)	Cdc42
1380317_at	BF402765	cadherin 10	Cdh10
1391146_at	BE111632	cadherin 11	Cdh11
1369425_at	NM_138889	cadherin 13	Cdh13
1368887_at	NM_019161	cadherin 22	Cdh22
1387194_at	U51013	centaurin, alpha 1	Centa1
1397549_at	AW526039	centaurin, gamma 1	Centg1
1373256_at	BM391119	chromodomain helicase DNA binding protein 3	Chd3
1387235_at	NM_021655	chromogranin A	Chga
1368034_at	NM_012526	chromogranin B	Chgb
1368287_at	NM_032083	chimerin (chimaerin) 1	Chn1
1387462_at	NM_012527	cholinergic receptor, muscarinic 3	Chrm3
1395429_at	BF281401	Cholinergic receptor, nicotinic, alpha polypeptide 7	Chrna7
1394334_at	BF545197	carbohydrate (N-acetylgalactosamine 4-0) sulfotransferase 8 (predicted)	Chst8_predicted
1390566_a_at	BI301453	creatine kinase, mitochondrial 1, ubiquitous	Ckmt1
1372492_at	AI412937	claudin 10 (predicted)	Cldn10_predicted
1369731_at	AF102854	connector enhancer of kinase suppressor of Ras 2	Cnksr2
1369964_at	NM_130411	coronin, actin binding protein 1A	Coro1a
1368648_at	NM_053472	cytochrome c oxidase subunit IV isoform 2	Cox4i2
1398357_at	BI281575	complexin 1	Cplx1
1368584_a_at	NM_053878	complexin 2	Cplx2
1384780_at	BF402747	copine IV (predicted)	Cpne4_predicted
1368381_at	NM_134401	cartilage acidic protein 1	Crtac1
1368059_at	NM_053955	crystallin, mu	Crym
1368200_at	NM_134455	chemokine (C-X3-C motif) ligand 1	Cx3cl1
1369408_at	NM_080482	deleted in bladder cancer chromosome region candidate 1 (human)	Dbccr1
1374966_at	BE109057	doublecortin	Dcx
1388177_at	X96589	dendrin	Ddn
1387265_at	NM_013126	diacylglycerol kinase, gamma	Dgkg
1375433_at	AI412473	Dispatched homolog 2 (Drosophila) (predicted)	Disp2_predicted
1375139_at	BF406295	Discs, large homolog 2 (Drosophila)	Dlgh2
1392064_at	BF400590	distal-less homeobox 1	Dlx1

1377125_at	AW523481	DnaJ (Hsp40) homolog, subfamily C, member 6 (predicted)	Dnajc6_predicted
1368292_at	NM_080689	dynamin 1	Dnm1
1393299_at	BF567794	dipeptidylpeptidase 10	Dpp10
1376345_at	BG381734	dopamine receptor D1 interacting protein	Drd1ip
1368699_at	NM_133587	Down syndrome cell adhesion molecule	Dscam
1391246_at	BF390318	dystrobrevin alpha (predicted)	Dtna_predicted
1387025_at	NM_019234	dynein cytoplasmic 1 intermediate chain 1	Dync1i1
1367799_at	NM_012660	eukaryotic translation elongation factor 1 alpha 2	Eef1a2
1368443_at	NM_133415	EF hand calcium binding protein 2	Efcbp2
1383078_at	BG381007	ephrin B3 (predicted)	Efnb3_predicted
1383736_at	AI145457	ELAV (embryonic lethal, abnormal vision, Drosophila)-like 2 (Hu antigen B)	Elavl2
1368114_at	NM_053428	fibroblast growth factor 13	Fgf13
1375043_at	BF415939	FBJ murine osteosarcoma viral oncogene homolog	Fos
1387383_at	NM_031802	gamma-aminobutyric acid (GABA) B receptor 2	Gabbr2
1380828_at	AI145413	gamma-aminobutyric acid A receptor, alpha 1	Gabra1
1371057_at	AW520967	gamma-aminobutyric acid (GABA-A) receptor, subunit alpha 5	Gabra5
1369904_at	NM_012956	gamma-aminobutyric acid (GABA-A) receptor, subunit beta 1	Gabrb1
1391653_at	BE120391	gamma-aminobutyric acid A receptor, gamma 2	Gabrg2
1396238_at	AI763990	UDP-N-acetyl-alpha-D-galactosamine:polypeptide N-acetylgalactosaminyltransferase 14	Galnt14
1387696_a_at	X61159	glycine receptor, alpha 2 subunit	Glra2
1367633_at	BI296610	glutamate-ammonia ligase (glutamine synthase)	Glul
1387906_a_at	AF107845	GNAS complex locus	Gnas
1386660_at	BF565021	Guanine nucleotide binding protein, gamma 2	Gng2
1368272_at	D00252	glutamate oxaloacetate transaminase 1	Got1
1368786_a_at	NM_030831	G-protein coupled receptor 12	Gpcr12
1384004_at	AI030360	G protein-coupled receptor 158 (predicted)	Gpr158_predicted
1382319_at	BM389005	G protein-coupled receptor 68 (predicted)	Gpr68_predicted
1368299_at	NM_080411	G protein-coupled receptor 83	Gpr83
1387666_at	AF203907	G protein-coupled receptor 85	Gpr85
1375050_at	BI294558	G protein-regulated inducer of neurite outgrowth 1 (predicted)	Gprin1_predicted
1371013_at	BG376217	glutamate receptor, ionotropic, AMPA1 (alpha 1)	Gria1
1394578_at	BI299761	Glutamate receptor, ionotropic, AMPA2	Gria2
1368572_a_at	NM_017010	glutamate receptor, ionotropic, N-methyl D-aspartate 1	Grin1
1368306_at	U08259	glutamate receptor, ionotropic, NMDA2C	Grin2c
1387286_at	NM_017011	glutamate receptor, metabotropic 1	Grm1
1388189_at	AW522430	glutamate receptor, metabotropic 3	Grm3
1368611_at	NM_133570	gastrin releasing peptide	Grp
1369097_s_at	NM_012769	guanylate cyclase 1, soluble, beta 3	Gucy1b3
1379920_at	BG671844	Hyperpolarization-activated cyclic nucleotide-gated potassium channel 1	Hcn1
1374105_at	H31665	hypoxia induced gene 1	Hig1
1368255_at	NM_017354	neurotrimin	Hnt
1370454_at	AB003726	homer homolog 1 (Drosophila)	Homer1
1375765_at	BI296503	Hippocalcin-like 4	Hpcal4
1386953_at	NM_017080	hydroxysteroid 11-beta dehydrogenase 1	Hsd11b1
1373480_at	BG670210	heat shock 70kDa protein 12A (predicted)	Hspa12a_predicted
1387226_at	NM_019128	internexin, alpha	Inexa
1391036_at	BG376106	IQ motif and Sec7 domain 3	Iqsec3
1387291_at	NM_017351	inter-alpha trypsin inhibitor, heavy chain 3	Itih3
1368462_at	NM_031045	inositol 1,4,5-trisphosphate 3-kinase A	Itpka
1385562_at	AI059487	junctophilin 3 (predicted)	Jph3_predicted

1369043_at	NM_012971	potassium voltage-gated channel, shaker-related subfamily, member 4	Kcna4
1378738_at	BE097574	potassium voltage-gated channel, shaker-related subfamily, beta member 1	Kcnab1
1368524_at	NM_012856	potassium voltage gated channel, Shaw-related subfamily, member 1	Kcnc1
1370439_a_at	M34052	potassium voltage gated channel, Shaw-related subfamily, member 2	Kcnc2
1379863_at	AW528891	potassium voltage gated channel, Shal-related family, member 2	Kcnd2
1373987_at	AI410448	Kv channel-interacting protein 2	Kcnip2
1383220_at	BE114231	Kv channel interacting protein 4	Kcnip4
1373991_at	AI411366	Potassium inwardly-rectifying channel, subfamily J, member 16	Kcnj16
1369035_a_at	AB073753	potassium inwardly-rectifying channel, subfamily J, member 6	Kcnj6
1370111_at	NM_019314	potassium intermediate/small conductance calcium-activated channel, subfamily N, member 2	Kcnn2
1392785_at	AA800908	Potassium channel tetramerisation domain containing 12 (predicted)	Kctd12_predicted
1397505_at	BE115743	kinesin family member 1A	Kif1a
1380172_at	BE104278	kinesin family member 5C (predicted)	Kif5c_predicted
1378197_at	AW433953	kinesin family member C2	KIFC2
1369213_at	NM_017345	L1 cell adhesion molecule	L1cam
1386023_at	AI229354	leucine-rich repeat LGI family, member 1	Lgi1
1370078_at	NM_021758	lin-7 homolog b (C. elegans)	Lin7b
1382207_at	BE097085	similar to Cerebellin-2 precursor (Cerebellin-like protein)	LOC288979
1383571_at	BF411217	hypothetical protein LOC303515	LOC303515
1377615_at	AI112395	similar to hypothetical protein	LOC304280
1391513_at	BE110237	Similar to hypothetical protein FLJ20331	LOC310946
1383422_at	AW252401	hypothetical LOC362564	LOC362564
1380866_at	AA817746	similar to adenylate kinase 5 isoform 1	LOC365985
1378904_at	AW529244	similar to solute carrier family 7, member 14	LOC499587
1385950_at	AI454926	hypothetical protein LOC500102	LOC500102
1391030_at	AW524694	similar to calmodulin-binding transcription activator 1	LOC500591
1398659_at	AW528611	similar to crossveinless 2 CG15671-PA	LOC501231
1378857_at	AI716196	similar to transcription elongation factor A (SII)-like 5	LOC678833
1381132_at	AI501937	Similar to TAFA2 protein	LOC680647
1373648_at	AI102627	similar to Protein C6orf142 homolog	LOC681849
1376736_at	BG375419	hypothetical protein LOC683263	LOC683263
1396388_at	AW522161	similar to Potassium channel tetramerisation domain-containing protein 4	LOC684884
1396381_at	BE097451	hypothetical protein LOC684957	LOC684957
1378064_at	AI144892	Hypothetical protein LOC689106	LOC689106
1386119_at	BE110033	Hypothetical protein LOC689147	LOC689147
1398405_at	BI289917	similar to septin 6	LOC691335
1384942_at	AA818417	leucine rich repeat and fibronectin type III domain containing 5 (predicted)	Lrfn5_predicted
1368964_at	NM_030856	leucine rich repeat protein 3, neuronal	Lrrn3
1387947_at	U56241	v-maf musculoaponeurotic fibrosarcoma oncogene family, protein B (avian)	Mafb
1368137_at	NM_017212	microtubule-associated protein tau	Mapt
1387834_at	NM_021859	megakaryocyte-associated tyrosine kinase	Matk
1389605_at	AI101952	multiple coiled-coil GABABR1-binding protein	MGC125215
1376106_at	AI010157	similar to hypothetical protein MGC33926	MGC94782
1370831_at	AY081195	monoglyceride lipase	Mgll
1388300_at	AA892234	microsomal glutathione S-transferase 3 (predicted)	Mgst3_predicted
1378430_at	AI555053	monooxygenase, DBH-like 1	Moxd1
1370535_at	U48809	myelin transcription factor 1-like	Myt1l
1372953_at	AI101330	neurocalcin delta	Ncald
1367956_at	NM_053543	neurochondrin	Ncdn
1370815_at	AF031879	neurofilament, heavy polypeptide	Nefh

1370058_at	NM_031783	neurofilament, light polypeptide	Nefl
1370016_at	NM_031070	nel-like 2 homolog (chicken)	Nell2
1370977_at	X66022	neuronal d4 domain family member	Neud4
1387288_at	NM_019218	neurogenic differentiation 1	Neurod1
1369999_a_at	NM_053601	neuronatin	Nnat
1370517_at	U18772	neuronal pentraxin 1	Nptx1
1376362_at	BG380575	neuronal pentraxin receptor	Nptxr
1370211_at	BE106940	neurogranin	Nrgn
1370570_at	AF016296	neuropilin 1	Nrp1
1368261_at	NM_053817	neurexin 3	Nrxn3
1369689_at	AF142097	N-ethylmaleimide sensitive fusion protein	Nsf
1387817_at	NM_024128	neuron specific gene family member 1	Nsg1
1368972_at	NM_012731	neurotrophic tyrosine kinase, receptor, type 2	Ntrk2
1368939_a_at	L14447	neurotrophic tyrosine kinase, receptor, type 3	Ntrk3
1368688_at	NM_022695	neurotensin receptor 2	Ntsr2
1369079_at	NM_012994	neurexophilin 1	Nxph1
1368993_at	NM_020088	odd Oz/ten-m homolog 2 (Drosophila)	Odz2
1387927_a_at	U03415	olfactomedin 1	Olfm1
1369417_a_at	NM_053848	opioid binding protein/cell adhesion molecule-like	Opcml
1368958_at	NM_017294	protein kinase C and casein kinase substrate in neurons 1	Pacsin1
1395792_at	AI549034	Poly(rC) binding protein 2	Pcbp2
1384509_s_at	BF558981	protocadherin 17 (predicted)	Pcdh17_predicted
1391208_at	BG379836	protocadherin 20 (predicted)	Pcdh20_predicted
1368956_at	NM_022868	protocadherin 8	Pcdh8
1368089_at	NM_031079	phosphodiesterase 2A, cGMP-stimulated	Pde2a
1389597_at	BI293445	piggyBac transposable element derived 5 (predicted)	Pgbd5_predicted
1374862_at	AI764464	phytanoyl-CoA hydroxylase interacting protein	Phyhip
1387281_a_at	D86556	pregnancy upregulated non-ubiquitously expressed CaM kinase	Pnck
1368369_at	NM_013007	prepronociceptin	Pnoc
1370432_at	M72711	POU domain, class 3, transcription factor 1	Pou3f1
1382821_at	AA998957	protein tyrosine phosphatase, receptor type, f polypeptide (PTPRF), interacting protein (liprin), alpha 3	Ppfia3
1379374_at	AW526088	plasticity related gene 1	Prg1
1372382_at	AW527165	Protein kinase, AMP-activated, gamma 2 non-catalytic subunit	Prkag2
1389463_at	BG375376	protein kinase, cAMP dependent regulatory, type I, beta	Prkar1b
1369089_at	NM_012628	protein kinase C, gamma	Prkcc
1374593_at	AA799421	protein kinase C, epsilon	Prkce
1368421_at	NM_019253	protein tyrosine phosphatase, non-receptor type 5	Ptpn5
1371086_at	BE096879	protein tyrosine phosphatase, receptor type, F	Ptprf
1368358_a_at	NM_053594	protein tyrosine phosphatase, receptor type, R	Ptprr
1368674_at	NM_022268	liver glycogen phosphorylase	Pygl
1369004_at	NM_133580	RAB26, member RAS oncogene family	Rab26
1369816_at	NM_013018	RAB3A, member RAS oncogene family	Rab3a
1383826_at	AA924620	Rab40b, member RAS oncogene family (predicted)	Rab40b_predicted
1388632_at	BG665929	RAB6B, member RAS oncogene family (predicted)	Rab6b_predicted
1373631_at	BF284067	RAP1, GTPase activating protein 1	Rap1ga1
1371081_at	U78517	Rap guanine nucleotide exchange factor (GEF) 4	Rapgef4
1373666_at	AI102560	Rap guanine nucleotide exchange factor (GEF) 5	Rapgef5
1370372_at	AF134409	RASD family, member 2	Rasd2
1393081_at	AI145237	RasGEF domain family, member 1A (predicted)	Rasgef1a_predicted
1369093_at	NM_080394	reelin	Reln

1370989_at	AI639318	ret proto-oncogene	Ret
1392315_at	BE107351	REV1-like (S. cerevisiae) (predicted)	Rev1l_predicted
1384289_at	BI281651	similar to RIKEN cDNA 4631403P03	RGD1305276
1373414_at	BG380515	similar to Brain specific membrane-anchored protein precursor	RGD1305557
1383706_at	BF409331	similar to RIKEN cDNA 2900011O08	RGD1305733
1380852_at	AI112346	hypothetical LOC294883	RGD1305844
1390167_at	BI286834	similar to hypothetical protein FLJ30373 (predicted)	RGD1306256_predicted
1380228_at	BG672066	similar to hypothetical protein MGC47816 (predicted)	RGD1306880_predicted
1385744_at	BF389238	similar to KIAA1679 protein (predicted)	RGD1306938_predicted
1383887_at	AA924984	similar to Protein C20orf103 precursor	RGD1306991
1374176_at	AI408727	similar to DNA segment, Chr 4, Brigham & Womens Genetics 0951 expressed	RGD1308059
1376654_at	AW521378	similar to RIKEN cDNA B130016O10 gene (predicted)	RGD1308448_predicted
1393733_at	BF402788	similar to hypothetical protein FLJ20300 (predicted)	RGD1309567_predicted
1379894_at	AI501165	similar to 3632451O06Rik protein (predicted)	RGD1310110_predicted
1393841_at	AA859317	similar to hypothetical protein FLJ31810 (predicted)	RGD1310773_predicted
1376328_at	BI278776	similar to putative protein (5S487) (predicted)	RGD1310819_predicted
1383794_at	AI575277	similar to RIKEN cDNA A930038C07 (predicted)	RGD1311080_predicted
1390865_at	AW524822	similar to Ca2+-dependent activator for secretion protein 2 (predicted)	RGD1559440_predicted
1383800_at	AW523537	similar to expressed sequence AW121567 (predicted)	RGD1559498_predicted
1376901_a_at	AA964675	Similar to Hypothetical protein 6330514E13 (predicted)	RGD1559693_predicted
1376460_at	BI286710	similar to ataxin 2-binding protein 1 isoform 2 (predicted)	RGD1560070_predicted
1391308_at	AI101675	Similar to vacuolar protein sorting 13C protein (predicted)	RGD1560364_predicted
1373985_at	BI282311	Similar to KIAA1183 protein (predicted)	RGD1560435_predicted
1393408_at	BF567707	similar to NEX-1 (predicted)	RGD1562793_predicted
1396206_at	BG665525	similar to Docking protein 5 (Downstream of tyrosine kinase 5) (Protein dok-5) (predicted)	RGD1562846_predicted
1376459_at	AW533060	similar to AP2 associated kinase 1 (predicted)	RGD1563580_predicted
1375305_at	BI282028	RGD1563912 (predicted)	RGD1563912_predicted
1389086_at	BF408444	similar to RIKEN cDNA E430021N18 (predicted)	RGD1564043_predicted
1380901_at	AW527298	similar to synaptotagmin XIV-related protein Strep14 (predicted)	RGD1564654_predicted
1379460_at	BF387898	similar to RIKEN cDNA 3110007P09 (predicted)	RGD1564957_predicted
1388705_at	BI282694	similar to selenoprotein SelM (predicted)	RGD1565037_predicted
1374785_at	BG380471	similar to CD69 antigen (p60, early T-cell activation antigen) (predicted)	RGD1565373_predicted
1379564_at	AW528486	similar to cajalin 2 isoform a (predicted)	RGD1565556_predicted
1383704_at	BF410844	similar to actin-related protein 3-beta (predicted)	RGD1565759_predicted
1392003_at	AA943753	similar to KIAA0316 protein (predicted)	RGD1566031_predicted
1381462_at	BI294541	similar to mKIAA1940 protein (predicted)	RGD1566130_predicted
1389937_at	BF404834	Similar to Neuropilin- and tolloid-like protein 1 (predicted)	RGD1566269_predicted
1384202_at	BI287326	similar to Tescalcin (predicted)	RGD1566317_predicted
1377008_at	BI296868	similar to GTL2, imprinted maternally expressed untranslated (predicted)	RGD1566401_predicted
1368144_at	AF321837	regulator of G-protein signaling 2	Rgs2
1368505_at	NM_017214	regulator of G-protein signaling 4	Rgs4
1368373_at	NM_019343	regulator of G-protein signaling 7	Rgs7
1395991_at	BE107556	RIM binding protein 2	Rimbp2
1368662_at	NM_134374	ring finger protein 39	Rnf39
1376110_at	AI009623	ribonuclease P 25 subunit (human)	Rpp25
1372690_at	AI137471	reticulon 4 receptor-like 1	Rtn4rl1
1382088_at	AI548753	Ryanodine receptor 2, cardiac	Ryr2
1369210_at	NM_030875	sodium channel, voltage-gated, type I, alpha	Scn1a
1369662_at	NM_012647	sodium channel, voltage-gated, type 2, alpha 1 polypeptide	Scn2a1
1368256_at	NM_053779	serine (or cysteine) peptidase inhibitor, clade I, member 1	Serpini1

1391032_at	AI112194	seizure related 6 homolog (mouse)	Sez6
1374825_at	BG380338	seizure related 6 homolog (mouse)-like 2 (predicted)	Sez6l2_predicted
1370419_a_at	AF230520	SH3-domain kinase binding protein 1	Sh3kbp1
1396040_at	BE108568	SH3 and multiple ankyrin repeat domains 1	Shank1
1370069_at	NM_134363	solute carrier family 12, (potassium-chloride transporter) member 5	Slc12a5
1368564_at	NM_053427	solute carrier family 17 (sodium-dependent inorganic phosphate cotransporter), member 6	Slc17a6
1368986_at	NM_053859	solute carrier family 17 (sodium-dependent inorganic phosphate cotransporter), member 7	Slc17a7
1383444_at	AA964069	solute carrier family 24 (sodium/potassium/calcium exchanger), member 2	Slc24a2
1387380_at	NM_031782	solute carrier family 32 (GABA vesicular transporter), member 1	Slc32a1
1373326_at	AI716512	Solute carrier family 4, sodium bicarbonate transporter-like, member 10	Slc4a10
1368170_at	NM_024371	solute carrier family 6 (neurotransmitter transporter, GABA), member 1	Slc6a1
1391019_at	BF285698	SLIT and NTRK-like family, member 1 (predicted)	Slitrk1_predicted
1368991_at	NM_053605	sphingomyelin phosphodiesterase 3, neutral	Smpd3
1387073_at	NM_030991	synaptosomal-associated protein 25	Snap25
1367977_at	NM_019169	synuclein, alpha	Snca
1369924_at	NM_080777	synuclein, beta	Sncb
1389752_at	BE109861	sortilin-related VPS10 domain containing receptor 3 (predicted)	Sorcs3_predicted
1367812_at	NM_019167	spectrin beta 3	Spnb3
1394252_at	BG668764	sparc/osteonectin, cwcv and kazal-like domains proteoglycan 3 (predicted)	Spock3_predicted
1367762_at	NM_012659	somatostatin	Sst
1369770_at	NM_012719	somatostatin receptor 1	Sstr1
1368782_at	NM_019348	somatostatin receptor 2	Sstr2
1368157_at	NM_024346	stathmin-like 3	Stmn3
1370315_a_at	AF026530	stathmin-like 4	Stmn4
1387360_at	BI290256	syntaxin 1A (brain)	Stx1a
1368352_at	NM_012700	syntaxin 1B2	Stx1b2
1368562_at	NM_031641	sulfotransferase family 4A, member 1	Sult4a1
1368682_at	NM_057210	synaptic vesicle glycoprotein 2a	Sv2a
1369251_a_at	NM_019133	synapsin I	Syn1
1369482_a_at	NM_019159	synapsin II	Syn2
1390209_at	BE097982	synaptogyrin 3 (predicted)	Syngr3_predicted
1368865_at	BG666364	synaptoporin	Synpr
1368276_at	NM_012664	synaptophysin	Syp
1373896_at	AA943569	synaptotagmin I	Syt1
1374427_at	AI144986	Synaptotagmin XIII	Syt13
1369309_a_at	BG671061	tachykinin 1	Tac1
1387138_at	NM_019162	tachykinin 2	Tac2
1370150_a_at	NM_012703	thyroid hormone responsive protein	Thrsp
1369651_at	NM_012673	thymus cell antigen 1, theta	Thy1
1374257_at	BM389265	T-cell lymphoma invasion and metastasis 1	Tiam1
1387850_at	NM_023020	transmembrane protein with EGF-like and two follistatin-like domains 1	Tmeff1
1397227_at	BE120895	transmembrane protein 35	Tmem35
1376721_at	BF400666	Triple functional domain (PTPRF interacting)	Trio
1371618_s_at	AI229029	tubulin, beta 3	Tubb3
1384927_at	AI230430	tubulin, beta 4	Tubb4
1397612_at	BF391002	Ubiquitin protein ligase E3A (predicted)	Ube3a_predicted
1395054_at	BF416262	ubiquitin specific protease 29 (predicted)	Usp29_predicted
1373510_at	BF281373	vesicle-associated membrane protein 1	Vamp1
1377146_at	AI412212	vasoactive intestinal polypeptide	Vip

1376893_at	AI406821	vesicular membrane protein p24 (predicted)	Vmp_predicted
1368853_at	NM_012686	visinin-like 1	Vsnl1

CLUSTER 3

Affymetrix ID	GenBank ID	Gene Name	Gene Symbol
1384603_at	AI602131	ATP-binding cassette, sub-family A (ABC1), member 4 (predicted)	Abca4_predicted
1370464_at	AF286167	ATP-binding cassette, sub-family B (MDR/TAP), member 1A	Abcb1a
1394483_at	AW535310	A disintegrin-like and metallopeptidase (reprolysin type) with thrombospondin type 1 motif, 5 (aggrecanase-2)	Adamts5
1367974_at	NM_012823	annexin A3	Anxa3
1372601_at	BM391471	activating transcription factor 5	Atf5
1398431_at	BI294910	carbonic anhydrase 8	Car8
1387818_at	NM_053736	caspase 4, apoptosis-related cysteine peptidase	Casp4
1379935_at	BF419899	chemokine (C-C motif) ligand 7	Ccl7
1379582_a_at	AA998516	cyclin A2	Ccna2
1371150_at	X75207	cyclin D1	Ccnd1
1374139_at	BG671589	cerebellar degeneration-related 2	Cdr2
1376193_at	AA819658	Kohjirin	Chrdl1
1384068_at	BI295150	cytoskeleton associated protein 2 (predicted)	Ckap2_predicted
1377765_at	AA848723	chloride intracellular channel 4	Clic4
1384211_at	BM388456	procollagen, type XI, alpha 1	Col11a1
1387854_at	BI282748	procollagen, type I, alpha 2	Col1a2
1373245_at	BE111752	procollagen, type IV, alpha 1	Col4a1
1370895_at	AI179399	procollagen, type V, alpha 2	Col5a2
1370269_at	X00469	cytochrome P450, family 1, subfamily a, polypeptide 1	Cyp1a1
1368990_at	NM_012940	cytochrome P450, family 1, subfamily b, polypeptide 1	Cyp1b1
1369590_a_at	NM_024134	DNA-damage inducible transcript 3	Ddit3
1389533_at	AA944398	fibulin 2	Fbln2
1374726_at	AI411941	fibronectin type III domain containing 1	Fndc1
1371331_at	BG665037	follistatin-like 1	Fstl1
1379440_at	AW144239	follistatin-like 3	Fstl3
1368947_at	NM_024127	growth arrest and DNA-damage-inducible 45 alpha	Gadd45a
1372273_at	AA944212	glycophorin C (Gerbich blood group)	Gypc
1387273_at	NM_013037	interleukin 1 receptor-like 1	Il1rl1
1376845_at	AA819034	putative ISG12(b) protein	isg12(b)
1387144_at	NM_030994	integrin alpha 1	Itga1
1372870_at	BM391302	KDEL (Lys-Asp-Glu-Leu) endoplasmic reticulum protein retention receptor 3 (predicted)	Kdelr3_predicted
1372478_at	AI137605	similar to chemokine-like factor super family 7	LOC501065
1378094_at	BM389654	Similar to pleckstrin homology-like domain, family B, member 2	LOC685611
1384231_at	BE108276	similar to Shc SH2-domain binding protein 1	LOC687121
1368171_at	NM_017061	lysyl oxidase	Lox
1372006_at	BM391274	Lysyl oxidase-like 2 (predicted)	Loxl2_predicted
1388102_at	U66322	leukotriene B4 12-hydroxydehydrogenase	Ltb4dh
1367912_at	NM_021587	latent transforming growth factor beta binding protein 1	Ltbp1
1368448_at	NM_021586	latent transforming growth factor beta binding protein 2	Ltbp2
1390585_at	AI169829	mannan-binding lectin serine peptidase 1	Masp1
1376055_at	AA859768	minichromosome maintenance deficient 5, cell division cycle 46 (S. cerevisiae) (predicted)	Mcm5_predicted
1371074_a_at	U17565	minichromosome maintenance deficient 6 (MIS5 homolog, S. pombe) (S. cerevisiae)	Mcm6

1374775_at	AI714002	antigen identified by monoclonal antibody Ki-67 (predicted)	Mki67_predicted
1370854_at	AA799423	nexilin	Nexn
1372559_at	AI103527	Ng23 protein	Ng23
1387454_at	NM_022242	niban protein	Niban
1388618_at	BM389302	nidogen 2	Nid2
1371052_at	AA859752	noggin	Nog
1388340_at	BF281153	NS5A (hepatitis C virus) transactivated protein 9	Ns5atp9
1368547_at	NM_130402	osteoclast inhibitory lectin	Ocil
1393129_at	AI711403	procollagen-proline, 2-oxoglutarate 4-dioxygenase (proline 4-hydroxylase), alpha polypeptide III	P4ha3
1367949_at	NM_017139	proenkephalin 1	Penk1
1385182_at	BG371843	plakophilin 1 (predicted)	Pkp1_predicted
1388539_at	BE113268	plakophilin 2	Pkp2
1384558_at	BI276313	placenta-specific 9 (predicted)	Plac9_predicted
1393982_at	AI070935	polymerase (DNA directed), epsilon 2 (p59 subunit) (predicted)	Pole2_predicted
1372729_at	AI137406	protein C receptor, endothelial	Procr
1368259_at	NM_017043	prostaglandin-endoperoxide synthase 1	Ptgs1
1374284_at	AI227769	Ras association (RalGDS/AF-6) domain family 4	Rassf4
1389107_at	AI008974	Similar to KIAA1749 protein (predicted)	RGD1304623_predicted
1380243_at	BE098614	similar to CG14803-PA (predicted)	RGD1304693_predicted
1373447_at	BF281350	similar to HN1-like protein	RGD1305117
1393451_at	BI295149	similar to RIKEN cDNA 2610510J17	RGD1310953
1371970_at	AA799328	similar to expressed sequence AW413625 (predicted)	RGD1560913_predicted
1374805_at	AW251849	similar to hypothetical protein MGC5528 (predicted)	RGD1561749_predicted
1376231_at	BF389244	similar to Hypothetical UPF0080 protein KIAA0186 (predicted)	RGD1562246_predicted
1375857_at	AW917760	similar to Myoferlin (Fer-1 like protein 3) (predicted)	RGD1564216_predicted
1373250_at	AI229404	similar to Anillin (predicted)	RGD1566097_predicted
1377967_at	AI112987	retroviral integration site 2 (predicted)	Ris2_predicted
1389408_at	BG379338	ribonucleotide reductase M2	Rrm2
1368519_at	NM_012620	serine (or cysteine) peptidase inhibitor, clade E, member 1	Serpine1
1388569_at	AI179984	serine (or cysteine) peptidase inhibitor, clade F, member 1	Serpinf1
1387134_at	NM_053687	schlafen 3	Slfn3
1393041_at	AW535052	SMC2 structural maintenance of chromosomes 2-like 1 (yeast) (predicted)	Smc2l1_predicted
1373026_at	BI303598	spindle pole body component 24 homolog (S. cerevisiae) (predicted)	Spbc24_predicted
1390107_at	BG670294	synaptotagmin-like 2 (predicted)	Sytl2_predicted
1367570_at	NM_031549	transgelin	Tagln
1389555_at	BM387190	transcription factor 19	Tcf19
1367859_at	NM_013174	transforming growth factor, beta 3	Tgfb3
1375951_at	AA818521	thrombomodulin	Thbd
1374529_at	AI406660	Thrombospondin 1	Thbs1
1372926_at	AI009159	Tissue inhibitor of metalloproteinase 3 (Sorsby fundus dystrophy, pseudoinflammatory)	Timp3
1373401_at	AI176034	Tenascin C	Tnc
1379331_at	AA965084	tenascin N (predicted)	Tnn_predicted
1368838_at	NM_012678	tropomyosin 4	Tpm4
1368912_at	M12138	thyrotropin releasing hormone	Trh
1370694_at	AB020967	tribbles homolog 3 (Drosophila)	Trib3
1372639_at	AA800245	tripartite motif-containing 54	Trim54
1379448_at	BE110883	Ttk protein kinase (predicted)	Ttk_predicted
1384506_at	H33706	unc-5 homolog C (C. elegans)	Unc5c
1368463_at	NM_053653	vascular endothelial growth factor C	Vegfc

1368359_a_at	NM_030997	VGF nerve growth factor inducible	Vgf
1369484_at	NM_031590	WNT1 inducible signaling pathway protein 2	Wisp2

- 3.4 -

Population coding in neuronal hippocampal networks

Broccard FD, Bonifazi P, Ruaro ME, Torre V

Paper in preparation

Population coding in networks of rat hippocampal neurons

Frédéric D. Broccard, Paolo Bonifazi, Maria Elisabetta Ruaro, and Vincent Torre

International School for Advanced Studies (SISSA/ISAS)
Area Science Park, S.S.14 Km163,5 - 34012 Basovizza (TS) - ITALY

Correspondence should be addressed to:

Vincent Torre
Scuola Superiore di Studi Avanzati (SISSA)
Area Science Park, S.S.14 Km163,5
34012 Basovizza (TS)
Italy
E-mail torre@sissa.it
Tel. +39 040 3756513
fax +39 040 3756502

Abbreviated title: Rate and temporal coding in neuronal cultures
Number of figures and tables: 7
Number of pages:
Keywords: rate coding, temporal coding, first evoked spike latency, population coding, distributed code, pooling, multielectrode array, multi-site stimulation, neuronal cultures

Abstract

Population coding was analyzed in dissociated hippocampal cultures, grown on multielectrode array. The efficiency of different coding schemes was considered and quantitatively compared by using criteria from information theory and pattern recognition. When neurons are tuned for the same stimulus, pooling or averaging evoked action potentials (APs) provides a nearly optimal coding. On the contrary, when neurons are tuned for different stimuli a distributed coding is advantageous. Among the different distributed coding schemes examined, a distributed code based on the post-stimulus time histogram (PSTH) provided the highest decoding performance. A distributed temporal coding based on the latency of the first evoked APs provided very similar performances as a rate coding integrating action potentials APs over a short time window of 10-20 ms. Our data also indicate that dissociated hippocampal cultures could use different encoding strategies, such as spike count or temporal patterns of population firing, to represent the intensity and spatial location of stimuli. Taken altogether, our results bear striking similarities with population coding strategies used *in vivo* in the somatosensory system and provide evidence of distributed processing in neuronal cultures with random connectivity, as proposed some years ago.

Introduction

Information processing in the nervous system is thought to be distributed (Rumelhart & McClelland, 1986) because information is spread across populations or ensembles of neurons and each neuron contributes to the processing of many stimulus features. A fundamental problem of information processing in neuronal networks is to characterize and to identify the optimal coding and decoding strategies which are used (Dayan & Abbott, 2001). Decoding refers to the map from the firing of the neuronal population to the stimulus, problem often equivalent to retrieve the stimulus from the neuronal firing. To date, several decoding strategies have been proposed in diverse neuronal networks. Experimental evidence have shown that the firing of individual neurons is noisy and unreliable and that a reduction of the variability necessary to reliably process stimuli could be readily achieved by averaging the firing of some dozens of neurons (Shadlen & Newsome, 1998; Bonifazi et al., 2005). The firing rate of each neuron can also be pooled together (Darian-Smith et al., 1973; Shadlen et al., 1996) or considered separately or distributed, i.e. a population rate vector is constructed and coding is based on the statistics of these vectors (Georgopoulos et al., 1986; Sanger, 2003). On the other hand, spike timing in population of neurons could be relevant as information can be coded in the precise temporal firing (O'Keefe & Recce, 1993; Hopfield 1995; Decharms & Merzenich 1996) such as in the latency of the first spike (Thorpe et al., 2001; Johansson & Birznieks, 2004) or in the synchrony of firing (Gray et al., 1989; Singer & Gray, 1995; Ritz & Sejnowski, 1997). In the latter case, correlations improve the encoding of information, whereas in other cases correlations can either be deleterious (Shadlen & Newsome, 1998) or have no effect at all (Nirenberg & Latham, 2003).

Two classes of decoding procedures have been proposed so far. One procedure is based on information theory and makes use of the mutual information between features of evoked trains of action potentials (APs) and the stimulus (Borst & Theunissen, 1999). This procedure requires an estimate of several probabilities, and, due to our limited set of trials, they can be computed reliably only when two or at most three neurons are considered. Alternatively, procedures based on pattern recognition and/or classification can be used (Foffani & Moxon, 2004). These procedures are based on training or learning step, in which the correct mapping between evoked APs trains and stimulus is learned. The *K*-nearest neighbor procedure, possibly the simplest methods of classification, is often used.

In order to gain some insights and find an optimal decoding strategy, we analyzed population coding quantitatively and compared diverse rate and temporal decoding schemes. Extracellular electrical stimuli differing in their intensity and spatial location were randomly delivered to hippocampal networks grown on MEA. The efficiency of various decoding scheme was then quantified using criteria from information theory (Shannon & Weaver, 1949) and pattern recognition (Nicolelis et al., 1998; Foffani & Moxon, 2004). In particular, we compared the efficiency of pooled rate code with that of distributed rate code and looked at the overall efficiency of several other distributed codes; binary coding in which the neuronal response of each neuron consisted in a string of 0's and 1's, latency of the first spike and post-stimulus time

histogram (PSTH). The influence of the neuron pool size was also considered. For neurons with similar tuning properties, a simple pooling of evoked APs provided a good decoding performance not significantly lower than of a more complex distributed coding. When stimuli differed in their amplitude and their spatial location, a distributed coding was necessary to achieve a good efficiency. Among the different distributed coding schemes examined, a distributed code based on the post-stimulus time histogram (PSTH) provided the highest decoding performance. A distributed temporal coding based on the latency of the first evoked spike provided very similar performances as a rate coding integrating spikes over a short time window of 10-20 ms. Our results bear striking similarities with those obtained in vivo in the monkey (Nicolelis et al., 1998) and rat (Panzeri et al., 2003) somatosensory cortex and provide evidence for distributed information processing in neuronal cultures with random connectivity, as proposed some years ago (Potter, 2001). This could have interesting implications for the creation of hybrid computational device (Ruaro et al., 2005).

Materials and Methods

Neuronal culture preparation.

Hippocampal neurons from Wistar rats (P0-P2) were prepared as previously described (Ruaro et al., 2005). Cells were plated on polyorhitine/matrigel pre-coated MEA (Ruaro et al, 2005) at a concentration of 8 x 10^5 cells/cm^2 and maintained in Minimal Essential Medium with Earle's salts (GIBCO-Brl) supplemented with 5% fetal calf serum, 0.5% D-glucose, 14 mM Hepes, 0.1 mg/ml apo-transferrin, 30 μg/ml insulin, 0.1 μg/ml D-biotin, 1 mM Vit. B12, and 2μg/ml gentamycin. After 48 hours 5 μM cytosine-β-D-arabinofuranoside (Ara-C) was added to the culture medium, in order to block glial cell proliferation. Half of the medium was changed twice a week.. Neuronal cultures were kept in an incubator providing a controlled level of CO_2 (5%), temperature (37^{o}C) and moisture (95%).

Electrical recordings and electrode stimulation.

The multi electrode array (MEA) system used for electrophysiology was commercially supplied by Multi Channel Systems (Reutlingen, Germany). MEA dishes had 10x6 TiN electrodes with an intra-electrode spacing of 500 μm and each metal electrode had a diameter of 30 μm. The MEA was connected to a 60 channel, 10 Hz – 3 kHz bandwidth pre-amplifier/filter-amplifier (MEA 1060-AMP) which redirected the signals towards a further electronic processing (i.e. amplification and AD conversion), operated by a board lodged inside a high performance PC. Signal acquisitions were managed under software control and each channel was sampled at a frequency of 20 kHz. One electrode was used as ground. Sample data were transferred in real time to the hard disk for later processing. In order to keep the desired environmental conditions during the electrical recordings, the dish was moved to a different incubator providing only a controlled level of CO_2 (5%) and of temperature (37^{o}C). It was also sealed with a Teflon cap supplied by MultiChannelSystem in order to eliminate evaporation and contamination (Potter & DeMarse, 2001). The neuronal culture was then allowed to settle for about 1 hour in order to reach a stationary state. The medium was changed and the dish was moved back to the original incubator once the experiment was terminated, usually after 3 to 10 hours.

The amplitude of the voltage pulse was selected between 300 and 900 mV. The minimum amplitude required to evoke an electrical response varied between 300 and 450 mV depending on the responsiveness of the culture and on the geometry of the stimulus. Analogously, the lowest amplitude giving the maximum response varied between 750 and 900 mV. In order to avoid invasive effects due to the stimulus itself, intensities higher that 900 mV were never applied. Once the lowest and highest intensity for a specific culture were selected, an intermediate value was chosen to complete the experiment. In most of the experiments the intensities applied were 300 or 450, 600 and 900 mV. Patterns of six electrodes were used for stimulation in figure 2 to 7. A total of nine different spatial patterns of three different intensities (i.e. a total of 27 distinct patterns) were used for stimulation (see Fig. 1A). In other experiments, a single pattern consisting of six stimulating electrodes arranged in a horizontal bar was also used (Fig.

7). In this case the effect of inhibitors of NMDA and $GABA_A$ receptors was also investigated. For all patterns of stimulation, each pattern was delivered hundred times at 0.25 Hz via a 8-channel stimulator (STG2008, Multichannelsystems) and the stimulation order was randomized.

Pharmacology.

In some experiments the following chemicals were used as synaptic blockers: 2-amino-5-phosphonovalerate (APV, Sigma-Aldrich), bicuculline (Sigma-Aldrich) and 6-cyano-7-nitroquinoxaline-2,3-dione disodium salt (CNQX, Sigma-Aldrich). Synaptic blocker/s was/were added to the extracellular medium in their required amount. After completion of the planned measurements, blockers were washed out by four medium replacements and the original extracellular medium was restored.

Data analysis.

Acquired data were analyzed using MATLAB (The Mathworks, Inc.). An artifact lasting 5 – 20 ms, generated by the electrical stimulation, was induced on the recording and was removed during data analysis (Wagenaar & Potter, 2002; Ruaro et al., 2005). As the artifact removal was not reliable during the first 2 ms following the stimulation, the first 2 ms following stimulation were excluded from the analysis. Antidromically evoked APs were identified in two different ways: first, all APs observed in the presence of a cocktail of synaptic blockers (50 μM APV, 10 μM bicuculline and 100 μM CNQX) were classified as antidromic APs; second, – in agreement with Wagenaar et al., (2004) - all APs with a reliability close to 100% and with a temporal jitter of less than 0.25 ms were classified as antidromic (Wagenaar et al., 2004). APs classified as antidromic were excluded from the analysis. For each individual electrode, we computed the standard deviation (σ) of the noise, ranging from 3 to 6 μV, and only action potentials (APs) crossing the threshold of -5σ were considered. Since each electrode could record the activity of several neurons, varying between 1 and 5, we define here as a multiunit recording the electrical (or neural) activity recorded by a single electrode. AP sorting was carried out using principal component analysis and MATLAB open source toolboxes for the analysis of multi-electrode data (Egert et al., 2002).

Calculation of correlation.

The degree of correlation of firing in the network was measured by averaging the cross-correlation analyzed among electrical recordings obtained from pairs of electrodes. The correlation of the spontaneous activity was computed in the following way: the spontaneous activity was recorded for about 30 minutes and the number of APs recorded at each electrode in a given bin width was computed, so to obtain a time series (SA_1, …, SA_n). For each pair of electrodes (i, j), the cross correlation between the time series (SA_{i1}, …, SA_{in};) (SA_{j1}, …, SA_{jn}) was calculated according to the equation (Papoulis, 1984):

$$\frac{\sum_{k=1}^{n}(SA_{ik}-\overline{SA_i})(SA_{jk}-\overline{SA_j})}{\sqrt{\left(\sum_{k=1}^{n}(SA_{ik}-\overline{SA_i})^2\right)\left(\sum_{k=1}^{n}(SA_{jk}-\overline{SA_j})^2\right)}} \qquad (1)$$

and the average cross-correlation over all the possible pairs of electrodes was computed The correlation of the evoked activity was obtained in the following way: for each electrode the APs evoked in the time bin following the stimulation were counted at each single trial so to obtain a series of single trial responses depending on the bin width. For each pair of electrodes, the cross-correlation between the "trial" series was calculated according to equation (1) and the obtained cross-correlation was averaged over all the possible pairs of electrode to obtain the average network correlation. The average network correlation for the spontaneous and evoked activity shown in Fig. 2 was obtained by varying the size of the bin width.

Neural coding mechanisms.

Given a set of different stimuli S_i, we investigated how information about S_i could be encoded in the evoked APs trains. Four distributed mechanisms were considered: a rate code, post-stimulus time histogram (PSTH) coding, a 1st evoked APs code (latency code or $1/\tau$) and a binary code. For each trial, a population vector was computed in the time window Δt following the stimulus (see Fig. 1B and C). The vector dimension N was equal to the number of neurons included in the population (or to the number of active electrodes when multiunit recordings were considered). A single time window Δt following the stimulation was considered, as we are interested in fast coding mechanisms. In the case of the rate code, the number of APs (FR_i) evoked in the time window Δt was counted for each neuron (electrode) *i* and the vector (FR_1,… , FR_N) was constructed. For PSTH coding, the time window Δt was binned with bins of equal width and spikes were counted in each bin. In this case a vector of (Δt/bin size) * number of neurons was constructed. Different bin sizes were considered. In the first evoked APs code, for each neuron (electrode) *i*, the inverse of the latency τ_i of the first evoked AP was considered and the vector ($1/\tau_1$,….,$1/\tau_N$) was constructed. When the latency was larger than the time window Δt, the latency was considered as infinite, i.e. the neuron was supposed not to fire. For the binary coding, the activity detected in the time window Δt was converted to "0" when no APs were evoked or to "1" when one or more APs were evoked and a vector of 0s and 1s was obtained. Given S different stimuli and T repetitions of the same stimulus, a total of S*T vector responses were collected for each different coding mechanisms. For the population rate code (pooling), for each single trial, the APs evoked in the neural pool (FR_1,…,FR_N) were summed (ΣFR_i). All coding schemes were investigated for different time window Δt.

Evaluation of neural coding mechanisms: mutual information and efficiency of decoding.

In order to extract the information about the stimulus from the firing of populations of neurons, we used two different procedures: information theory (Shannon & Weaver, 1949) and classification analysis (Foffani & Moxon, 2004). Information theory was used to compare the information carried by single neurons and pairs of neurons. In order to calculate the mutual information, a reliable estimate of conditional probabilities is required and this was not possible when more than two neurons were considered, due to the limited set of trials. The mutual information I (Shannon & Weaver, 1949) was calculated as follow:

$$I \equiv I(R,S) = \sum_{s \in S} p(s) \sum_{r \in R} p(r|s) \cdot \log_2 (p(r|s)/p(r)) \qquad (2)$$

where

$$p(r) = \sum_{s \in S} p(s) \cdot p(r|s) \qquad (3)$$

and $p(r)$ is the total probability of observing the response r. In our case, all stimuli occurred with equal probability, $p(s)$. The response r could be the firing rate FR_i of a single neuron i, or the distributed firing rate (population vector response) (FR_i, FR_j) of neuron i and neuron j, or the pooled firing rate ($FR_i + FR_j$) of neuron i and neuron j. The response was measured in the time window Δt following the stimulus. In order to minimize the effects of finite sample size on our estimates of information, the real response r was binned into different intervals, following the methods of Panzeri and Treves (1996).

In order to measure the information encoded in the response of a neural population, classification analysis was used and the efficiency of decoding was calculated. Given a set of S different stimuli, a set of S templates was constructed. These templates represented the average neural response and were vectors for the distributed codes and a scalar for the population rate code (pooling). Two cross-validation methods were used to construct the S templates (Duda et al., 2000). In the *bootstrap method*, half of the T trials were randomly selected to construct the S templates and the remaining half was used for testing. In order to eliminate any effect due to the random sample of the training trials, the complete cross-validation procedure was repeated 50 times and average values were considered. In the *leave-one-out method*, the S templates were constructed with T-1 trials and the remaining trial was used for testing. This procedure was repeated T times and average values were considered. For both cross-validation methods, the Euclidean distance between test trials and all stimuli templates were computed, and trials were assigned to the closest template (Foffani & Moxon, 2004). The decoding performance was the fraction of correct assignments over the total number of assignments. The analysis reported in Fig. 5 show how the decoding performance varies as a function of the size of the ensemble of neurons (electrodes). When subsets of N elements (neurons or electrodes) were considered out of N_{max} possible elements, only a

maximum of 1000 combinations were randomly selected and averages were calculated. The error bars in the graphics represent standard deviation calculated for 5 different experiments. The analysis shown in Fig. 5 and 6 shows the maximal efficiency of retrieval which was computed for the bin width giving the maximal efficiency.

Measures of the tuning properties of the neurons.

The choice of the most appropriate coding scheme depends on the stimuli which have to be coded and on the properties of the neurons under consideration. Considering the average number of spikes fired by neuron i in the time window Δt following the stimulus S_k ($AFR_i(S_k)$), $N_i(S_k)$ scales the response of neuron N_i to the stimulus S_k with an integer value between 1 and 10, where 1 and 10 correspond respectively to minimal response ($min\ AFR_i$) and to maximal response ($max\ AFR_i$) of neuron i to the all T different stimuli according to:

$$min\ AFR_i = min_{k=\{1,\ldots,T\}}(\ AFR_i(S_k)\ ) \qquad (4)$$

$$max\ AFR_i = max_{k=\{1,\ldots,T\}}(\ AFR_i(S_k)\ ) \qquad (5)$$

When three stimuli or more (S_1,…, S_N) are considered it is important to establish whether neurons respond to them in a "progressive-like way". For instance, it is possible that the response, given by the neuron i to these stimuli, satisfies the condition:

$$AFR_i(S_1) < AFR_i(S_2) < \ldots\ldots < AFR_i(S_N)$$

This is the case when the stimuli differ in their intensity (with the intensity of S_j larger than the intensity of S_k when $j>k$) and the average firing rate of neuron i increases monotonically with the stimulus intensity. This kind of behavior can be detected by plotting $AFR_i(S_j)$ versus $AFR_i(S_k)$. If points cluster in one semisector for all pairs of stimuli (S_j, S_k) then the neuron i responds to the stimuli in a progressive-like way.

Results

Nervous system are able to process visual stimuli varying for their intensity and location in the visual field and mechanical stimuli applied to different regions of the skin with a different pressure. We tested if neuronal cultures were able to retrieve such stimulus' features based on the response of a population of neurons. Hippocampal neurons from neonatal rats were grown over a 10 x 6 MEA. After three or four weeks of culture a well developed neuronal network was observed exhibiting bursts of spontaneous activity. The MEA on which neurons are grown allows the recording of extracellular voltage signals, produced by action potentials (APs) of all neurons establishing a good electrical contact with MEA electrodes. Extracellular APs larger than 100 μV were often measured. The neuronal culture was stimulated with brief bipolar voltage pulses applied through the electrodes. Stimuli could differ in intensity and in their spatial location, i.e. different pattern of stimulated electrodes (Fig. 1A, see Methods). The electrical stimulation produced an artifact lasting 5 – 20 ms (removed off-line, see Methods) in all electrodes, followed by clear evoked APs. Extracellular signals larger than five times the standard deviation of the voltage noise (5σ) were considered. The total number of neurons recorded by a MEA ranged from few dozens to hundreds of units. Out of these, it was possible to identify APs originating from individual neurons and its number ranged from 10 to 40 units in different experiments (see Methods for APs sorting). As neurons in our cultures had long axons, some detected APs were produced by a direct antidromic stimulation of the neuron and were not evoked through synaptic pathways (Wagenaar et al. 2004). In order to identify these antidromic evoked APs, recordings in the absence and in the presence of a cocktail of synaptic blockers (50 μM APV, 10 μM bicuculline and 100 μM CNQX) were compared as described previously (Bonifazi et al., 2005; see Methods).

(Fig.1 near here)

Given N distinct neurons (or electrodes, when multiunit recordings are considered, see Methods), the firing rate of the neurons can be summed (known as pooled population rate code or pooling) or can be considered as distributed (distributed rate coding). Distributed codes based on the latency of the first evoked APs were also analyzed ($1/\tau$, Fig. 1B). These coding schemes were compared in term of their ability to recover the stimulus and its characteristics in every trial (Dayan & Abbott, 2001). In this view, decoding is adopted as the criteria to evaluate coding mechanisms. 27 different stimuli (9 spatial locations * 3 intensities) were used in order to test the different decoding scheme described above. Hundred repetitions of these 27 stimuli were randomly applied to the MEA to avoid any bias. Neurons responded diversely, but reliably, to the diverse stimuli. Figure 1C shows the responses of three representative neurons to stimuli of diverse intensities and spatial locations. The responses depended on the neurons' locations relative to the spatial position of the electrodes' pattern (Fig. 1C, upper panels) as well as the stimulus intensity applied (Fig. 1C, lower panels). In agreement with previous work (Jimbo et al., 2000), for all neurons, the early phase of the evoked activity was more reliable across trials than the late phase, independently of the stimulus intensity or location.

Correlation of the spontaneous and evoked electrical activity

The amount of correlation among neurons is a key element of neural coding (Averbeck et al., 2006). Therefore, we investigated in detail the degree of correlation in the electrical activity of the neuronal culture in bin width of increasing duration. The cross-correlation among the number of APs detected on pairs of electrodes was computed as described in the Methods. Figure 2A and B illustrate the average network correlation from collected data of 5 cultures for the spontaneous and evoked electrical activity respectively. When a small bin width of 5 ms was used, the average network correlation was close to 0.05 for both spontaneous and evoked activity. Increasing the bin width from 5 to 200 ms slightly increased the correlation of the spontaneous activity from 0.0646 ± 0.0212 to 0.4173 ± 0.0514 (Fig. 2A) and from 0.0496 ± 0.0128 to 0.2453 ± 0.0357 for the evoked activity (Fig. 2B), respectively. The difference of correlation between spontaneous and evoked activity became significant for bin widths larger than 15 ms (*t*-test, $p<0.05$).

(Fig.2 near here)

Tuning properties of the neurons in response to stimuli varying in intensity and in spatial location

We looked at the tuning properties of the neurons and verified that all neurons increased their firing rate with the stimulus intensity (intensity tuning) and that they responded differentially to diverse spatial stimuli (spatial tuning) and were not bias towards any of the stimulus applied. For the intensity tuning, neurons responded to stimuli differing in intensity in a “progressive-like way” (see Methods), meaning that the number of evoked APs increased as the stimulus’ intensity increased. This property is illustrated for three different stimuli differing in their relative location and number of stimulation electrodes (Fig. 3A-C) and was observed for all patterns (data not shown). The average number of spikes evoked by a stronger stimulus is plotted against the average number of spikes evoked by a weaker stimulus and the great majority of points clustered in one semi sector (see Methods). In contrast, neurons did not fire in a progressive-like way when stimuli of different spatial location were considered (spatial tuning), both for single (fig. 3D) or pairs (fig. 3E) of electrodes patterns. This different tuning originates from the facts that a neuron responding to a stimulus of weak intensity responds also to the same stimulus but with stronger intensity and that spatially distinct stimuli evoked response in different neurons. This different selectivity determines optimal distinct coding mechanisms.

(Fig.3 near here)

Coding the location and the intensity of the stimulus: population and distributed rate code

As neurons have different tuning properties for the intensity and spatial location of the stimulus, we then studied how these two features were encoded in the firing of a population of neurons. Information theory and classification analysis were used to measure the decoding or retrieval efficiency. Given N neurons with a firing FR_i in a time window Δt, we compared the population rate code based on the pooled response (i.e. ΣFR_i) and the distributed rate code based on the vector (FR_1, …, FR_N). We distinguished intensity coding, in which the responses of a given spatial pattern for three intensities were considered and spatial coding, in which the responses of all spatial stimuli of a given intensity were considered. Information theoretic analysis (Fig. 4) revealed that the information encoded by the firing rate *FR* of single neurons was generally low both for intensity (Fig. 4A) and spatial coding (Fig. 4C). Indeed, for intensity coding, the mutual information between the firing rate *FR* and the stimulus was maximum for the pattern of stimulation having four groups of six electrodes and was on average 0.135 ± 0.118 bits (Fig. 4A, right panel). Similarly, for spatial coding, the mutual information was higher for high stimulus intensity and was on average 0.367 ± 0.187 bits when spatial stimuli were considered for an intensity of 900 mV (Fig. 4C, right panel). The information encoded in the rate slightly increased when pairs of neurons were considered (Fig. 4B and D). Comparison of the information encoded in pairs of neurons in the pooled, I_{pool}, and distributed, I_{dist}, responses showed that the distributed rate code was more advantageous than the pooled response, both for intensity (Fig. 4B) and spatial (Fig. 4D) coding. For intensity coding, this advantage was more obvious when the number of stimulating electrode increased i.e. when the pattern of stimulation was global rather than local, and for high stimuli intensities. A restricted local pattern of stimulation will likely evoked APs in few neurons and the contribution of silent neurons to the distributed schemes will be null, seriously limiting its efficiency. Similarly, high intensities will ensure that most, if not all, neurons will respond to a particular pattern and allow a certain degree of response diversity among neurons with different spatial tuning. For intensity coding, the averaged mutual information over all patterns for I_{dist} and I_{pool} was, considering a time window of 20 ms, 0.692 ± 0.096 bits and 0.317 ± 0.029 bits, respectively. In the case of stimuli differing in their spatial location (spatial coding), for several pairs of neurons I_{dist} was larger than I_{pool}. In this case, the average mutual information averaged over all patterns for a given intensity and for all intensities for I_{dist} and I_{pool} was, considering a time window of 20 ms, 0.552 ± 0.137 bits and 0.248 ± 0.036 bits, respectively. A distributed rate code is thus more advantageous when neurons in the pair are tuned to different spatial stimuli, as observed in Fig. 3D-E.

(Fig.4 near here)

Figure 5 shows how retrieval is affected when the best predictors (neurons with the highest mutual information) were removed one by one from the neuronal population. As neuron ensemble size varied in diverse experiments, we removed the worst predictors of bigger neuronal population so to have the same ensemble size (31 neurons) for all experiments. Considering the total neuronal population, the ensemble performance to retrieve a particular stimulus was always largely bigger for the distributed rate code than for the pooled population rate code (*t*-test, $p<0.05$) both for patterns of stimulation comprising single and pairs of electrode patterns. For the distributed rate code, the ensemble performance decreased smoothly for both cross-validation methods and for all patterns of stimulation comprising single and pairs of electrode patterns. An example of the ensemble performance decrease when a single pattern of six electrodes was used for stimulation is shown in Fig. 5A. By using the leave-one-out method, the ensemble performance for the whole population was 65.81 ± 10.24 % and 18.04 ± 18.63 % for the distributed rate code and the pooled population rate code respectively. Decoding performance above chance level was still reached for small population of 5 neurons for both cross-validation methods. For the population rate code (pooling), the ensemble performance was very low for all patterns (data not shown) of stimulation except for the one involving all four patterns of electrodes, in which case the ensemble performance of pooling was similar to a distributed rate code (compare Fig. 5A and B). This particular pattern of stimulation evoked APs in a bigger number of neurons than did any other pattern of stimulation, thus biasing the decoding procedure and insuring a high decoding performance. In this case too, performance above chance level was still reached for small population of 5 neurons for both cross-validation methods. Altogether, the ensemble performance of the whole population (31 neurons) was largely unaffected by the cross-validation used. Averaging the ensemble performance of all experiments across all the patterns of stimulation (Fig. 5C) shows that, overall, a pooled population rate code performed poorly relative to a distributed rate code (see also Fig. 6A). Thus, the smooth degradation of the distributed rate code and the low performance of the pooled population rate code confirm that the information is distributed in the population response.

(Fig.5 near here)

Comparison of distributed codes: rate, first AP and binary codes

First evoked APs are the fastest signals in the nervous system. In addition, they are usually highly reliable and often carry most of the relevant information (Abeles, 1991; Gawne & Richmond 1993; Panzeri et al., 2001; Thorpe et al., 2001; Van Rullen & Thorpe, 2001; Delorme & Thorpe, 2001; Delorme, 2003; Johansson & Birznieks, 2004; Bonifazi et al. 2005) and are ideal candidates for an efficient and fast code. Given an ensemble of N neurons and a time window Δt following the stimulus, three distinct vectors describing the population response were computed: a rate vector, the inverse of the first AP latency vector ($1/\tau$) and a binary vector (see Methods and Fig. 1B). Moreover, a PSTH code was also considered by binning the firing rate. We compared

these four distributed neural coding mechanisms and the population rate code (pooling) on the decoding performance of all patterns (intensity coding) and spatial location (spatial coding). The results presented in Figure 6 were obtained using a time window Δt of 20 ms and the leave-one-out method (see Methods), which was computationally less expensive. Similar results were obtained using the bootstrap method (data not shown).

(Fig. 6 near here)

All four distributed codes outperformed pooling for both intensity (Fig. 6A) and spatial (Fig. 6B) coding. PSTH and first evoked AP latency gave the highest decoding performance followed by rate and binary coding that scored identically. A higher decoding performance was observed both for intensity and spatial coding for stimuli consisting of a single group of six stimulating electrodes compared to stimuli having two groups of stimulating electrodes. We first computed the decoding performance to retrieve the intensity and spatial location of a given stimulus (intensity coding, Fig. 6A). For stimuli consisting of a single group of six stimulating electrodes, the decoding performance was on average 84.33 ± 6.71 % for PSTH coding, 71.87 ± 9.58 % for first evoked AP latency coding, 66 ± 8.39 % for rate coding, 63.08 ± 8.92 % for binary coding and 13.46 ± 12.25 % for pooling. For stimuli having pairs of pattern of six electrodes, the decoding performance was on average 83 ± 8.18 % for PSTH coding, 72.54 ± 12.12 % for first evoked AP latency coding, 63.29 ± 10.82 % for rate coding, 58.83 ± 8.82 % for binary coding and 14.64 ± 10.24 % for pooling. The overall decoding performance considering all stimuli was statistically different between PSTH coding and all the other coding schemes considered (*t*-test, $p<0.05$; Fig. 6A) and was on average 84.61 ± 7.66 % for PSTH coding, 73.44 ± 11.17 % for first evoked AP latency coding, 65.81 ± 10.24 % for rate coding and 61.44 ± 9.17 % for binary coding. In contrast, the decoding performance for pooling was on average 18.04 ± 18.63 % and was slightly above chance level for all stimuli but for the medium and high intensity of the stimulus having four group of six stimulating electrodes (last two grey circles in Fig. 6A). These latter stimuli represent special cases as they evoked more APs than any other stimulus thus biasing the decoding performance. For the medium intensity, decoding performance by the pooling scheme for this stimulus was above chance level at 57.23 ± 5.33 %. For the highest intensity, this stimulus was one of the highest decoding performance for PSTH coding and the best for all other decoding schemes, ranking at 83 ± 7.07 % for pooling. A closer inspection of the decoding performance of individual stimuli revealed that the decoding performance of stimuli formed by a single group of six stimulating electrodes was independent of the stimulus intensity, whereas it increased with stimulus intensity for all stimuli of two or four groups of six stimulating electrodes (Fig. 6A and B). We also computed the decoding performance to only retrieve the spatial location of a stimulus, independently of its intensity (spatial coding). In this case, for a given spatial location, single trials giving the correct spatial location but the wrong intensity were pooled together with those giving the correct spatial location and intensity. The decoding performance was obviously higher than for intensity coding and was similar for all distributed coding scheme (Fig. 6B). It was on average, 92.13 ± 4.89 % for PSTH coding, 86.85 ± 4.99 % for the first evoked AP latency coding, 80.8 ± 5.33 % for rate

coding and 77.7 ± 5.19 % for binary coding. Pooling was still slightly above chance level and was on average 23.81 ± 14.56 %.

In order to investigate whether the temporal structures of the neurons' responses carried additional information, we examined the influence of the length of the time window Δt on the decoding performance. To this end, we integrated neurons' responses in time windows Δt of various lengths. For all coding schemes considered, the decoding performance was similar for time windows smaller than 50 ms (Fig. 6C-G). In contrast, increasing the time window's length to 50 or 100 ms significantly reduced the decoding performance of the rate, binary and first evoked APs coding schemes for all stimuli but the one with four groups of six stimulating electrodes (Fig. 6C-E). As discussed above, stimuli consisting in four groups of six stimulating electrodes are special cases for which the decoding performance is biased. Increasing the time window Δt from 10 to 100 ms decreased the overall decoding performance (averaged over all stimuli) from 69.78 ± 10.18 % to 41.19 ± 12.7 % for rate coding (*t*-test, $p<0.05$; Fig. 6C), and from 67.43 ± 9.19 % to 42.5 ± 11.5 % for binary coding (*t*-test, $p<0.05$; Fig. 6D), respectively, and had no effect on the first evoked AP latency (72.61 ± 11.34 % for 10 ms and 73.26 ± 11.4 % for 100 ms; Fig. 6E). On the other hand, the decoding performance of the pooling (Fig. 6F) and PSTH (Fig. 6G) coding schemes were unaffected by changes of the time window's length. However, the decoding performance of the PSTH coding scheme was dependent on the bin size used to construct the PSTH and decreased when bigger bins were considered (Fig. 6H). In this case, for a given time window, increasing the bin size consequently decreased the number of bins and PSTH approached rate coding. When the bin size was increased from 2 to 10 ms, the decoding performance decreased from 84.61 ± 6.11 % to 70.19 ± 10.4 % for a time window of 20 ms (*t*-test, $p<0.05$; Fig. 6H), from 84.93 ± 7.66 % to 73.07 ± 10.21 % for a time window of 50 ms (*t*-test, $p>0.05$; data not shown) and 84.93 ± 7.8 % to 72.68 ± 10.26 % for a time window of 100 ms (*t*-test, $p>0.05$; data not shown), respectively. Taking altogether, these results indicate that good decoding performance could be obtained considering a small time window Δt of 10-20 ms, in agreement with previous studies showing that most of the information is contained in the first milliseconds of the neuronal response (Petersen et al., 2002).

Distributed analysis of pooled signals and effect of APV and bicuculline

Hippocampal neuronal cultures are composed of GABAergic and glutamatergic neurons (Bonifazi et al. 2005). In the final step of our analysis, we performed a pharmacological dissection of synaptic pathways mediated by NMDA and $GABA_A$ receptors to study the influence of the excitatory/inhibitory balance on distributed coding schemes. Stimuli were a horizontal bar of six electrodes (inset of Fig. 7A) stimulated at three different intensities. In this analysis, reported in the graphs of Fig. 7, all APs recorded at each electrode were averaged (multiunit recordings, see Methods). We did this because AP sorting was computationally very demanding or impossible when $GABA_A$ receptors were blocked, due to the high number of spikes present in the disinhibited network. Therefore, given N electrodes, vector responses (of N dimensions) were computed as for single neurons (see Methods and Fig. 1) but the number of evoked

APs and the latency of the first evoked AP ($1/\tau$) were measured in the pool of neurons recorded by each electrode. In this way the variability of firing of each element is reduced. When excitatory synaptic pathways mediated by NMDA receptors were blocked by the addition of 50 μM APV, the average network correlation was drastically reduced for all bin widths and was less than 0.05 and 0.15 for the spontaneous (Fig. 7A) and evoked (Fig. 7B) activity respectively. The average network correlation of the evoked activity in normal conditions and in the presence of APV (Fig. 7B) was significantly different only for bin width larger than 60 ms (*t*-test, $p<0.05$), i.e. when the late phase of the evoked response, mediated by the NMDA receptors, was considered (Jimbo et al., 2000). A very different effect was observed when $GABA_A$ receptors were blocked with 10 μM bicuculline. In this case, the average network correlation for both the spontaneous (Fig. 7A) and the evoked (Fig. 7B) activity was always significantly larger with respect to normal conditions (*t*-test, $p<0.05$). Moreover, even at a bin width of 25 ms the electrical activity showed a high correlation, larger than 0.5.

(Fig. 7 near here)

When the retrieval was based on the responses of 32 electrodes, the maximal average efficiency obtained with the two codes, compared to normal conditions, increased of about 10 % in the presence of 50 μM APV (*t*-test, $p<0.05$) and decreased of about 15% in the presence of 10 μM bicuculline (*t*-test, $p<0.05$). Therefore, blockage of excitatory pathways mediated by NMDA receptors improves information processing, whereas the opposite effect was observed when inhibitory pathways mediated by $GABA_A$ receptors were blocked. For a given condition, when the three distributed codes (rate, first evoked AP and binary) were compared, the maximal retrieval efficiency was not significantly different both in normal conditions (Fig. 7C, black bars) (n=5, *t*-test, $p>0.05$) and in presence of 50 μM of APV (fig. 7C, white bars). Only in the presence of 10 μM bicuculline, the rate code was slightly less efficient compared to the other two codes (n=5, *t*-test, $p<0.05$). None of the distributed codes outperformed the others. In fact all distributed codes were similarly influenced by synaptic blockers, and the correlation of the electrical activity played the same role for all of them.

A difference between the three distributed codes was observed varying the time window Δt where optimal response was measured. For the largest ensemble considered (32 electrodes, second panel from the right), the dependence of the average retrieval efficiency on Δt was different for the three conditions and for the three codes. In normal conditions (fig. 7D), the efficiency reached its maximum for a Δt about 20 ms and it remained constant at larger Δt for the first AP code. In fact, neurons with the largest latencies poorly contribute to the coding since the weight of their response is $1/\tau$. On the contrary, later APs do contribute to the binary and rate coding. Since APs evoked at later times are more variable (Bonifazi et al. 2005), their firing at larger Δt degrades the efficiency of these codes. When inhibitory synaptic pathways were blocked (Fig. 7C) and the late phase is prolonged, there are consequently more variable APs for longer values of Δt and the rate and binary codes deteriorate even more. On the contrary, no significant difference was observed between the three codes, when the excitatory synaptic pathways were blocked (Fig. 7C), as the late phase of the evoked response was either reduced or abolished in the presence of APV (Jimbo et al., 2000).

Discussion

We used neuronal cultures of rat hippocampal neurons grown on MEA to study population coding scheme based on the response of a population of neurons. Although anticipated some years ago (Potter, 2001), the possibility of using multielectrode array to study distributed processing has received very little attention and previous work focused mainly on pooling of the neuronal responses (Ruaro et al., 2005; Bonifazi et al., 2005). Stimuli consisted of brief bipolar voltage pulses applied through patterns of extracellular electrodes, differing in their intensity and spatial location. Decoding performance on a variety of population coding scheme was estimated using criteria from information theory and classification analysis. By using this latter, we found striking similarities with previous in vivo population coding studies carried out in the somatosensory system (Nicolelis et al., 1998; Panzeri et al., 2003) and provide the first compelling evidence that neuronal cultures with apparently random connectivity can use different distributed codes to retrieve stimuli's features. Small populations of cultured neurons (~30) were able to identify correctly the intensity and spatial location of stimulus on a single trial basis, by relying on several distributed coding strategies, based either on the firing rate, first AP latency, PSTH or binarization of the neuronal responses. All of these distributed coding schemes had similar decoding performance and largely outperformed pooling of the population rate coding when neuronal responses were integrated over a short time window of 10-20 ms (Fig. 6). Our results also indicate that the temporal structure of the neuronal response of neurons matters and that rat hippocampal neuronal cultures could use different encoding strategies, such as mean firing rate, binarization or temporal patterns of population firing (PSTH) to represent stimulus's intensity and spatial location, as observed in the monkey somatosensory system (Nicolelis et al., 1998). Finally, the decoding performance depended critically on the balance between excitation and inhibition and the resulting pattern of correlation (Fig. 7): decreasing the correlation in the electrical activity via blockade of the NMDA receptors increased successful decoding, whereas increasing the correlation via blockade of the $GABA_A$ receptors had the opposite effect.

Pooled versus distributed responses

Considering the number of APs evoked in an ensemble of neurons, when APs are pooled and averaged (pooling) the relevant information is reduced to a scalar quantity, when the activity of neurons is considered separately (distributed rate coding) a vector of numbers is obtained. It is evident that, whenever it is possible, pooling the activity is computationally economic and therefore advantageous. As shown in Figures 5 and 6, it is possible to use pooling to code and retrieve the intensity of a stimulus, in agreement with previous work in hippocampal cultures (Bonifazi et al 2005). In this case, increasing the ensemble size from few neurons to dozens of neurons, both the distributed and the pooled responses allow us to reach a high decoding performance (Fig. 5B). As shown in Fig.5, the efficiency of pooling requires a larger ensemble of neurons.

The choice between pooled and distributed response is strictly linked to the tuning properties of the neurons to the different stimuli. The diversity of neuronal

responses for two neurons with different tuning properties will be conserved for a distributed code and lost by pooling. Pooling has been previously shown to be the right strategy to handle information from neurons with similar tuning characteristics, as in cortical columns where neurons in the sensory motor cortex respond to deflections of the same whisker (Panzeri et al., 2003) or in the visual cortex to visual stimuli with the same orientation and/or direction (Levit & Lund, 2002). In the present investigation we showed that pooling can be used when neurons respond in a progressive-like way (see Fig. 3) to the stimuli, as in the case of stimuli differing for their intensity. In this case, the firing rate of neurons increases monotonically with the stimulus intensity. On the contrary, a distributed coding is the appropriate strategy for neurons with different tuning characteristics, such as those belonging to distinct cortical columns where neurons respond to deflections of the different whiskers (Panzeri et al., 2003) or in the visual cortex to visual stimuli, with the different orientation and/or direction. In our investigation we showed that a distributed coding is advantageous when neurons were tuned to different spatial stimuli (Fig. 4D). Note that, in our case, tuning was considered for stimulus' features such as intensity and spatial location but tuning could also be observed for other stimulus' feature (e.g. stimulus frequency).

Comparison of distributed codes and retrieval of information

The comparison of the retrieval efficiency of differently distributed coding (see Fig. 6 and 7) shows that distributed codes based on the mean firing rate, latency of the first APs and a binary code provide very similar results. All these distributed schemes seem to be equivalent, even in the presence of synaptic blockers such as APV and bicuculline (see Fig.7). The equivalence of a rate and of a temporal coding using small time window of 10-20 ms is not surprising: within 10-20 ms neurons respond to stimuli with one or at most two APs and a rate coding becomes very similar to a coding based on the first evoked AP. Indeed, as shown in Fig.7 the optimal time window Δt to retrieve correctly the stimulus from the population response is only about 20 ms, which appears to be the time required for one elementary computation. This was clearly shown by the code based on the first evoked AP, when the response of each neuron decayed as the inverse of the latency of the first AP. In this way, early responses contribute more to the retrieval of the stimulus. An integration time of about 20 ms is also suggested by several biophysical mechanisms occurring in that time scale, such as processing in dendrites (Koch, 1999) and timing-dependent synaptic plasticity rule required for hebbian-like learning (Song et al., 2000). The short time needed for the retrieval of the stimulus prevents a significant role of NMDA receptors known to generate slow and long lasting synaptic potentials (Lester et al., 1990). Moreover, in the 20 ms following the stimulus, the correlation present in the network activity is low (Fig. 7A) while it seems to be more relevant at larger time windows when NMDA receptors are contributing to the network activity (compare open and closed circles of Fig. 7A). In agreement with our results, it has been shown that retrieval and memory encoding depends on AMPA receptor and NMDA in the hippocampus (Bast et al. 2005). Analogously, we previously showed for hippocampal cultures how after LTP-induction- which requires the involvement of

NMDA receptors - pattern recognition, i.e. stimulus retrieval, was obtained by pooling APs in few tens of ms, the time domain of AMPA contribution.

Even when small time windows of 10-20 ms are considered, decoding performance of a PSTH based code emphasis that the temporal structure of the neuronal response still matter. Increasing bin size significantly decreased PSTH's decoding performance (Fig. 6G) as temporal precision was reduced. This suggest that similarly to somatosensory neurons (Nicolelis et al., 1998; Foffani & Moxon, 2004), population of cultured neurons could use different encoding strategies such as mean firing rate or temporal patterns of population firing to represent the intensity and location of a stimulus. This means that for our stimuli set, neuronal cultures can be considered, to some extent, as a kind of topographic sensory map in which distributed coding schemes can be used to decode the information about the intensity and spatial location of a stimulus.

The role of inhibition and excitation and the contribution of the correlation in stimulus retrieval

Inhibition and excitation greatly determine the efficiency of retrieval of all considered coding schemes (see Fig.7). In agreement with our previous investigation (Bonifazi et al., 2005), blockage of excitatory synaptic pathways mediated by NMDA-receptors substantially increased the decoding performance of the distributed coding schemes explored. An opposite effect was observed when inhibitory synaptic pathways mediated by $GABA_A$ receptors were blocked. The correlation of the electrical activity in the network, which is clearly present in the spontaneous activity in normal conditions (fig. 2 A), was highly affected by the balanced presence of inhibition and excitation and therefore played a fundamental role in the decoding performance. Nevertheless, in normal conditions, the spontaneous activity was clearly correlated even for short time windows of few dozens of ms, the presence of balanced inhibition and excitation allowed to maintain a low correlation in the evoked electrical activity and, as a consequence, it allowed the efficient retrieval of the stimuli. At a large bin width (>80 ms) when the excitatory synaptic pathways mediated by NMDA-receptors contributed to the evoked response, the correlation of the evoked response significantly increased and, as a consequence, the efficiency of rate and of the binary code decreased (fig. 6 central upper panel and fig. 7A second panel from the right). When longer time window are considered, the late phase of the evoked response (Jimbo et al., 2000) will influence the decoding performance due to its variability. This increase in the neuronal response variability is responsible for the decrease of the decoding performance of a distributed code based on the mean firing rate (Fig. 6). Increasing the time window also increases the probability of observing APs. Thus, some elements of the vector response which had a zero for small time window will now likely have non-zero values. This is especially true for the first APs latency and binary schemes, in which a zero means an absence of AP for a particular time window. As a consequence of longer time window, the diversity of neuronal responses for the first AP latency and binary coding scheme will decrease, resulting in a decrease of the decoding performance (Fig. 6).

Acknowledgements

This work was supported by the EU grant NEURO, by a FIRB grant from the Italian Ministers and by the CIPE grant (GRAND FVG). We thank Manuela Schipizza Lough for carefully reading the manuscript and G. Pastore for preparing some of the cell cultures.

References

Abeles, M. (1991) *Corticonics*. Cambridge University Press.

Averbeck, B.B., Latham, P.E., Pouget, A. (2006) Neural correlations, population coding and computation. Nat. Rev. Neurosci. **7**, 358-366.

Bast, T., da Silva, T.M. and Morris, R.G. (2005) Distinct contributions of hippocampal NMDA and AMPA receptors to encoding and retrieval of one-trial place memory. *J. Neurosci.* **25**: 5845-5856.

Borst, A. & Theunissen, F.E. (1999) Information theory and neural coding. *Nat. Neurosci.* **2:**947-957.

Darian-Smith, I., Johnson, K.O., Dykes, R. (1973) 'Cold' fiber population innervating palmar and digital skin of the monkey: responses to cooling pulses. *J. Neurophysiol.* **36**:325-346.

Dayan, P. & Abbott, L.F. (2001) *Theoretical Neuroscience. Computational and mathematical modeling of neural systems.* MIT Press. Cambride, MA, USA.

Delorme, A., Thorpe, S.J. (2001) Face identification using one spike per neuron: resistance to image degradations. *Neural. Netw.* **14**:795-803.

Delorme, A. (2003) Early cortical orientation selectivity: how fast inhibition decodes the order of spike latencies. *J. Comput. Neurosci*. **15**: 357-365.

Duda, R.O., Hart, P.E. & Stork, D.G. (2000) *Pattern Classification, 2nd Edition (Wiley-Interscience, 2001).*

Egert, U., Knott, T. Schwarz, C. Nawrot, M., Brandt, A., Rotter, S., Diesmann, M. (2002) MEA-Tools: an open source toolbox for the analysis of multi-electrode data with MATLAB. *J. Neurosci. Meth.*. **17**: 33-42.

Foffani, G. Moxon, K.A. (2004) PSTH-based classification of sensory stimuli using ensembles of single neurons. *J. Neurosci. Meth.* **135**: 107-120.

Gawne, T.J., Richmond, B.J. (1993) How independent are the messages carried by adjacent inferior temporal cortical neurons? *J. Neurosci.* **13**:2758-2771.

Georgopoulos, A.P., Schwartz, A.B., Kettner, R.E. (1986) Neuronal population coding of movement direction. *Science* **233**:1416-1419.

Gray, C.M., König, P., Engel, A.K., Singer, W. (1989) Oscillatory responses in cat visual cortex exhibit inter-columnar synchronization which reflects global stimulus properties. *Nature* **338:** 334-337.

Hopfield, J.J. (1995) Pattern recognition computation using action potential timing for stimulus representation. *Nature* **376**:33-36.

Jimbo, Y., Kawana, A., Parodi, P., Torre, V. (2000) The dynamics of a neuronal culture of dissociated cortical neurons of neonatal rats. *Biol. Cybern.* **83**: 1-20.

Johansson, R.S., Birznieks, I. (2004) First spikes in ensembles of human tactile afferents code. *Nat. Neurosci.* **6**: 750 – 757.

Koch, C. (1999) *Biophysics of computation*. Oxford University Press, New York.

Lester, R.A., Clements, J.D., Westbrook, G.L., Jahr, C.E. (1990) Channel kinetics determine the time course of NMDA receptor-mediated synaptic currents. *Nature* **346**: 565-567.

Levit, J.B. and Lund, J.S. (2002) The spatial extent over which neurons in macaque striate cortex pool visual signals. *Vis. Neurosci.* **19**: 439-452.

Nicolelis, M.A., Ghazanfar, A.A., Stambaugh, C.R. Oliveira, L.M., Laubach, M., Chapin, J.K., Nelson, R.J., Kaas, J.H. (1998) Simultaneous encoding of tactile information by three primate cortical areas. *Nat. Neurosci.* **1**:621-630.

Nirenberg, S. and Latham, P.E. (2003) Decoding neuronal spike trains: how important are correlations? *PNAS USA* **100**: 7348–7353.

Panzeri, S., Treves, A. (1996) Analytical estimates of limited sampling biases in different information measures. *Network Comput. Neural. Syst.* **7**:87–107.

Panzeri, S., Petersen, R.S., Schultz, S.R., Lebedev, M., Diamond, M.E. (2001) The role of spike timing in the coding of stimulus location in rat somatosensory cortex. *Neuron* **29**:769-777.

Panzeri, S., Petroni, F., Petersen, R.R., Diamone, M.E. (2003) Decoding neuronal population activity in rat somatosensory cortex: role of columnar organization. *Cereb. Cortex* **13**:45-52.

Petersen, R.S., Panzeri, S., Diamond, M.E. (2002) Population coding in somatosensory cortex. *Curr. Opin. Neurobiol.* **12**: 441-447.

Papoulis, A. (1984) *Probability, random variables and stochastic processes*. McGraw-Hill, New York.

Potter, S.M. (2001) Distributed processing in cultured neuronal networks. *Prog. Brain Res.* **130**:49-62.

Potter, S.M. and DeMarse, T.B. (2001) A new approach to neural cell culture for long-term studies. *J. Neurosci. Meth.* **110**:17-24.

Rieke, F.D., Warland, R.R., de Ruyter van Steveninick R, Bialek W (1997) *Spikes: Exploring the neural code.* MIT Press. Cambride, MA, USA.

Ritz, R., Sejnowski, T.J. (1997) Synchronous oscillatory activity in sensory systems: new vistas on mechanisms.*Curr. Opin. Neurobiol.* **7:** 536-46.

Ruaro, M.E., Bonifazi, P., Torre, V. (2005) Towards the neurocomputer: image processing and pattern recognition with neuronal cultures. *IEEE Trans. Biomed. Eng.* **52**:371-383.

Rumelhart, D.E. and McClelland, J.L., Eds. (1986). *Parallel Distributed Processing: Explorations in the Microstructure of Cognition Vol 1: Foundations*. MIT Press.

Sanger, T.D. (2003) Neural population codes. *Curr. Opin. Neurobiol.* **13:** 238-249.

Shannon, C.E., Weaver, W. (1949) A mathematical theory of communication. In: *The mathematical theory of communication*. Urbana, IL: University of Illinois.

Shadlen, M.N., Britten, K.H., Newsome, W.T., Movshon, J.A. (1996) A computational analysis of the relationship between neuronal and behavioural responses to visual motion. *J. Neurosci.* **16**:1486-1510.

Shadlen, M.N., Newsome, W.T. (1998) The variable discharge of cortical neurons: implications for connectivity, computation, and information coding. *J. Neurosci.* **18**:3870-3896.

Singer, W. & Gray, C.M. (1995) Visual feature integration and the temporal correlation hypothesis. *Annu. Rev. Neurosci.* **18:**555-86.

Song, S., Miller, K.D., Abbott, L.F. (2000) Competitive Hebbian learning through spiketiming-dependent synaptic plasticity. *Nature* **3**: 916-926.

Thorpe, S., Delorme, A. Van Rullen, R. (2001) Spike-based strategies for rapid processing *Neural Network* **14**:715-725.

Van Rullen, R., Thorpe, S.J. (2001) Rate coding versus temporal order coding: what the retinal ganglion cells tell the visual cortex. *Neural Comput*. **3**:1255-1283.

Wagenaar, D.A., & Potter, S.M. (2002) Real-time multi-channel stimulus artifact suppression by local curve fitting. *J. Neurosci. Meth.* **120**:113-120.

Wagenaar, D.A., Pine J., Potter, S.M. (2004) Effective parameters for stimulation of dissociated cultures using multi-electrode arrays. *J. Neurosci. Meth.* **138**:27-37.

Figure legends

Figure 1. Stimuli of different spatial location and vector responses. **A.** *Left*, Sketch of the 60 MEA electrodes with the four different patterns of electrodes used for stimulation (A-D). Each square represents an individual electrode. Gray squares indicate the position of the three neurons whose activity is shown in C. Distance between electrodes is 500 μm. *Right*, disposition of the 9 spatial patterns. Each pattern consists of one of, or combination of, the four patterns depicted on the left. Three different intensities were used for each spatial pattern, resulting in a total of 27 different patterns of stimulation (9 spatial x 3 intensities). **B.** Schematic representation of the single-trial response of an ensemble of *n* neurons (or electrodes when multiunit recordings are considered, see Methods) to the stimulus. The delivery of the stimulation is indicated by the black vertical arrow. The population response was evaluated in the time window Δt of variable size. τ_i represents the latency of the first evoked AP in the neuron *i* (i=1..n). For the three distributed neural codes examined, binary code (BIN 0-1), first evoked AP ($1/\tau$) and rate, the response is represented by a vector. For the binary coding, the activity measured in each bin was converted to "0" when no APs were detected or to "1" when one or more APs were detected. For the first evoked AP code, the inverse of the latency τ_i was considered. When the latency was larger than a time window Δt, the latency was considered as infinite, i.e. the neuron was supposed not to fire. For the rate code, the numbers of APs fired within each bin are counted. The time window Δt was binned in the case of PSTH coding. For the population rate code, the APs fired within each bin in the all ensemble of neurons were pooled, i.e. summed. **C.** Single-trial responses. *Top*, rasterplots of the single-trial responses of three neurons depicted in grey in A (1-3) for three different spatial stimuli, showing the reliability of responses for a given spatial pattern and the diversity of neuronal responses to diverse spatial patterns. Each line of the rasterplot correspond to a different trial. *Bottom*, rasterplots of the single-trial responses of the same three neurons as *top*, but for three different intensities, showing the reliability of responses for a given intensity and the diversity of neuronal responses to diverse intensities. The spatial pattern was the one shown in the left panel of A. For a given neuron, responses were reliable for a given intensity and the diversity of neuronal responses to diverse intensities.

Figure 2. Correlation in the electrical activity of the network. The results are averaged over 5 different preparations. For each dish, the average correlation was calculated between the firing rate of all possible pairs of electrodes. Closed circles, open circles and open squares correspond respectively to control conditions, 50μM APV and 10μM bicuculline. **A.** Average cross-correlation of the spontaneous activity for different time bins. The electrical activity was binned into firing rate so to obtain a time series. The cross-correlation between the time series of each pair of electrodes was calculated according to equation (1). **B.** Average cross-correlation of the evoked activity for different time bins. For each single trial and each single electrode, the number of APs evoked in the bin following the stimulus was calculated. The cross-correlation between the trial time series of each pair of electrodes was calculated according to equation (1).

Figure 3. Tuning properties of the neurons for the distinct stimuli features. **A-C.** *Upper plots*, average firing rate in response to the highest intensity (y-axis) in function of the lowest intensity (x-axis) for each neuron and for three different spatial patterns displayed on top of the graphs. *Lower plots*, average firing rate in response to the highest intensity (y-axis) in function of the intermediate intensity (x-axis) for each neuron and for three different spatial patterns displayed on top of the graphs. Most of the neuronal responses cluster in one semisector, indicative of a progressive-like response (see Methods). This means that a given neuron always fires more APs for the highest intensity. The average firing rate was determined in a 20 ms time window following the stimulation onset. **D.** Average firing rate in response to single patterns of electrodes. The spatial location of patterns A-D is shown in C. **E.** Same as D, but for pairs of electrode patterns. In D and E, Different neurons respond differentially to different spatial stimuli, indicating that neurons exhibit spatial tuning.

Figure 4. Statistics of the mutual information encoded in the rate response of single neurons and of pairs of neurons. Analysis distinguishes stimuli of different intensity and spatial location. For pairs of neurons the response was pooled or considered as distributed (i.e. a vector). **A-B.** Mutual information for intensity coding. **A.** Distributions of the mutual information for single neurons for the spatial patterns shown on top. **B.** Mutual information of pairs of neurons for stimuli of variable intensity. The mutual information of the pooled response (I_{pool}) is plotted versus the mutual information of the distributed response (I_{dist}). Intensities used were 400, 650 and 900 mV. **C-D.** Mutual information for spatial coding. **C.** Distributions of the mutual information for single neurons for the three intensities indicated on top. **D.** Mutual information of pairs of neurons for stimuli of variable intensity. The mutual information of the pooled response (I_{pool}) is plotted versus the mutual information of the distributed response (I_{dist}) for stimuli of variable location. In **B** and **D,** the diagonal line represent $I_{pool} = I_{dist}$. In both intensity and spatial coding, a distributed rate code is more efficient than a pooled code as indicated by clusterization of neuron pairs in the upper semisector. Comparison between intensity and spatial coding further reveals that single neurons carry more information on the spatial location than on the intensity.

Figure 5. Ensemble performance stimulus single-trial classification for different neuronal population size. The size of the neuronal population was varied by removing best predictors (neurons with highest mutual information) one by one. The ensemble performance corresponds to the fraction of trial classified correctly. Left and right column correspond to the ensemble performance computed according to the bootstrap and leave-one-out methods respectively (see Methods). **A.** Ensemble performance for a pattern of stimulation involving a single pattern of six electrodes. A distributed rate code performs better than a pooled population rate code and decreased smoothly as best predictors were removed. Note that the performance of the pooled population rate code was lower than chance level. **B.** Ensemble performance for a pattern of stimulation involving four patterns of six electrodes. In this case, distributed rate code and pooled population rate code performed equally. In this case, the number of neurons responding is bigger than for any other pattern of stimulation, facilitating the decoding procedure. The intensity of the stimulus in **A** and **C** was 900 mV. **C.** Ensemble performance

averaged over all experiments (n=5) and across all 27 patterns of stimulation, showing that a distributed rate code always outperformed a pooled population rate code, independently of the cross-validation method used. Dashed lines correspond to chance level.

Figure 6. Efficiency of stimulus single-trial classification for different coding schemes. **A.** Ensemble performance for all 27 stimuli (9 spatial location * 3 intensities) for four different distributed codes and one pooled population rate code (pooling, grey circle). APs are considered in a 20 ms time window. Distributed codes are firing rate (black square), binary (BIN 0-1, blue triangle), the first evoked AP ($1/\tau$, green circle) and the post-stimulus time histogram (PSTH, red diamond). Time window was binned with 2 ms bins for the PSTH coding. The ensemble performance for 3 intensities (low, medium and high) is plotted for each of the 9 spatial patterns indicated on the x ordinate. Distributed codes outperformed pooling but for the last pattern of stimulation with four patterns of six electrodes, in which case ensemble performance was similar to binary coding for the medium and high intensity. **B.** Same as A, but considering only the spatial location of the single-trial, independently of the intensity, i.e. a single-trial was considered as correctly classified if only the spatial location was identified, even though the intensity could be misclassified. PSTH coding gave the best performance and the three other distributed codes (rate, binary and first evoked AP) performed almost equally. In **A** and **B**, ensemble performance represents mean value (n=5) and was computed using the leave-one-out method for cross-validation (see Methods). Error bar have been omitted for the sake of clarity. Dashed lines correspond to chance level. **C-G.** Influence of the time window length Δt on the ensemble performance for two patterns and the average of all patterns. Increasing the time window length increases the variability of the firing pattern which in turn decreases the ensemble performance of all distributed codes (C-E) but PSTH (G). Pooling (F) was largely unaffected by change of the time window and performed below chance level for all patterns of stimulation but the one involving four patterns of six electrodes. This pattern of stimulation constitutes a special case (see text) and the retrieval efficiency was unaffected by changes of the time window length for all coding schemes considered. **H.** Influence of the bin size on the ensemble performance for the PSTH coding scheme. Decreasing the number of bin led to a decrease of the ensemble performance as PSTH coding became roughly equivalent to rate coding.

Figure 7. Pharmacological dissection of distributed coding schemes. Blockage of $GABA_A$ receptors with bicuculline (10 μM, open circles) increased the correlation of both spontaneous (**A**) and evoked (**B**) activity relative to normal conditions (filled circles), whereas blocking NMDA receptors with APV (50 μM, open squares) had the opposite effect. The pattern of stimulation was a horizontal bar of six electrodes indicated by the black squares of the MEA grid's sketch representation depicted in the inset of panel A. The electrical activity of each electrode was binned into firing rate so to obtain time series from which cross-correlation was computed (see Methods). **C.** Influence of the balance between excitation and inhibition on the decoding performance. Decreasing network excitation with APV slightly increases decoding performance for distributed codes. Δperformance refers to a difference from the decoding performance with drug relative to performance in normal conditions. **D.** Influence of the time window length on

the decoding performance for the distributed codes, rate, binary and first evoked AP ($1/\tau$). A time window of 20-40 ms is optimal for these distributed codes.

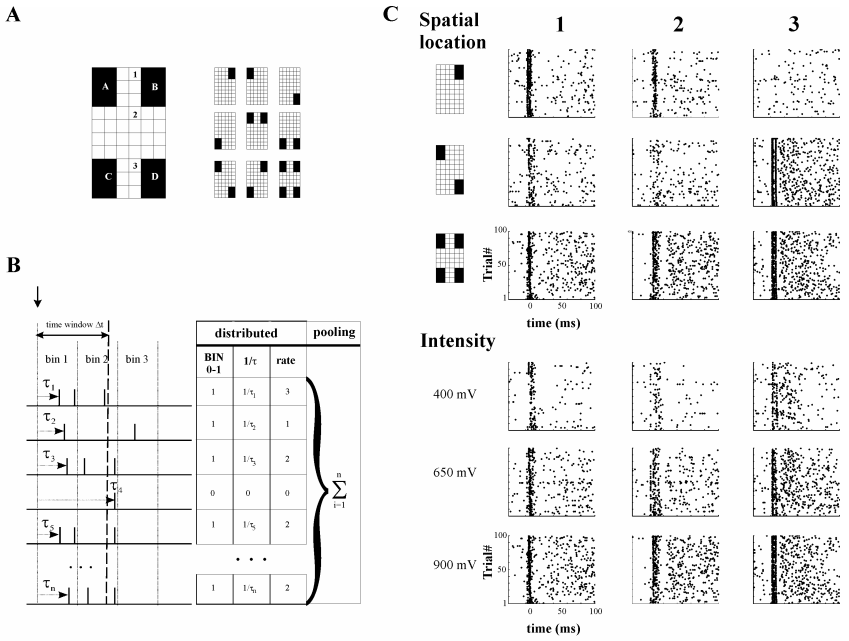
A
B
C
Spatial location
1
2
3
Intensity
400 mV
650 mV
900 mV
Trial#
time (ms)
time window Δt
bin 1
bin 2
bin 3
distributed
pooling
BIN 0-1
1/τ
rate

Fig. 1

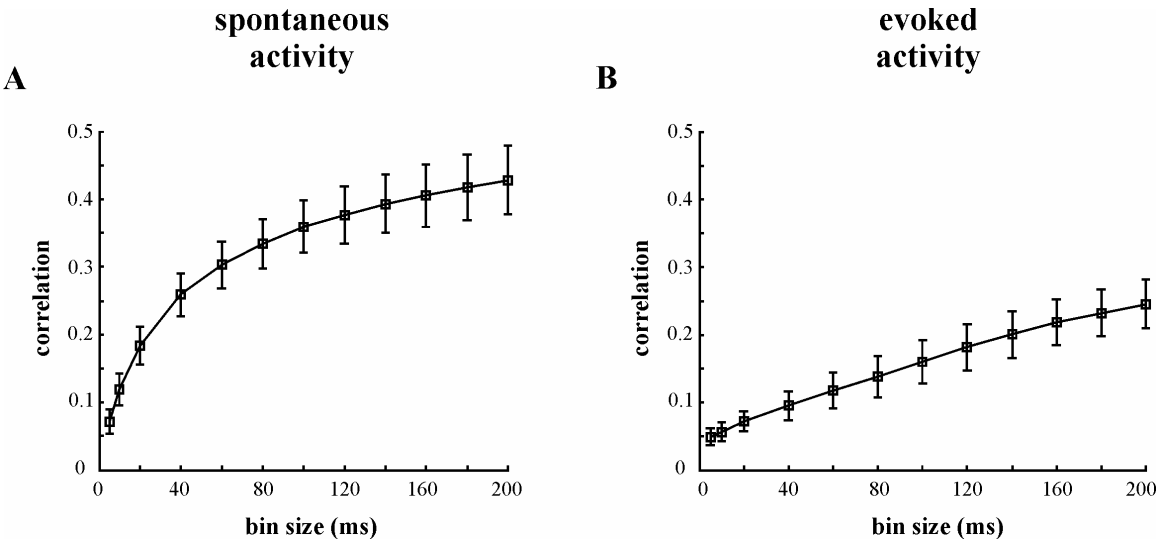
A
spontaneous activity
B
evoked activity
correlation
bin size (ms)
0
0.1
0.2
0.3
0.4
0.5
40
80
120
160
200

Fig. 2

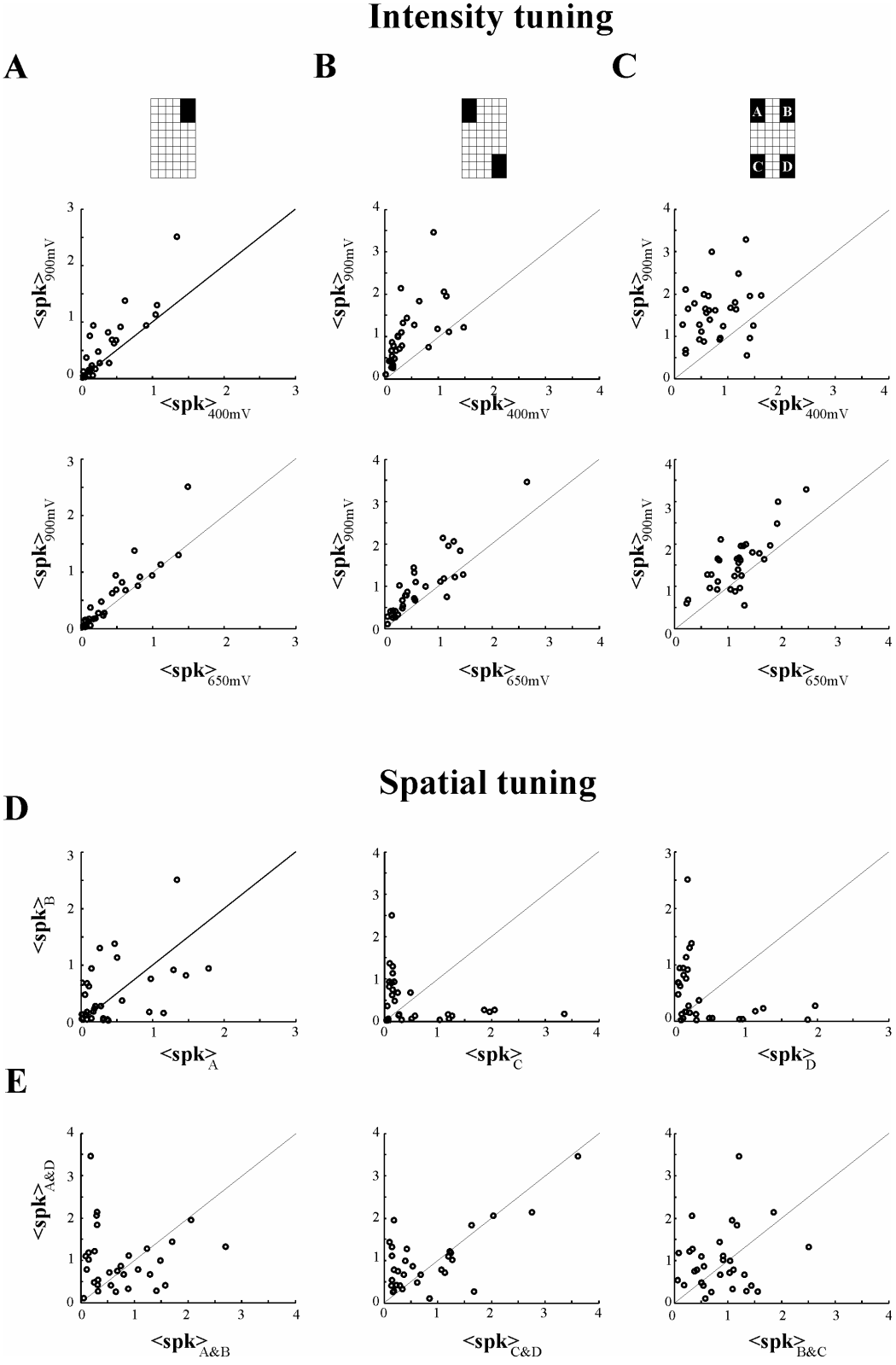
Intensity tuning
A
B
C
A
B
C
D
<spk>900mV
<spk>400mV
<spk>650mV
Spatial tuning
D
E
<spk>B
<spk>A
<spk>C
<spk>D
<spk>A&D
<spk>A&B
<spk>C&D
<spk>B&C

Fig. 3

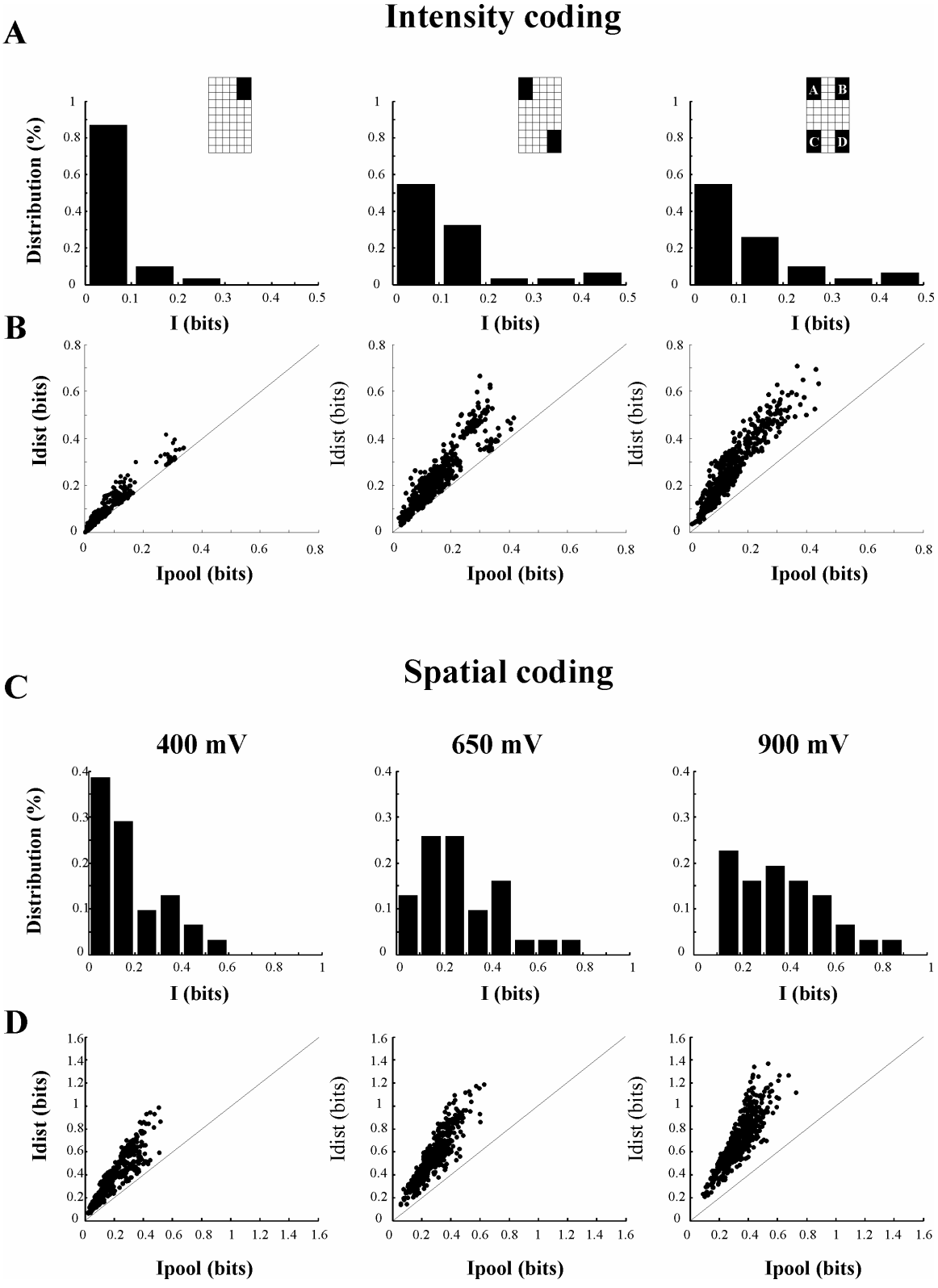
A
Intensity coding
Distribution (%)
I (bits)
A
B
C
D
B
Idist (bits)
Ipool (bits)
C
Spatial coding
400 mV
650 mV
900 mV
Distribution (%)
I (bits)
D
Idist (bits)
Ipool (bits)

Fig. 4

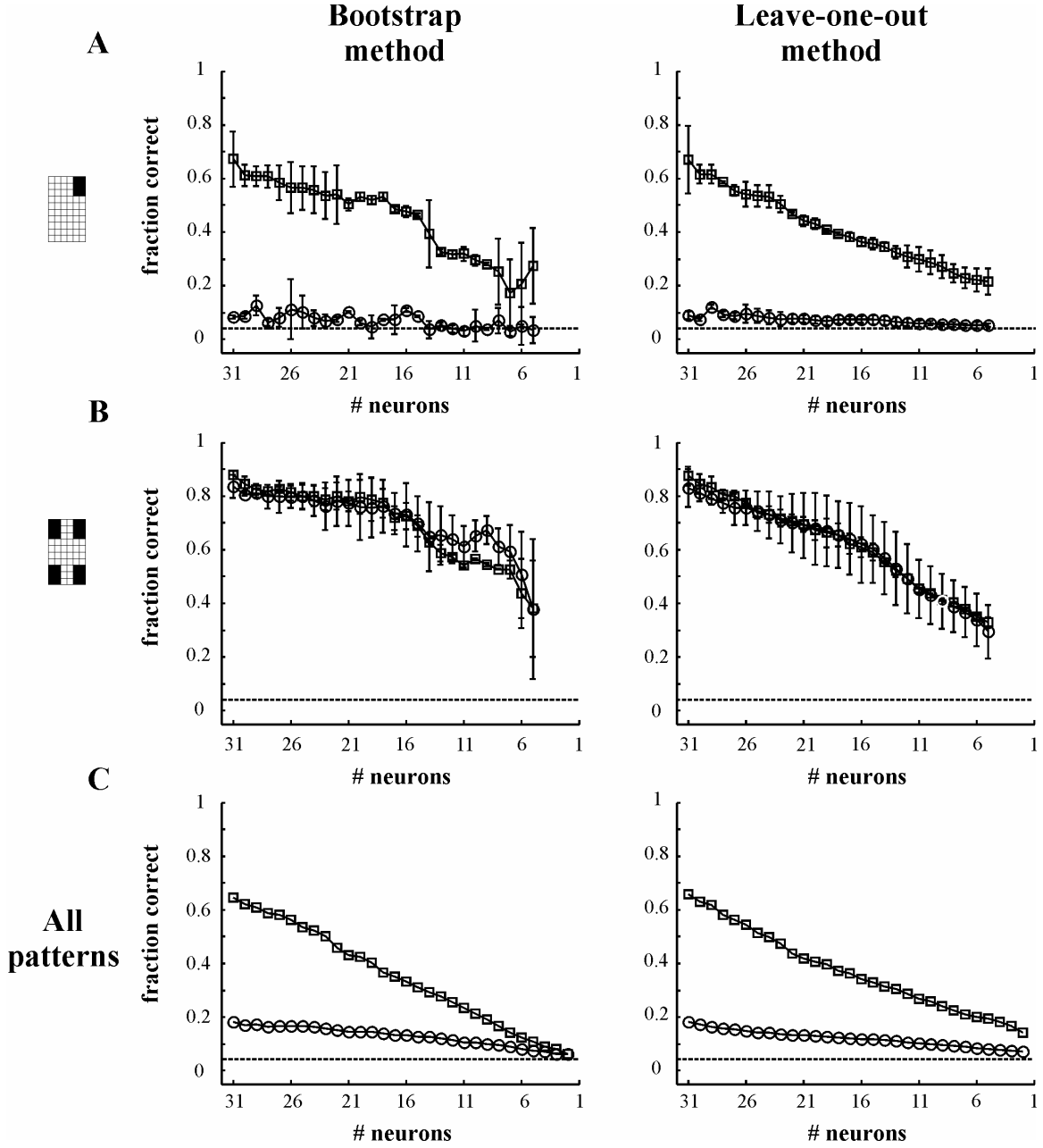
A
B
C
All patterns
Bootstrap method
Leave-one-out method
fraction correct
neurons
1
0.8
0.6
0.4
0.2
0
31
26
21
16
11
6
1

Fig. 5

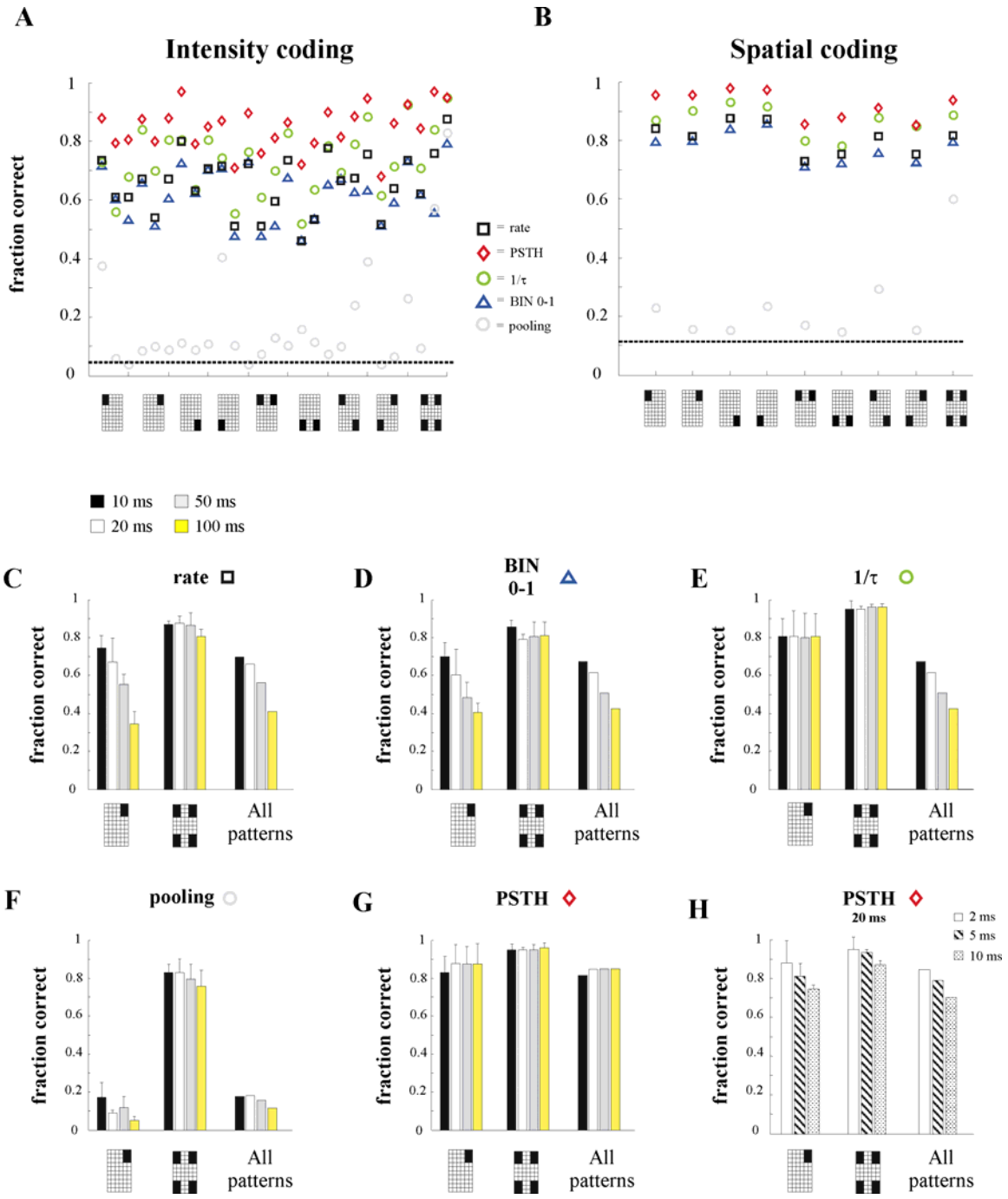
A
Intensity coding
fraction correct
1
0.8
0.6
0.4
0.2
0
= rate
= PSTH
= 1/τ
= BIN 0-1
= pooling
B
Spatial coding
10 ms
50 ms
20 ms
100 ms
C
rate
D
BIN 0-1
E
1/τ
All patterns
F
pooling
G
PSTH
H
PSTH
20 ms
2 ms
5 ms
10 ms

Fig. 6

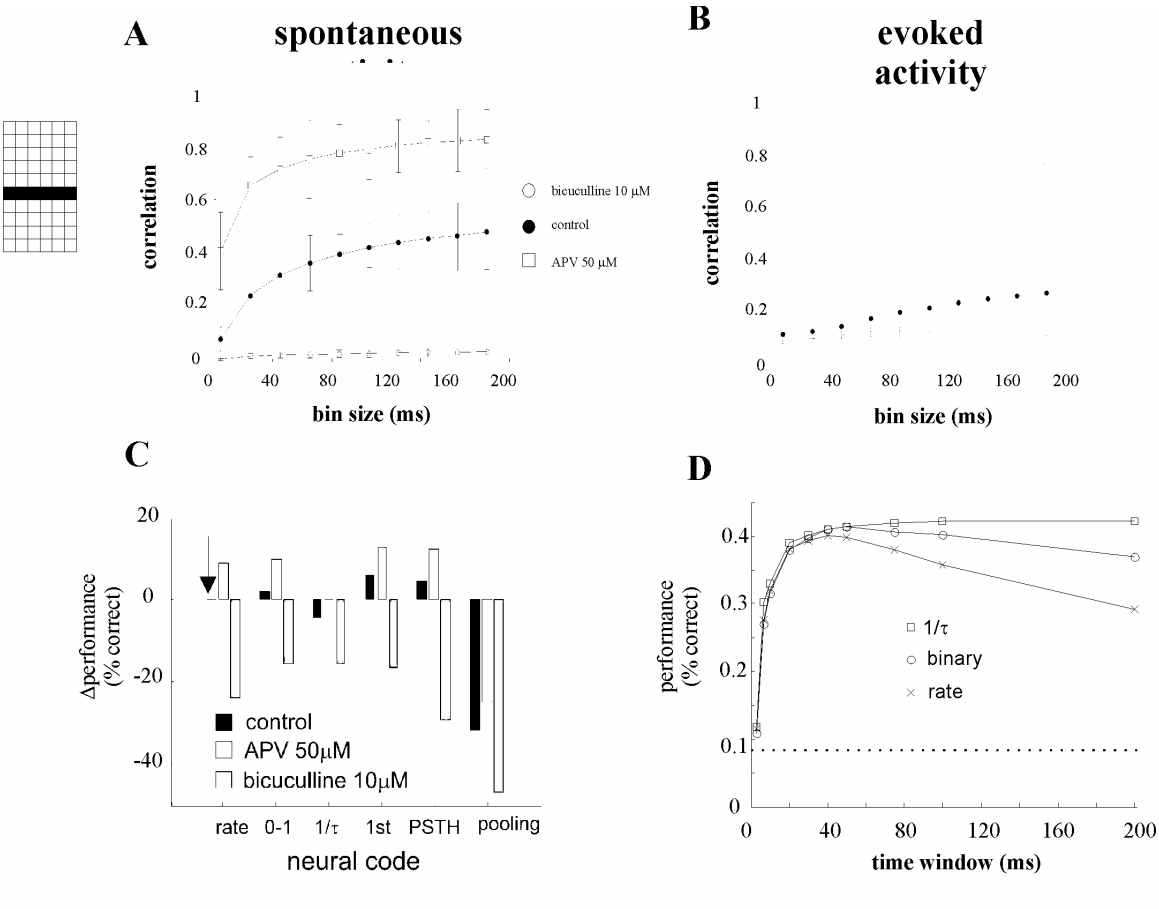
A
spontaneous
correlation
bin size (ms)
bicuculline 10 µM
control
APV 50 µM
B
evoked
activity
correlation
bin size (ms)
C
Δperformance
(% correct)
control
APV 50µM
bicuculline 10µM
rate
0-1
1/τ
1st
PSTH
pooling
neural code
D
performance
(% correct)
1/τ
binary
rate
time window (ms)

Fig. 7

4 – CONCLUSION AND PERSPECTIVES

The experiments described in this thesis aimed at investigating network functions of dissociated cultures of rat hippocampal neurons. These neuronal cultures form random networks that share many developmental, structural and functional aspects of *in vivo* networks. My major research findings concern the usefulness of studying random cultured hippocampal networks using multi-electrode array to probe a large variety of network functions and can be summarized in three main achievements.

First, I characterized the network spontaneous activity dynamics and compared it with that of another network studied in our laboratory, the intact leech ganglia. We found that these two very different networks share several features. In particular, in both networks: i) the inter-spike intervals distribution of the spontaneous firing of single neurons is either regular or periodic or bursting, with the fraction of bursting neurons depending on the network activity; ii) bursts of spontaneous spikes have the same broad distributions of size and duration; iii) the degree of correlated activity increases with the bin width, and the power spectrum of the network firing rate has a 1/f behavior at low frequencies, indicating the existence of long-range temporal correlations; iv) the activity of excitatory synaptic pathways mediated by NMDA receptors is necessary for the onset of the long-range correlations and for the presence of large bursts; and v) blockage of inhibitory synaptic pathways mediated by $GABA_A$ receptors causes instead an increase in the correlation among neurons and leads to a burst distribution composed only of very small and very large bursts. These results were explained in the context of the self-organized criticality (SOC) framework (Jensen, 1998). SOC has been described at several levels of investigation from MEG and EEG time series in the developing and adult human brain (Linkenkaer-Hansen et al., 2001; Freeman, 2004; Tatcher et al., 2008) to LFP in acute slices and organotypic cultures of rat cortex (Beggs & Plenz, 2003). All these networks have a specific functional architecture. Our findings of SOC in cultured hippocampal networks and in intact leech ganglia provide the first demonstration of SOC in random networks as well as in invertebrate networks, thus generalizing SOC dynamics, and indicating that such dynamics might be a generic property of neuronal networks. Moreover, SOC seems also present in the rat spinal cord culture (J. Streit, personal

communication) suggesting that this dynamics is a rather ubiquitous phenomenon in a large variety of nervous systems.

In agreement with diverse neural network models exhibiting SOC and having different topologies, such as cellular automata-like (Chen et al., 1995), global coupling (Eurich et al., 1999, 2002) and small-world networks (Lin & Chen, 2005), SOC dynamics, at the experimental level, seems thus independent from the network's topology. A possible explanation for this would be that networks follow some common organizational underlying principles. Comparison of the developmental pattern of rat cultured cortical and hippocampal networks grown on MEAs support this hypothesis. Cortical (Maeda et al., 1995; van Pelt et al., 2004) and hippocampal (data not shown) developing networks exhibit similar firing rate profile and patterns of synchronous bursting activity after the first week *in vitro*. Moreover, as in cortical networks (Maeda et al., 1995), my own experiments in hippocampal networks indicate that the site of initiation, or seed, of bursts varied randomly (data not shown).

More importantly, networks having SOC dynamics can switch among three distinct regimes of activity depending on the strength of interactions among neurons (Eurich et al., 2002). This indicates that SOC dynamics could play a role in information processing (Beggs & Plenz, 2003; Beggs, 2008). Previous work in our laboratory on the information processing capacities of the same cultured hippocampal networks (Bonifazi et al., 2005) showed that the mutual information between stimuli and response was the highest when NMDA receptors were blocked with APV, whereas the propagation of activity was the lowest. Conversely, mutual information was the lowest and activity propagation the highest when $GABA_A$ receptors were blocked with bicuculline. Moreover, on the one hand, reduction of the bursting activity by APV (subcritical regime in SOC theory) reduces propagation of the electrical activity, allowing better local information processing and resulting in higher mutual information. On the other hand, increasing the bursting activity (supercritical regime in SOC theory) with bicuculline (BIC) or gabazine (GBZ) increases propagation of the electrical activity but it seriously limits information processing as stimulation triggers large bursts invading the entire networks. In this case discriminability drops. This demonstrates the importance of a correct balance between excitation and inhibition, and in the light of the results on SOC

dynamics in these networks, the critical state observed in control conditions seems to represent a trade-off between propagation of the electrical activity and information processing capacity. This can be summarized by the following table:

SOC regime	**Sub-critical**	**critical**	**super-critical**
induced by	APV	normal conditions	BIC/GBZ
bursting	low	medium	high
mutual info.	high	medium	low
info propagation	low	medium	high

My second major achievement was to use a protocol allowing the investigation of both spontaneous and evoked activity network plasticity at the molecular and electrical level. In contrast to the classical electrical protocols, I induced network plasticity pharmacologically by exposing transiently networks to inhibitors of $GABA_A$ receptors, such as bicuculline or gabazine.

On the one hand, $GABA_A$ inhibitors trigger large synchronized bursts invading the entire network. As in the developing hippocampus, retina and spinal cord networks, network hyperexcitability was necessary and sufficient to generate synchronous patterns of bursting activity. Interestingly, this spontaneous pattern of bursting activity persisted 24 h after drug washout in most cases and sometimes up to several days, indicating that plastic changes took place during drug application. By combining top-down (MEA) and bottom-up (DNA microarrays) approaches, we characterized the time course of the electrical and molecular events underlying these plastic changes and the persistence of this bursting pattern of activity. The combination of MEA and DNA microarray to study neuronal plasticity was originally developed by Bading's group (Arnold et al., 2005) but has been limited to the plasticity of the spontaneous activity and did not identify specific genes. Also, previous works on neuronal plasticity usually focused on few genes and our data rather suggest that the regulation of hundreds – rather than tens or thousands – of genes is necessary to sustain it.

On the other hand, the evoked activity was potentiated for several hours after the drug washout. This represents the first demonstration of a pharmacological induction of a LTP form in MEAs. This is particularly important as a recent review of the classical electrical protocols used so far to induce functional plasticity in MEAs by several groups (Wagenaar & Potter 2006), revealed that changes concomitant with induction were no larger in magnitude than changes that occurred spontaneously. This group failed to repeat all of the protocols claimed to induce functional plasticity. Thus, pharmacological induction of functional plasticity could be an interesting alternative. The mechanism by which the evoked activity was potentiated can be accounted for by the fact that the synchronous bursting patterns of activity provide hebbian conditions for induction of plasticity, as it has been proposed in developing networks.

A second reason for the importance of functional plasticity is that it is a prerequisite for the creation of versatile hybrid devices, composed of biological neurons and artificial elements, capable of massive parallel computation. The creation of hybrid devices is one of the long-term goals of our laboratory and functional plasticity could serve as a kind of programming way to store patterns of activity.

Previous works combining MEA and DNA microarrays focused mainly on the patterns of gene expression without much emphasis on the functional characterization of the concomitant electrical changes (Valor et al., 2006; Xiang et al., 2007). To our knowledge, our results are the first to describe the time course of both cellular and electrical changes during a form of network plasticity. In a wider context, combining electrophysiology, pharmacology and genetics will likely prove to be a valuable approach to dissect and investigate network functions. Recent advances in genetics open up the possibility of silencing diverse neuronal types (White et al., 2001; Wulff & Wisden, 2005) with high specificity in the very near future. Such ‘circuit breaking’ could reveal how a single type of neuron contributes to network properties, such as plasticity, oscillations and ultimately to animal behavior. Similarly, the contribution and role of a single type of neuron during developmental processes could be investigated. However, any silencing procedure or interference, whether pharmacologic or genetic, should ideally be reversible in a time frame of milliseconds to seconds, otherwise compensations or adaptation mechanisms will fog the interpretation of experiments. Another exciting

application of genetic tools applied to networks is the possibility of engineering networks genetically with specific properties in order to potentially generate new generations of computing devices.

A future project which will start soon in our laboratory will aim at characterizing gene regulation taking place during the potentiation of the evoked activity. To this end, the same procedure as the one used to study the spontaneous activity plasticity will be used. A comparison of the gene regulation patterns observed in the plasticity of both spontaneous and evoked activity is envisaged. It would be also very informative to carry out gene regulation analysis when different protocols of induction of plasticity are used and compare the pattern of gene expression among different LTP induction protocols. This would reveal similarities and differences of gene regulation patterns in diverse forms of plasticity and give insights for further research *in vitro* and in living animals.

The third achievement of my thesis consisted in comparing and identifying several candidate coding schemes used for computation in random networks of rat hippocampal neurons. By using classification criteria from pattern recognition theory, we found striking similarities with *in vivo* population coding strategies used in the somatosensory cortex of rat (Petersen et al., 2003) and monkey (Nicolelis et al., 1998). Distributed codes proved to be more efficient than pooling of the neuronal responses to be able to correctly identify a stimulus' intensity and spatial location. As in the rat barrel cortex, pooling was found to be advantageous only when neurons had similar tuning properties. Among the different distributed coding schemes tested, PSTH has a slightly higher decoding performance than other distributed codes based on the mean firing rate, first AP latency or binarized vectors (that all performed similarly among them). This means that, like in the monkey somatosensory system, different encoding strategies could be used by random networks of rat hippocampal neurons. This is particularly interesting as the neuronal cultures used in this thesis have a random connectivity and lack any fnctional organization. Despite this latter, in our case, random networks of rat hippocampal neurons could be seen as a kind of topographic sensory map from which stimulus' intensity and spatial location can be efficiently retrieved by using distributed coding schemes.

Taken altogether, these results provide the first compelling evidence that simple computational tasks can rely on distributed population coding schemes in random networks of rat hippocampal neurons. Although proposed some years ago (Potter, 2001), this idea received little attention in the MEA community, especially for those working with dissociated cultures. Indeed, previous work on population of neurons using MEA and random cultures either focused on pooling (Bonifazi et al., 2005; Ruaro et al., 2005) or on the response of the individual neurons/electrodes following focal stimulation (Jimbo et al., 1999; Marom and Shahaf , 2001; Cozzi et al., 2006). A future line of research would be to investigate whether distributed coding schemes could be used to efficiently decode more complex stimulus features like for example the stimulus frequency or more complex stimuli, like time-varying stimuli. This would allow to generalize the usefulness of distributed coding schemes in such cultures and would be a prerequisite for the above mentioned long-term goal of our laboratory, the creation of hybrid devices.

In summary, MEA proved to be an extremely useful tool to characterize network functions. Thanks to their numerous and non-invasive extracellular electrodes, MEA provide the possibility to record the activity of a very large number of neurons for long periods of time. It allowed me to investigate network functions as diverse as the spatiotemporal dynamics of the spontaneous activity, network plasticity mechanisms and computational properties of random networks of rat hippocampal neurons. Despite the lack of functional organization, these networks bear striking biochemical and functional similarities with their *in vivo* counterpart from brain regions where the neurons come from. The results presented in this thesis are in complete agreement with this notion and encourage further work using random cultures as a generic network model. However, a major drawback of such networks is the difficulty of access to the network's topology. Knowing this latter would provide a better understanding of network functions and some insights on the relationship between structure and function. An alternative solution would be to construct a network of a given topology and recent progress in network patterning should soon make it feasible. As mentioned above, combining electrophysiology, pharmacology and genetics will also likely prove to be a valuable approach to dissect and

investigate network functions in the near future. This would allow one to isolate the function(s) and contribution(s) of diverse network components. Nonetheless, one should not forget that networks are nonlinear and that most network functions emerge from the interactions among neurons and often do not rely on a single specific component and/or mechanism.

5- REFERENCES

Abraham WC, Bear MF (1996) Metaplasticity: the plasticity of synaptic plasticity. *TINS* **19**, 126-130.

Adrian ED, Zotterman Y (1926) The impulses produced by sensory nerve endings: Part II: The responses of a single end organ. *J. Physiol. (Lond.)* **61**, 151-171.

Antal A, Keri S, Kovacs G, Janka Z and Benedek G (2000) Early and late components of visual categorization: an event-related potential study. *Brain Res. Cogn. Brain Res.* **9**, 117-119.

Arieli A, Shoham D, Hildesheim R, Grinvald A (1995) Coherent spatiotemporal patterns of ongoing activity revealed by real-time optical imaging coupled with single-unit recording in the cat visual cortex. *J. Neurophysiol.* **73**, 2072-2093.

Arieli A, Sterkin A, Grinvald A, Aertsen A (1996) Dynamics of ongoing activity: explanation of the large variability in evoked cortical responses. *Science* **273**, 1868-1871.

Azouz R, Gray CM (1999) Cellular mechanisms contributing to response variability of cortical neurons in vivo. *J. Neurosci.* **19**, 2209-2223.

Bair W, Koch C (1996) Temporal precision of spike trains in extrastriate cortex of the behaving macaque monkey. *Neural Comput.* **8**, 1185-1202.

Bak P, Tang C, Wiesenfeld K (1988) Self-organized criticality. *Physical Review A: Atomic, Molecular, and Optical Physics* **38**, 364–374.

Baker RE, Corner MA, van Pelt J (2006) Spontaneous neuronal discharge patterns in developing organotypic mega co-cultures of neonatal rat cerebral cortex. *Brain Res.* **1101**, 29-35.

Ban J, Bonifazi P, Pinato G, Broccard FD, Studer L, Torre V, Ruaro ME (2007) Embryonic derived stem cell-derived neurons form functional networks in vitro. *Stem Cells* 25(3), 738-749.

Bear MF, Connors BW, Damasio MA (1996) *Neurosciences: Exploring the brain.* Williams & Wilkins, USA.

Bedard C, Kroger H, Destexhe A (2006) Does the 1/f frequency scaling of brain signals reflect self-organized critical states ? *Phys. Rev. Lett.* **97**, 118102.

Beggs JM, Plenz D (2003) Neuronal avalanches in neocortical circuits. *J. Neurosci.* **23**, 11167-77.

Beggs JM, Plenz D (2004) Neuronal avalanches are diverse and precise activity patterns that are stable for many hours in cortical slice cultures. *J Neurosci* **24**, 5216-5229.

Beggs JM (2008) The criticality hypothesis: how local cortical networks might optimize information processing. *Phil Trans R Soc A Math. Phys. Eng. Sci.* **366**, 329-343.

Ben-Ari Y, Cherubini E, Corradetti R, Gaïarsa JL (1989) Giant synaptic potentials in immature rat CA3 hippocampal neurones. *J. Physiol. (Lond)* **416**, 303-325.

Ben-Ari Y, Khazipov R, Leinekugel X, Caillard O, Gaiarsa J.-L (1997) GABAA, NMDA and AMPA receptors: a developmental regulated 'ménage à trois'. *TINS* **20**, 523-529.

Ben-Ari Y (2001) Developing networks play a similar melody. *TINS* **24**, 353-360.

Ben-Ari Y (2002) Excitatory actions of GABA during development: the nature of the nurture. *Nat. Rev. Neurosci.* **3**, 728-739.

Ben-Ari Y, Gaiarsa J.-L, Tyzio R, Khazipov R (2007) GABA : a pioneer transmitter that excites immature neurons and generates primitive oscillations. *Physiol. Rev.* **87**. 1215-1284.

Benda J, Longtin A, Maler L (2006) A synchronization-desynchronization code for natural communication signals. *Neuron* **52**, 347-58.

Berry MJ, Warland DK, Meister M (1997) The structure and precision of retinal spike trains. *PNAS USA* **94**, 5411-5416.

Bertalanffy L (1969) *General System Theory, Theory, Fondations, Development, Applications* (George Braziller, New York, 1969).

Bialek W, Rieke F (1992) Reliability and information transmission in spiking neurons. *TINS* **1**, 428-434.

Bolea S, Avignone E, Berretta N, Sanchez-Andres JV, Cherubini E (1999) Glutamate controls the induction of GABA-mediated giant depolarizing potentials through AMPA receptors in neonatal rat hippocampal slices. *J. Neurophysiol.* **81**, 2095-2102.

Bonifazi P, Ruaro ME, Torre V (2005) Statistical properties of information processing in neuronal networks. *Eur. J. Neurosci.* **22**, 2953-2964.

Bucher V, Graf M, Stelzle M, Nisch W (1999) Low impedance thin-film polycrystalline silicon microelectrodes for extracellular stimulation and recording. *Biosens. Bioelectron.* **14**, 639-649.

Buracas GT, Zador AM, DeWeese MR, Albright TD (1998) Efficient discrimination of temporal patterns by motion-sensitive neurons in primate visual cortex. *Neuron* **20**, 959-969.

Buzsáki G, Draguhn (2004) Neuronal oscillations in cortical networks. *Science* **304**, 1926-1929.

Carr CE (1993) Processing of temporal information in the brain. *Ann. Rev. Neurosci.* **16**, 223-243.

Catalano SM, Shatz CJ (1998) Activity-dependent cortical target selection by thalamic axons. *Science* **281**, 559-562.

Cattaneo A, Maffei L and Morrone C (1981) Patterns in the discharge of simple and complex visual cortical cells. *Proc. R. Soc. Lond. B* **212**, 279-297.

Chapin JK, Nicolelis MAL (1999) Population coding in simultaneously recorded neuronal ensemble in ventral posteromedial (VPM) thalamus: multidimensional sensory representations and population vectors. *J. Neurosci. Meth.* **94**, 121-140.

Chen D.-M, Wu S, Guo A, Yang ZR (1995) Self-organized criticality in a cellular automaton model of pulse-coupled integrate-and-fire neurons. *J. Phys. A: Math. Gen.* **28**, 5177-5182.

Chialvo DR (2006) Are our senses critical ? *Nature Phys.* **2**, 301-302.

Chub N, O'Donovan MJ (1998) Blockade and recovery of spontaneous rhythmic activity after application of neurotransmitter antagonists in to spinal network of the chick embryo. *J. Neurosci.* **18**, 294-306.

Connolly P, Curtis A, Dow J, Wilkinson C (1990) An extracellular microelectrode array for monitoring electrogenic cells in culture. *Biosens. Bioelectron.* **5**, 223-234.

Corner MA (1994) Reciprocity of structure-function relations in developing neural networks. *Prog. Brain Res.* **102**, 3-31.

Cozzi L, D'Angelo P, Sanguineti V (2006) Encoding of time-varying stimuli in populations of cultured neurons. *Biol. Cybern.* **94**, 335-349.

Crick F (1984) Function of the thalamic reticular complex: the searchlight hypothesis. *PNAS USA* **81**, 4586-4590.

Crochet S, Fuentealba P, Cissé Y, Timoeef I, Steriade M (2006) Synaptic plasticity in local cortical network in vivo and its modulation by the level of neuronal activity. *Cereb. Cortex* **16**, 618-631.

Dantzker JL, Callaway EM (1998) The development of lacal, layer-specific visual cortical axons in the absence of extrinsic influences and intrinsic activity. *J. Neurosci.* **18**, 4145-4154.

Dayan P, Abbott LF (2001) *Theoretical Neuroscience. Computational and mathematical modeling of neural systems.* MIT Press. Cambride, MA, USA.

Davis GW, Bezprozvanny I (2001) Maintaining the stability of neural function: A homeostatic hypothesis. *Annu. Rev. Physiol.* **63**, 847-869.

Dear SP, Fritz J, Haresign M, Ferragamo M and Simmons JA (1993) Tonotopic and functional organization in the auditory cortex of the big brown bat, *Eptesicus fuscus*. *J. Neurophysiol.* **70**, 1988-2009.

DeCharms, R.C., Merzenich, M.M. (1996). Primary cortical representation of sounds by the coordination of action-potential timing. *Nature* **381,** 610-613.

Delorme A, Thorpe SJ (2001) Face identification with one spike per neuron: resistance to image degradations. *J. Neural Networks* **14**, 795-803.

Destexhe A, Paré D (1999) Impact of network activity on the integrative properties of neocortical pyramidal neurons in vivo. *J. Neurophysiol.* **81**, 1531-1547.

Destexhe A, Rudolph M, Paré D (2003) The high-conductance state of neocortical neurons in vivo. *Nat. Rev. Neurosci.* **4**, 739-751.

Destexhe A, Contreras D (2006) Neuronal computations with stochastic network states.
Science **314**, 85-90.

DeValois RL, DeValois KK (1993) A multi-stage color model. *Vision Res.* **33**, 1053-1065.

Durand GM, Kovalchuk A, Konnerth A (1996) Long-term potentiation and functional synapses induction in developing hippocampus. *Nature* **381**, 71-75.

Edeline JM, Dutrieux G, Manunta Y, Hennevin E (2001) Diversity of receptive field changes in auditory cortex during natural sleep. *Eur. J. Neurosci.* **14**, 1865-1880.

Engel AK, Fries P, Singer W (2001) Dynamic predictions: oscillations and synchrony in top-down processing. *Nat. Rev. Neurosci*. **2**, 704-716.

Ermentrout GB, Kleinfeld D (2001) Travelling electrical waves in cortex: insights from phase dynamics and speculation on a computational role. *Neuron* **29**, 33-44.

Eurich CW, Conradi T, Schwegler H (1999) Critical and non-critical avalanche behavior in network of integrate-and-fire neurons. ESANN ISBN 2-600049-9-X, 411-416.

Eurich CW, Herrmann JM, Ernst UA (2002) Finite-size effects of avalanche dynamics. *Phys. Rev. E* **66**, 066137.

Eytan D, Brenner N, Marom S (2003) Selective Adaptation in networks of cortical neurons. *J. Neurosci.* **23**, 9349-9356.

Fabre-Thorpe M, Richard G and Thorpe SJ (1998) Rapid categorization of natural imagesby rhesus monkeys. *Neuroreport* **9**, 303-308.

Feller MB, Wellis DP, Stellwagen D, Werblin FS, Shatz CJ (1996) Requirement for cholinergic synaptic transmission in the propagation of spontaneous retinal waves. *Science* **272**, 1182-1187.

Feller MB, Butts DA, Aaron HL, Rokhsar S, Schatz CJ (1997) Dynamic properties shape spatiotemporal properties of retinal waves. *Neuron* **19**, 293-306.

Feller MB (1999) Spontaneous correlated activity in developing neural circuits. *Neuron* **22**, 653-656.

Fellous J.-M, Rudolph M, Destexhe A, Sejnowski TJ (2003) Synaptic background noise controls the input/output characteristics of single cells in an *in vitro* model of *in vivo* activity. *Neuroscience* **122**, 811-829.

Fiser J, Chiu C, Weliky M (2004) Small modulation of ongoing cortical dynamics by sensory input during natural vision. *Nature* **431**, 573-578.

Fisher KF, Lukas PD, Wong ROL (1998) Age-dependent and cell class-specific modulation of retinal ganglion cell bursting activity by GABA. *J. Neurosci.* **18**, 3767-3778.

Fox MD, Raichle ME (2007) Spontaneous fluctuations in brain activity observed with functional magnetic resonance imaging. *Nat. Rev. Neurosci.* **8**, 700-711.

Franklin JL, Fickbohm DJ, Willard AL (1992) Long-term regulation of neuronal calcium currents by prolonged changes of membrane potential. *J. Neurosci.* **12**, 1726-1735.

Freeman MP, Watkins NW, Riley DJ (2000) Power law distributions of burst duration and interburst interval in the solar wind: Turbulence or dissipative self-organized criticality ? *Phys. Rev. E* **62**, 8794-8797.

Freeman W.J. Origin, structure, and role of background EEG activity. Part 2. Analytic phase. *Clin. Neurophys.* **115**, 2089-2107 (2004).

Furukawa S, Middlebrooks JC (2002). Cortical representation of auditory space:
information-bearing features of spike patterns. *J. Neurophysiol.* **87**,1749-1762.

Gaiarsa JL, McLean H, Congar P, Leinekugel X, Khazipov R, Tseeb V, Ben-Ari Y (1995) Postnatal maturation of gamma-aminobutyric acidA and B-mediated inhibition in the CA3 hippocampal region of the rat. *J. Neurobiol.* **26**, 339-349.

Galli L, Maffei L (1988) Spontaneous impulse activity of rat retinal ganglion cells in prenatal life. *Science* **242**, 90-91.

Garaschuk O, Linn J, Eilers J, Konnerth A (2000) Large-scale osillatory calcium waves in the immature cortex. *Nat. Neurosci.* **3**, 452-459.

Georgopoulos AP, Schwartz AB, Kettner RE (1986) Neuronal population coding of movement direction. *Science* **233**, 1416-1419.

Gonzales-Islas C, Wenner P (2006) Spontaneous network activity in the embryonic spinal cord regulates AMPAergic and GABAergic synaptic strength. *Neuron* **49**, 563-575.

Gray, C.M., Konig, P., Engel, A.K., Singer, W. (1989). Oscillatory responses in cat visual cortex exhibit inter-columnar synchronization which reflects global stimulus properties. *Nature* **338,** 334-337.

Gross GW, Williams AN, Lucas JH (1982) Recording of spontaneous activity with photoetched microelectrode surfaces from mouse spinal neurons in culture. *J. Neurosci. Meth.* **5**, 13-22.

Gross GW, Rhoades BK, Jordan RJ (1992) Neuronal networks for biochemical sensing. *Sensors and Actuators* **6**, 1-8.

Gross GW, Rhoades BK, Azzazy HME, Wu M.-C (1995) The use of neuronal networks on multielectrode arrays as biosensors. *Biosens. Bioelectron.* **10**, 553-567.

Gross GW, Harsh A, Rhoades B, Göpel W (1997) Odor, drug and toxin analysis with neuronal networks in vitro: extracellular array recording of network responses. *Biosens. Bioelectron.* **12**, 373-393.

Gu X, Spitzer NC (1997) Breaking the code: regulation of neuronal differentiation by spontaneous calcium transients. *Dev. Neurosci.* **19**, 33-41.

Haider B, Duque A, Hasenstaub AR, McCormick DA (2006) Neocortical network activity in vivo is generated through a dynamic balance of excitation and inhibition. *J. Neurosci.* **26**, 4535-4545.

Haider B, Duque A, Hasenstaub AR, Yu Y, McCormick DA (2007) Enhancement of visual responsiveness by spontaneous local network activity in vivo. *J. Neurophysiol.* **97**, 4186-4202.

Hanson MG, Landmesser LT (2004) Normal patterns of spontaneous activity are required for correct motor axon guidance and the expression of specific guidance molecules. *Neuron* **43**, 687-701.

Hanson MG, Landmesser LT (2006) Increasing the frequency of spontaneous rhythmic activity disrupts pool-specific axon fasciculation and pathfinding of embryonic spinal motoneurons. *J. Neurosci.* **26**, 12769-12780.

Hamburger V (1976) The developmental history of motor neuron. *Neurosci. Res. Prog. Bull.* **15**, 1-37.

Hebb D. *The organization of behavior* (Wiley, New York, 1949).

Herz AV, Hopfield JJ (1995) Earthquake cycles and neural reverberations: collective oscillations in systems with pulse-coupled threshold elements. *Phys. Rev. Lett.* **75**, 1222-1225.

Higgins D, Banker G (1998) Primary dissociated cell cultures. In: G. Banker and K. Goslin, Editors, *Culturing Nerve Cells*, The MIT Press, Cambridge, MA (1998), pp. 37–78.

Ho SM, Waite PM (1999) Spontaneous activity in the perinatal trigeminal nucleus of the rat. *NeuroReport* **10**, 659-664.

Horton JC, Hocking DR (1996) An adult pattern of ocular dominance columns in striate cortex of newborn monkeys prior to visual experience. *J. Neurosci.* **16**, 1791-1807.

Ibarretxe G, Perrais D, Jaskloski F, Vimeney A, Mulle C (2007) Fast regulation of axonal growth cone motility by electrical activity. *J. Neurosci.* **27**, 7684-7695.

Israel D, Barry W, Edell D, Mark R (1984) An array of microelectrodes to stimulate and record from cardiac cells in culture. *Am. J. Physiol.* **247**, H669-H674.

Janhsen H, Llinas R (1984) Electrophysiological properties of guinea-pig thalamic neurones: an in vitro study. *J. Physiol*. **349**, 205–226.

Jen PH, Sun XD and Lin PJ (1989) Frequency and space representation in the primary auditory cortex of the frequency modulating bat Eptesicus fuscus. *J. Comp. Physiol. [A]* **165**, 1-14.

Jensen HJ (1998) *Self-Organized Criticality – Emergent Complex Behavior in Physical and Biological Systems*. Cambridge: Cambridge University Press.

Jimbo Y, Kawana A (1992) Electrical stimulation and recording from cultured neurons using a planar microelectrode array. *Bioelectrochem. Bioenerg.* **29**, 193-204.

Jimbo Y, Tateno T, Robinson HPC (1999) Simultaneous induction of pathway-specific potentiation and depression in networks of cortical neurons. *Biophys. J.* **76**, 670-678.

Jimbo Y, Kawana A, Parodi P, Torre V (2000) The dynamics of a neuronal culture of dissociated cortical neurons of neonatal rats. *Biol. Cyb.* **83**, 1-20.

Johansson RS, Birznieks I (2004) First spikes in ensembles of human tactile afferents code complex spatial fingertip events. *Nat. Neurosci.* **7**, 170-177.

Kamioka H, Maeda E, Jimbo Y, Robinson HP, Kawana A (1996) Spontaneous periodic synchronized bursting during formation of mature patterns of connections in cortical cultures. *Neurosci. Lett.* **206**, 109-112.

Kandel ER, Schwartz JH, Jessel TM (2000) Principles of neural science. 4th Edition (McGraw Hill Companies)

Katz LC, Shatz CJ (1996) Synaptic activity and the construction of cortical circuits. *Science* **274**, 1133-1138.

Kenet T, Bibitchkov D, Tsodkys M, Grinvald A, Arieli A (2003) Spontaneously emerging cortical representations of visual attributes. *Nature* **425**, 954-956.

Khazipov R, Leinekugel X, Khalilov I, Gaiarsa JL, Ben-Ari Y (1997) Synchronization of GABAergic interneuronal network in CA3 subfield of neonatal rat hippocampal slices. *J. Physiol.* **498**(Pt 3), 763-772.

Kinouchi O, Copelli M (2006) Physics of psychophysics: Dynamic range of excitable networks is optimized at criticality. *Nature Phys.* **2**, 348-352.

Kisley MA, Gerstein GL (1999) Trial-to-trial variability and state-dependent modulation of auditory-evoked responses in cortex. *J. Neurosci.* **19**, 10451-10460.

Kitano H (2002) Systems biology: A brief overview. *Science* **295**, 1662-1664

Knierem JJ, van Essen DC (1992) Neuronal responses to static textures in area V1 of the alert Macaque monkey. *J. Neurophysiol.* **67**, 961-980.

Krahe R, Gabbiani F (2004) Burst firing in sensory systems. *Nat. Rev. Neurosci.* **5**, 13-24.

Kreiter AK & Singer W (1996) Stimulus-dependent synchronization of neuronal responses in the visual cortex of the awake monkey. *J. Neurosci.* **16**, 2381-2396.

Lauder JM (1993) Neurostransmitters as growth regulatory signals: role of receptors and second messengers. *TINS* **16**, 233-240.

Leblanc MO, Bland BH (1979) Developmental aspects of hippocampal electrical activity and motor behavior in the rat. *Exp. Neurol.* **66**, 220-237.

Leinekugel X, Medina I, Khalilov I, Ben-Ari Y, Khazipov R (1997) Ca2+ oscillations mediated by the synergestic excitatory actions of GABA(A) and NMDA receptors in the neonatal hippocampus. *Neuron* **18**, 243-255.

Leinekugel X, Khalilov I, Ben-Ari Y, Khazipov R (1998) Giant depolarizing potentials: the septa pole of the hippocampus paces the activity of the developing intact septohippocampal complex *in vitro*. *J. Neurosci.* **18**, 6349-6357.

Leinekugel X, Khazipov R, Cannon R, Hirase H, Ben-Ari Y, Buzsaki G (2002) Correlated bursts of activity in the neonatal hippocampus in vivo. *Science* **296**, 2049-2052.

Leinekugel X (2003) Developmental patterns and plasticities: the hippocampal model. *J Physiol (Paris)* **97**, 27-37.

Lewicki MS, Konishi M (1995) Mechanisms underlying the sensitivity of songbird forebrain neurons to temporal order. *PNAS USA* **92**, 5582-5586.

Lin DM, Wang F, Lowe G, Gold GH, Axel R, Ngai J, Brunet L (2000) Formation of precise connections in the olfactory bulb occurs in the absence of odorant-evoked neuronal activity. *Neuron* **26**, 69-80.

Lin M, Chen T (2005) Self-organized criticality in a simple model of neurons based on small-world networks. *Phys. Rev. E* **71**, 016133.

Linkenkaer-Hansen K, Nikouline VV, Palva JM, Ilmoniemi RJ (2001) Long-range temporal correlations and scaling behaviour in human brain oscillations. *J. Neurosci.* **21**,1370-1377.

Lippe WR (1994) Rythmic spontaneous activity in the avian auditory system. *J. Neurosci.* **14**, 1486-1495.

Livingstone MS, Freeman DC and Hubel DH (1996) Visual responses in V1 of freely viewing monkeys. *Cold Spring Harb. Symp. Quant. Biol.* **61**, 27-37.

Llinas E, Jahnsen H (1982) Electrophysiology of mammalian thalamic neurons. *Nature* **297**, 406-408.

Luck SJ, Chelazzi L, Hillyard SA, Desimone R (1997) Neural mechanisms of spatial selective attention in areas V1, V2, V4 of macaque visual cortex. *J. Neurophysiol.* **77**, 24-42.

MacKay D, McCulloch WS (1952) The limiting information capacity of a neuronal link. *Bull. Math. Biophys.* **14**, 127-135.

Maeda E, Robinson HPC, Kawana A (1995) The mechanisms of generation and propagation of synchronized bursting in developing networks of cortical neurons. *J. Neurosci.* **15**, 6834-6845.

Maeda E, Kuroda Y, Robinson HPC, Kawana A (1998) Modification of parallel activity elicited by propagating bursts in developing networks of rat cortical neurons. *Eur. J. Neurosci.* **10**, 488-496.

Malamud BD, Morein G, Turcotte DL (1998) Forest fires: an example of self-organized critical behavior. *Science* **281**, 1840-1842.

Markram H, Lubke J, Frotscher M, Sakmann B (1997) Regulation of synaptic efficacy by coincidence of postsynaptic APs and EPSPs. *Science* **275**, 213-215.

Marom S, Eytan D (2005) Learning in ex-vivo developing networks of cortical neurons. *Prog. Brain Res.* **14**, 189-198.

Martinoia S, Bove M, Carlini G, Ciccarelli C, Grattarola M, Storment C, Kovacs G (1993) A general purpose system for long-term recording from a miroelectrode array coupled to excitable cells. *J. Neurosci. Meth.* **48**, 115-121.

Masuda N, Aihara K (2007) Dual coding hypotheses for neural information representation. *Math. Biosci.* **207**, 312-321.

Mattson MP (1988) Neurotransmitters in the regulation of neuronal cytoarchitecture. *Brain Res. Rev.* **13**, 179-212.

McLean HA, Caillard O, Khazipov R, Ben-Ari Y, Gaiarsa JL (1996) Spontaneous release of GABA activates GABAB receptors and controls network activity in the neonatal rat hippocampus. *J. Neurophysiol.* **76**, 1036-1046.

McLean HA, Caillard O, Ben-Ari Y, Gaiarsa JL (1996b) Bideirectional plasticity expressed by GABAergic synapses in the neonatal hippocampus. *J. Physiol.* **496**(Pt 2), 471-477.

Menendez de la Prida L, Bolea S, Sanchez-Andres JV(1998) Origin of the synchronized network activity in the rabbit developing hippocampus. *Eur. J. Neurosci.* **10**, 899-906.

Metzner W, Koch C, Wessel R and Gabbiani F (1998) Feature extraction by burst-like spike patterns in multiple sensory maps. *J. Neurosci.* **18**, 2283-2300.

Milner LD, Landmesser LT (1999) Cholinergic and GABAergic inputs drive patterned spontaneous motoneuron activity before target contact. *J. Neurosci.* 19, 3007-3022**.**

Ming G, Henley J, Tessier-Lavigne M, Song H, Poo M (2001) Electrical activity modulates growth cone guidance by diffusible factors. *Neuron* **29**, 441-452.

Mooney R, Penn AA, Gallego R, Schatz CJ (1996) Thalamic relay of spontaneous retinal activity prior to vision. *Neuron* **17**, 863-874.

Morefield S, Keefer E, Chapman K, Gross G (2000) Drug evaluation using neuronal networks cultured on microelectrode arrays. *Biosens. Bioelectron.* **15**, 383-396.

Morin FO, Yuzuru T, Tamiya E (2005) Investigating neuronal activity with planar microelectrode arrays: achievements and new perspectives. *J. Biosci. Bioeng.* **100**(2), 131-143.

Morrow TJ, Casey KL (1992) State-related modulation of thalamic somatosensory responses in the awake monkey. *J. Neurophysiol.* **67**, 305-317.

Murakami M, Kashiwadani H, Kirino Y, Mori K (2005) State-Dependent Sensory Gating in Olfactory Cortex. *Neuron* **46**, 285-296.

Murphy BK, Miller KD (2003) Multiplicative gain changes are produced by excitation or inhibition alone. *J. Neurosci.* **23**, 10040-10051.

Murthy VN, Fetz EE (1992) Coherent 25- to 35-Hz oscillations in the sensorimotor cortex of awake behaving monkeys. *PNAS USA* **89**, 5670-5674.

Nakagami Y, Saito H, Matsuki N (1996) Optical recording of rat enthorhino-hippocampal system in organotypic cuclture. *Neurosci. Lett.* **216**, 211-213.

Nicolelis MA, Ghazanfar AA, Faggin BM, Votaw S, Oliveira LM (1997) Reconstructing the engram: simultaneous, multisite, many single neuron recordings. *Neuron* **18**, 529-37.

Nicolelis MA, Ghazanfar AA, Stambaugh CR, Oliveira LM, Laubach M, Chapin JK, Nelson RJ, Kaas JH (1998) Simultaneous encoding of tactile information by three primate cortical areas. *Nat. Neurosci.* **1,** 621-630.

Novak J, Wheeler B (1986) Recording from the aplysia abdominal ganglion with a planar microelectrode array. *IEEE Trans. Biomed. Eng.* **33**, 196-202.

O'Donovan MJ (1989) Motor activity in the isolated spinal cord of the chick embryo: synaptic drive and firing pattern of single motoneurons. *J. Neurosci.* **9**, 943-958.

O'Donovan MJ (1999) The origin of spontaneous activity in developing networks of the vertebrate nervous system. *Curr. Opin. Neuronbiol.* **9**, 94-104.

Pancrazio JJ, Bey PP, Lolee A, Manne SR, Chao HC, Howard LL, Gosney WM, Borkholder DA, Kovacs GTA, Manos P, Cuttino DS, Stenger DA (1998) Description and demonstration of a CMOS amplifier-based-system with measurement and stimulation capability for bioelectrical signal transduction. *Biosens. Bioelectron.* **13**, 971-979.

Panzeri S, Petersen RS, Schultz SR, Lebedev M, Diamond ME (2001) The role of spike timing in the coding of stimulus location in rat somatosensory cortex. *Neuron* **29**, 769-777.

Petersen RS, Panzeri S, Diamond ME (2001) Population coding of stimulus location in rat somatosensory cortex. *Neuron* **32**, 503–14.

Parker D (2006) Complexities and uncertainties of neuronal network function. *Phil. Trans. R. Soc. B.* **361**, 81-99.

Patterson WR, Song YK, Bull CW, Ozden I, Deangellis AP, Lay C, McKay JL, Nurmikko AV, DonoghueJD, Connors BW (2004) A microelectrode/microelectronic hybrid device for brain implantable neuroprosthesis applications. *IEEE Trans. Biomed. Eng.* **51**, 1845-1853.

Penn AA, Riquelme PA, Feller MB, Schatz CJ (1998) Competition in retinogeniculate patterning driven by spontaneous activity. *Science* **279**, 2108-2112.

Perkel DH, Bullock TH (1968) Neural coding. *Neurosci. Res. Prog. Bull.* **63**, 221-348.

Petersen CCH, Hahn TTG, Mehta M, Grinvald A, Sakmann B (2003) Interaction of sensory responses with spontaneous depolarization in layer 2/3 barrel cortex. *PNAS* **100**, 13638-13643.

Pine (1980) Recording action potentials from cultured neurons with extrcellular microcircuit electrodes. *J. Neurosci. Meth.* **2**, 19-31.

Plenz D, Kitai ST (1996) Generation of high frequency oscillations in cortical circuits of somatosensory cortex cultures. *J. Neurophysiol.* **76**, 4001-4005.

Potter SM, DeMarse TB (2001) A new approach to neural cell culture for long-term studies. *J. Neurosci. Meth.* **110**, 17-24.

Potter SM (2001) Distributed processing in cultured neuronal networks. *Prog. Brain Res.* **130**, 49-62.

Pouget A, Dayan P, Zemel R (2000) Information processing with population codes. *Nat. Rev. Neurosci.* **1**, 125-132.
Raichle ME, Mintun MA (2006) Brain work and brain imaging. *Annu. Rev. Neurosci.* **29**, 449-476.

Prut Y, Vaadia E, Bergmann H, Haalman I, Slovin H, Abeles M (1998) Spatiotemporal structure of cortical activity: properties and behavioral relevance. *J. Neurophysiol.* **79**, 2857-2874.

Reid RC, Soodack RE, Shapley RM (1991) Directional selsctivity and spatiotemporal strucure of receptive fields of simple cells in cat striate cortex. *J. Neurophysiol.* **66**, 505-529.

Richmond B, Wiener M (2004) Recruitment order: a powerful neural ensemble code. *Nat. Neurosci.* **7**, 97-98.

Rieke FD, Warland RR, de Ruyter van Steveninick R, Bialek W (1997) *Spikes: Exploring the neural code.* MIT Press. Cambride, MA, USA.

Ritz R, Sejnowski TJ (1997) Synchronous oscillatory activity in sensory systems: new vistas on mechanisms. *Curr. Opin. Neurobiol.* **7**, 536-546.

Rosanova M, Timofeev I (2005) Neuronal mechanisms mediating the variability of somatosensory evoked potentials during sleep oscillations in cats. *J. Physiol.* **562**, 569-582.

Roskies A (1999) The binding problem. *Neuron* **24**, 7-9.

Ruaro ME, Bonifazi P, Torre V (2005) Toward the neurocomputer: image processing and pattern recognition with neuronal cultures. *IEEE Trans. Biomed. Eng.* **52**, 371-383.

Rudolph M, Destexhe A (2003) A fast-conducting, stochastic integrative mode for neocortical neurons in vivo. *J. Neurosci.* **23**, 2466-2476.

Rudolph M, Destexhe A (2003b) Gain modulation and frequency locking under conductance noise. *Neurocomputing* **52**, 907-912.

Rumerlhart DE, Hinton GE, McClelland JL (1986) A general framework for parallel distributed processing. in *Parallel Distributed Processing: Explorations in the Microstructure of Cognition. Vol.1: Fondations* (eds. Rumelhart DE, McClelland JL and the PDP Reasarch Group) (MIT Press, Cambridge, Massachusettes, 1986).

Salinas E, Sejnowski TJ (2001) Correlated neuronal activity and the flow of neural information. *Nat. Rev. Neurosci.* **2**, 539-550.

Sanger TD (2003) Neural population codes. *Curr. Opin. Neurobiol.* **13**, 238-249.

Segundo JP, Moore GP, Sensaas LG and Bullock TH (1963) Sensitivity of neurons in aplysia to temporal pattern of arriving impulses. *J. Exp. Biol.* **40**, 643-667.

Sejnowski T (2003) The computational self. *Ann. NY Acad. Sci.* **1001**, 262-271.

Selinger JV, Pancrazio JJ, Gross GW (2004) Measuring synchronization in neuronal networks for biosensor applications. *Biosens. Bioelectron.* **19**, 675-683.

Shadlen MN, Newsome WT (1994) Noise, neural codes and cortical organization. *Curr. Opin. Neurobiol.* **4**, 569-579.

Shadlen MN, Newsome WT (1998) The variable discharge of cortical neurons: implications for connectivity, computation, and information coding. *J. Neurosci.* **18**, 3870-3896.

Shahaf G, Marom S (2001) Learning in neworks of cortical neurons. *J. Neurosci.* **21**, 8782-8788.

Singer W and Gray CM (1995) Visual features integration and the temporal correlation hypothesis. *Annu. Rev. Neurosci.* **18**, 555-586.

Softky WR (1995) Simple codes versus efficient codes. *Curr. Opin. Neurobiol.* **5**, 239-247.

Spitzer NC (1994) Spontaneous Ca^{2+} spikes and waves in embryonic neurons: signaling systems for differentiation. *TINS* **17**, 115-118.

Staley KJ, Longacher M, Bains JS, Yee A (1998) Presynaptic modulation of CA3 network activity. *Nat. Neurosci.* **1**, 201-209.

Stent GS (1973) A physiological mechanism for Hebb's postulate of learning. *PNAS USA* **70**, 997-1001.

Steriade M, McCormick DA, Sejnowski TJ (1993) Thalamocortical oscillations in the sleeping and aroused brain. *Science* **262**, 679-685.

Steriade M, Contreras D, Curró Dossi R, Nuñez A (1993b) The slow (< 1 Hz) oscillation in reticular thalamic and thalamocortical neurons: scenario of sleep rhythm generation in interacting thalamic and neocortical networks. *J. Neurosci.* **13**, 3284-3299.

Steriade M (2000) Corticothalamic resonance, states of vigilance and mentation. *Neuroscience* **101**, 243-276.

Stett A, Egert U, Guenther E, Hoffman F, Meyer T, Nisch W, Hammerle H (2003) Biological applications of microelectrode arrays in drug discovery and basic research. *Anal. Bioanal. Chem.* **377**, 486-495.

Tatcher RW, North DM, Biver CJ (2008) Self-organized criticality and the development of EEG phase reset. *Hum. Brain Mapp.* In press.

Tateno T, Jimbo Y (1999) Activity-dependent enhancement in the reliability of correlated spike timings in cultured cortical neurons. *Biol. Cyb.* **80**, 45-55.

Tateno T, Jimbo Y, Robinson HPC (2005) Spatio-temporal cholinergic modulation in cultured networks of rat cortical neurons : evoked activity. *Neuroscience* **134**, 439-448.

Thomas CA, Springer PA, Loeb GE, Berwald-Netter Y & Okun LM (1972) A miniature microelectrode array to monitor the bioelectric activity of cultured cells. *Exp. Cell Res.* **74**, 61-66.

Thorpe SJ, Imbert M (1989) Biological constraints on connectionist models. In R. Pfeifer, Z. Schreter and F. Fogelman-Soulié, *Connectionism in perspective* (pp. 63-92). Amsterdam: Elsevier.

Thorpe S, Delorme A, Van Rullen R (2001) Spike-based strategies for rapid processing. *Neural Networks* **14**, 715-725.

Timofeev I, Contreras D, Steriade M (1996) Synaptic responsiveness of cortical and thalamic neurones during various phases of slow sleep oscillations in cat. *J. Physiol.* **494**, 265-278.

Tscherter A, Heuschkel MO, Renaud P, Streit J (2001) Spatiotemporal characterization of rhythmic activity in rat spinal cord slice cultures. *Eur. J. Neurosci.* **14**, 179-190.

Tsodyks M, Kenet T, Grinvald A, Arieli A (1999) Linking spontaneous activity of single neurons and the underlying functional architecture. *Science* **286**, 1943-1946.

Turrigano GG, Nelson SB (2004) Homeostatic plasticity in the developing nervous system. *Nat. Rev. Neurosci.* **5**, 97-107.

Tyzio R, Represa A, Jorquera I, Ben-Ari, Y, Gozlan H, Aniksztejn L (1999) The establishment of GABAergic and glutamatergic synapses on CA1 pyramidal neurons is sequential and correlates with the development of the apical dendrite. *J. Neurosci.* **19**, 10372-10382.

van Pelt J, Wolters PS, Corner MA, Rutten WLC, Ramakers GJA (2004) Long-term characterization of firing dynamics of spontaneous bursts in cultured neural networks. *IEEE Trans. Biomed. Eng.* **51**, 2051-2062.

van Pelt J, Vajda I, Wolters PS, Corner MA, Ramakers GJA (2005) Dynamics and plasticity in developing neuronal networks in vitro. *Prog. Brain Res.* **147**, 173-188.

Vassanelli S, Fromherz P (1997) Neurons from rat brain coupled to transistors. *Appl. Phys. Mater. Sci. Process.* **65**, 85-88.

Wagenaar DA, Potter SM (2004) A versatile all-channel stimulator for electrode arrays, with real-time control. *J. Neural Eng.* **1**, 39-44.

Wagenaar DA, Madhavan R, Pine J, Potter SM (2005) Controlling bursting in cortical cultures with closed-loop multi-electrode stimulation. *J. Neurosci.* **25**, 680-688.

Wagenaar DA, Pine J, Potter SM (2006) Searching for plasticity in dissociated cortical cultures on multi-electrode arrays. *J. Neg. Res. Biomed.* **5**, 16

Weliky M, Katz LC (1998) *Soc. Neurosci. Abstr.* **24**, 1517.

Wells JE, Porter JT, Agmon A (2000) GABAergic inhibition suppresses paroxysmal network activity in the neonatal rodent hippocampus and neocortex. *J. Neurosci.* **20**, 8822-8830.

Wilson MA, McNaughton BL (1993) Dynamics of the hippocampal code for space. *Science* **261**, 1055-1058.

Williford T, Maunsell JH (2006) Effects of spatial attention on contrast response functions in macaque area V4. *J. Neurophysiol.* **96**, 40-54.

Wong RO, Chernjawski A, Smith SJ, Shatz CJ (1995) Early functional neural networks in the developing retina. *Nature* **374**, 716-718.

Wong ROL (1999) Retinal waves and visual system development. *Annu. Rev. Neurosci.* **22**, 29-47.

Wulff P & Wisden W (2005) Dissecting neural circuitry by combining genetics and pharmacology. *TINS* **28**, 44-50.

Yuste R, Peinado A, Katz LC (1992) Neuronal domain in developing neocortex. *Science* **257**, 665-669.

Zador (1998) Impact of synaptic unreliability on the information transmitted by spiking neurons. *J. Neurophysiol.* **79**, 1219-1229.

Zapperi S, Baekgaard LK, Stanley HE (1995) Self-organized branching processes: mean-field theory for avalanches. *Phys. Rev. Lett.* **75**, 4071-4074.

Zhang LI, Tao HW, Holt CE, Harris WA, Poo M (1998) A crtitical window for cooperation and competition among developing retinotectal synapses. *Nature* **395**, 37-44.

Zhang LI, Tao HW, Poo M (2000) Visual input induces long-term potentiation of developing retinotectal synapses. *Nat. Neurosci.* **3**, 708-715.

Zheng C, Feinstein P, Bozza T, Rodriguez I, Mombaerts P (2000) Peripheral olfactory projections are differentially affected in mice deficient in a cyclic nucleotide-gated channel subunit. *Neuron* **26**, 81-91.

ACKNOWLEDGEMENTS

____ first of all, I'd like to express my gratitude to my supervisor Vincent "the Vincent" Torre for his genuine inter-disciplinary approach of Neurosciences. First person I met that talk to me about **NEurocomputer** and neuronal machines. . . . old school **cybernetics** term I'm fond of. . . . quindi grazie Vincent, anche per avermi sopportato per aver creduto in me per più di 4 anni ed aver lasciarmi dei spazi nella ricerca . . . ! ____ grazie a tutti miei colleghi del laboratorio qui m'ont adopté dès la première minute, una seconda **famiglia** con cui ho condiviso tante risate, frustrazioni, conversazioni su tutti i temi possibili ed inimmaginabili ed anche tanto cibo.. tanto.....loro che hanno sopportatto miei deliri surreali. . . . frase italiane di un altro secolo con una **grammatica** incerta ed una pronuncia di sbornione epitellico fievroso convulsivo . . . ed anche mie legioni di domande linguistiche recurrenti. . . . *galanterie oblige*, les femmes d'abord; tutte le biogirls, fonte di motivazione perenne. . .: Elisabetta "la madre superiore dell'ES", collega, amica e padrona di casa !! Giulietta, une autre maman, **fluorescente** celle-ci e torinese, parlando anche il francese ed il danese !! con loro, tante conversazioni interessantissime dalla biologia molecolare, electrofisiologia e canali ionici alla storia dell'Italia ***en passant*** par les conseils avisés sur la science and the best different ways to deal with the PhD student's frustrations . . . . Radio Jelena, trasmissione continua.. et son indissociable sara, les blagues bosniaques, sa bonne humeur à toute épreuve, giretti primaverili al asilo, e il su'optimismo in **cemento** aramato blindato. . . . Silvia, mia cara compagna di **scrivania** per più di 2 anni, a condividere mattine in mancanza di sonno, chocolat e banana, dialoghi doppio-multi-senso interminabili, illusioni e delusioni sissaiene, I love **bicuculline** ! _____then the indian **brigade**: Jummiji, darling miss Eternal whose smiles and laughs enlighted da lab. . . . Raaaaahhhaaahhhhaaaajesh Mr. Spiritual the wise braman still perfectioning his **levitation** skills, the ninja tablas master who taught me indian mythology and helped me in my effort to learn some sanskrit, only Ganesh knows. . . ! Shripad **Mr. Criminal** the meditation brother, flabbergasting me with his MATLAB magic. . . . Anil Mr. Casual, enigmatic Corel-Draw-skilled dude, knowing a hell of keyboard short-cuts and that shared some of the most tantalizing animal stories from south India_____the vector men, Reza & Walter-Trinita-one-of-glance's-eye, other matlab magicians, the talented voice of Walter during our **surrealistic** radiophonic experiments_____and all the others, Franceso son of Bob, bother of all… **Pifidus Activus** la mascotta del lab. . . . the **leech** gang, Liz "Colonel" Garcia, Alberto le sandiniste. Mille grazie anche a Manuela for critically reading the thesis et pour sa disponibilité, sa gentillesse et son rire communicatif de chaque jour. Pano *tricchecus codegus* & Mario Metal Dotti, compagni sempre pronti per qualisasi tipo di deliro musicale, improbabili collaboratori di Radiogeno et véritables amateurs de la langue française, des sacrés **lascars** ces deux-là...! Michel mon ami & Sudhir, **mini-pub** do' for goddam cheap junk-food, beers and long talkin' & Simone le troisième laron that helps me improve useful italian words during rainy sundays in the **Galileo submarine** while trying to patch-clamp vicious vomeronasal cells. _____i pazzi del Malamachi's lab che hanno resistato alle mie incurzione invasive dal **corridorio**, i gomoristi Nicola il maratonista e Marco il filosofo **virulente** e le tre ninfe: Paola la giovana vicking zingarelliana, Giulia la poetessa e Assunta la santa _____tante grazie anche ai tutti miei colleghi del settore di Neurobiologia ed all'Italia in generale ! un grand merci (et bref, car impossible de résumer plus de 2 ans de folie quotidienne en quelques lignes hélas!) au crew del **Pendice dello scoglietto 5/3** con le sue cene allegre e feste estive sul teto del palazzo coll'approvazione di un MAuri claudicante ma sereno: 'astard'Ino qui a paratagé mes **tribulations** MEAesques, camomille et Clorindo, congressi e meeting, il cardinale Knull e il Walker Texas Joker, unlikely encoding of the decoding of the recoding. . . ; **'ngeniere** prof. FelixusPellegrino, fagiola e lentiche mattinale, canzonette napoletane, challenger della battaglia di coniglio, aperitivi da Roby a parlare di rete artificiale e musica e vità in generale; Yolanda la **pittrice**, ultima coinquilina divenuto in poco tempo padrona della casa e maestra della decorazione interiora e delle feste improvvisate a colpo di gastronomia spagnola e giocchi alti in colore. Ci rivederemmo tutti in 2022. . . _____da **Tetris** posse, Il Gorillo, GianPi, Bronco, Sarah, Ilaria, Federico… keepin' rockin' TS baby ! _____all the bro @ gva_____également tant de reconnaissance à l'onlce J alias le Rais **Akbar** ben Salah, membre des collectifs individuels **OD** Prod. et MegaLowRecord, Sound Repair for No-Fi looping experimentation, St-Oyen and the attack of the clowns, et le bureau de la t[our de Bael… manaaz'. . . . _____et merci à Natalia pour son soutien moral et physique lors de la dernière année mouvementée et chaotique de la thèse. . .